

Supplementary wavelength calibration methods for SALT/RSS spectropolarimetric observations

Justin Cooper

B.Sc. (Hons) *cum laude*

Submitted in partial fulfillment of the requirements for the degree

Master of Science in Astrophysics

in the Faculty of Natural and Agricultural Sciences

Department of Physics

University of the Free State

South Africa

November 2024

Supervised by: Prof. B. van Soelen, Department of Physics

Abstract

The Southern African Large Telescope ([SALT](#)) is the largest optical telescope in the Southern Hemisphere. Onboard [SALT](#) is the Robert Stobie Spectrograph ([RSS](#)), which is capable of performing linear spectropolarimetry at optical wavelengths. This, along with its wide wavelength coverage and dynamic observing queue, make [SALT/RSS](#) spectropolarimetric observations ideal for high-energy sources. [Active Galactic Nuclei \(AGN\)](#) are one such high-energy source, powered by the accretion of material onto a central supermassive black hole. Blazars represent a subset of [AGN](#) with relativistic jets closely aligned to our line of sight, and whose high apparent luminosities display variability on periods from less than one day up to years. The optical emission of blazars is often dominated by the polarized, non-thermal emission arising in the jets, with an underlying non-polarized, thermal emission component arising from the host galaxy, dusty torus, and accretion disk components. Optical spectropolarimetry of blazars during both flaring and quiescent states can be used, alongside multi-wavelength observations, to disentangle the polarized and non-polarized components. This provides better constraints to model the [Spectral Energy Distribution \(SED\)](#), allowing a deeper understanding of the mechanisms and structures powering such highly energetic sources. [SALT/RSS](#) spectropolarimetric observations are reduced using an adaption of the beta version of the [POLSAIT](#) (*Polarimetric reductions for SALT*) software. Wavelength calibrations are, in general, the most time-consuming and error-prone manual step in the data reduction process, while also being the most pivotal. Furthermore, the wavelength solutions for complementary *O*- and *E*-beams may, seemingly, be independently well calibrated, but may be inconsistent with each other – essential for accurate polarization results. To improve the time-efficiency of [SALT/RSS](#) spectropolarimetric data reductions, and to ensure consistent wavelength solutions across the *O*- and *E*-beams, this study presents [STOPs](#) (*Supplementary Tools for POLSAIT Spectropolarimetry*), as well as its development and testing. The [STOPs](#) software addresses limitations in the existing wavelength calibration method, allowing for external wavelength calibrations, such as [IRAF](#), while also providing tools to verify the consistency of the wavelength solutions, epoch-to-epoch or across polarimetric beams. Rigorous testing, through both synthetic and real data, has been conducted to ensure the reliability and accuracy of [STOPs](#). The blazar 3C 279 was observed during periods of enhanced and flaring γ -ray activity in 2017. The normalized relative flux spectrum of 3C 279 shows a notable dip in the $\sim 6000 - 9000 \text{ \AA}$ range during the period of flaring as compared to epochs of enhanced activity. The degree of polarization for 3C 279 was found to be $\Pi \approx 13.3\%$, and 21.1% during epochs of enhanced activity, and 8.7% during flaring, respectively. The degree of polarization shows good agreement across grating angles and remains fairly constant over the observed wavelength range while still varying from epoch to epoch, as expected from the transient nature of 3C 279. The polarization angle was found to be $\theta \approx 53.3^\circ$, and 77.7° during epochs of enhanced activity, and 63.3° during flaring, respectively. The polarization angle remains consistent across the observed wavelength range, with a slight deviation between grating angles during flaring. Further, Hiltner 652 was observed with the [SALT/RSS](#) in linear spectropolarimetry mode on 10 June 2022. The reduced, P_Q and P_U , Stokes parameters show no major deviation from previously published results which further ensures that there is no interference introduced into the Stokes parameter calculations for alternate wavelength calibrations as handled by [STOPs](#). The application of [STOPs](#), during the reductions presented, supports the feasibility of alternate wavelength calibration methods while ensuring efficient, accurate, and consistent wavelength solutions.

Keywords: Optical Astronomy: [SALT](#), [RSS](#) – Spectropolarimetry – Astronomy software: [POLSAIT](#), [IRAF](#), [STOPs](#) – Astronomy data reduction: wavelength calibration – High-energy astrophysics: Blazars

In loving memory of my grandpa and oupa,

Boyd McGowan Fichardt Cooper
1942 – 2021

Jacobus Pieter ‘Koos’ van der Merwe
1947 – 2024

Acknowledgements

I hereby acknowledge and express my sincere gratitude to the following parties for their invaluable support and contributions.

Firstly, I would like to thank my supervisor, Prof. Brian van Soelen. Your guidance, patience, and willingness to put up with all of my ‘Dear sir’ emails is greatly appreciated.

I acknowledge the financial support from the Department of Physics, UFS, whose funding made this project possible. To my colleagues and friends at UFS, notably Natalie and Joleen, thank you for your support and encouragement, without which this project would not have been as fun or enjoyable as it was. To Daniel and J.P., I can’t believe we made it this far, but I’m glad we did.

I would also like to acknowledge the [SAAO/SALT](#) teams for making this project possible, notably Dr. Daniël Groenewald for her instruction in getting the [POLSLALT](#) software running.

For their continuous love and support I thank my parents, Samantha and Juan Barnard, André and Sarah van der Merwe, as well as my brother Jacob van der Merwe.

Thank you, too, to those who may as well be family, the van der Walt’s, and the Litch’s. You have been a constant source of support and love, and I am grateful for you all.

Finally, to my friends, your unfailing friendships have kept me sane and smiling. Thank you. To Monica, you were the year-long push I needed to get this done. Truly, I would not have finished this if it weren’t for you. To Johané, you have shown me how kind and caring a person can be, and I am proud to call you friend. To Wian, thank you for being weirder than me and showing me that there’s a world outside of university. To Candes, thank you for always being a great friend, even when I disappear for months at a time.

“Oh, and in case I don’t see ya,
good afternoon,
good evening,
and goodnight!”

– Truman Burbank

Contents

1	Introduction	1
1.1	Outline	3
2	Spectropolarimetry and the SALT/RSS	5
2.1	Spectroscopy	5
2.1.1	Telescope Optics	5
2.1.2	Slit	6
2.1.3	Collimator	6
2.1.4	Dispersion Element	6
2.1.5	Camera Optics	7
2.1.6	Detector	7
2.1.7	Dispersion of Light	7
2.1.8	Detector and Spectroscopic Calibrations	11
2.2	Polarimetry	17
2.2.1	Polarization	18
2.2.2	Polarization Measurement	21
2.2.3	Polarimetric Calibrations	24
2.3	Spectropolarimetry	25
2.3.1	Spectropolarimetric Measurement	26
2.3.2	Spectropolarimetric Calibrations	27
2.4	The Southern African Large Telescope	28
2.4.1	The Primary Mirror	28
2.4.2	Tracker and Tracking	29
2.4.3	SALT Instrumentation	30
3	Existing and Developed Software	33
3.1	POLSALT	33
3.1.1	Raw Image Reductions	34
3.1.2	Wavelength Calibrations	34
3.1.3	Spectral Extraction	35
3.1.4	Raw Stokes Calculations	35
3.1.5	Final Stokes Calculations	36
3.1.6	Visualization	36
3.1.7	Post-Processing Analysis	36
3.1.8	The Need for Supplementary Tools	37

3.2	IRAF	38
3.2.1	Identify	39
3.2.2	Reidentify	39
3.2.3	Fitcoords	41
3.2.4	Transform	42
3.3	STOPS	43
3.3.1	Splitting	43
3.3.2	Joining	45
3.3.3	Sky Lines	49
3.3.4	Cross Correlation	50
3.4	General Reduction Procedure	51
3.4.1	Initial Setup	51
3.4.2	POLSLT Pre-Reductions	53
3.4.3	Wavelength Calibration	54
3.4.4	POLSLT Reduction Completion	56
4	Testing and Application	59
4.1	Testing STOPS	59
4.1.1	The split Method	60
4.1.2	The join Method	61
4.1.3	The correlate Method	63
4.1.4	The skylines Method	63
4.2	Application of STOPS	66
4.2.1	Buckley et al. (2019)	67
4.2.2	Proceeding, HEASA (2021)	68
4.2.3	Spectropolarimetric observations of 3C 279	70
4.2.4	Comparison of Hiltner 652 to VLT/FORS observations	73
4.2.5	Schutte et al. (2022)	74
5	Conclusions	77
5.1	A Broad Overview of STOPS	77
5.2	Scientific results using STOPS	78
5.3	Future Development	79
Bibliography		81
A The Modified Reduction Process		93
B STOPS Source Code		101
C Proceedings		143

List of Acronyms and Symbols

ADC	Atmospheric Dispersion Compensator
AGN	Active Galactic Nucleus
Ar	Argon
BAT	Burst Alert Telescope
CCD	Charged-Coupled Device
CLI	Command Line Interface
CMOS	Complementary Metal-Oxide-Semiconductor
CuAr	Copper-Argon
CRR	Cosmic Ray Rejection
ESO	European Southern Observatory
EW	Equivalent Width
<i>Fermi</i> -LAT	<i>Fermi</i> Large Area Telescope
<i>Fermi</i> LCR	<i>Fermi</i> Light Curve Repository
FITS	Flexible Image Transport System
FORS	Focal Reducer and Low Dispersion Spectrograph
FSRQ	Flat Spectrum Radio Quasar
FWHM	Full Width at Half Maximum
GRB	Gamma-ray Burst
GUI	Graphical User Interface
HDU	Header and Data Unit
HEASA	High Energy Astrophysics South Africa
HET	Hobby-Eberly Telescope
HRS	High Resolution Spectrograph
IRAF	<i>Image Reduction and Analysis Facility</i>
L+45°	Linear +45° Polarized
L−45°	Linear −45° Polarized
LCP	Left Circularly Polarized
LHP	Linear Horizontally Polarized

LVP	Linear Vertically Polarized
HgAr	Mercury-Argon
Ne	Neon-Argon
NIR	Near Infra-Red
NIRWALS	Near Infra-Red Washburn Labs Spectrograph
POLSALT	<i>Polarimetric reductions for SALT</i>
PyPI	Python Package Index
RCP	Right Circularly Polarized
RMS	Root Mean Square
RSS	Robert Stobie Spectrograph
SAAO	South African Astronomical Observatory
SAC	Spherical Aberration Corrector
SALT	Southern African Large Telescope
SALTICAM	SALT Imaging Camera
SED	Spectral Energy Distribution
SNR	Signal-to-Noise Ratio
STOPS	<i>Supplementary Tools for POLSALT Spectropolarimetry</i>
<i>Swift</i>	Neil Gehrels <i>Swift</i> Observatory
ThAr	Thorium-Argon
UV	Ultraviolet
UVOT	Ultraviolet Optical Telescope
VLT	Very Large Telescope
VPH	Volume Phase Holographic
Xe	Xenon

Chapter 1

Introduction

Data reductions and, by extension, the software enabling them, are an often overlooked aspect of astrophysical research. They are the foundation upon which scientific results are built. With ever increasingly complex and sensitive observational techniques and instruments, coupled with the ever-increasing volume of data, the need for efficient and accurate data reductions are a critical aspect of astronomical research.

One such instrument, installed on the Southern African Large Telescope ([SALT](#)) ([Buckley et al., 2006](#)), is the Robert Stobie Spectrograph ([RSS](#)) ([Burgh et al., 2003](#)). The [SALT/RSS](#) is currently capable of performing, point-source and diffuse (spatial), long-slit linear spectropolarimetry, allowing for the simultaneous observation of, wavelength dependent, intensity and polarization ([Nordsieck et al., 2003](#)).

The [POLSLAT](#) (*Polarimetric reductions for SALT*) software is a Python 2 based software package that provides a complete reduction pipeline for [SALT](#) spectropolarimetric data, from pre- to final reductions, and the plotting of the spectropolarimetric results ([Crawford et al., 2010](#)). As of 2024, data reductions for [SALT/RSS](#) spectropolarimetric observations are generally completed using an adaption of the beta version of the [POLSLAT](#) software.¹ A [Graphical User Interface \(GUI\)](#) is implemented through the beta version, providing limited interactivity during the reduction process. The user can complete the full reduction process purely using [POLSLAT](#), but this does not mean the software is without its limitations.

Erroneous inputs or key presses from the user can lead to unexpected program crashes, and the wavelength calibration process is time-consuming and inflexible. This makes recalibrating the wavelength solutions unfeasible for anything larger than a handful of observations. Furthermore, the wavelength calibration of the *O*- and *E*-beams are entirely independent of each other. This allows good fits to each polarimetric beam, but does not ensure that the wavelength solutions are consistent across the two beams, leading to potential systematic errors in the final results.

¹As of writing, the versions used for [POLSLAT](#) are as follows: [POLSLAT](#) (0.2.dev144), [PySALT](#) (0.5dev), [PyRAF](#) (1.8.1), and [IRAF](#) (2.14).

To address these challenges, the objective of this study is to develop supplementary tools to aid in the spectropolarimetric reduction process. The aims of these supplementary tools, named **STOPS** (*Supplementary Tools for POLSALT Spectropolarimetry*), are:

- to provide a more interactive approach to the wavelength calibration process,
- to allow integration of alternate wavelength calibration methods into the standard **POLSALT** reduction procedure,
- to ensure the accuracy of spectropolarimetric wavelength solutions, and
- to improve the overall efficiency and wavelength calibration process for spectropolarimetric wavelength calibrations.

The **STOPS** software should allow for efficient and accurate wavelength calibrations. It is designed to be used in conjunction with the **POLSALT** software, allowing for more interactive wavelength calibration processes to be used in place of the built-in **POLSALT wavelength calibration** method. This means that **STOPS** does not perform the wavelength calibration itself, but should rather parse the **Flexible Image Transport System (FITS)** files from and to the **POLSALT** format before and after the wavelength calibration process, respectively. **STOPS** should also be expected to handle any additional calibrations which are completed during the **POLSALT** wavelength calibration process, such as the wollaston tilt corrections and **Cosmic Ray Rejection (CRR)**.

Further secondary aims were to make the installation and usage of the software as user-friendly as possible, and to ensure the software is easily maintainable and extendable. These secondary aims, thankfully, relate to design choices, and are controlled through the choice of programming language and distribution method. Python 3 is the language of choice due to the current widespread use of Python in the astronomical community. The software will be distributed through GitHub for version control, with the option to later publish to the **Python Package Index (PyPI)** once a stable release is developed. Lastly, Python relies on the Python package manager, pip, which allows the installation of **STOPS** to be handled natively.

The development of **STOPS** was initiated to be used as part of ongoing research which uses **SALT** to study the polarimetric properties of **Active Galactic Nuclei (AGN)**, in particular, blazars. **AGN** are the cores of galaxies powered by accretion onto a super-massive black hole. Blazars represent the subclass of radio-loud **AGN** with relativistic jets closely aligned to our line of sight ($\theta \lesssim 10^\circ$), known for their rapid and high degree of variability across the electromagnetic spectrum (Urry and Padovani, 1995). Blazar **Spectral Energy Distributions (SEDs)** show two clear components: a lower energy component produced through leptonic synchrotron processes (spanning the radio to **Ultraviolet (UV)**/soft X-ray regimes) and a higher energy component (spanning the X-ray to γ -ray regimes) which is proposed to be produced through either leptonic or hadronic processes (Böttcher et al., 2013). The optical emission from blazars comprises of polarized, non-thermal, synchrotron emission arising in the jets, with underlying non-polarized, thermal, emission arising from the host galaxy, dusty torus, and accretion disk components (Ghisellini et al., 2009). Optical spectropolarimetry, coupled with multi-wavelength observations, during both flaring and quiescent states can be used to disentangle the polarized and non-polarized components in blazar **SEDs**, providing better constraints for the non-thermal particle distribution (Schutte et al., 2021, 2022).

The **SALT/RSS** PG0300 grating, and accompanying **Ar** arc lamp, provided the widest wavelength range and highest throughput, making them ideal for optical observations of blazars during differing states of flaring and quiescence. These spectropolarimetric observations are, however, particularly challenging to reduce as the **Ar** arc lamp exhibits sparse spectral features across the wavelength range, with a partial overlap of a higher order at longer wavelengths. Due to these difficulties, a backlog of unanalyzed data existed.

Integrating alternate wavelength calibrations for **SALT/RSS** spectropolarimetry has broad implications for astronomical research, particularly in studies involving sources which display high degrees of polarization, such as high-energy sources. By providing alternate reliable and efficient methods of wavelength calibration, this dissertation directly enhances the efficiency of the **SALT/RSS** to produce high-quality spectropolarimetric results, allowing the interplay between polarization and spectral features to be further investigated.

1.1 Outline

The layout of the rest of the dissertation is as follows:

Chapter 2 lays a foundation for spectroscopy, polarimetry, and spectropolarimetry as well as the implementation of these principles through instrumentation, focusing specifically on principles as relating to the **SALT/RSS**. These principles provide an understanding of spectropolarimetric data as well as describe the reduction and calibration processes to be completed for the acquisition of spectropolarimetric results.

Chapter 3 describes the existing **POLSALT** (used for spectropolarimetric reductions) and **IRAF (*Image Reduction and Analysis Facility*)** (used for wavelength calibrations) software, the developed **STOPS** software, and provides a general reduction process for spectropolarimetric data. The principles, application, and challenges faced when using the existing software for spectropolarimetric data reductions are broadly described, with greater emphasis placed on the developed software, **STOPS**, which was designed to streamline the data reduction process and overcome the limitations of the existing software.

Chapter 4 provides the testing of the developed software and discusses its application within published articles and proceedings. Testing was conducted on a ‘per-module’ basis aligning with the usage of **STOPS**.

Chapter 5 concludes the dissertation proper by summarizing the development and testing of the **STOPS** software, noting the current application of **STOPS** in publications. The possible routes for future development are described, focusing on stability, further integration with **POLSALT**, and development of improved features.

Finally, the appendices, **Appendix A**, **B**, and **C**, contain a complete, generalized, working reduction procedure (referred to in **Chapter 3**), the **STOPS** source code, and Proceedings produced from conferences (referred to in **Chapter 4**), respectively.

Chapter 2

Spectropolarimetry and the SALT/RSS

This chapter gives an overview of the basics of spectropolarimetry (§ 2.3), and how it functions, following from the principles of both spectroscopy (§ 2.1) and polarimetry (§ 2.2). Further, it is discussed how these techniques are practically implemented for SALT (§ 2.4), using the RSS (§ 2.4.3), and how the spectropolarimetric reduction process is completed (§ 2.4.3).

2.1 Spectroscopy

Spectroscopy originated in its most basic form with Newton's examinations of sunlight through a prism (Newton and Innys, 1730) but came to prominence as a field of scientific study with Wollaston's improvements to the optics elements (Wollaston, 1802), Fraunhofer's use of a diffraction grating instead of a prism (der Wissenschaften, 1824), and Bunsen and Kirchoff's classifications of spectral features to their respective chemical elements (Kirchhoff and Bunsen, 1861).

The simplest spectrometer schematic, as shown in Figure 2.1, consists of incident light collected from the telescope's optics, labelled A, being focused onto a slit, B, and passed through a collimator, C. The collimator collimates the light allowing a dispersion element, D, to disperse the light into its constituent wavelengths. The resultant spectrum is focused by camera optics, E, onto a focal plane, F. Viewing optics are situated at the focal plane in the case of a spectroscope and a detector is situated at the focal plane in the case of a spectrograph.

2.1.1 Telescope Optics

The telescope optics refers simply to all the components of a telescope necessary to acquire a focal point at the spectrometer entrance, labelled B. The focal point in most traditional telescope designs is fixed relative to the telescope and so the spectrometer may be mounted at that point. In cases where the telescope is designed to have a moving focal point relative to the telescope (see Buckley et al., 2006; Cohen, 2009; Ramsey et al., 1998), the spectrometer, or a signal transfer method such as a fibre feed to the spectrometer, must also move along the telescope's focal path.

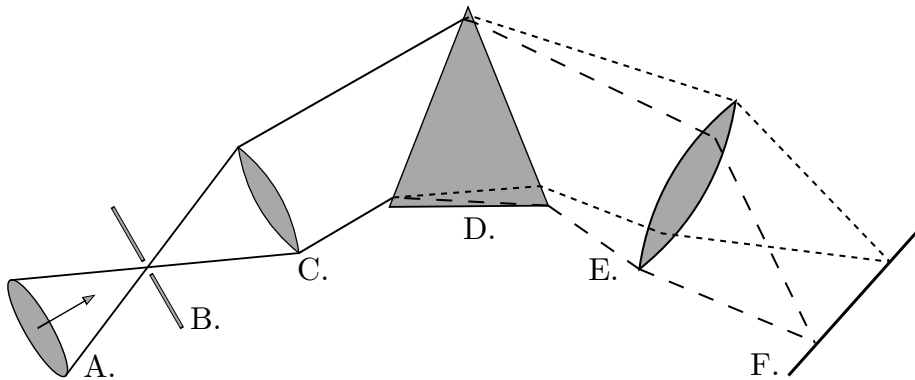


Figure 2.1: Layout depicting the light path through a spectrometer. Diagram adapted from [Birney et al. \(2006\)](#).

2.1.2 Slit

The slit's function is to control the amount of incident light entering a spectrometer and, along with the exposure time of the detector, prevents over-exposures of bright sources on highly sensitive detectors ([Tonkin, 2013](#)). If a source is spatially resolvable, or larger than the seeing conditions, the slit additionally acts to spatially limit the source to increase the spectral resolution, resulting in sharper features in the resultant spectrum. Without the slit the spectral resolution would be determined by the projected width of the source on the detector, or the seeing if the source was a star-like point source. Increasing the spectral resolution comes with the trade-off of decreasing the light collected from the source and thus acquiring a less intense resultant spectrum. Multiple spectra may be acquired simultaneously when the slit is positioned such that collinear sources lie along the slit.

The spectrometer is usually situated at the focal point. In cases where this is not feasible due to restrictions, for example restrictions of weight or size, a fibre feed may be situated behind the slit on the telescope. This allows the signal to be routed away from the telescope to a controlled environment with only minuscule losses.

2.1.3 Collimator

The collimators function is to collimate the focused light from the telescope, ensuring that all light rays run parallel before reaching the dispersion element. The focal ratio of the collimator (f_c/D_c , where f refers to the focal length and D refers to the diameter) should ideally match the focal ratio of the telescope (f_T/D_T).

2.1.4 Dispersion Element

Including a dispersion element in the optical path is what defines a spectrometer. As the name suggests, a dispersion element disperses the light incident on it into its constituent wavelengths and produces a spectrum. There are two types of dispersion elements, namely the prism and the diffraction grating, which operate on different principles, as discussed in § 2.1.7.

2.1.5 Camera Optics

The lens functions similarly to that of the telescope's optics but in this case focuses the dispersed light onto a receiver situated at the focal plane. As mentioned previously, an eye piece is fixed to the focal point for a spectroscope while a spectrograph employs a detector.

2.1.6 Detector

The two most prevalent detector types in spectroscopy are the [Charged-Coupled Device \(CCD\)](#) and [Complementary Metal-Oxide-Semiconductor \(CMOS\)](#) detectors. In astronomical spectroscopy however, sources are fainter and exposure times are much longer and so the [CCD](#) detectors are by far the preferred detector as their output has a higher-quality and lower-noise when compared to [CMOS](#) cameras under the same conditions ([Janesick et al., 2006](#)).

The [CCD](#) is a detector composed of many thousands of pixels which can store a charge so long as a voltage is maintained across the pixels. Each pixel detects incoming photons using photo-sensitive capacitors through the photoelectric effect and converts the photons to a charge ([Buil, 1991](#)). There are also thermal agitation effects which introduce noise to the charge accumulated by a pixel, further discussed in § 2.1.8. Once the exposure is finished the accumulated charge is read column by column, row by row, through an Analog-to-Digital Converter which produces a two-dimensional array of ‘counts’.

2.1.7 Dispersion of Light

Light can be broken up into its constituent wavelengths through two different physical phenomena, namely dispersion and diffraction, which dispersive elements use to create spectra. Dispersive prisms and diffractive gratings each have their strengths and weaknesses and a wide spectrum of instruments exist which implement either, or both, concepts. Regardless of the specific element, dispersive elements all have a resolving power, R , and an angular dispersion. Generally, while the angular dispersion is a more involved process to determine, the resolving power of a spectrograph can be measured as:

$$R = \frac{\lambda}{FWHM}, \quad (2.1)$$

where λ is the wavelength of an incident monochromatic beam and [Full Width at Half Maximum \(FWHM\)](#) refers to the width of the feature on the detector at half of its maximum intensity.

Prism

The prism operates on the principle that the refractive index of light, n , varies as a function of its wavelength, λ . Prisms were the only dispersive elements available for early spectroscopic studies, but they were not without flaw. The angular dispersion of a prism is given by:

$$\frac{\partial\theta}{\partial\lambda} = \frac{B}{a} \frac{dn}{d\lambda}, \quad (2.2)$$

where θ is the angle at which the refracted light differs from the incident light, λ is the wavelength of the incident light, B is the longest distance the beam would travel through

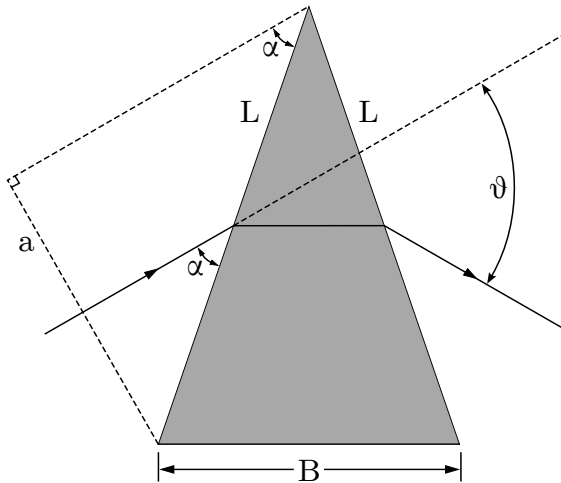


Figure 2.2: Geometry of a prism refracting an incident monochromatic beam at a minimum deviation angle. Diagram adapted from Birney et al. (2006).

the prism. $a = L \sin(\alpha)$ is the maximal beam width that would fit onto a prism with a transmissive surface of length L for a given angle, α , at which a beam would strike the transmissive surface, as shown in Figure 2.2.

The refractive index of a material as a function of its wavelength, $n(\lambda)$, can be approximated by Cauchy's equation:

$$n(\lambda) = A_C + \frac{B_C}{\lambda^2} + \frac{C_C}{\lambda^4} + \dots, \quad (2.3)$$

where A_C, B_C, C_C are the Cauchy coefficients and have known values for certain materials. Cauchy's equation is a much simpler approximation of the refractive index that remains very accurate at visible wavelengths (Jenkins and White, 1976). Taking only the first term of the derivative of the Cauchy equation allows us to approximate the angular dispersion of a prism,

$$\frac{\partial \theta}{\partial \lambda} = -\frac{B}{a} \frac{2B_C}{\lambda^3} \propto -\lambda^{-3}, \quad (2.4)$$

which shows that the angular dispersion of a prism is wavelength dependent and furthermore that longer wavelengths are dispersed less than shorter wavelengths (Birney et al., 2006; Hecht, 2017). The dependence of the angular dispersion, $d\theta/d\lambda$, on the wavelength, λ , is crucial for the formation of a spectrum but this cubic, non-linear, relation results in a non-linear spectrum. Since prisms rely on the refractive index of the material they are made of, they have low angular dispersions.

Multiple prisms can be used to increase the angular dispersion but as the dispersion is non-linear it becomes increasingly more difficult to calibrate. The more material and material boundaries the light must pass through, the more its intensity decreases due to attenuation effects and Fresnel losses. Even so, the transmittance of modern prisms for their selected wavelength range is generally very high due to improved manufacturing methods as well as improved transmitting materials.¹

¹See manufacturers technical specifications, [THORLABS](#), or [Edmund Optics](#) for example.

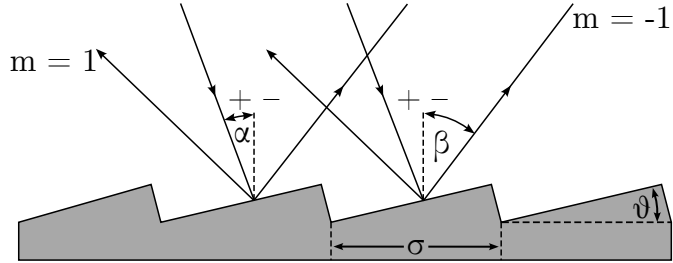


Figure 2.3: Geometry of a reflective blazed grating refracting an incident monochromatic beam. Diagram adapted from Birney et al. (2006).

Diffraction Grating

The alternative dispersing element is a diffraction grating, which operates on the principle that as light interacts with a grating where the groove size is comparable to the light's wavelength, the light is dispersed through constructive and destructive interference. This interference results in multiple diffracted beams m , called orders, either side of a central reflected, or transmitted, beam such that $m \in \mathbb{Z}$, where $m = 0$ is the non-dispersed, or reflected, beam.

An example of a reflective blazed grating is illustrated in Figure 2.3. Here a monochromatic beam is incident on the grating at an angle of α from the grating normal. Due to the interference, a diffracted beam of wavelength λ is found at an angle of β from the grating normal. The relation between the incident and diffracted beams is given by the grating equation:

$$m\lambda = \sigma(\sin(\alpha) \pm \sin(\beta)), \quad (2.5)$$

where σ is the groove spacing of the grating and m is the order of the diffracted beam being considered. The grating equation also applies to transmission gratings, though care should be taken for the signs of α and β .

Equation 2.5 also shows that different diffracted beams may share an angle of dispersion for beams not in the same order. The regions of an order that do not overlap with another order are called free spectral ranges. An order-blocking filter may be used to account for the overlaps and increase the free spectral range. A diffraction grating can also be blazed by an angle θ , as illustrated in Figure 2.3. Blazing refers to the fact that the grooves on the surface of the grating are not symmetrical. The asymmetry of the grooves diffracts the incident beam such that most of the beam's intensity is found in a reflected, zeroth order, beam. The wavelength at which a blazed spectrograph is most effective is called the blaze wavelength, λ_b , which is determined by:

$$\begin{aligned} m\lambda_b &= 2\sigma \sin(\theta) \cos(\alpha - \theta), \text{ where} \\ 2\theta &= \alpha + \beta. \end{aligned} \quad (2.6)$$

Taking the derivative of Equation 2.5 with respect to λ while keeping α constant, allows us to determine the angular dispersion of a diffraction grating,

$$\frac{\partial \beta}{\partial \lambda} = \frac{m}{\sigma \cos(\beta)}. \quad (2.7)$$

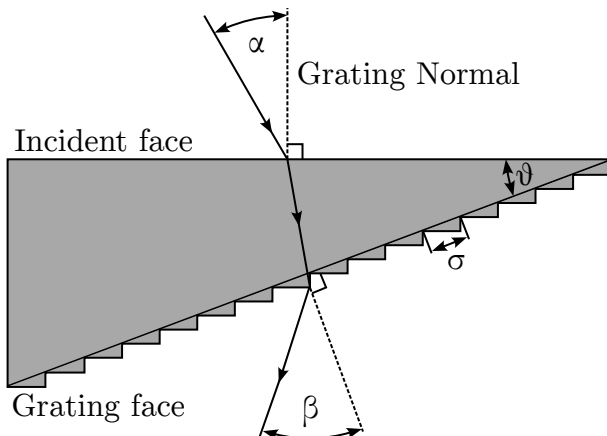


Figure 2.4: Diagram of a grism for an incident monochromatic beam of light and a diffracted beam of order $m = 1$. Diagram adapted from Birney et al. (2006).

Substituting m/σ with the grating equation results in

$$\frac{\partial \beta}{\partial \lambda} = \frac{\sin(\alpha) + \sin(\beta)}{\lambda \cos(\beta)} \propto \lambda^{-1}. \quad (2.8)$$

Similar to the dispersion of a prism, Equation 2.8 shows that the dispersion of a grating is wavelength dependent, but this dependence is only inversely proportional and thus more uniform across a wavelength range than that of a prism. Furthermore, shorter wavelengths are refracted less than longer wavelengths since there is no negative relation between the angular dispersion and the wavelength (Birney et al., 2006; Hecht, 2017).

Alternate Diffraction Elements

As mentioned before, multiple subgroups exist for both dispersive prisms and diffractive gratings. For prisms, along with the single and multiple prism setups mentioned, there also exists grisms and immersed gratings. A grism (Grating Prism), as shown in Figure 2.4, refers to a transmissive grating etched onto one of the transmissive faces of a prism and allows a single camera to capture both spectroscopic and photometric images without needing to be moved, with and without the grism in the path of the beam of light, respectively. An immersed grating refers to a grism modified such that the transmissive grating is coated with reflective material. The primary source of dispersion for both grisms and immersive gratings is the grating and any aberration effects from the prism are negligible in comparison.

Other types of gratings include the Volume Phase Holographic (VPH) grating as well as the echelle grating. The VPH grating consists of a photoresist, which is a light-sensitive material, sandwiched between two glass substrates. Diffraction is possible since the photoresist's refractive index varies near-sinusoidally perpendicularly to the gratings lines, as seen in Figure 2.5. This allows for sharper diffraction orders and low stray light scattering as compared to more traditional gratings but since blazing is not possible the efficiency is decreased. An echelle grating refers to a diffraction grating with higher groove spacing which is optimized for use at high orders. The high order of the diffracted beam

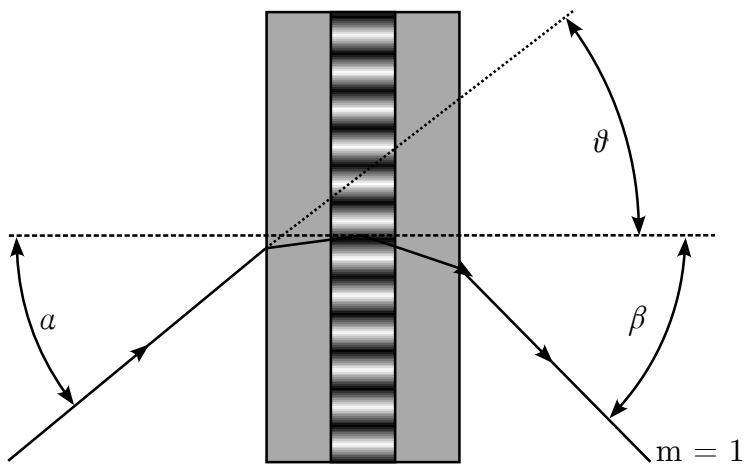


Figure 2.5: Diagram of a VPH grating for an incident monochromatic beam of light. Diagram adapted from Birney et al. (2006).

allows for greater angular dispersion which is most useful when combined with another dispersion element to cross-disperse a spectrum, resulting in a high resolution spectrum.

2.1.8 Detector and Spectroscopic Calibrations

Acquiring a spectrum from observations is more involved than simply reading out the data recorded on the [CCD](#). A raw science image, which is the raw counts of the observed source read from the [CCD](#) with no calibrations applied, has on it a combination of useful science data as well as noise. The noise is a combination of random noise introduced through statistical processes and systematic noise introduced through the instrumentation and the observation conditions the source was observed under. This noise causes an uncertainty in the useful data and can be minimized, predominantly by calibrating for the systematic noise, but never fully removed ([Howell, 2006](#)).

The dominant source of noise in a raw image is detector noise. [CCDs](#) are manufactured to have a small base charge in each pixel, called the ‘bias’ current which allows the readout noise, a type of random noise, to better be sampled. There is also an unintentional additional charge which is linearly proportional to the exposure time and originates from thermal agitation of the [CCD](#) material, called the ‘dark’ current. The dark current can be minimized and possibly ignored if the [CCD](#) is adequately cooled. These types of noise add to the charge held by a pixel and are thus considered additive.

The [CCD](#) is not a perfect detector and the efficiency of it and the optics of the telescope also contribute noise to the image. The efficiency of a [CCD](#) is referred to as the Quantum Efficiency, and it is a measure of what percentage of light striking the detector is actually recorded and converted to a charge. The efficiency of the [CCD](#) and telescope optics is also wavelength dependent and so the noise that results from them is more complex than that of additive noise. This type of noise is referred to as multiplicative noise.

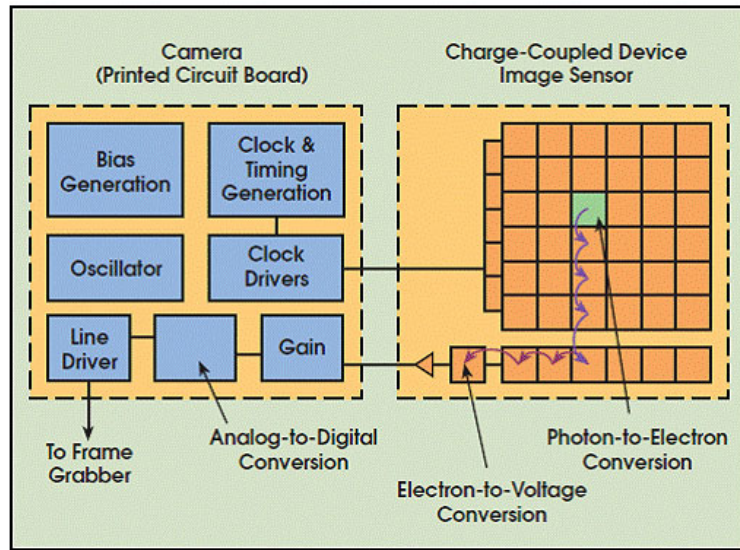


Figure 2.6: Diagram of the inner logic of a **CCD**. Figure adapted from [Litwiller \(2001\)](#).

Additive noise, such as bias and dark currents, is inherent to **CCD** images, and as such needs to be subtracted out first when performing calibrations. Bias currents can be found by taking a bias image or by adding an overscan region to each image. A bias image is an image where the charges on the **CCD** are reset and then immediately read off without exposing anything on the detector, effectively taking an image with zero exposure time. Alternatively, to save time during an observational run, overscan regions may be added to the images. An overscan region refers to adding a few cycles to the readout of each column of the **CCD** such that the base current is read out and appended to each image.

Dark currents can be found by taking an image with nothing exposed onto the detector for a certain exposure time. This resultant dark image can then be scaled to the science images exposure time since the dark current should be linearly proportional to exposure time. When the detector is capable of being held at precise temperatures, dark images may be taken over multiple hours during the day to produce a high quality master dark image that may then be scaled and subtracted from all subsequent images.

Next, multiplicative noise, such as a **CCD**'s pixel-to-pixel response, should be accounted for. This pixel-to-pixel response should be uniform across the image and to achieve this an average response may be divided out. The average response is referred to as a ‘flat’ image or flat-field and may be acquired by observing a uniformly illuminated surface to determine the pixel-to-pixel response.

Dome flats are images taken of a relatively flat surface, usually the inside of a telescopes dome, and are used in both photometry and spectroscopy. The surface is uniformly and indirectly illuminated by a projector lamp, ideal for flat-field images. Alternate flat-fielding methods, such as night sky and twilight flats, are available but are suited solely for photometry.

Night sky flats are produced from science images containing mostly sky. The science images are combined using the ‘mode’ statistic which removes any celestial objects at the cost of a low **Signal-to-Noise Ratio (SNR)** flat-field.

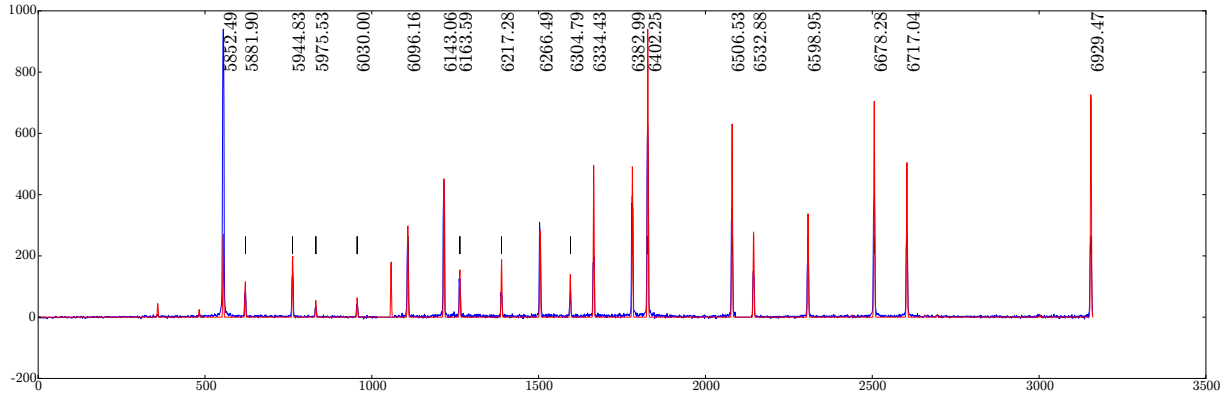


Figure 2.7: Example of an arc spectrum for NeAr taken with SALT’s RSS using the PG1800 grating at a grating angle of 34.625° , an articulation angle of 69.258° , and covering a wavelength range of $\sim 5600 - 6900 \text{ \AA}$. Plot adapted from SALT’s published Longslit Line Atlases, (2023).²

Twilight flats are produced from images of the twilight (or dawn) sky. They are taken when the Sun has just set, in the opposite direction, at $\sim 20^\circ$ from zenith and provide a better SNR at the cost of careful timing of the images.

A flat-field must be normalized before being used to correct any science images since it only acts to account for the pixel-to-pixel response and not for the additive errors. A normalized spectroscopic flat image, $F_\lambda^n(x, y)$, can be calculated as:

$$F_\lambda^n(x, y) = \frac{F_\lambda(x, y) - B(x, y) - (\frac{t_S}{t_D})D(x, y)}{\text{med}_{lp}(F_\lambda(x, y) - B(x, y) - (\frac{t_S}{t_D})D(x, y))}, \quad (2.9)$$

where $F_\lambda(x, y)$ is the non-corrected flat image, $B(x, y)$ is the bias image, $D(x, y)$ is the dark image which is scaled by the exposure time of the science image, t_S , and the dark image, t_D . med_{lp} is a low-pass median filter which smoothes out any rapid changes in the pixel-to-pixel response, removing the illumination contribution.

The calibrated science image, $S_\lambda^*(x, y)$, which accounts for the bias and dark currents as well as the flat fielding can then be calculated as:

$$S_\lambda^*(x, y) = \frac{S_\lambda(x, y) - B(x, y) - (\frac{t_S}{t_D})D(x, y)}{F_\lambda^n(x, y)}. \quad (2.10)$$

When multichannel CCDs are used, which consist of multiple CCDs or a CCD with multiple output amplifiers, additional calibrations, specifically cross-talk corrections and mosaicking, are required. Cross-talk noise refers to contamination that occurs during readout in one channel from another channel with a high signal and occurs because the signals can not be completely isolated from one another. Cross-talk corrections therefore account for this signal contamination between channels being read out at the same time (Freyhammer et al., 2001). Mosaicking is necessary for multichannel CCDs since the digitized signal read out from the detector has no reference of the physical location of the pixel it was detected at. Mosaicking, therefore, correctly orients the data acquired from a multichannel detector so that a single correctly oriented image is produced.

²NeAr plot sourced from <https://astronomers.salt.ac.za/data/salt-longslit-line-atlas/>

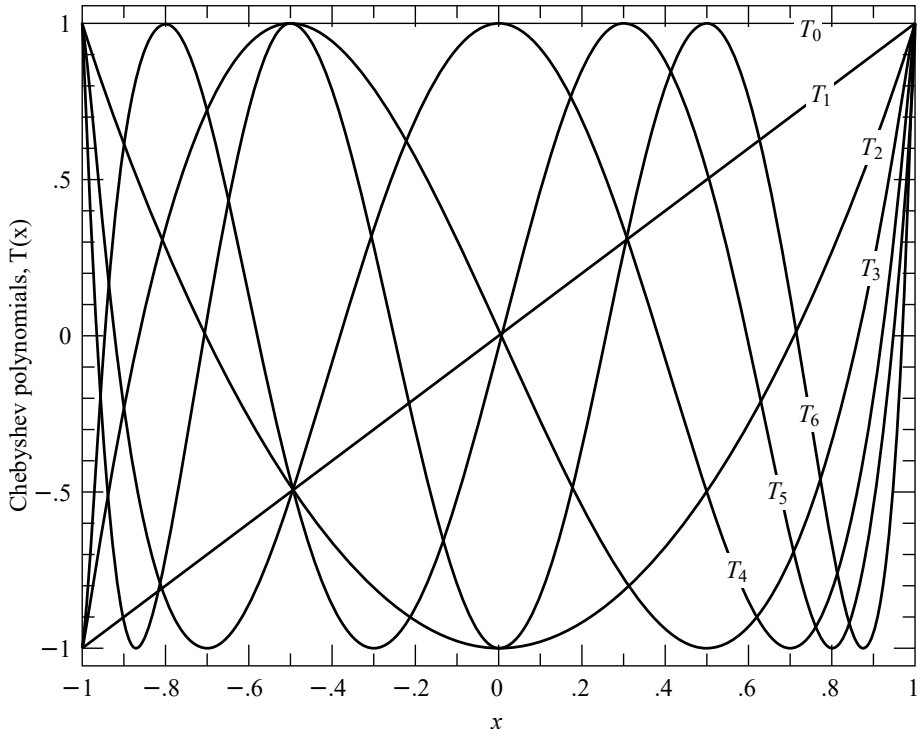


Figure 2.8: The first seven Chebyshev polynomials (T_0 through T_6) as defined by Equation 2.12 over the region $[-1, 1]$ for which they are orthogonal. Plot adapted from (Press et al., 2007).³

Wavelength Calibration

Finally, since the dispersion element breaks the incident light into its constituent wavelengths non-linearly (§ 2.1.7), the relation between the pixel on a detector and the wavelength of the light incident on it is unknown. Ideally, the spectrometer’s optics would be modeled to produce a reliable pixel to wavelength calibration (see e.g., Liu and Hennelly, 2022), but this becomes increasingly more difficult for spectrometers with complex, non-sedentary, optical paths.

Alternatively, a source with well-defined spectral features, with said features evenly populating the wavelength region of interest, such as in Figure 2.7 may be observed. The observed frame is commonly referred to as an ‘arc’ frame, after the arc-lamps used to acquire the spectra, and should be observed alongside the science frames over the course of an observation run.

It is important that the arc frame is observed at the same observing conditions and parameters as the science frames since the optical path will vary over the course of an observing run and for different observing parameters, invalidating previously acquired arc frames. The wavelength calibrations then consist of defining a two-dimensional pixel-to-wavelength conversion function from the arc frame which may later be applied to calibrate the science frames. The two most common approximations for wavelength calibrations are the Chebyshev and Legendre polynomial approximations.

³Excellent resources on Chebyshev and Legendre polynomials are available digitally at www.numerical.recipes/book.

Chebyshev Polynomials The Chebyshev polynomials are defined explicitly as:

$$T_n(x) = \cos(n \cos^{-1}(x)), \quad (2.11)$$

or recursively as:

$$\begin{aligned} T_0(x) &= 1, \\ T_1(x) &= x, \text{ and} \\ T_{n+1}(x) &= 2xT_n(x) - T_{n-1}(x), \text{ for } n \geq 1, \end{aligned} \quad (2.12)$$

where T is a Chebyshev polynomial of order n .⁴ An important property of Chebyshev polynomials is that they are orthogonal polynomials. This means that the inner product of any two differing Chebyshev polynomials, $T_i(x)$ and $T_j(x)$, over the range $[-1, 1]$ is zero, as shown by:

$$\int_{-1}^1 T_i(x) T_j(x) \frac{1}{\sqrt{1-x^2}} dx = \begin{cases} 0, & i \neq j \\ \pi/2, & i = j \neq 0 \\ \pi, & i = j = 0 \end{cases}, \quad (2.13)$$

where $1/\sqrt{1-x^2}$ is the weighting factor for Chebyshev polynomials. This property is important because it means that the coefficients in the Chebyshev polynomial expansion are independent of one another, allowing for a unique solution when approximating an unknown function (Arfken and Weber, 1999; Press et al., 2007). A Chebyshev approximation of an unknown wavelength calibration function is given by:

$$f(x) \approx \sum_{i=0}^N c_i T_i(u), \text{ or} \quad (2.14)$$

$$F(x, y) \approx \sum_{i=0}^N \sum_{j=0}^M c_{ij} T_i(u) T_j(v), \quad (2.15)$$

for a one- or a two-dimensional wavelength surface function, respectively. Here N and M are the desired x and y orders, and c_i and c_{ij} are the Chebyshev polynomial coefficients (Florinsky and Pankratov, 2015; Leng, 1997). Since the orthogonality property of the Chebyshev polynomials only holds true over the range $[-1, 1]$, the $(x, y) \in ([0, a], [0, b])$ pixel coordinates must be remapped to $u, v \in [-1, 1]$ following the relation:

$$(u, v) = \frac{2(x, y) - a - b}{b - a}. \quad (2.16)$$

The Chebyshev polynomials are more suited for wavelength calibrations than standard polynomials since they are orthogonal and have minima and maxima located at $[-1, 1]$, as seen in Figure 2.8. This means that the Chebyshev approximation is exact when $x = x_n$, where x_n are the positions of the $n - 1$ x -intercepts of $T_N(x)$. These properties greatly minimize the error in the Chebyshev approximation, even at lower orders (Arfken and Weber, 1999).

⁴Chebyshev polynomials are denoted T as a hold-over from the alternate spelling of ‘Tchebycheff’.

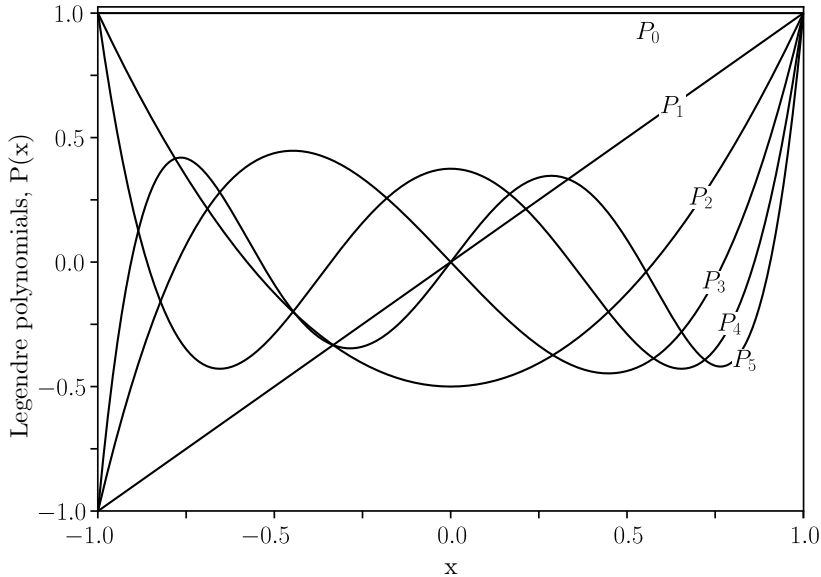


Figure 2.9: The first six Legendre polynomials (P_0 through P_5) as defined by Equation 2.20 over the region $[-1, 1]$ for which they are orthogonal. Plot adapted from Geek3, CC BY-SA 3.0, via Wikimedia Commons (2023).

Legendre Polynomials Similar to the Chebyshev polynomials, the Legendre polynomials may be defined explicitly as:

$$P_n(x) = \frac{1}{2^n n!} \frac{d^n}{dx^n} (x^2 - 1)^n, \quad (2.17)$$

or recursively as:

$$\begin{aligned} P_0(x) &= 1, \\ P_1(x) &= x, \text{ and} \\ (n+1)P_{n+1}(x) &= (2n+1)xP_n(x) - nP_{n-1}(x), \text{ for } n \geq 1, \end{aligned} \quad (2.18)$$

where P is a Legendre polynomial of order n . Legendre polynomials also hold the property of orthogonality. This means that the inner product of any two differing Legendre polynomials, $P_i(x)$ and $P_j(x)$, over the range $[-1, 1]$ is zero, as shown by:

$$\int_{-1}^1 P_i(x) P_j(x) dx = \begin{cases} 0, & i \neq j \\ \frac{2}{2n+1}, & i = j \end{cases}, \quad (2.19)$$

where a weight of 1 is the weighting factor for Legendre polynomials (Dahlquist and Björck, 2003; Press et al., 2007). A Legendre approximation of an unknown wavelength calibration function is given by:

$$f(x) \approx \sum_{n=0}^N a_n P_n(u), \text{ or} \quad (2.20)$$

$$F(x, y) \approx \sum_{i=0}^N \sum_{j=0}^M a_{ij} P_i(u) P_j(v), \quad (2.21)$$

for a one-dimensional wavelength function or a two-dimensional surface function, respectively. Here N and M are the desired x and y orders, u and v are the same mapping variable as in Equation 2.16, and a_{ij} are the Legendre polynomial coefficients.

Legendre polynomials benefit from having the orthogonality condition with no weight necessary ($w = 1$) which makes their coefficients computationally easier to compute but increases the error in a Legendre approximation when compared to that of the error in a Chebyshev approximation for functions of the same order, N (Ismail, 2005).

Regardless of which method of polynomial approximation is chosen, the polynomials are fit by varying the relevant coefficients using the least squares method. The resultant minimized function may then be used to convert the science frames from an (x -pixel, y -pixel) coordinate system to a (λ , y -pixel) coordinate system.

2.2 Polarimetry

Both Huygens and Newton came to the conclusion that light demonstrates transversal properties (Huygens, 1690; Newton and Innys, 1730), which was later further investigated and coined as ‘polarization’ by Malus (Malus, 1809). Malus also investigated the polarization effects of multiple materials including some of which were birefringent, such as optical calcite, which he referred to as Iceland spar after Bartholinus’ investigations of the material (Bartholinus, 1670).

Fresnel built on Malus’ work showing that two beams of light, polarized at a right angle to one another, do not interfere, conclusively proving that light is transversal in nature, opposing the widely accepted longitudinal nature of light due to the prevalent belief in the ether. He later went on to correctly describe how polarized light is reflected and refracted at the surface of optical dielectric interfaces, without knowledge of the electromagnetic nature of light. Fresnel’s equations for the reflectance and transmittance, R and T , are defined as:

$$\begin{aligned} R_s &= \left| \frac{Z_2 \cos \theta_i - Z_1 \cos \theta_t}{Z_2 \cos \theta_i + Z_1 \cos \theta_t} \right|^2, \\ R_p &= \left| \frac{Z_2 \cos \theta_t - Z_1 \cos \theta_i}{Z_2 \cos \theta_t + Z_1 \cos \theta_i} \right|^2, \\ T_s &= 1 - R_s, \text{ and} \\ T_p &= 1 - R_p, \end{aligned} \tag{2.22}$$

where s and p are the two polarized components of light perpendicular to one another, Z_1 and Z_2 are the impedance of the two media, and θ_i , θ_t , and θ_r are the angles of incidence, transmission, and reflection, respectively (Fresnel, 1870).

Nicol was the first to create a polarizer, aptly named the Nicol prism, where the incident light is split into its two perpendicular polarization components, namely the ordinary and extraordinary beams. Faraday discovered the phenomenon where the polarization plane of light is rotated when under the influence of a magnetic field, known as the Faraday effect. Brewster calculated the angle of incidence, $\theta_B = \arctan n_2/n_1$, at which incident polarized light is perfectly transmitted through a transparent surface, with refractive indexes of n_1 and n_2 , while non-polarized incident light is perfectly polarized when reflected and partially polarized when refracted.

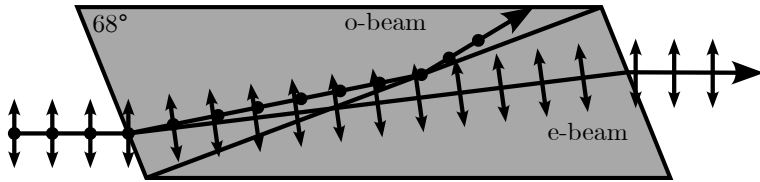


Figure 2.10: Diagram of a Nicol prism for incident non-polarized light. Diagram adapted from Fred the Oyster, CC BY-SA 4.0, via Wikimedia Commons (2023).

Stokes' work created the first consistent description of polarization and gave us the Stokes parameters which describe an operational approach to measuring polarization (discussed further in § 2.2.1) (Stokes, 1852). Hale was the first to apply polarization to astronomical observations, using a Fresnel rhomb and Nicol prism as a quarter-wave plate and polarizer, respectively (Hale, 1908, 1979). Wollaston also created a prism, similarly named the Wollaston prism, which allowed simultaneous observation of the ordinary and extraordinary beams due to the smaller deviation angle (Wollaston, 1802). Finally, Chandrasekhar's work furthered our understanding of astrophysical polarimetry by explaining the origin of polarization observed in starlight as well as mathematically modeling the polarization of rotating stars, which came to be named Chandrasekhar polarization (Chandrasekhar, 1950).

2.2.1 Polarization

Maxwell's equations for an electromagnetic field propagating through a vacuum are given as:

$$\begin{aligned} \nabla \cdot \mathbf{E} &= 0, \\ \nabla \cdot \mathbf{B} &= 0, \\ \nabla \times \mathbf{E} &= -\frac{1}{c} \frac{\partial \mathbf{B}}{\partial t}, \text{ and} \\ \nabla \times \mathbf{B} &= \frac{1}{c} \frac{\partial \mathbf{E}}{\partial t}, \end{aligned} \quad (2.23)$$

where \mathbf{E} and \mathbf{B} are the electric and magnetic field vectors, and c is the speed of light. In a right-handed (x, y, z) coordinate system, a non-trivial solution of an electromagnetic wave following Maxwell's Equations propagating along the z -axis, towards a hypothetical observer, is described by:

$$\begin{aligned} \mathbf{E} &= E_x \cos(kz - \omega t + \Phi_x) \hat{x} + E_y \cos(kz - \omega t + \Phi_y) \hat{y}, \text{ and} \\ \mathbf{B} &= \frac{1}{c} E_y \cos(kz - \omega t + \Phi_y) \hat{x} + \frac{1}{c} E_x \cos(kz - \omega t + \Phi_x) \hat{y}, \end{aligned} \quad (2.24)$$

where E_x , E_y , Φ_x , and Φ_y are all parameters describing the amplitude and phase of the electric field vector in the (x, y) plane, and with the magnetic field vector proportional and perpendicular to the electric field vector (Griffiths, 2005).

Considering only the electric field component and rewriting Equation 2.24 using complex values allows us to simplify the form of the solution to:

$$\mathbf{E} = \Re(\mathbf{E}_0 e^{-i\omega t}), \quad (2.25)$$

where we only consider the real part of the equation, and where \mathbf{E}_0 is defined as:

$$\mathbf{E}_0 = E_x e^{i\Phi_x} \hat{x} + E_y e^{i\Phi_y} \hat{y}, \quad (2.26)$$

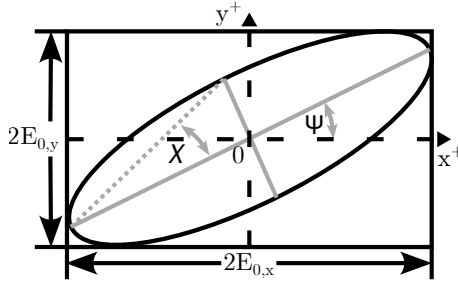


Figure 2.11: The polarization ellipse for an electric field vector propagating through free space. Diagram adapted from Inductiveload, PDM 1.0, via Wikimedia Commons (2023).

and is referred to as the polarization vector since it neatly contains the parameters responsible for the polarization properties (Degl'Innocenti, 2014).

For an electric field vector with oscillations in some combination of the x and y axes, the tip of the vector sweeps out an ellipse, as depicted in Figure 2.11. This ellipse is referred to as the polarization ellipse and has the form:

$$\left(\frac{\mathbf{E}_x}{\mathbf{E}_{0,x}}\right)^2 + \left(\frac{\mathbf{E}_y}{\mathbf{E}_{0,y}}\right)^2 - \frac{2\mathbf{E}_x\mathbf{E}_y}{\mathbf{E}_{0,x}\mathbf{E}_{0,y}} \cos \Phi = \sin^2 \Phi, \quad (2.27)$$

where $\Phi = \Phi_x - \Phi_y$ is the phase difference between the x and y phase parameters. The degree of polarization for the polarization ellipse is related to the eccentricity of the ellipse and the angle at which it is rotated relates to the polarization angle. Since $\mathbf{E}_{0,x}$, $\mathbf{E}_{0,y}$, Φ_x , and Φ_y describe the wave, the polarization ellipse that results from these parameters is fixed as the wave continues to propagate.

Since observations consist of images taken over a desired exposure time, time averaging of Equation 2.27 over the exposure time is necessary. Given the periodical nature and high frequencies of the fields, the time averaging may be found over a single oscillation using:

$$\langle \mathbf{E}_i \mathbf{E}_j \rangle = \lim_{dt \rightarrow \infty} \frac{1}{T} \int_0^T \mathbf{E}_i \mathbf{E}_j dt, \quad \text{for } i, j \in (x, y), \quad (2.28)$$

where T is the total averaging time over the electric field vectors \mathbf{E}_i and \mathbf{E}_j (Collett, 2005). Applying the time averaging to Equation 2.27 and simplifying results in:

$$(E_{0x}^2 + E_{0y}^2)^2 - (E_{0x}^2 - E_{0y}^2)^2 - (2E_x E_y \cos \Phi)^2 = (2E_x E_y \sin \Phi)^2. \quad (2.29)$$

The expressions inside the parentheses can be found through observation and may also be represented as:

$$\mathbf{S} = \begin{pmatrix} S_0 \\ S_1 \\ S_2 \\ S_3 \end{pmatrix} = \begin{pmatrix} I \\ Q \\ U \\ V \end{pmatrix} = \begin{pmatrix} E_{0x}^2 + E_{0y}^2 \\ E_{0x}^2 - E_{0y}^2 \\ 2E_{0x}E_{0y} \cos \Phi \\ 2E_{0x}E_{0y} \sin \Phi \end{pmatrix}, \quad (2.30)$$

where S_0 to S_3 are referred to as the Stokes (polarization) parameters. The parameters describe the: S_0 , total intensity (often normalized to 1); S_1 , ratio of the Linear Horizontally Polarized (LHP) to Linear Vertically Polarized (LVP) light; S_2 , ratio of the Linear $+45^\circ$ Polarized ($L+45^\circ$) to Linear -45° Polarized ($L-45^\circ$) light; and S_3 , ratio of the Right Circularly Polarized (RCP) (clockwise) to Left Circularly Polarized (LCP)

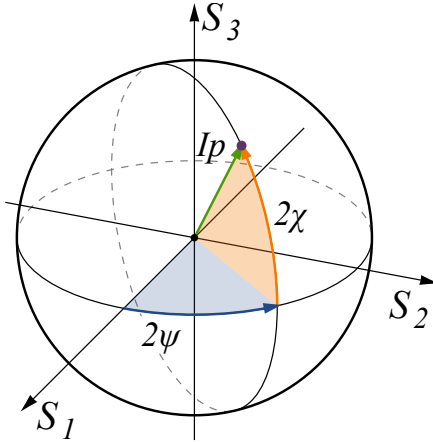


Figure 2.12: The Poincaré sphere describing the polarization properties of a wave-packet propagating through free space. Diagram adapted from Inductiveload, PDM 1.0, via [Wikimedia Commons](#) (2023).

(counter-clockwise) light. When the intensity is normalized, the Stokes parameters range from 1 to -1 , based on the dominating component of the parameter ([Chandrasekhar, 1950](#); [Stokes, 1852](#)).

From [Equation 2.29](#) and [2.30](#), the polarization parameters are related by:

$$I^2 = Q^2 + U^2 + V^2, \quad (2.31)$$

for entirely polarized light. Only beams of completely polarized light could be accounted for before Stokes' work on polarization. Using the [Stokes parameters](#), we can now account for partially polarized light such that:

$$I^2 \geq Q^2 + U^2 + V^2, \quad (2.32)$$

where I , Q , U , and V are the normalized polarization parameters, often symbolized as

$$\bar{Q} = \frac{Q}{I}, \quad \bar{U} = \frac{U}{I}, \quad \text{and} \quad \bar{V} = \frac{V}{I}. \quad (2.33)$$

Similar to the polarization ellipse, the Stokes parameters may be depicted using the Poincaré sphere in spherical coordinates $(IP, 2\Psi, 2\chi)$, such that:

$$\begin{aligned} I &= S_0, \\ P &= \frac{\sqrt{S_1^2 + S_2^2 + S_3^2}}{S_0}, \text{ for } 0 \leq P \leq 1, \\ 2\Psi &= \arctan \frac{S_3}{\sqrt{S_1^2 + S_2^2}}, \text{ and} \\ 2\chi &= \arctan \frac{S_2}{S_1}, \end{aligned} \quad (2.34)$$

where I denotes the total intensity, P denotes the degree of polarization, or the ratio of polarized to non-polarized light in the wave-packet, χ denotes the polarization angle, and Ψ denotes the ellipticity angle of the polarization ellipse.

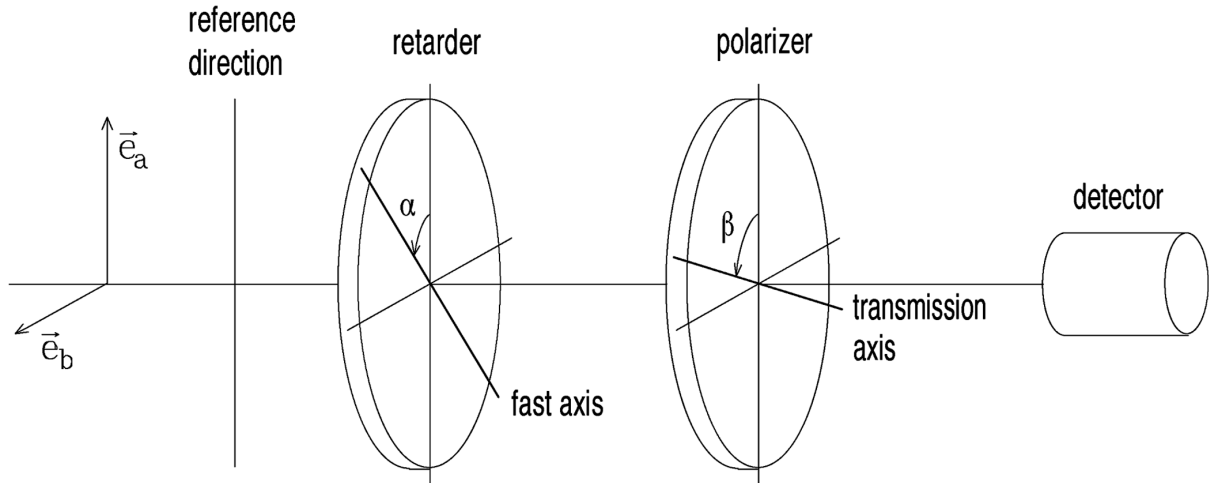


Figure 2.13: A diagram of an ideal polarimeter. Diagram adapted from [Degl'Innocenti and Landolfi \(2004\)](#).

2.2.2 Polarization Measurement

Except for polarimetry in the radio-wavelength regime, the polarization of a beam can not be directly measured. The polarization properties may, however, be recovered from the beam through the manipulation of the four parameters given in [Equation 2.24](#). This so-called manipulation is achieved by passing the beam through optical elements which vary the beam for differing amplitudes and phases. These matrix operations may be represented by their corresponding Mueller matrices.

For ideal components, the resultant beam \mathbf{S}' after passing through an optical element is given by $\mathbf{S}' = \mathbf{MS}$, where \mathbf{S} is the beam incident on the optical element and \mathbf{M} represents the 4×4 Mueller matrix representing the optical element. Mueller matrices are especially useful when dealing with paths through optical elements as they observe the ‘train’ property ([Priebe, 1969](#)). This means that an incoming beam \mathbf{S} passing, in order, through elements with known Mueller matrices $(\mathbf{M}_0, \dots, \mathbf{M}_N)$ results in an outgoing beam \mathbf{S}' such that:

$$\mathbf{S}' = \mathbf{M}_N \dots \mathbf{M}_0 \mathbf{S}. \quad (2.35)$$

Some Mueller Matrices are given below with angles related to those in Figure 2.13, measured counter-clockwise in a right-handed coordinate system.

General Rotation The Mueller matrix for coordinate space rotations about the origin by an angle θ ,

$$\mathbf{R}(\theta) = \begin{bmatrix} 1 & 0 & 0 & 0 \\ 0 & \cos 2\theta & \sin 2\theta & 0 \\ 0 & -\sin 2\theta & \cos 2\theta & 0 \\ 0 & 0 & 0 & 1 \end{bmatrix}. \quad (2.36)$$

General Linear Retardance The Mueller matrix for retardance where α is the angle between the incoming vector and fast axis, and δ is the retardance introduced by the retarder,

$$\mathbf{W}(\alpha, \delta) = \begin{bmatrix} 1 & 0 & 0 & 0 \\ 0 & \cos^2 2\alpha + \sin^2 2\alpha \cos \delta & \cos 2\alpha \sin 2\alpha(1 - \cos \delta) & \sin 2\alpha \sin \delta \\ 0 & \cos 2\alpha \sin 2\alpha(1 - \cos \delta) & \cos^2 2\alpha \cos \delta + \sin^2 2\alpha & -\cos 2\alpha \sin \delta \\ 0 & -\sin 2\alpha \sin \delta & \cos 2\alpha \sin \delta & \cos \delta \end{bmatrix}. \quad (2.37)$$

The retarder is often referred to by this retardance, e.g., if the retardance is $\delta = \pi$ or $\pi/2$, the retarder is referred to as a half- or quarter-wave plate, respectively.

General Linear Polarization The Mueller matrix for linear polarization where β is the angle between the incoming vector and transmission axis,

$$\mathbf{P}(\beta) = \frac{1}{2} \begin{bmatrix} 1 & \cos 2\beta & \sin 2\beta & 0 \\ \cos 2\beta & \cos^2 2\beta & \cos 2\beta \sin 2\beta & 0 \\ \sin 2\beta & \sin 2\beta \cos 2\beta & \sin^2 2\beta & 0 \\ 0 & 0 & 0 & 0 \end{bmatrix}. \quad (2.38)$$

These matrices in combination with Equation 2.35 allow us to describe how the incoming Stokes parameters would change when passing through the various optical elements. For a setup similar to Figure 2.13, the detected Stokes parameters can be described by:

$$\begin{aligned} S'(\alpha, \beta, \gamma) \propto \frac{1}{2} \{ & I + [Q \cos 2\alpha + U \sin 2\alpha] \cos(2\beta - 2\alpha) \\ & - [Q \sin 2\alpha + U \cos 2\alpha] \sin(2\beta - 2\alpha) \cos \gamma \\ & + V \sin(2\beta - 2\alpha) \sin \gamma \}, \end{aligned} \quad (2.39)$$

where the retardance angle, α , polarization angle, β , for a wave plate with a relative phase difference, γ , may be varied to acquire a system of equations that can be solved to retrieve the Stokes polarization parameters (Bagnulo et al., 2009).

Several or more frames taken under differing configurations may be used to reduce a system of equations to extract all four Stokes polarization parameters, but it is possible to extract the I , Q and U polarization parameters using only four frames, or two dual-beam frames, for well-chosen configurations and assuming ideal components. This ideal configuration varies the retarder angle such that $\Delta\alpha = \pi/8$ while keeping the polarizer stationary. More frames for additional retarder angles are advisable and often necessary, however, as they correct for any differences in sensitivity, such as may arise in a polarized flat field and which is further discussed in § 2.2.3 (Patat and Romaniello, 2006). From Equation 2.39 we see that the linear retarder element is the driving element of a polarizer as the first three Stokes parameters (S_{0-2} , or I , Q , and U) may be found by changing only the angle of retardance, α .

Wave Plates Wave plates, also commonly referred to as retarders, are generally made from optically transparent birefringent crystals. A wave plate has a fast and slow axis, which are perpendicular to one another and both perpendicular to an incident beam. Due to the birefringence of the wave plate medium, the phase velocity of the beam polarized

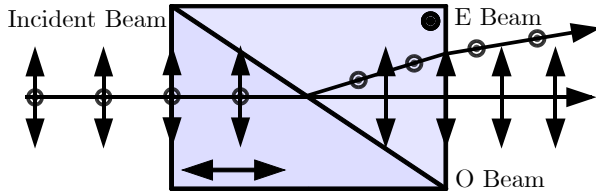


Figure 2.14: Diagram of a Rochon prism. Included in the diagram are the optical axes of the differing sections of the birefringent material as well as polarizing directions of the incident beam, denoted using the \leftrightarrow and \odot symbols, for the O - and E -beams, respectively. Figure adapted from ChrisHodgesUK, CC BY-SA 3.0, via Wikimedia Commons (2023).

parallel to the fast axis, namely the extraordinary beam, slightly increases while that of the beam polarized parallel to the slow axis, namely the ordinary beam, remains unaffected. This difference in the perpendicular component's phase velocities introduces a relative phase difference between the two beams, γ , which is given by:

$$\gamma = \frac{2\pi\Delta n L}{\lambda_0} \quad (2.40)$$

where Δn and L refer to the birefringence and thickness of the wave plate medium, respectively, and λ_0 refers to the vacuum wavelength of the beam (Hecht, 2017).

This relative phase difference determines the name of the wave plate, such that the $\gamma = m(\pi/2)$ and $\gamma = m(\pi/4)$ phase differences, for $m \in \mathbb{Z}^+$, refer to the half- and quarter-wave plates (which are the most common wave plate phases), respectively. Phase differences with an integer multiple of one another relate to the same phase difference and are referred to as multiple-order wave plates, while wave plates with a phase difference less than an integer multiple are referred to as zero-order wave plates. Several multiple-order wave plates can be combined by alternatively aligning the fast axis of one to the slow axis of another to create a compound zero-order wave plate (Hale and Day, 1988).

Polarizers Polarizers are typically made from two prisms, of a birefringent material, cemented together with an optically transparent adhesive. The actual effect of separating the perpendicular polarization components is achieved using varying effects, namely through:

- absorption of one of the polarized components, such as in Polaroid polarizing filters,
- total internal reflection of a single polarized component, such as in a Nicol prism (Figure 2.10),
- Refraction of a single polarized component, such as in a Rochon prism (Figure 2.14), or
- Refraction of both polarization components in differing directions, such as in a Wollaston prism (Figure 2.15).

Wollaston Prisms The Wollaston prism consists of two right-angle prisms consisting of a birefringent monoaxial material, cemented together with an optically transparent adhesive along their hypotenuses with their optical axes orthogonal, as seen in Figure 2.15. The Wollaston prism is a common optical polarizing element in astrophysical polarimetry which separates an incident beam into two linearly polarized O - and E -beams, orthogonal to one another, and deviated from their common axis equally. The deviation angle of the

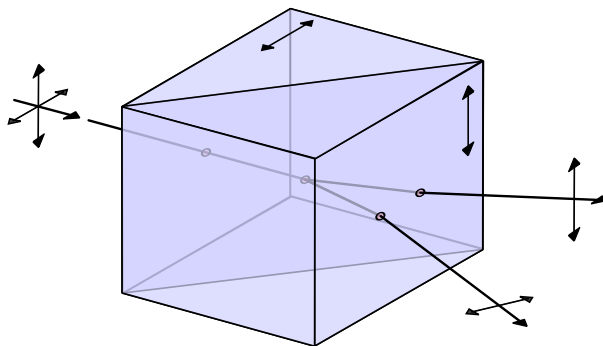


Figure 2.15: Diagram of a Wollaston prism. Included in the diagram are the optical axes of the differing sections of the birefringent material as well as polarizing directions of the incident beam, denoted using the \leftrightarrow and \updownarrow symbols, for the *O*- and *E*-beams, respectively. Diagram adapted from fgalore, CC BY-SA 3.0, via Wikimedia Commons (2023).

polarized beams is determined by the wedge angle which is defined as the angle from the common hypotenuse to that of the outer transmission face of either prism.

Wollaston prisms benefit over simpler elements (such as those listed in the [polarizer](#) paragraph) since a single frame allows for the observation of both orthogonal polarization components. This halves the observational time required to collect enough data to calculate the Stokes parameters, at the cost of an increase in calibration and reduction difficulty ([Simon, 1986](#)).

2.2.3 Polarimetric Calibrations

The raw science images acquired during polarimetric observations contain a combination of useful science data as well as noise. Corrections and calibrations related to the detector remain unchanged from those described in § 2.1.8, while those related to correcting for the optical elements relate to corrections for spurious polarization effects.

Flat Fielding

Once the [CCD](#) calibrations have been completed, the polarization intrinsic to the optical elements needs to be accounted for such that the pixel-to-pixel response is made uniform. Flat-fielding is, once again, used to correct for this. The flats taken for polarimetry, however, introduce an additional challenge as the targets for conventional flats are polarized, such as twilight and dome flats which are polarized by light scattering in the atmosphere and the reflective surface of the dome, respectively.

If no unpolarized flat images can be taken for flat field calibrations then, when possible due to the polarimeter design, the wave plate may be constantly rotated to act as a depolarizing element; this is effective so long as the wave plate rotation period is much faster than the flat's exposure time. Alternatively, polarized flats may be taken at the same set of half-wave plate angles used for science observations and averaged together to achieve a similar depolarizing effect.

Observing additional ‘redundant’ exposures for the science and flat images increases the depolarizing effect up to the maximum of 16 half-wave plate positions, where exposures with a half-wave plate angle differing by $\pi/4$ from another are considered redundant due to the *O*- and *E*-beams swapping between the related exposures.

Increasing the amount of redundant observations proportionally increases the time needed to observe all the exposures, which in turn introduces time-dependent effects such as fringing or intensity variations of the flat source. As such, a middle ground must be found for the amount of redundant frames observed ([Patat and Romanielo, 2006](#); [Peinado et al., 2010](#)).

Dual-Beam Extraction and Alignment

After calibrations for the [CCD](#) and light path are accounted for, the *O*- and *E*-beams can be extracted and further reduced. The extraction depends heavily on the layout of the polarimeter but often a simple cropping of the differing sections is enough to separate the two images.

After extracting the *O*- and *E*-beams for a specific half-wave plate angle, the images need to be aligned such that the sources present in them overlap. The Wollaston prism needs to be corrected for as it introduces a beam deviation which differs across both images. The aligning of the *O*- and *E*-beams is crucial as the comparison of the dual images is what allows for the calculation of the polarization properties.

Sky Subtraction

The polarization introduced by the sky introduces a difference in the intensity of the background sky and needs to be removed as it will influence the polarization results of the target source. Thankfully, the background polarization is an additive type of noise and may be subtracted out across the frames. This subtraction is done independently for both beams in a frame and for each frame since the background intensity of all observed polarimetric beams will differ based on the observational parameters.

2.3 Spectropolarimetry

As the name suggests, spectropolarimetry is the measurement of the polarization of light for a chosen spectral range and provides polarimetric results as a function of wavelength. As spectropolarimetry is so closely reliant on both spectroscopy and polarimetry, advancements in spectropolarimeters have always been gated by the advancements of spectrometers and polarimeters (as described in [§ 2.1](#) and [§ 2.2](#)).

The most notable historical contributions of spectropolarimetry are those of spectropolarimetric studies instead of instrumental developments. Spectropolarimetry provides further insights into a materials physical structure, chemical composition, and magnetic field, allowing spectropolarimetry to be useful across multiple disciplines. In astronomy in particular, spectropolarimetry has been used to study the magnetic field, chemical composition, and underlying structure and emission processes of multiple types of celestial objects (see for example [Antonucci and Miller, 1985](#); [Donati et al., 1997](#); [Wang and Wheeler, 2008](#)).

Along with common points of consideration when developing any instrumentation for observational astronomy, such as resolution and sensitivity, spectropolarimeters need also consider the spectral response of the polarimetric components as well as the polarization

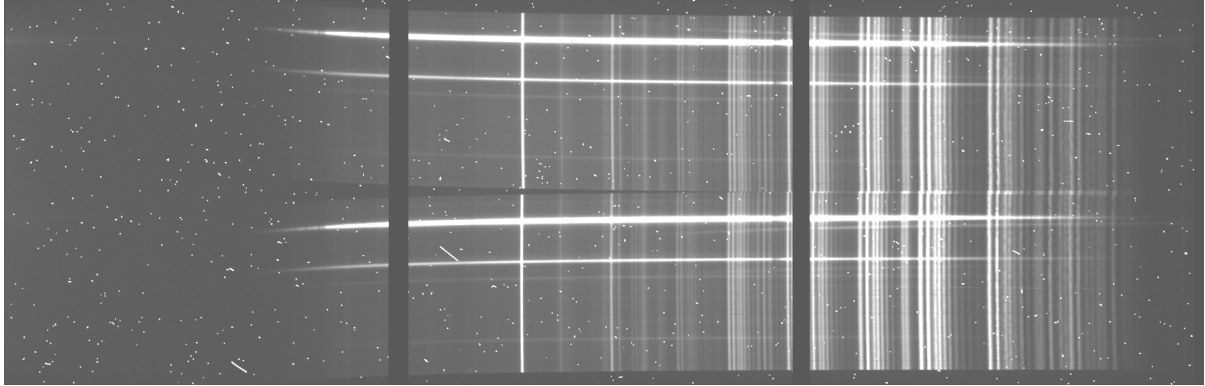


Figure 2.16: A spectropolarimetric target exposure as observed by the SALT RSS in spectropolarimetry mode.

response of the spectroscopic components as both are simultaneously in the light-path during observations and have noticeable affects on one another. Time is another constraint for spectropolarimetry as the incident light is separated both by wavelength and by polarization states. This division of the incident light results in increased exposure times for both target observations and observations necessary for calibrations.

Figure 2.16 illustrates a typical science image taken with a spectropolarimeter. The image contains the O - and E -beams which are both dispersed into their spectra. Spectropolarimetric results are acquired from measurements and calibrations of these images alongside any necessary calibration images.

2.3.1 Spectropolarimetric Measurement

The derived relations given in § 2.2.1, such as the Stokes parameters, describe polarization in general and are valid for both polarimetry and spectropolarimetry. Due to the time averaging of the observed light (Equation 2.28), any minor temporal variation, partial polarization, or monochromatic nature of the spectropolarimetric polarization parameters are accounted for.

For linear spectropolarimetry using a dual-beam polarizing element, an exposure measures the O - and E -beam wavelength dependent intensities, $f_{O,i}(\lambda)$ and $f_{E,i}(\lambda)$, for a given wave plate angle θ_i at angle i . These intensities thus relate to the wavelength dependent Stokes parameters as:

$$\begin{aligned} f_{O,i}(\lambda) &= \frac{1}{2}[I(\lambda) + Q(\lambda) \cos(4\theta_i) + U(\lambda) \sin(4\theta_i)], \text{ and} \\ f_{E,i}(\lambda) &= \frac{1}{2}[I(\lambda) - Q(\lambda) \cos(4\theta_i) - U(\lambda) \sin(4\theta_i)]. \end{aligned} \quad (2.41)$$

At least four linear equations are required to solve for three variables in a system of linear equations and thus at least two exposures must be taken to solve for the linear ($I(\lambda)$, $Q(\lambda)$, and $U(\lambda)$) polarization parameters (Degl’Innocenti et al., 2006; Keller, 2002).

The first Stokes parameter, $I(\lambda)$, may be recovered for each dual-beam exposure using

$$I_i(\lambda) = f_{O,i}(\lambda) + f_{E,i}(\lambda). \quad (2.42)$$

By calculating the $I_i(\lambda)$ Stokes parameter for each wave plate position i , the variation of the target over the course of observation may be corrected for, resulting in the $I(\lambda)$ Stokes parameter.

Next, the $Q(\lambda)$ and $U(\lambda)$ Stokes parameters are found by first defining the normalized difference in relative intensities, $F_i(\lambda)$, as:

$$F_i(\lambda) \equiv \frac{f_{O,i}(\lambda) - f_{E,i}(\lambda)}{f_{O,i}(\lambda) + f_{E,i}(\lambda)}, \quad (2.43)$$

which allows Equation 2.41 to be written, as

$$F_i(\lambda) = \bar{Q}(\lambda) \cos(4\theta_i) + \bar{U}(\lambda) \sin(4\theta_i) = P \cos(4\theta_i - 2\chi), \quad (2.44)$$

in terms of the normalized Stokes parameters, or, alternatively, the degree of polarization, P , and polarization angle, χ (as described in Equation 2.33 and 2.34).

The optimal change in wave plate angle is $\Delta\theta_i = \pi/8$ as it allows the normalized Stokes polarization parameters to be calculated as:

$$\begin{aligned} \bar{Q}(\lambda) &= \frac{2}{N} \sum_{i=0}^{N-1} F_i(\lambda) \cos\left(\frac{\pi}{2}i\right), \text{ and} \\ \bar{U}(\lambda) &= \frac{2}{N} \sum_{i=0}^{N-1} F_i(\lambda) \sin\left(\frac{\pi}{2}i\right), \end{aligned} \quad (2.45)$$

where N is the number of exposures taken, limited such that $N \in [2, 16]$ (Patat and Romaniello, 2006).

2.3.2 Spectropolarimetric Calibrations

Just as the elements of a spectropolarimeter are an amalgamation of both a spectrometer and polarimeter, it naturally follows that the calibrations necessary to reduce spectropolarimetric data are a combination of the calibrations needed for spectroscopy and polarimetry, discussed further in § 2.1.8 and § 2.2.3. Even though the spectrometer and polarimeter components both have an effect on an incident beam following the light-path through the spectropolarimeter, the calibration procedures for both methods remain mostly independent of one another and as such need not be repeated here.

Spectropolarimetric calibrations are, however, more involved when compared to the same calibrations for either spectroscopy or polarimetry. Minor deviations in the calibrations across both the spectra and the polarized beam compound, especially when dealing with the wavelength calibration, resulting in poor SNRs. Generally, more exposures over longer timespans are required to acquire enough redundancy and signal for the calculation of the Stokes parameters on top of the time necessary for calibrations to be completed. It should therefore be noted just how important the calibrations are when dealing with spectropolarimetry.

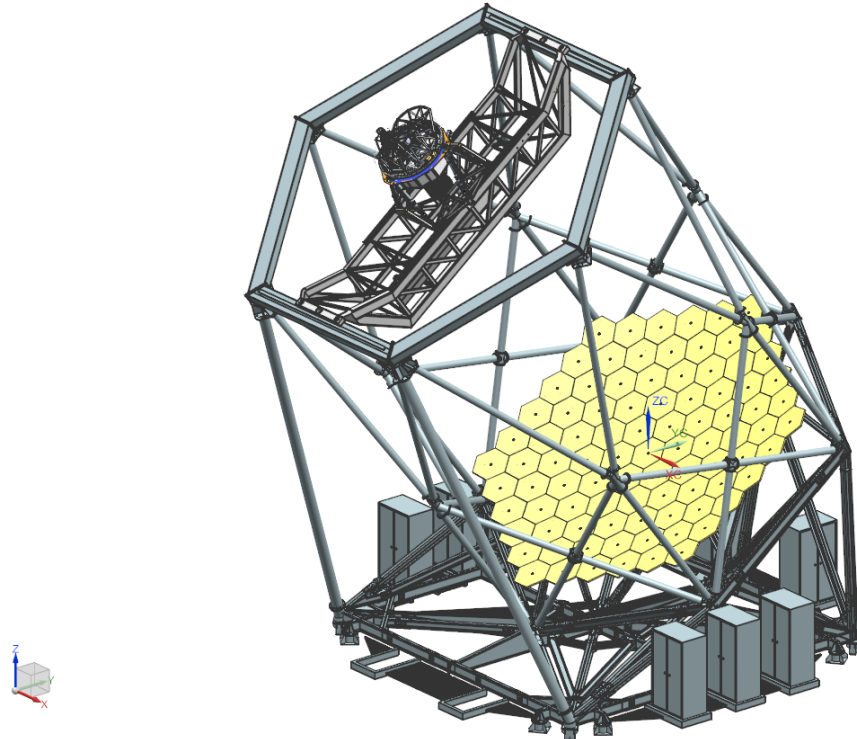


Figure 2.17: The tracker, supporting structure, and primary mirror of SALT. Figure adapted from the SALT call for proposals (SALT Ast. Ops., 2024).

2.4 The Southern African Large Telescope

Southern African Large Telescope (SALT) is a 10 m class optical/near-infrared telescope situated at the South African Astronomical Observatory (SAAO) field station near Sutherland, South Africa (Burgh et al., 2003). The operational design was based on the Hobby-Eberly Telescope (HET) situated at McDonald Observatory, Texas, which limits the pointing of the telescope’s primary mirror to a fixed elevation (37° from zenith in the case of SALT) while still allowing for full azimuthal rotation (Ramsey et al., 1998). Both SALT and HET utilize a spherical primary mirror which is stationary during observations and a tracker housing most of the instrumentation that tracks the primary mirrors spherically shaped focal path. Figure 2.17 depicts SALTs tracker (top left), supporting structure, and primary mirror (bottom right).

2.4.1 The Primary Mirror

The primary mirror is composed of 91 individual 1 m hexagonal mirrors which together form an 11 m segmented spherical mirror. Each mirror segment can be adjusted by actuators allowing the individual mirrors to approximate a single monolithic spherical mirror. The fixed elevation means that SALTs primary mirror has a fixed gravity vector allowing for a lighter, cost-effective supporting structure when compared to those of a more traditional altitude-azimuthal mount but with the trade-off that the control mechanism and tracking have increased complexity (Buckley et al., 2006).

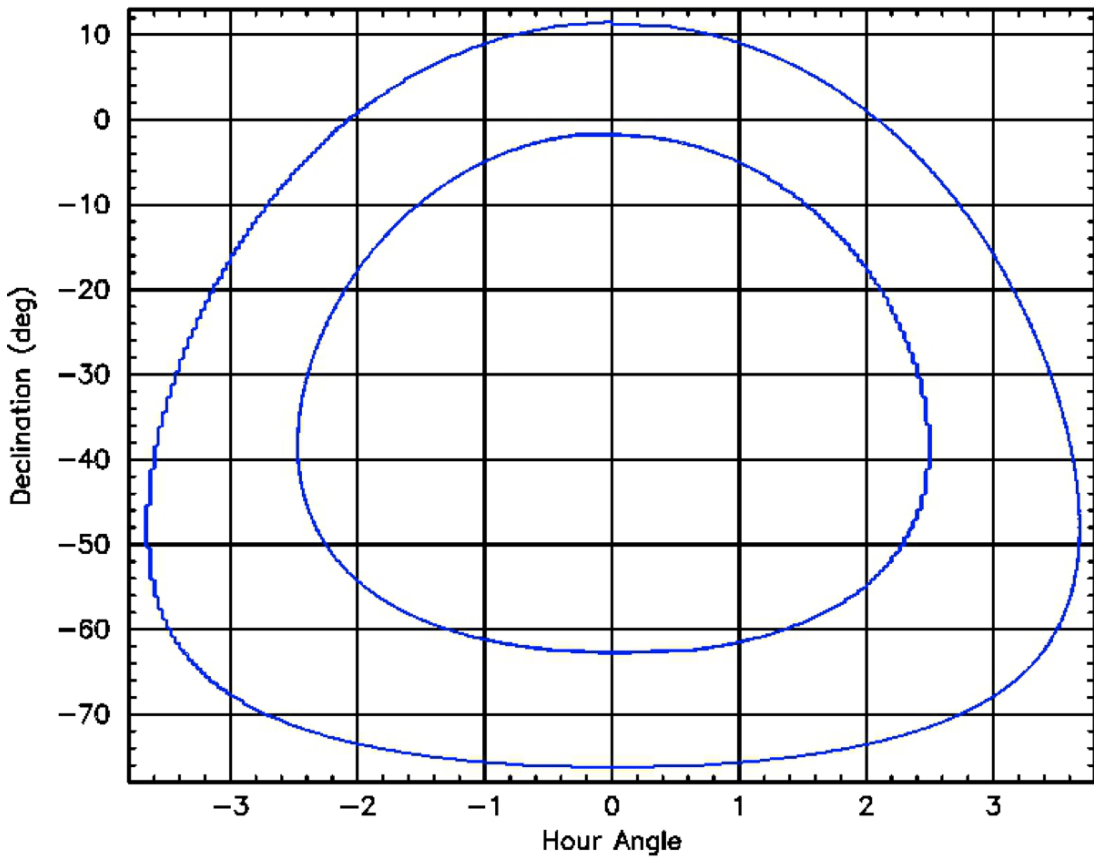


Figure 2.18: The visibility annulus of objects observable by SALT. Figure adapted from the SALT call for proposals (SALT Ast. Ops., 2024).

2.4.2 Tracker and Tracking

During observations the primary mirror is stationary and the tracker tracks celestial objects across the sky by moving along the primary focus. The tracker is capable of 6 degrees of freedom with an accuracy of $\sim 5 \mu\text{m}$ and is capable of tracking $\pm 6^\circ$ from the optimal central track position. Targets at declinations from 10.5° to -75.3° , as shown in Figure 2.18 are accessible during windows of opportunity. As the tracker moves along the track the effective collecting area varies and thus SALT has a varying effective diameter of $\sim 7 \text{ m}$ to 9 m when the tracker is furthest and closest to the optimal central position, respectively.

The tracker is equipped with a Spherical Aberration Corrector (SAC) (O'Donoghue, 2000), and an Atmospheric Dispersion Compensator (ADC) (O'Donoghue, 2002), which corrects for the spherical aberration caused by the geometry of the primary mirror and allows access to wavelengths as short as 3200 \AA . These return a corrected flat focal plane with an $8'$ diameter field of view at prime focus on to the science instruments, with a $1'$ annulus around it used by the tracker in a closed-loop guidance system. The tracker also houses the calibration system which contains the Ar, CuAr, HgAr, Ne, ThAr, and Xe wavelength calibration lamps (Buckley et al., 2008).

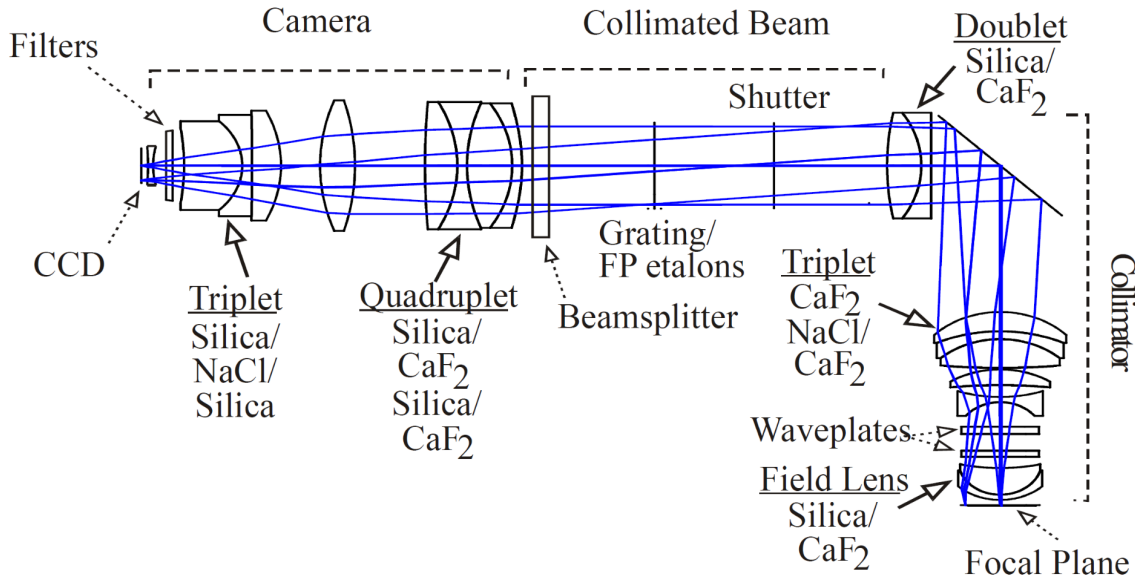


Figure 2.19: The optical path of the SALT RSS. Figure adapted from the SALT call for proposals (SALT Ast. Ops., 2024).

2.4.3 SALT Instrumentation

SALT is equipped with the SALT Imaging Camera (SALTICAM) and the RSS science instruments onboard the tracker, and the High Resolution Spectrograph (HRS) and Near Infra-Red Washburn Labs Spectrograph (NIRWALS) science instruments which are fibre-fed from the tracker to their own climate controlled rooms. The RSS is currently the only instrument used for spectropolarimetry.

NIRWALS

The Near Infra-Red Washburn Labs Spectrograph (NIRWALS) is currently being commissioned and will have a wavelength coverage of 8000 to 17000 Å, providing medium resolution spectroscopy at $R = 2000 - 5000$ over Near Infra-Red (NIR) wavelengths (Brink et al., 2022; Wolf et al., 2022). NIRWALS is fibre-fed from its integral field unit, containing 212 object fibers, along with a separate sky bundle, containing 36 fibers, housed in the SALT fibre instrument feed. It is ideally suited for studies of nearby galaxies.

HRS

The High Resolution Spectrograph (HRS) echelle spectrograph was designed for high resolution spectroscopy at $R = 37000 - 67000$ covering a wavelength range of 3700 – 8900 Å (Barnes et al., 2008; Bramall et al., 2010, 2012) and consists of a dichroic beam splitter and two VPH gratings (Nordsieck et al., 2003). This instrument is capable of stellar atmospheric and radial velocity analysis.

Table 2.1: Gratings available for use with the RSS. Table adapted from the SALT call for proposals (SALT Ast. Ops., 2024).

Grating Name	Wavelength Coverage (Å)	Usable Angles (°)	Bandpass per tilt (Å)	Resolving Power (1.25'' slit)
PG0300 ⁵	3700 – 9000		3900/4400	250 – 600
PG0700 ⁵	3200 – 9000	3.0 – 7.5	4000 – 3200	400 – 1200
PG0900	3200 – 9000	12 – 20	~ 3000	600 – 2000
PG1300	3900 – 9000	19 – 32	~ 2000	1000 – 3200
PG1800	4500 – 9000	28.5 – 50	1500 – 1000	2000 – 5500
PG2300	3800 – 7000	30.5 – 50	1000 – 800	2200 – 5500
PG3000	3200 – 5400	32 – 50	800 – 600	2200 – 5500

SALTICAM

The SALT Imaging Camera (SALTICAM) functions as the acquisition camera and simple science imager with various imaging modes, such as full-mode and slot-mode imaging, and supports low exposure times, down to 50 ms (O'Donoghue et al., 2006). This enables photometry of faint objects, especially at fast exposure times.

RSS

The Robert Stobie Spectrograph (RSS) functions as the primary spectrograph on SALT and can operate in long-slit spectroscopy and spectropolarimetry modes, a narrowband imaging mode, and multi-object and high resolution spectroscopy modes (for an in-depth discussion on operational modes see Kobulnicky et al., 2003; SALT Ast. Ops., 2024).

The Detector The RSS detector consists of a mosaic of 3 CCD chips with a total pixel scale of 0.1267'' per unbinned pixel with varying readout times depending on the binning and readout mode. The mosaicking results in a characteristic double ‘gap’ in the frames and resultant spectra taken with the RSS, as seen in Figure 2.16.

The Available Gratings The RSS is equipped with a rotatable magazine of six VPH gratings, as listed in Table 2.1. Observations may be planned using simulator tools provided by SALT and are performed in the first order only. The RSS has a clear filter, as well as three UV (with differing lower filtering ranges) and one blue order blocking filter available, used in conjunction with the various gratings to block out contamination from the second order.

RSS Spectropolarimetry Spectropolarimetry using the RSS is currently commissioned for long-slit linear spectropolarimetry, (I, Q, U), where observations are taken following the waveplate pattern lists as in Table 2.2. Circular, (I, V), and all-Stokes, (I, Q, U, V), spectropolarimetry modes are in commissioning with observations including redundant half-wave plate pairs to be commissioned thereafter.⁶

⁵The PG0300 surface relief grating has been replaced with the PG0700 VPH grating as of November 2022 but has been included here as observations using the PG0300 are used in later sections.

⁶Commission status sourced from the latest SALT ‘Polarimetry Observers Guide’ (2024).

Table 2.2: Spectropolarimetry waveplate patterns defined for the RSS. The stated angles refer to the angle of the half ($\frac{1}{2}$ -) and quarter ($\frac{1}{4}$ -) waveplate's optical axis from the perpendicular of the dispersion axis. Table adapted from the SALT call for proposals ([SALT Ast. Ops., 2024](#)).

Linear (°)		Linear-Hi (°)		Circular (°)		Circular-Hi (°)		All Stokes (°)	
$\frac{1}{2}$	$\frac{1}{4}$	$\frac{1}{2}$	$\frac{1}{4}$	$\frac{1}{2}$	$\frac{1}{4}$	$\frac{1}{2}$	$\frac{1}{4}$	$\frac{1}{2}$	$\frac{1}{4}$
0	-	0	-	0	45	0	45	0	0
45	-	45	-	0	-45	0	-45	45	0
22.5	-	22.5	-			22.5	-45	22.5	0
67.5	-	67.5	-			22.5	45	67.5	0
		11.25	-			45	45	0	45
		56.25	-			45	-45	0	-45
		33.75	-			67.5	-45		
		78.75	-			67.5	45		

Chapter 3

Existing and Developed Software: An Overview of POLSALT, IRAF, and STOPS

This chapter contains an overview of `POLSALT` and the limitations faced during `POLSALT` wavelength calibrations (§ 3.1), a brief overview of the `IRAF` tasks relevant for spectropolarimetric wavelength calibrations (§ 3.2), and an overview of `STOPS`, the software developed to supplement the `POLSALT` reduction process (§ 3.3). Finally, a discussion of the updated reduction process, an example of which may be found in Appendix A, is included (§ 3.4).

3.1 `POLSALT` - *Polarimetric reductions for SALT*

The `POLSALT` (*Polarimetric reductions for SALT*) pipeline is the official reduction pipeline for spectropolarimetric data taken using `SALT/RSS` (Crawford et al., 2010).¹ The newest version of the software, aptly named the ‘beta version’ (‘version’ 23 January 2020), was the version adapted in this study. It includes a `GUI`, depicted in Figure 3.1, which allows for limited interactivity during key steps in the reduction process.² The `POLSALT` pipeline is written in Python 2, and it is suggested that a Python environment manager, such as `anaconda` (`Anaconda`), is installed.

The steps that make up the `POLSALT` reduction pipeline include raw image reductions, wavelength calibrations, background subtraction and spectral extraction, raw Stokes calculations, final Stokes calculations, and visualization of the results. Accurate reductions at each step are crucial for accurate results and are thus briefly discussed below. Further details for the reduction process may be found at the `POLSALT` GitHub wiki.³

¹ `POLSALT` is made freely available via the `POLSALT` GitHub repository, available at <https://github.com/saltastro/polsalt>. It is strongly advised to follow the wiki for installation instructions.

² Installation files and instructions for the ‘beta version’ utilizing the `GUI` are available at <http://www.saao.ac.za/~ejk/polsalt/code/> in a TAR GZIP file.

³ The GitHub wiki for `POLSALT` is available at <https://github.com/saltastro/polsalt/wiki>.

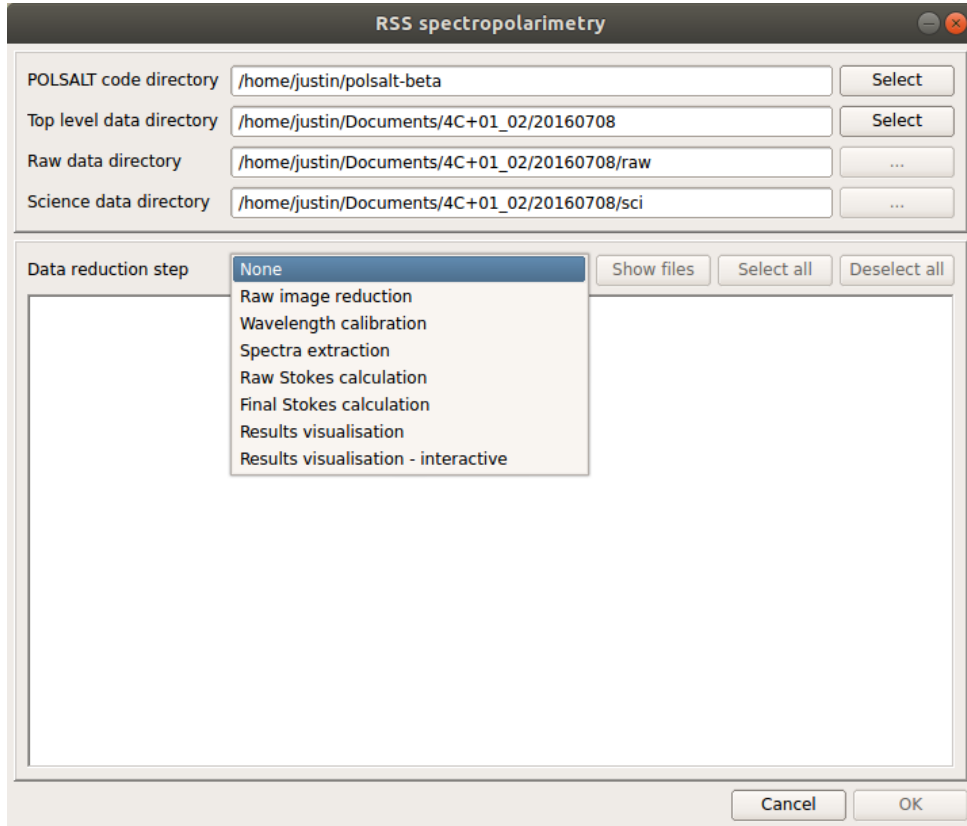


Figure 3.1: The layout of the [POLSALT GUI](#), including the contents of the reduction steps accessible via the dropdown menu. Note that there is no trailing forward slash after the ‘Top level data directory’. Figure created from a local instance of the [POLSALT GUI](#).

3.1.1 Raw Image Reductions

Raw image reductions are run via `imred.py` and apply the necessary basic reductions to the raw data before any calibrations are applied. These reductions include overscan subtractions, gain corrections, crosstalk corrections, and mosaicking as well as attaching the bad pixel maps and pixel variance information. Files with raw image reductions performed have “`mxgbp`” prepended to their names. As of February 2022, raw image reductions are automatically run for all RSS spectropolarimetric observations as part of the default SALT basic reduction pipeline that is run daily.

3.1.2 Wavelength Calibrations

Wavelength calibration and cosmic-ray rejection is performed via `specpolwavmap.py` and separately calibrates the *O*- and *E*-beams, based on the arc frames, and applies a simple cosmic-ray rejection for all science frames. This step is interactive and allows the user to individually fit wavelength calibration maps to each beam. The importance of an accurate correlation between both beams has been touched on previously (§ 2.3.2) and will be further discussed in § 3.1.8. The wavelength calibrated results are saved as an additional ‘`WAV`’ wavelength extension to each science FITS file, which are prefixed with a “`w`”, and the *O*- and *E*-beams of the extensions are split into their own sub-extensions.

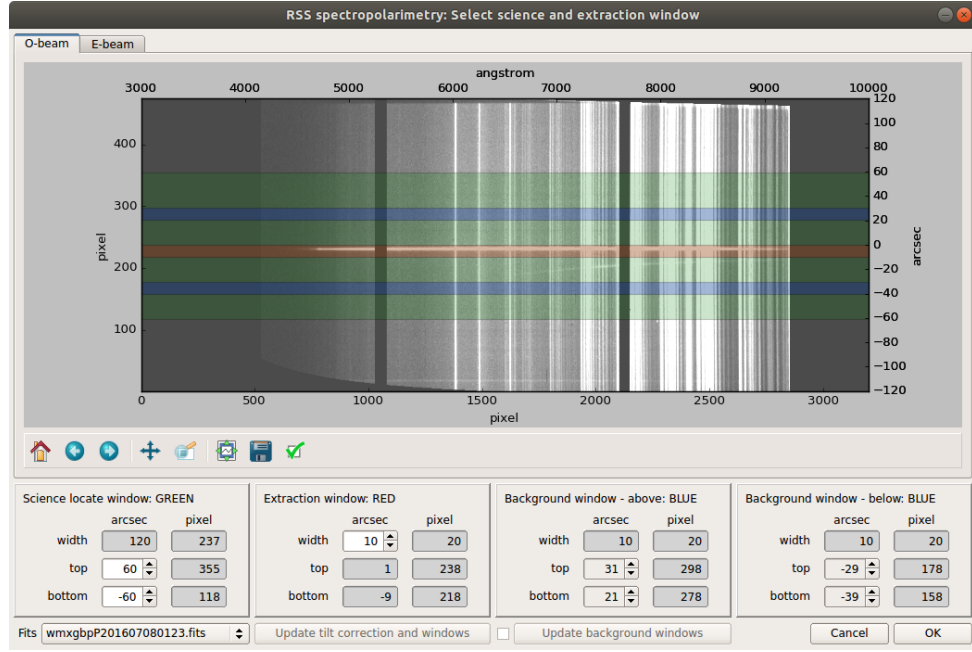


Figure 3.2: The layout of the interactive `POLSALT spectra extraction` GUI after selecting the ‘update tilt correction and windows’ button along the bottom border of the window. Figure created from a local instance of the `POLSALT` GUI.

3.1.3 Spectral Extraction

Background subtraction and spectral extraction is run via `specpoleextract_dev.py` which corrects for the beam-splitter distortion and tilt, performs sky subtraction, and extracts a one dimensional wavelength dependent spectrum for each beam sub-extension. This step is interactive with Figure 3.2 showing the interactive window used for spectral extraction. The user, using the brightest trace in the image as a reference, defines regions which span the wavelength axis which define the background and trace regions for the sky subtraction and spectral extraction. Files with background and geometric corrections applied are saved with “c” prepended to their names and files which contain the extracted one dimensional spectrum have “e” further prepended to their names.

3.1.4 Raw Stokes Calculations

The raw Stokes calculations are performed via `specpolrawstokes_dev.py` and identify waveplate pairs for which the intensity, I , and a ‘raw Stokes’ signal, S , are calculated as:

$$I = \frac{1}{2}(O_1 + O_2 + E_1 + E_2), \text{ and} \quad (3.1)$$

$$S = \frac{1}{2} \left[\left(\frac{O_1 - O_2}{O_1 + O_2} \right) - \left(\frac{E_1 - E_2}{E_1 + E_2} \right) \right]. \quad (3.2)$$

The raw Stokes signal is calculated as the normalized difference of the O - and E -beams, for a waveplate pair, taken perpendicular to one another. The created files contain the raw Stokes information and use a very specific naming style; most notably the indexes of the related waveplate pairs, from Table 2.2, are included in the file names.

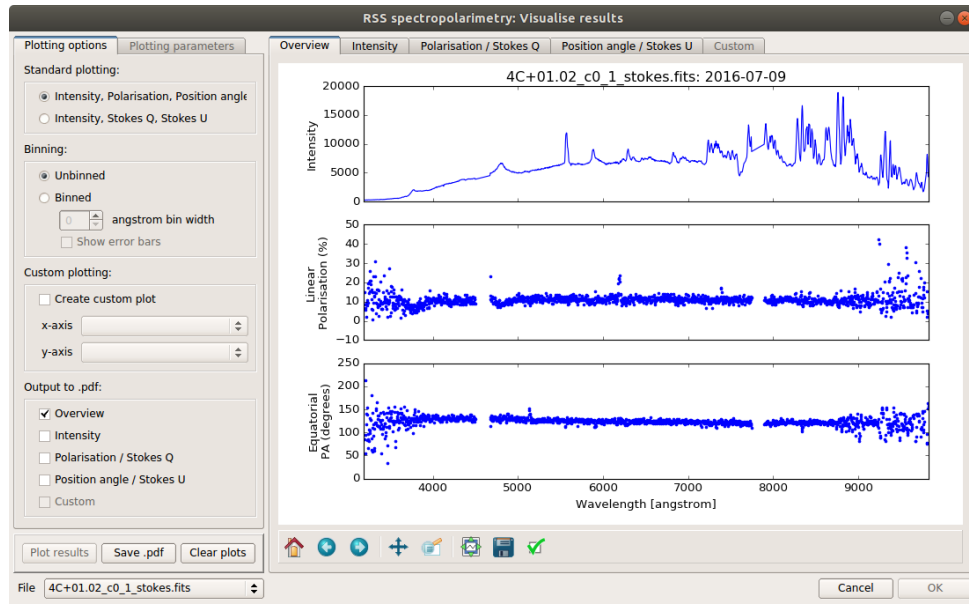


Figure 3.3: The layout of the interactive `POLSALT` visualization GUI after selecting the ‘Plot results’ button along the bottom border of the window. Figure created from a local instance of the `POLSALT` GUI.

3.1.5 Final Stokes Calculations

The Final Stokes calculations are performed via `specpolfinalstokes.py` and, using the waveplate pattern along with the raw Stokes signals, calibrates for the polarimetric zero-point and waveplate efficiency, and calculates the final Stokes parameters. Before the final Stokes calculations are performed, and if a sufficient number of redundant exposures were taken, the raw Stokes signals are culled to eliminate outlier signals which may arise from, for example, temporary atmospheric conditions affecting the signal. The culling is performed by comparing observation cycles against one another, comparing the deviation of the signal means which estimate the baseline systematic polarization fluctuations (due to imperfections in repeatability), and performing a χ^2 analysis to eliminate any statistical outliers.

3.1.6 Visualization

Plotting the results of the spectropolarimetric reduction process is done using `specpolview.py`, which generates a plot of the Intensity, Linear Polarization (%), and Equatorial Polarization Angle ($^\circ$) against a shared wavelength axis, as seen in Figure 3.4. This step is interactive allowing the user control over various options, such as the wavelength range, binning, etc., with the GUI shown in Figure 3.3.

3.1.7 Post-Processing Analysis

Generally, the plot of the spectropolarimetric results is the stopping point for most reduction procedures as it contains or creates the desired results. However, additional tools exist which may be used after the polarization reductions, and which are not represented in the GUI, namely, flux calibration and synthetic filtering.

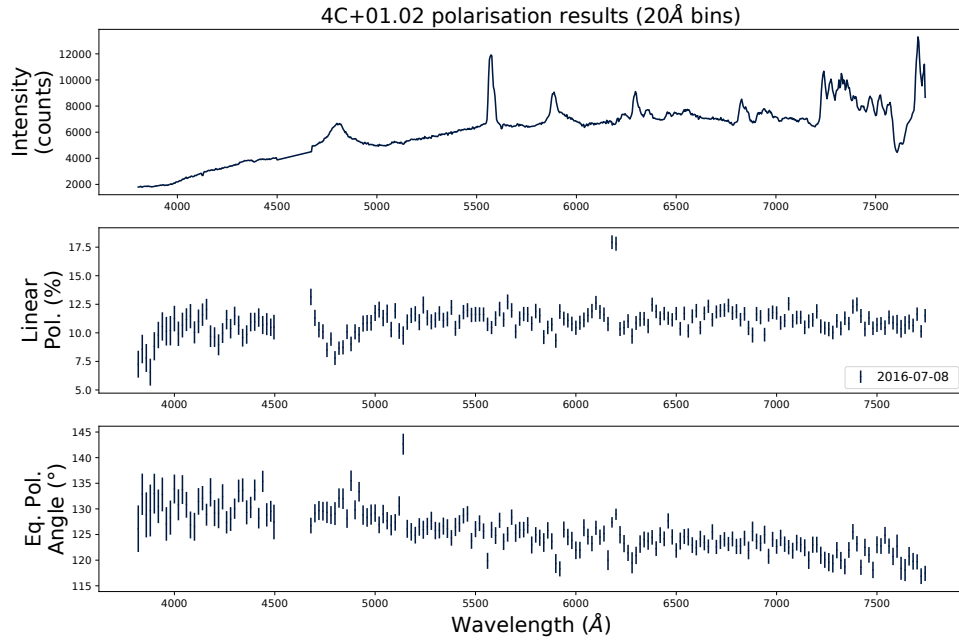


Figure 3.4: A typical plot resulting from the reduction process. Figure adapted from (Cooper et al., 2022).

Flux-calibrations are performed via `specpolflux.py` and are only intended for shape corrections of the spectrum. Additionally, a flux database file must exist for the observed standard and must be included in the working science directory.

Synthetic filtering is calculated via `specpolfilter.py` and computes the synthetically filtered polarization results. Any wavelength dependent throughput filter curve may be synthesized when defined by the user, but a few pre-defined filter curves are available, namely: the SALTICAMs *U*, *B*, *V*, *R*, and *I* Johnson-Cousins photometric system filter curves.

3.1.8 POLSALT Limitations and the Need for Supplementary Tools

The creation of supplementary tools for `POLSALT` spectropolarimetric reductions stemmed from the limitations of the wavelength calibration process and a need to compare wavelength solutions across the perpendicular *O*- and *E*- polarization beams. The process of calibrating wavelength solutions using the `POLSALT` pipeline is time-consuming for the average user, and often results in unexpected program crashes when receiving erroneous inputs or key presses. Due to the time-consuming process of recalibrating the wavelength solutions it is not feasible to perform the wavelength calibrations time and time again for anything larger than a handful of observations. This is particularly true for observations performed with the `SALT` PG0300 grating as the sparse spectral features of the `Ar` arc lamp are not handled well by the `POLSALT` pipeline.

Since PG0300 provided the widest wavelength range and highest throughput, it was almost exclusively used for observations of flaring blazars, resulting in a large backlog of unanalyzed data. The only arc available for the PG0300 grating with a close enough articulation and grating angle ($\sim 10.68^\circ$ and $\sim 5.38^\circ$, respectively), was the `Ar` arc lamp which displays sparse spectral features with large gaps over the wavelength range at these grating and articulation angles (Figure 3.5). This often led the `POLSALT` pipeline to create

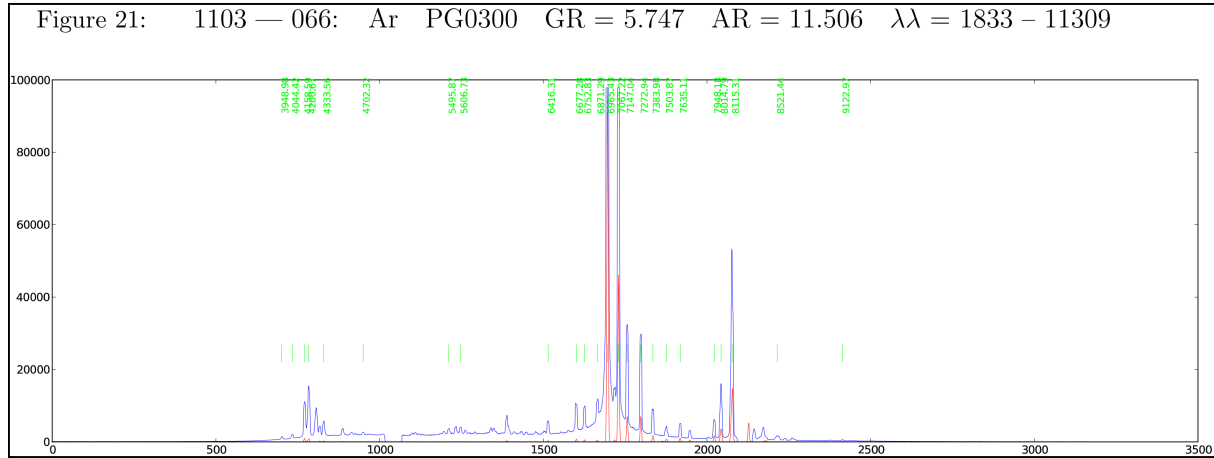


Figure 3.5: One of many Ar arc lamp spectra as provided by **SALT** for line identification. Plot adapted from **SALT**'s published Longslit Line Atlases (as of 2024), resized to fit within the document margins but otherwise unchanged.⁴

inconsistent wavelength solutions, or to fail to create a wavelength solution altogether, since minor deviations of identified spectral features resulted in large deviations in regions with no spectral features. To only further compound the difficulty of the wavelength calibrations, the spectrum of the Ar arc lamp contains a partial overlap of a higher order at longer wavelengths (§ 2.1.7, Equation 2.5).

The chosen solution to overcome the limitations of the wavelength calibration process was to use a well established wavelength calibration software which allowed for rapid recalibrations and provided a familiar interface. **IRAF** provides this familiar environment and reliability, in part thanks to its [continued community development](#).

Unfortunately, **IRAF** is unable to natively parse the data structure implemented by **POLSALT** ‘as is’ and so the files must be restructured. This restructuring works both ways as once the **IRAF** reductions are complete the data structure must be restructured to match that of the **POLSALT** [wavelength calibration](#) output such that the reduction process may be completed in **POLSALT**.

3.2 IRAF - *Image Reduction and Analysis Facility*

The **IRAF** (*Image Reduction and Analysis Facility*) software is a collection of software designed specifically for the reduction and analysis of astronomical images and spectra (Tody, 1986, 1993). The software consists of many tasks which perform specific operations and which are grouped into relevant packages. Only a brief overview of the tasks will be provided here. Help documentation for any of the **IRAF** tasks may be found online at https://astro.uni-bonn.de/~sysstw/lfa_html/iraf/iraf.html or through the **IRAF** Command Line Interface (CLI) through the ? or .:help ‘cursor commands’ when running interactive tasks.⁵

⁴The ‘low resolution’ Ar plot sourced from <https://astronomers.salt.ac.za/data/salt-longslit-line-atlas/>

⁵Online help for **IRAF** is also available at <https://iraf.net/irafdocs/>.

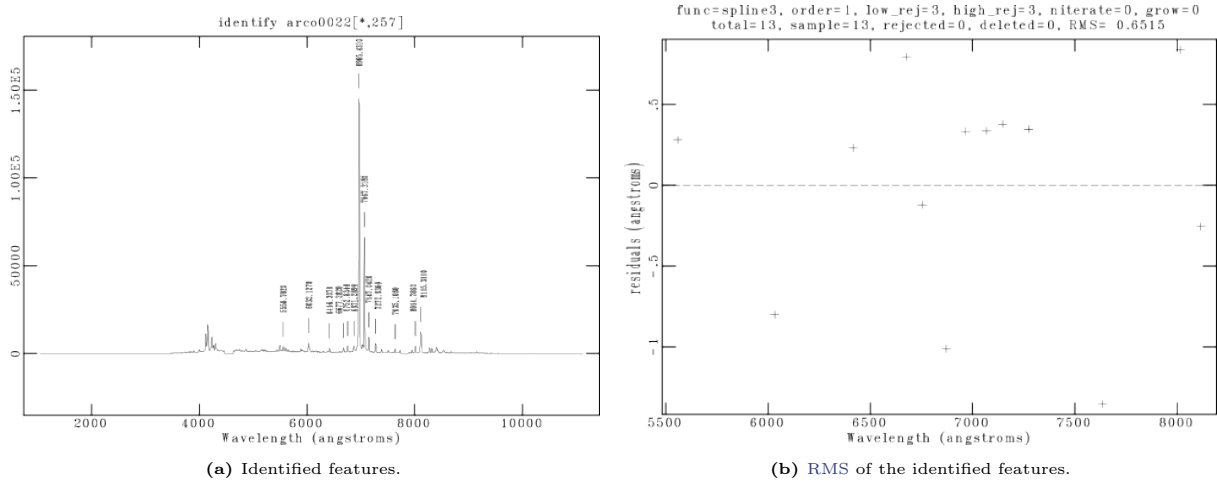


Figure 3.6: A plot and the Root Mean Square (RMS) of the identified features found using the `IRAF identify` task. Figures created using the `IRAF identify` task.

Useful `IRAF` tasks that deserve a brief mention are: the `mkscript` task in the `system` package which allows the user to create and save a task along with the defined parameters as a file which can later be called as a script, the `implot` task in the `plot` package which allows the rows or columns of an image to be interactively displayed, and the `eparam` task in the `language` package which allows the parameters of a task to be edited within the `IRAF CLI`.

For the wavelength calibration of `SALT` spectropolarimetric data, the relevant tasks are the `identify` and `reidentify` tasks located in the `noao.onedspec` package, and the `fitcoords` and the (optional) `transform` tasks located under the `noao.twodspec.longslit` package. These tasks produce a two-dimensional wavelength solution which must be obtained separately for the *O*- and *E*-beam.

3.2.1 Identify

The `identify` task is used to interactively determine a one-dimensional wavelength function across a chosen row of an arc exposure by identifying features in the spectrum with known wavelengths. The task creates the first approximation of the wavelength solution (see Figure 3.6) as well as a local database in which the solution is saved (see Listing 3.1). The initial solution is built on in subsequent tasks, and it is, therefore, imperative that the initial solution is well-fit to minimize errors further along the calibration process.

The execution of `identify` consists of identifying known features spanning the entire wavelength range and then removing any features which negatively impact the wavelength solution. A balance must be found between the number of identified features, the parameters of the fit, and the deviation of the fit from the known features.

3.2.2 Reidentify

The `reidentify` task is used to run the `identify` task autonomously and repeatedly across the entirety of the arc frame at defined (row) intervals. The task uses the one-dimensional wavelength solution stored in the database created by the initial `identify` call and refits the positions of the relevant spectral features. The task may fail based on

Listing 3.1: An example of the `identify` database contents. See <https://iraf.net/irafdocs/formats/identify.php> for a detailed explanation of the identify database contents.

```
# Thu 15:19:16 13-May-2021
begin    identify arc00057[*,237]
id      arc00057
task      identify
image     arc00057[*,237]
units      Angstroms
features   35
      53.61 5944.74989  5944.834  13.0 1 1 15257
    140.19 6029.9793   6029.997  13.0 1 1 4652
   185.30 6074.34644  6074.338  13.0 1 1 13396
  207.49 6096.15873  6096.161  13.0 1 1 21700
  255.23 6143.0493   6143.063  13.0 1 1 33330
  276.13 6163.56995  6163.594  13.0 1 1 11344
  330.89 6217.29293  6217.281  13.0 1 1 13705
  381.10 6266.51524  6266.495  13.0 1 1 21747
  420.21 6304.8113   6304.789  13.0 1 1 10226
  450.49 6334.45415  6334.428  13.0 1 1 36235
  500.18 6383.04826  6382.991  13.0 1 1 35824
  519.85 6402.26802  6402.248  13.0 1 1 70163
  626.70 6506.56147  6506.528  13.0 1 1 46165
  653.73 6532.91083  6532.882  13.0 1 1 21413
  721.60 6598.98642  6598.953  13.0 1 1 26396
  803.21 6678.31069  6678.277  13.0 1 1 51338
  843.15 6717.0732   6717.043  13.0 1 1 36780
1099.95 6965.36335  6965.431  13.0 1 1 5618.4 ar
1169.57 7032.38598  7032.413  13.0 1 1 100000
1317.05 7173.89814  7173.938  13.0 1 1 5000 decrease
1391.52 7245.11148  7245.167  13.0 1 1 73545
1537.20 7383.93022  7383.981  13.0 1 1 5557.5 ar
1595.02 7438.83545  7438.898  13.0 1 1 15000 decrease
1663.64 7503.86263  7503.869  13.0 1 1 30000 ar; increase
1697.46 7535.84584  7535.774  13.0 1 1 8000 increase
1802.64 7635.07335  7635.106  13.0 1 1 20000 ar; decrease
2209.19 8014.79559  8014.786  13.0 1 1 3000 ar; decrease
2604.58 8377.66137  8377.607  13.0 1 1 14543
2734.54 8495.41423  8495.359  13.0 1 1 8765
2763.48 8521.52355  8521.442  13.0 1 1 4537.5 ar
2840.92 8591.20799  8591.258  13.0 1 1 2000 decrease
2889.39 8634.67334  8634.647  13.0 1 1 3059
2911.42 8654.39264  8654.383  13.0 1 1 3000 decrease
2926.56 8667.93501  8667.944  13.0 1 1 702.5 ar
3135.72 8853.77575  8853.867  13.0 1 1 1820

function legendre
order 4
sample *
nverage 1
niterate 0
low_reject 3.
high_reject 3.
grow 0.
coefficients     8
 2.
 4.
53.60757446289061
3135.715576171875
7425.420339270724
1457.513831286474
-26.15751926622308
-3.000903509842187
```

Listing 3.2: An example of the `fitcoords` database contents. See <https://iraf.net/irafdocs/formats/fitcoords.php> for a detailed explanation of the `fitcoords` database contents.

```
# Thu 15:26:55 13-May-2021
begin    arc00057
task      fitcoords
axis      1
units    angstroms
surface  33
      1.
      5.
      5.
      1.
      1.
      3199.
      1.
      474.
      7419.096745914063
      1510.03933621895
      -21.10886852752348
      -2.079553916887794
      0.06772631420528228
      0.7720164913117386
      -1.506773900054024
      0.1341878190232142
      -0.01659697703758917
      0.0251087019569153
      -3.318493303995171
      -0.3612632489821799
      0.003270665801371641
      -0.0157962041414068
      -0.003073690871589242
      0.007533453962924031
      0.02839687304474069
      -0.003233465769521899
      0.00174111456659807
      0.00645177595090841
      0.0105080093855621
      -0.01157827440314294
      -0.007789479002470706
      -0.006562085282926231
      -0.002321476801926803
```

a number of conditions, most common of which is the loss of features as the task moves further from the row at which the user manually ran `identify`.

When running `reidentify` non-interactively, it is recommended to set the `verbose` parameter to ‘yes’ as this will provide immediate confirmation if the task quit early. Regardless of whether the task quit successfully, the newly defined wavelength solutions are appended to the local database following the `identify` task database format, an example of which is given in Listing 3.1.

3.2.3 Fitcoords

The `fitcoords` task is used to find a two-dimensional surface function from the one-dimensional wavelength solutions found for specific rows in the previous steps. The usage of `fitcoords` is similar to that of `identify` and consists of examining the distribution of identified points and eliminating any points that `reidentify` may have misidentified (see Figure 3.7).

By eliminating outliers with bad residuals and modifying the two-dimensional surface function’s type and degree, the overall error of the fit is decreased, aligning more closely to what the ‘true’ wavelength solution is. This surface function is the final two-dimensional wavelength solution for each two-dimensional spectrum. It is saved using the `fitcoords` database format, an example of which is given in Listing 3.2, as the list of parameters and function coefficients required to recreate the closest two-dimensional model. The `IRAF` wavelength solution is used by the `STOPS join` method to create the ‘`WAV`’ extension required by `POLSLAT`, further described in § 3.3.2.

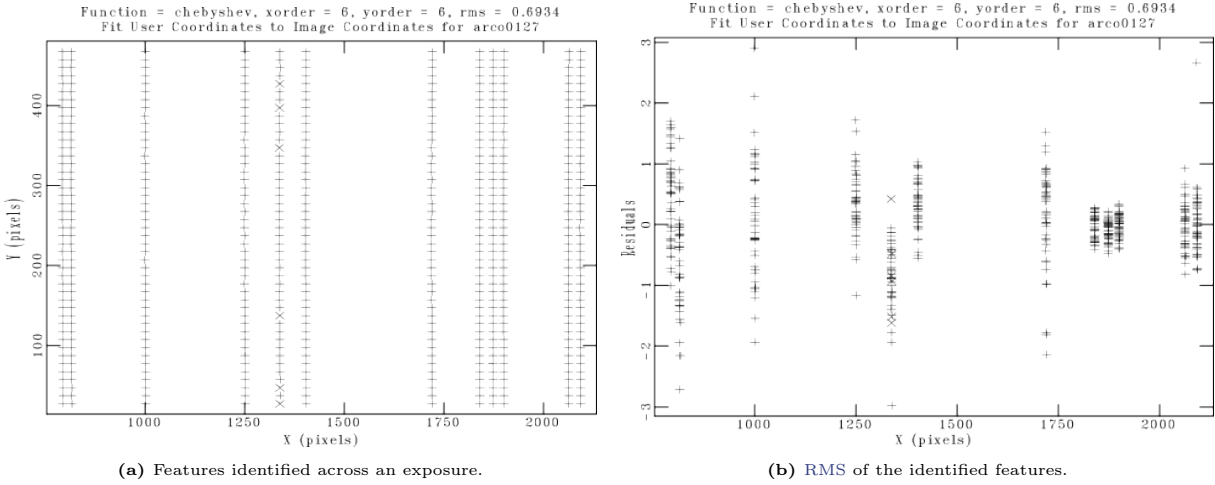


Figure 3.7: A plot and the RMS of the features identified across the exposure using the `IRAF fitcoords` task. Figures created using the `IRAF fitcoords` task.

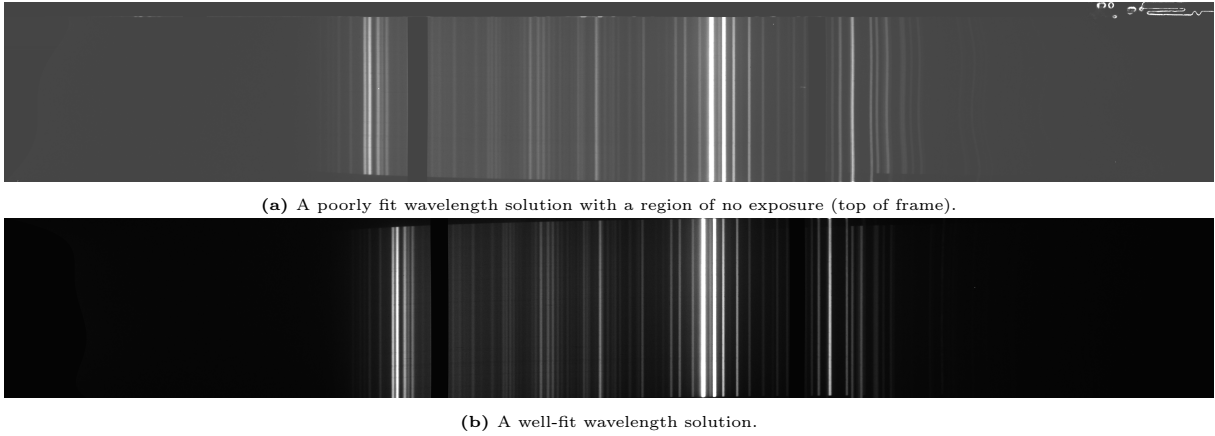


Figure 3.8: Examples of a poor fit (a) and well-fit (b) wavelength solution applied to the O- and E-beams of an arc image. The contrast of the figures were scaled to best capture any deviation of the arc lines. Figures created by the `IRAF transform` task.

3.2.4 Transform

The `transform` task is the optional final step in the `IRAF` wavelength calibration process. Simply put, `transform` converts the (x_p, y_p) pixel units of an exposure to (λ, y_p) wavelength units which allows for an immediate check of whether the wavelength solution is consistent across the frame. Any general error in the wavelength solution may be spotted in the transformed images; ranging from minor errors, such as the arc lines or sky lines not being purely vertical across the frame, to more major errors, such as an incorrect wavelength solution skewing the exposure beyond recognition.

For example, Figure 3.8a shows a good fit to the wavelength solution, as after transformation all the sky lines run exactly vertical. Figure 3.8b, on the other hand, shows a seemingly good fit, but closer inspection reveals that the sky lines (especially towards the right of the frame) deviate from the vertical, indicating a poor fit to the wavelength solution.

3.3 STOPS - *Supplementary Tools for POLSALT Spectropolarimetry*

STOPS (*Supplementary Tools for POLSALT Spectropolarimetry*) provides supplementary tools which convert the **POLSALT** and **IRAF** formats back and forth, allowing **IRAF** to be used for wavelength calibrations of **SALT** spectropolarimetric data. It also provides additional tools to check the accuracy of the wavelength calibration. STOPS is written in, and requires, Python 3 (3.11+) to run, as well as **Astropy** (6.0.0+) ([Astropy Collaboration et al., 2013, 2018, 2022](#)), **ccdproc** (2.4.1+) ([Craig et al., 2017](#)), **Matplotlib** (3.5.2+) ([Hunter, 2007](#)), **NumPy** (1.26.4+) ([Harris et al., 2020](#)), and **SciPy** (1.13.0+) ([Virtanen et al., 2020](#)).

The parsing of **POLSALT** data into an **IRAF** usable format and the reformatting of the **IRAF** wavelength calibrated data back into a **POLSALT** usable format, referred to as *splitting* and *joining*, is performed by the **STOPS** **split** and **join** methods, respectively.

Methods to verify the validity of the wavelength calibrations were also added to **STOPS**. The **skyline** method checks the sky line (λ) wavelength positions across the frame as well as the variation of the sky lines across the (y_{pos}) positional axis of the frame. The **correlate** method checks the correlation of the *O*- and *E*-beams either within a given **FITS** file or across multiple files (comparing only the *O*- and *E*-beams for each). With these two additional methods, the user is able to verify that the wavelength solutions do not conflict across the *O*- and *E*-beams and that no unexpected deviations are included in the wavelength solutions.

Help on the usage of **STOPS** in a **CLI** can be viewed by running:

```
$ python ~/STOPS --help
# OR
$ python ~/STOPS [split|join|correlate|skylines] --help
```

which retrieves and prints the help documentation to the **CLI** from [Listing B.1](#) (in [Appendix B](#)), such as how to enable logging or increase the verbosity, or change default parameters of the various methods. Finally, help documentation for the specific **STOPS** methods may be found within this section ([Listing 3.3](#) to [3.6](#)) or in [Appendix B](#).

3.3.1 Splitting

As mentioned previously, the format of the **FITS** file created by **POLSALT** after basic CCD reductions and the format expected by **IRAF** to be used for the wavelength calibrations are incompatible. Basic **POLSALT** CCD reductions return **FITS** files which contain a primary header along with extensions for the science, variance, and ‘BPM’ images. These extensions carry the image of the trace (see [Figure 3.9](#)), the variance of the image, and a map of the pixels to be masked out, split into sub-extensions for both polarimetry beams, respectively.

While **IRAF** is capable of dealing with multiple traces in an extension or lists of input files, it is not as capable when dealing with multiple wavelength solutions contained in a single extension (as expected by the **POLSALT wavelength calibration**) or extensions containing sub-extensions (as expected by the **POLSALT spectral extraction**).

Listing 3.3: The ‘docstring’ for **split.py**

The `Split` class allows for the splitting of `polsalt` FITS files based on the polarization beam. The FITS files must have basic `polsalt` pre-reductions already applied (`mxgbp...` FITS files).

Parameters

`data_dir : str | Path`
The path to the data to be split

`fits_list : list[str], optional`
A list of pre-reduced `polsalt` FITS files to be split within `data_dir`.
(The default is None, `Split` will search for `mxgbp*.fits` files)

`split_row : int, optional`
The row along which to split the data of each extension in the FITS file.
(The default is SPLIT_ROW (See Notes), the SALT RSS CCD’s middle row)

`no_arc : bool, optional`
Decides whether the arc frames should be recombined.
(The default is False, `polsalt` has no use for the arc after wavelength calibrations)

`save_prefix : dict[str, list[str]], optional`
The prefix with which to save the O & E beams. Setting `save_prefix` = `None` does not save the split O & E beams.
(The default is SAVE_PREFIX (See Notes))

Attributes

`arc : str`
Name of arc FITS file within `data_dir`. `arc` = `""` if `no_arc` or not detected in `data_dir`.

`o_files, e_files : list[str]`
A list of the ‘O’- and ‘E’-beam FITS file names. The first entry is the arc file if `arc` defined.

`data_dir`

`fits_list`

`split_row`

`save_prefix`

Methods

`split_file(file: os.PathLike) -> tuple[astropy.io.fits.HDUList]`
Handles creation and saving the separated FITS files

`split_ext(hdulist: astropy.io.fits.HDUList, ext: str = 'SCI') -> astropy.io.fits.HDUList`
Splits the data in the `ext` extension along the `split_row`

`crop_file(hdulist: astropy.io.fits.HDUList, crop: int = CROP_DEFAULT) -> tuple[numpy.ndarray]`
Crops the data along the edge of the frame, that is,
‘O’-beam cropped as [crop:], and
‘E’-beam cropped as [:-crop].

`update_beam_lists(o_name: str, e_name: str) -> None`
Updates `o_files` and `e_files`.

`save_beam_lists(file_suffix: str = 'frames') -> None`
Creates and writes (overwrites if exists) the `[o|e]_files` to files named `[o|e]_{file_suffix}`.

`process() -> None`
Calls `split_file` and `save_beam_lists` on each file in `fits_list` for automation.

Other Parameters

`**kwargs : dict`
keyword arguments. Allows for passing unpacked dictionary to the class constructor.

Notes

Constants Imported (See `utils.Constants`):

- SAVE_PREFIX
- CROP_DEFAULT
- SPLIT_ROW

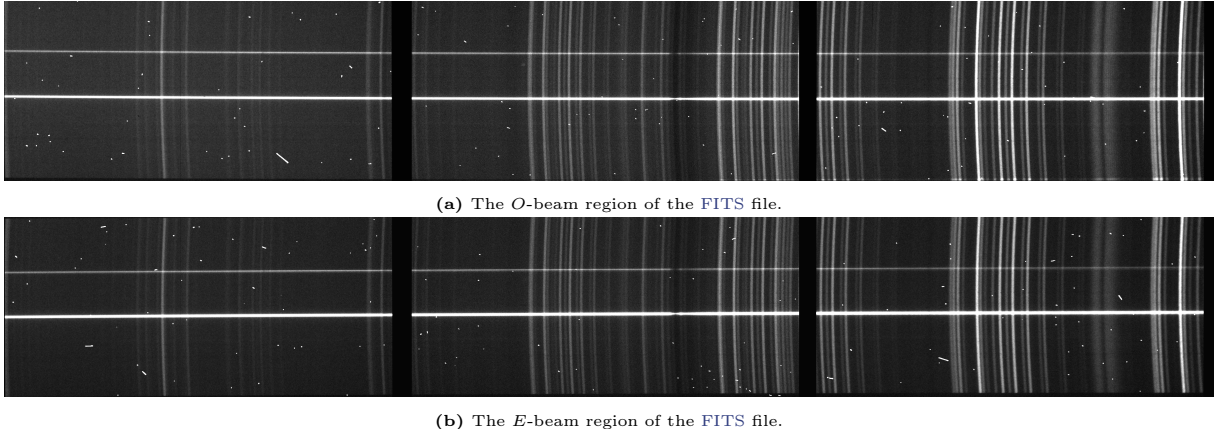


Figure 3.9: The split *O*- (a) and *E*-beams (b) as handed to **IRAF**. Figure created from the **STOPS** `split` method output.

To simplify the **IRAF** reduction procedure it was decided to separate the perpendicular polarization beams into their own files.

The files with **POLSALT** pre-reductions applied, namely **FITS** files with an ‘mxgbp’ prefix (§ 3.1), are used as the starting point for the supplementary tool’s `split` method. Running `split` finds all the **FITS** files for wavelength calibration within the working directory, creates two empty **Header and Data Unit (HDU)** structures for each **FITS** file (i.e., for both the *O*- and *E*-beam), and appends all header and science data necessary for wavelength calibration to the relevant **HDU** structure. Otherwise, defaults, such as which row to split the image along to separate the beams, were kept as close to the **POLSALT** pipeline as possible.

As the intent was always to parse the wavelength function back into **POLSALT** it was decided to keep these temporary **FITS** files as small as possible by only including the header and ‘SCI’ science extension. To aid the scripting of the **IRAF** wavelength calibration process, the `split` method also performs row cropping to exclude **CCD** regions which are not exposed to light, and creates files listing the split *O*- and *E*-beam **FITS** files which may be passed to the **IRAF** task inputs. Row cropping was decided on as **IRAF** does not handle rows with no exposure well, specifically when it comes to the autonomous `reidentify` task. The full **STOPS** `split` class docstring is given in Listing 3.3.

3.3.2 Joining

After the **IRAF** `fitcoords` task has been successfully run for both the *O*- and *E*-beams, the **STOPS** `join` method is used to extract and parse the wavelength solution from the **IRAF** database, and to create the wavelength calibrated **FITS** files required by the **POLSALT** pipeline. More specifically, the `join` method performs the following steps:

First, `join` parses the wavelength database file, described in § 3.2.3, for either a ‘Chebyshev’ or ‘Legendre’ solution, and calculates the wavelength at each (x_p, y_p) pixel position. This new image containing the corresponding wavelength values, seen in Figure 3.10, is appended to the wavelength calibrated **FITS** file as the ‘WAV’ extension.

Listing 3.4: The ‘docstring’ for `join.py`

The `Join` class allows for the joining of previously split files and the appending of an external wavelength solution in the `polsalt` FITS file format.

Parameters

`data_dir : str | Path`
The path to the data to be joined

`database : str, optional`
The name of the `IRAF` database folder.
(The default is "database")

`fits_list : list[str], optional`
A list of pre-reduced `polsalt` FITS files to be joined within `data_dir`.
(The default is ``None``, `Join` will search for `mxbgp*.fits` files)

`solutions_list: list[str], optional`
A list of solution filenames from which the wavelength solution is created.
(The default is ``None``, `Join` will search for `fc*` files within the `database` directory)

`split_row : int, optional`
The row along which the data of each extension in the FITS file was split.
Necessary when Joining cropped files.
(The default is 517, the SALT RSS CCD's middle row)

`save_prefix : dict[str, list[str]], optional`
The prefix with which the previously split 'O'- & 'E'-beams were saved.
Used for detecting if cropping was applied during the splitting procedure.
(The default is `SAVE_PREFIX` (See Notes))

`verbose : int, optional`
The level of verbosity to use for the Cosmic ray rejection
(The default is 30, i.e., `logging.INFO`)

Attributes

`fc_files : list[str]`
Valid solutions found from `solutions_list`.

`custom : bool`
Internal flag for whether `solutions_list` uses the `IRAF` or a custom format.
See Notes for custom solution formatting.
(Default (inherited from `solutions_list`) is False)

`arc : str`
Deprecated. Name of arc FITS file within `data_dir`.

`data_dir`

`database`

`fits_list`

`split_row`

`save_prefix`

Methods

`get_solutions(wavlist: list | None, prefix: str = "fc") -> (fc_files, custom): tuple[list[str], bool]`
Parse `solutions_list` and return valid solution files and if they are non-`IRAF` solutions.

`parse_solution(fc_file: str, x_shape: int, y_shape: int) -> tuple[dict[str, int], np.ndarray]`
Loads the wavelength solution file and parses keywords necessary for creating the wavelength extension.

`join_file(file: os.PathLike) -> None`
Joins the files, attaches the wavelength solutions, performs cosmic ray cleaning, masks the extension, and checks cropping performed in `Split`. Writes the FITS file in a `polsalt` valid format.

`check_crop(hdu: pyfits.HDUList, o_file: str, e_file: str) -> int`
Opens the split 'O'- and 'E'-beam FITS files and returns the amount of cropping that was performed.

`process() -> None`
Calls `join_file` on each file in `fits_list` for automation.

Other Parameters

`no_arc : bool, optional`
Deprecated. Decides whether the arc frames should be processed.
(The default is False, `polsalt` has no use for the arc after wavelength calibrations)

`**kwargs : dict`
keyword arguments. Allows for passing unpacked dictionary to the class constructor.

Notes

Constants Imported (See `utils.Constants`):

- `DATADIR,`
- `SAVE_PREFIX,`
- `SPLIT_ROW,`
- `CR_PARAMS`

Custom wavelength solutions must be formatted containing:
`x`, `y`, *coefficients...
where a solution are of order ('x' by 'y') and must contain x*y coefficients, all separated by newlines.
The name of the custom wavelength solution file must contain either "cheb" or "leg"
for Chebyshev or Legendre wavelength solutions, respectively.

Cosmic ray rejection is performed using `lacosmic [1]` implemented in `ccdproc` via `astroscrappy [2]`.

References

.. [1] van Dokkum 2001, PASP, 113, 789, 1420
(article : <https://adsabs.harvard.edu/abs/2001PASP..113.1420V>)

.. [2] <https://zenodo.org/records/1482019>

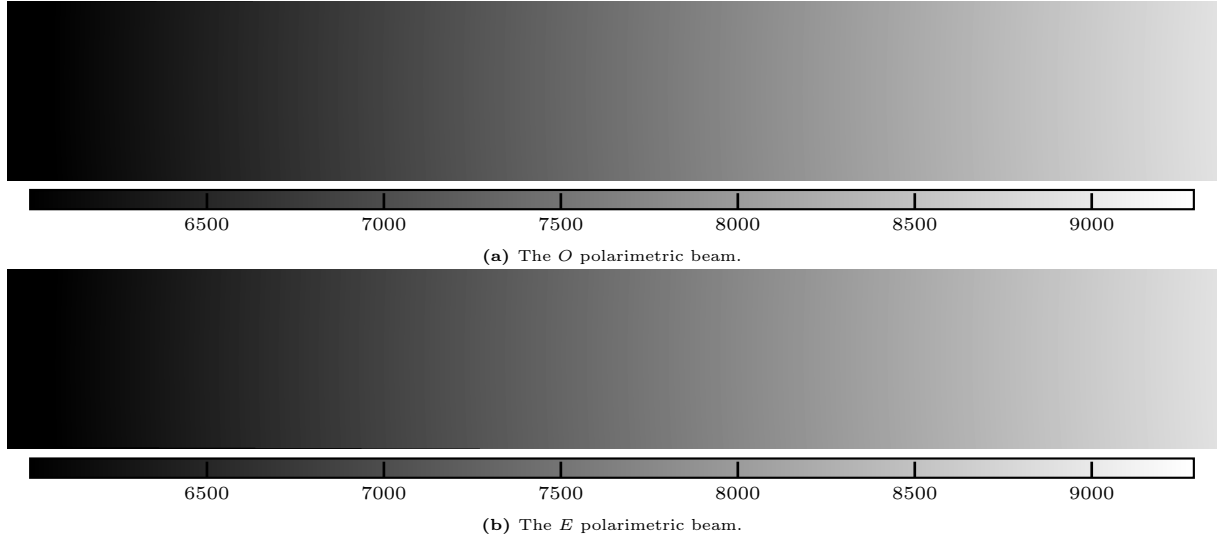


Figure 3.10: A representative ‘WAV’ extension of a FITS file, for the *O*- (a) and *E*-beam (b), ready to be processed by the `POLSLT` pipeline. The color bars show the wavelength in Å. Note that regions which fall outside the exposed region are masked by setting the corresponding pixel values of the wavelength and ‘BPM’ extensions to 0. Figure created from the `STOPS join` method output.

Second, cosmic-ray cleaning is performed on the ‘SCI’ extension using the `ccdproc` implementation of the `lacosmic` Python package which implements the L. A. Cosmic algorithm, based on Laplacian edge detection. The read noise and gain parameters used for cosmic ray cleaning were chosen based on the properties of the RSS, while the rest of the parameters were left as the default, following the publication and suggestions by the algorithm’s creator, as well as the implementation of the algorithm in the python `ccdproc` package (McCully et al., 2018; van Dokkum, 2001).⁶ The chosen parameters work well for most cosmic rays, as can be seen when comparing Figure 3.9 to Figure 3.11, but may be modified as needed.

Next, `join` updates the headers to be near-identical to those created by the `POLSLT wavelength calibration`, most notably updating the data shape, ‘CTYPE3’, and data type, ‘BITPIX’, keywords. The only difference in the header is the ‘NAXIS2’ keyword, due to the cropping performed by `split`. The cropped region could be reintroduced but would be masked out and further discarded in the following `POLSLT spectra extraction` process, making it redundant.

Finally, the ‘WAV’ extension is masked to remove any regions with no wavelength calibration, and masked for the skewing of the trace introduced by the wollaston element. The masking of the wollaston skewing is necessary since `POLSLT` introduces a wollaston correction during `spectra extraction`. The ‘BPM’ extension is masked to reflect the valid wavelength calibrated region, and the files are saved with the `POLSLT` wavelength calibrated ‘wmxgbp’ prefix. The full `STOPS join` class docstring is given in Listing 3.4.

⁶Suggested parameters for the `lacosmic` algorithm may be found at <http://www.astro.yale.edu/dokkum/lacosmic/pars.html>.

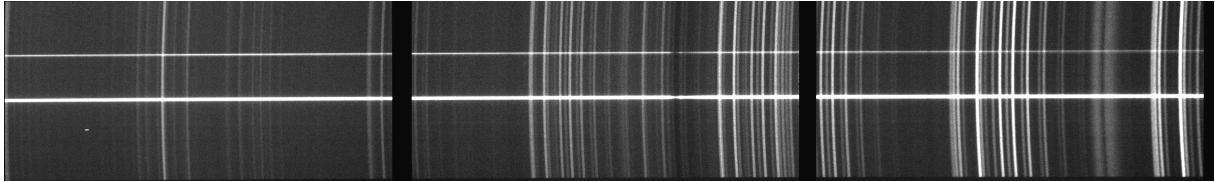
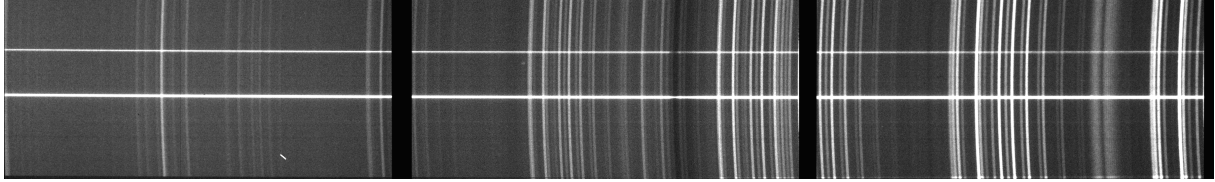
(a) The O polarimetric beam.(b) The E polarimetric beam.

Figure 3.11: A representative ‘SCI’ extension of a FITS file, for the O - (a) and E -beam (b), ready to be processed by the `POLSLT` pipeline. The observed intensity is displayed via the grayscale value at each pixel. Figure created from the `STOPs` join method output.

Listing 3.5: The ‘docstring’ for `skylines.py`

```
Class representing the Skyline object.

Parameters
-----
data_dir : Path
    The directory containing the data files.
filenames : list[str]
    The list of filenames to be processed.
beam : str, optional
    The beam mode, by default "OE".
plot : bool, optional
    Flag indicating whether to plot the continuum, by default False.
save_prefix : Path | None, optional
    The prefix for saving the data, by default None.
**kwargs
    Additional keyword arguments.

Attributes
-----
data_dir : Path
    The directory containing the data files.
fits_list : list[str]
    The list of fits file paths.
beams : str
    The beam mode.
can_plot : bool
    Flag indicating whether to plot the continuum.
save_prefix : Path | None
    The prefix for saving the data.
wav_unit : str
    The unit of wavelength.

Methods
-----
checkLoad(self, path1: str) -> np.ndarray:
    Checks and loads the data from the given path.
transform(self, wav_sol: np.ndarray, spec: np.ndarray) -> np.ndarray:
    Transforms the input wavelength and spectral data based on the given wavelength solution.
rmvCont(self) -> np.ndarray:
    Removes the continuum from the spectrum.
process(self) -> None:
    Placeholder method for processing the data.

See Also
-----
matplotlib custom style:
    https://matplotlib.org/stable/users/explain/customizing.html

Notes
-----
Constants imported (see utils.Constants):
    SAVE_SKY:
        The default save name for the skylines plot.
    FIND_PEAK_PARAMS:
        The default parameters for finding peaks in the spectrum.
```

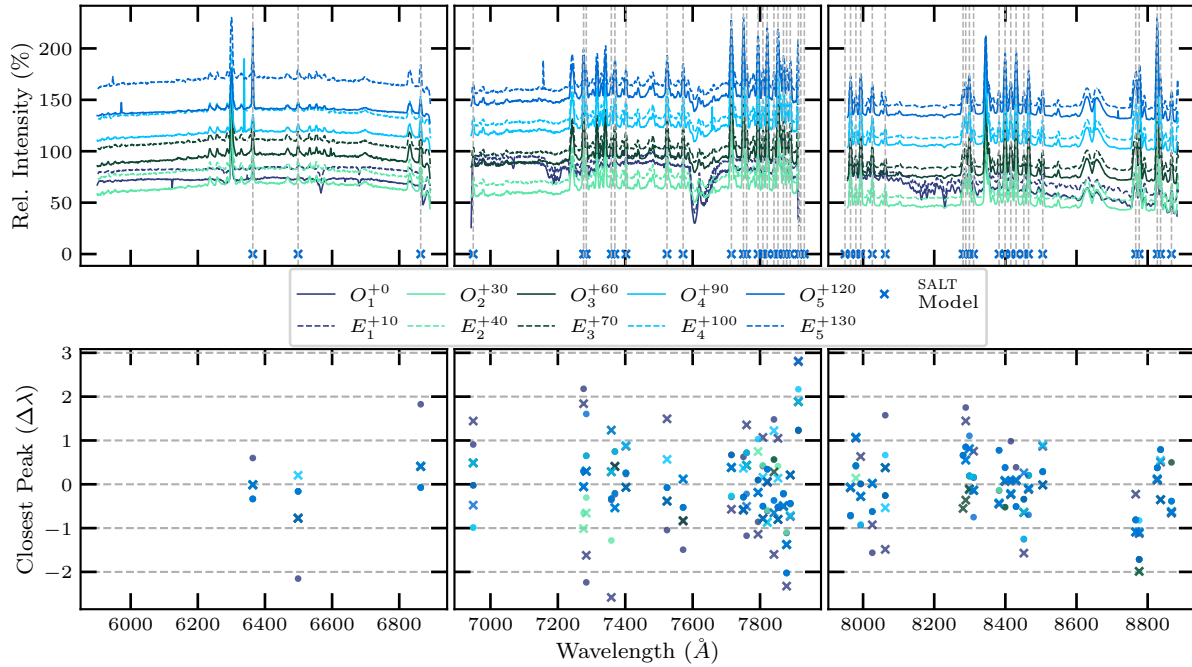


Figure 3.12: An example of a well calibrated wavelength solution, specifically shown for science images. Figure created via the `STOPS skyline` method.

3.3.3 Sky Lines

The `skyline` method has been implemented to compare the position of the sky lines on the ‘SCI’ extension, or arc lines in the arc exposure, to the known positions of the sky lines, or arc lines, as measured by `SALT`, respectively.⁷ This provides an additional check of the accuracy of the wavelength solution across the frame. This method accepts both the `IRAF transform` `FITS` file or the ‘wmxgbp’ `FITS` files created by the `join` method as the input.

The `skyline` method loads the wavelength calibrated files, masks the traces present in the frames, transforms the frames from (x_p, y_p) pixel to (λ, y_p) wavelength units if the frame was not transformed by `transform`,⁸ and compares the peak wavelength position of the sky lines to the reference sky lines as measured by `SALT`. Finally, a figure is created containing a plot of the background spectra (offset by the respective legend entries superscript) with the known sky lines marked with a vertical line, and a plot of the closest identified peaks of said spectra.

Minor variations in the comparison of the sky lines are expected, such as those seen in Figure 3.12, but any uniform trends, such as those in Figure 3.13 (bottom left), indicate an underlying poor fit across the horizontal axis of the wavelength solution. The full `STOPS skyline` class docstring is given in Listing 3.5.

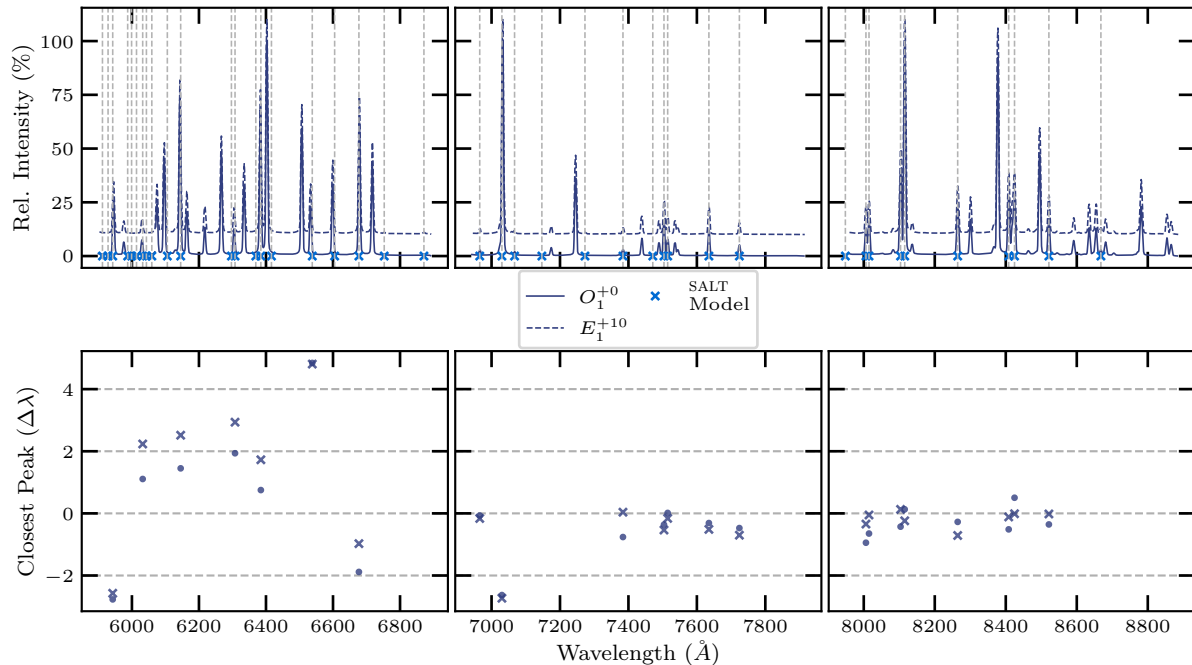


Figure 3.13: An example of a wavelength solution with a poor fit at shorter wavelengths (bottom left), specifically shown for an arc image. Arc lines are Figure created via the `STOPs skyline` method.

3.3.4 Cross Correlation

The `skyline` method allows for confirmation of a single wavelength solution, but has no means for comparing how the wavelength solutions of two polarization beams differ from each other. As the Stokes results, and thus final polarization results, are determined by the difference between the O - and E -beams, a direct comparison is not appropriate.

Any observed unpolarized light, however, will reflect equally in both polarization beams and so the general trend of the two spectra may reasonably be expected to follow one another. The `correlate` method was created to allow for comparisons between the wavelength solutions of the O - and E -beams of a single exposure or the O - or E -beams of differing exposures by cross correlating the spectra.

The `correlate` method loads the `POLSALT spectra extraction FITS` files, removes the continuum and separates the `CCD` regions. The relevant `CCD` regions are cross correlated and the correlation peak is plotted and specified in the plot legend, as seen in Figure 3.14.

Sources under spectropolarimetric observation are generally expected to vary over time and, as such, the ratio of polarized to unpolarized light is also expected to vary. The accuracy of correlation may decrease as features with differences in the polarized component of the polarization beams change, and it is up to the user to determine the validity of the correlation result taking into consideration the two spectra being correlated. The differences in the features of the different spectra are often negligible when compared

⁷Both sky and arc lines are available at <https://astronomers.salt.ac.za/data/salt-longslit-line-atlas/>.

⁸The transformation applied by the `skyline` method uses linear interpolation and is thus less accurate at flux conservation than the transformation applied by the `transform` method.



Figure 3.14: The resultant output plot of the `STOPs correlate` method. Figure created via the `STOPs correlate` method.

to the overall continuum of the spectra and are generally only reflected in a change in the intensity of said features when the continuum is removed. The full `STOPs split` class docstring is given in Listing 3.6.

3.4 General Reduction Procedure

This section aims to provide a comprehensive discussion of the modified reduction procedure, an example of which is provided in Appendix A. As users all employ a variety of operating systems, language environments, and software setups, not much emphasis will be placed on how to get the software running or the managing of files; instead, the general order, seen in Figure 3.15, and commands necessary to complete each step of the reduction process are discussed, assuming that the software is running as intended.

3.4.1 Initial Setup

It is important to note that while `POLSALT` was developed in Python 2 (2.7), the `STOPs` supplementary tools were developed in, and require, Python 3 (3.11+), as well as the other requirements mentioned in § 3.3. While managing multiple versions of Python introduces some extra complication, it would not have been reasonable to develop `STOPs` in Python 2, as it has been deprecated, nor would it have been reasonable to update `POLSALT` to Python 3.

It is therefore recommended that the different versions of Python are managed using separate virtual environments. While the `anaconda` package manager was used in this study and is recommended, any package manager may be used. The Python 2.7 `anaconda` environment is aliased to ‘`salt`’. When Listings are provided (see for example Listing A.1 or the Listings in § 3.4.2 below), the `anaconda` environment is activated at the start of the Listing, otherwise it is assumed the previously specified environment is still active.

Listing 3.6: The ‘docstring’ for `cross_correlate.py`

```
Cross correlate allows for comparing the extensions of multiple FITS files,
or comparing the $0$- and $E$-beams of a single FITS file.

Parameters
-----
data_dir : str | Path
    The path to the data to be cross correlated
filenames : list[str]
    The ecwmxgbp*.fits files to be cross correlated.
    If only one filename is defined, correlation is done against the two polarization beams.
split_ccd : bool, optional
    Decides whether the CCD regions should each be individually cross correlated.
    (The default is True, which splits the spectrum up into its separate CCD regions)
cont_ord : int, optional
    The degree of a chebyshev to fit to the continuum.
    (The default is 11)
plot : bool, optional
    Decides whether the continuum fitting should be plotted
    (The default is False, so no continua plots are displayed)
save_prefix : str, optional
    The name or directory to save the figure produced to. “.” saves a default name to the current working.
    A default name is also used when save_prefix is a directory.
    (The default is None, i.e., The figure is not saved, only displayed)

Attributes
-----
data_dir
fits_list
beams : str
    The mode of correlation. ‘OE’ for same file, and ‘O’ or ‘E’ for different files but same extension.
ccds : int
    The number of CCD’s in the data. Used to split the CCD’s if split_ccd is True.
cont_ord : int
    The degree of the chebyshev to fit to the continuum.
can_plot : bool
    Decides whether the continuum fitting should be plotted
offset : int, DEPRECATED
    The amount the spectrum is shifted, mainly to test the effect of the cross correlation.
    (The default is 0, i.e., no offset introduced)
save_prefix
wav_unit : str
    The units of the wavelength axis.
    (The default is Angstroms)
wav_cdel : int
    The wavelength increment.
    (The default is 1)
alt : Callable
    An alternate method of cross correlating the data.
    (The default is None)

Methods
-----
load_file(filename: Path) -> tuple[np.ndarray, np.ndarray, np.ndarray]
    Loads the data from a FITS file.
get_bounds(bpm: np.ndarray) -> np.ndarray
    Finds the bounds for the CCD regions.
remove_cont(spec: list, wav: list, bpm: list, plot_cont: bool) -> None
    Removes the continuum from the data.
correlate(filename1: Path, filename2: Path | None = None) -> None
    Cross correlates the data.
ftcs(filename1: Path, filename2: Path | None = None) -> None
    Cross correlates the data using the Fourier Transform.
plot(spec, wav, bpm, corrd, lagsdb) -> None
    Plots the data.
process() -> None
    Processes the data.

Other Parameters
-----
offset : int, optional
    The amount the spectrum is shifted, mainly to test the effect of the cross correlation.
    (The default is 0, i.e., no offset introduced)
**kwargs : dict
    keyword arguments.
    Allows for passing unpacked dictionary to the class constructor.
ftcs : bool, optional
    Boolean whether to use Fourier Transform for cross correlation.

See Also
-----
scipy - correlation:
    https://docs.scipy.org/doc/scipy/reference/generated/scipy.signal.correlate.html

matplotlib custom style:
    https://matplotlib.org/stable/users/explain/customizing.html

Notes
-----
Constants Imported (See utils.Constants):
    SAVE_CORR:
        The default save name for the correlation plot.
    OFFSET:
        The vertical offset of spectra in the output plot.
```

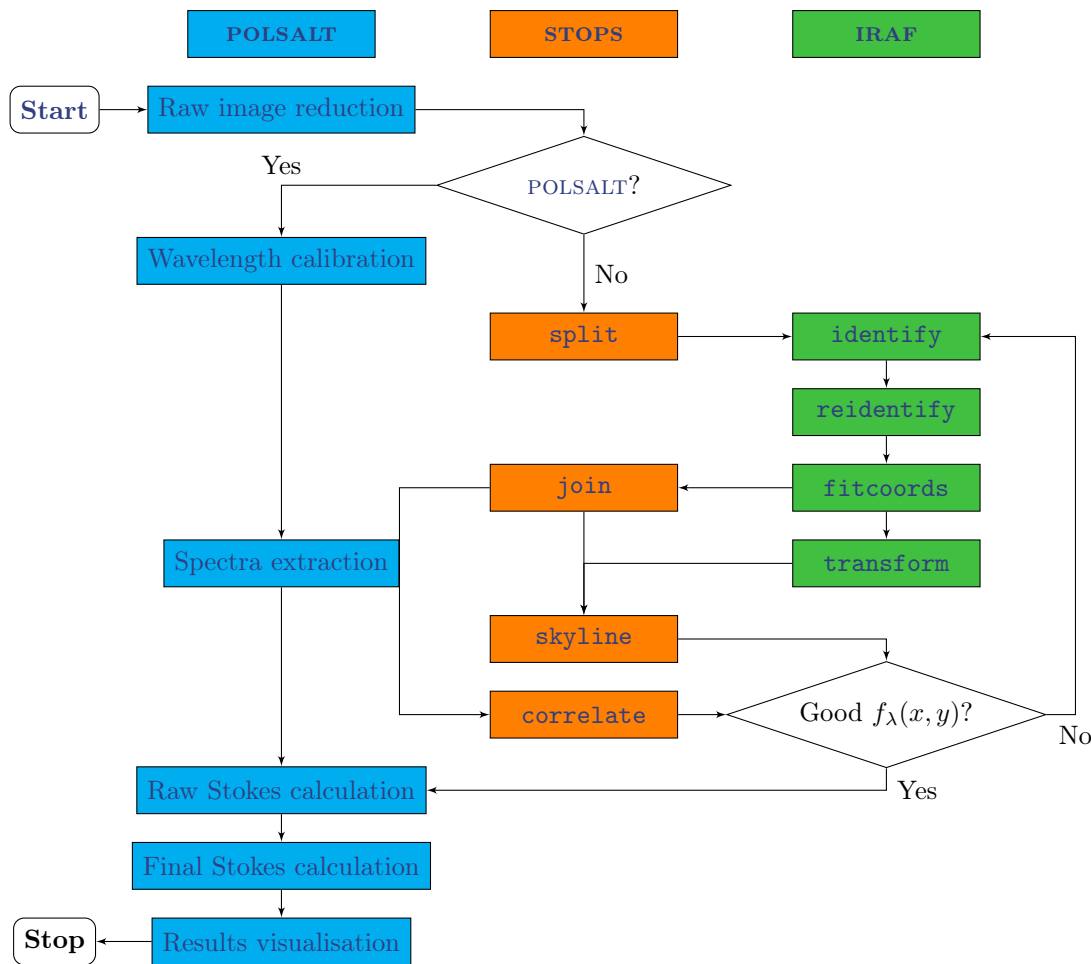


Figure 3.15: A general workflow for data reductions using a combination of **POLSALT**, **IRAF**, and **STOPs**. Diagram adapted from Cooper et al. (2022).

It is recommended to use **POLSALT** through the **GUI** as it provides the user-friendly environment while also sequentially listing each step of the reduction process in a dropdown menu, as seen in Figure 3.1. Reductions are possible, however, purely through the **CLI** using the **POLSALT** ‘beta’ scripts.

3.4.2 **POLSALT** Pre-Reductions

The **POLSALT** reduction process requires a file structure such that the raw data received from **SALT** is located in a folder named using the observing date with a sub-folder named `raw`, following the format `YYYYMMDD/raw/`. This directory structure allows **POLSALT** to create a ‘working’ directory following the format `YYYYMMDD/sci/` which contains all the files modified during the reduction process. Multiple reduction procedures using the same data may therefore be separated by simply renaming the `sci/` sub-folder.

The **POLSALT GUI** may be launched by opening a **CLI** and running the commands given in Listing A.1. Once the window, depicted in Figure 3.1, has launched, ensure that the first two paths at the top of the window point to the **POLSALT** and working directories, as seen in Figure 3.1. The ‘raw image reduction’ entry may then be selected from the dropdown menu and the pre-reductions run.

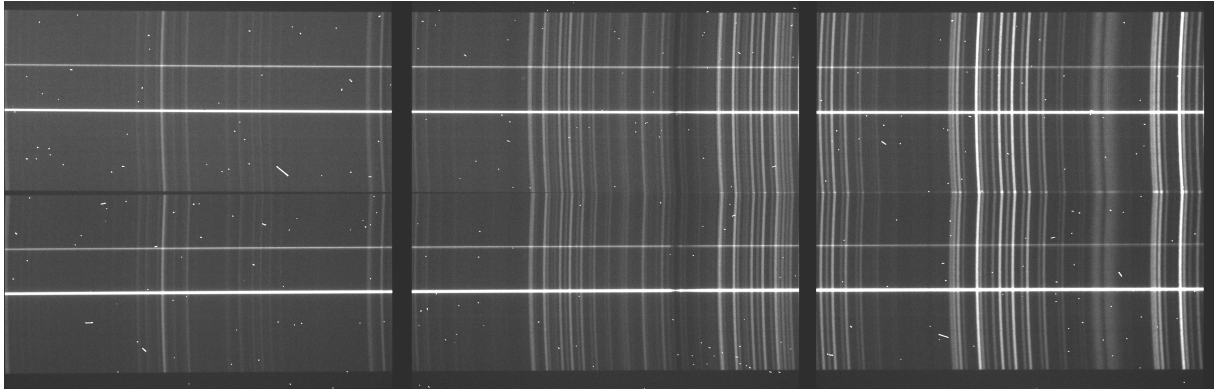


Figure 3.16: The ‘SCI’ extension of a typical spectropolarimetric **FITS** file taken with the **SALT/RSS**, after basic **POLSALT** **CCD** reductions have been completed. Figure created from the **STOPs split** output.

Alternatively, a **CLI** may be used to complete the initial pre-reductions using

```
$ cd <OBSDATE>/sci
$ conda activate salt
$ python ~/polsalt/scripts/reducepoldata_sc.py <OBSDATE>
```

which will start the full **POLSALT** reduction process. This process is quit once the **POLSALT wavelength calibration GUI** opens, and the alternate wavelength calibration procedure is followed.

3.4.3 Wavelength Calibration

The wavelength calibrations may now be completed in **IRAF**. This section concerns the procedure for parsing the **FITS** files to and from both **IRAF** and **POLSALT**, as well as the relevant task names and methods to be run to complete the calibrations. A base working case of each of the tasks and methods are presented in Listing A.2 to A.8, but it should be noted that the art of wavelength calibration consists of modifying the parameters to achieve a well-fit calibration function.

Preparing the Data for **IRAF**

Splitting the data is presented in Listing A.2. The **STOPs split** method may take multiple parameters, as seen in § 3.3, but default parameters should be used wherever possible. The most notable parameters are the directory, which defaults to the current working directory of the **CLI**, the split row, which defaults to **POLSALT**’s default center row, and the save prefix, which defaults to ‘beam0’ and ‘beam1’.

IRAF Wavelength Calibrations

The **IRAF** wavelength calibrations are performed using the tasks described in § 3.2, namely the **identify**, **reidentify**, **fitcoords**, and optionally **transform** tasks.

In general, these tasks are run directly in the **IRAF** terminal using:

```
cl> identify arc_files
cl> reidentify arc_ref arc_files
cl> fitcoords arc_files fit_2d
cl> transform files tr_file fit_2d
```

where ‘arc_files’ refers to a list or file containing the **FITS** files relevant to the task, ‘arc_ref’ refers to the **FITS** file previously identified, ‘fit_2d’ refers to the name to be used for the final two-dimensional wavelength solution, and ‘tr_file’ refers to the new name for the transformed input ‘files’.

The interactive tasks take up the bulk of the reduction time as this is where the fine-tuning of the reduction is done, through the use of cursor (or colon) commands, which allow modification of the parameters mid-reduction. Task parameters may, however, be edited beforehand within the **IRAF** terminal using the **eparam** task, and optionally saved, and quit or run using a combination of :w, and :q or :go cursor commands, respectively.

The reduction process in [Appendix A](#), namely [Listing A.4](#) to [A.7](#), describes how the tasks may be scripted and saved for posterity. It is recommended to create an **IRAF** Command Language (cl) script for each task to keep track of which parameters were used and for simple recalibrations. The scripts are created using the **mkscrip**t task which interactively asks for a task to script and parameters to use. Multiple tasks may be appended to an **IRAF** script, allowing for the parameters of both beams to be tracked.

Running an **IRAF** script may be done by running:

```
cl> cl < script_name.cl
```

but is not suggested for interactive scripts, which run best when simply copied from the <...>/sci/script_name.cl file to the **IRAF** terminal.

Preparing the Data for **POLSALT**

After the wavelength calibrations have been completed, the wavelength solution is parsed back into the format expected by **POLSALT**. Joining the separate beams with their respective wavelength solutions is performed in the **CLI** following [Listing A.8](#).

Similar to the **split** procedure, the **join** procedure has the same defaults defined. The onus of keeping track of any previously changed default parameters falls to the user, but logging is implemented in **STOPS** (see the discussion on help documentation in [§ 3.3](#)) which allows for later reference of any changed parameters.

Sky Line Checks

The optional **IRAF transform** task and **STOPS skylines** method are used to confirm the wavelength solution across the frame (see [§ 3.3.3](#)) by transforming and comparing known and observed sky line wavelength positions, respectively.

The **skyline** method is run in the **CLI** following [Listing A.9](#). As with the rest of **STOPS**, default parameters describe the overplotting behavior for the *O*- and *E*-beams, the skylines provided by **SALT**, and the calculated variation of the wavelength axis of a frame.

Cross Correlation Checks

The **correlate** method is run in the **CLI** following [Listing A.11](#). The input of the **correlate** method takes the output of the **POLSALT spectra extraction** and is thus

only run thereafter, but is mentioned here as the completion of the **POLSALT** reductions is not discussed in much depth. If the user wishes to compare the *O*- and *E*-beams of a single file then only that image name is to be provided, otherwise it is assumed that the user wishes to compare the same polarization beam across each file provided.

Cleaning Up the **IRAF** and **STOPS** Output

Before the final **POLSALT** reductions, it is recommended that the user ‘clean up’ the `sci/` directory of all **IRAF** and **STOPS** files since the ‘wmxgbp’ **FITS** files are all that is expected by **POLSALT**. The **POLSALT** methods use wildcard file collection and as such any errant detections of files added by the user will result in unexpected crashes. It is suggested to move any additional files to a new subfolder following [Listing A.10](#), but they may also be removed using:

```
$ rm beam*.fits arc*.fits frame* <any user created files>
```

3.4.4 **POLSALT** Reduction Completion

Reductions may now be completed using **POLSALT**. The reduction process consists of correcting for the wollaston tilt, extracting the spectra, creating the Stokes files, and displaying the results. The ‘beta’ version of **POLSALT** provides access to a **GUI** but may also be handled entirely through a **CLI** as scripts.

POLSALT Beta in the **GUI**

The reduction process using the **POLSALT GUI** is completed by selecting and, when applicable, interactively modifying the reduction step through the interactive windows, one-by-one, from the **GUI**’s dropdown menu, as explained in [Appendix A](#) (p. 98 onwards).⁹

POLSALT Beta through a **CLI**

Both **GUI** and **CLI** implementations of the **POLSALT** beta pipeline access the same script files. Although the **GUI** is more user-friendly, the **CLI** offers a more streamlined approach to the reduction process, allowing the reduction process to be automated once the **IRAF** wavelength solution is known and parsed into the ‘wmxgbp’ **FITS** file format. A modified version of the **POLSALT** beta `reducepoldata_sc.py` script (see [Listing 3.7](#)) is used to run the entire reduction process without needing to select which process to run next, using:

```
$ python reducepoldata_sc.py YYYYMMDD
```

where the only modification made to the `reducepoldata_sc.py` script file is the removal of a call to the `specpolwavmap` method.

The **POLSALT** beta `reducepoldata_sc.py` copies a `script.py` file into the science working directory, ‘YYYYMMDD/sci/’, which provides analysis scripts for analysis and modification of the **POLSALT** beta results. These tools consist of data culling for the final Stokes calculations, text and plot output, relative flux calibration corrections, and synthetic filtering of polarization results.

⁹See the official **POLSALT** [wiki](#) or alternative online resources such as the **SALT** [workshop slides](#).

Listing 3.7: The modified `reducepoldata_sc.py` script file.

```

import os, sys, glob, shutil
poldir = '/home/justin/polsalt-beta/'                                     # Will differ according to user
reddir=poldir+'polsalt/'
scrdir=poldir+'scripts/'
sys.path.extend((reddir,scrdir,poldir))

datadir = reddir+'data/'
import numpy as np
from astropy.io import fits as pyfits
from specpolview import printstokes
from imred import imred
from specpolwvmap import specpolwvmap
from specpolextract_sc import specpolextract_sc
from specpolrawstokes import specpolrawstokes
from specpolfinalstokes import specpolfinalstokes

print sys.argv
obsdate = sys.argv[1]
print obsdate
os.chdir(obsdate)
if not os.path.isdir('sci'): os.mkdir('sci')
shutil.copy(scrdir+'script.py','sci')
os.chdir('sci')

# basic image reductions
infilelist = sorted(glob.glob('../raw/P*fits'))
imred(infilelist, './', datadir+'bpm_rss_11.fits', crthresh=False, cleanup=True)

# basic polarimetric reductions
logfile='specpol'+obsdate+'.log'                                         # The following lines may be removed or commented out as below

# wavelength map
# infilelist = sorted(glob.glob('m*fits'))
# linelistlib=""
# specpolwvmap(infilelist, linelistlib=linelistlib, logfile=logfile)

#background subtraction and extraction
infilelist = sorted(glob.glob('wm*fits'))
extract = 10.    # star +/-5, bkg= +/- (25-35) arcsec: 2nd order is 9-20 arcsec away
locate = (-120.,120.)      # science target is brightest target in whole slit
#locate = (-20.,20.)

specpolextract_sc(infilelist,logfile=logfile,locate=locate,extract=extract)
#specpolextract_sc(infilelist,logfile=logfile,locate=locate,extract=extract, docomp=True, useoldc=True)

# raw stokes
infilelist = sorted(glob.glob('e*fits'))
specpolrawstokes(infilelist, logfile=logfile)

# final stokes
infilelist = sorted(glob.glob('*_h*.fits'))
specpolfinalstokes(infilelist, logfile=logfile)

```

The `POLSALT` analysis scripts may be run using:

```
$ python script.py
```

followed by `specpolfinalstokes.py`, `specpolview.py`, `specpolflux.py`, or `specpolfilter.py`, for the different analysis modes, respectively.¹⁰

¹⁰Please see <https://github.com/saltastro/polsalt/wiki/Linear-Polarization-Reduction---Beta-version> for a comprehensive discussion of the `POLSALT` beta analysis scripts.

Chapter 4

Testing and Application

This chapter contains an overview of the tests performed during the development of `STOPS` which includes the verification of the modified wavelength solutions (§ 4.1), as well as the application of `STOPS` on observations of both spectrophotometric standards and science targets (§ 4.2).

4.1 Testing `STOPS`

A fundamental requirement during the development of `STOPS` was ensuring that the software was compatible with both the `POLSLT` and `IRAF` file structures and that the ‘reduction-specific’ methods, namely the `STOPS` `split` and `join` methods, provided correct and consistent results. As development is an iterative process, `STOPS` was continually checked to ensure compatibility such that the varying `STOPS` method inputs were correctly parsed, and that their outputs were parsable by the relevant `IRAF` tasks or `POLSLT` methods.

To this end, observations which were verified to have been accurately reduced were duplicated for testing the ‘reduction-specific’ methods, allowing for continual checks of the `STOPS` pipeline to be made during the development process. The testing of the ‘reduction-specific’ methods are discussed in § 4.1.1 and § 4.1.2, respectively.

The secondary requirement during the development of `STOPS` was to provide a means to check the wavelength solutions. This was achieved through the ‘check-specific’ methods, namely the `STOPS` `correlate` and `skylines` methods, which were designed to validate the `IRAF` wavelength solutions, specifically after re-insertion of the wavelength solutions back into the `POLSLT FITS` file format. The file format distinction is necessary as `IRAF` provides immediate confirmation of the wavelength solutions during calibration through interactive `RMS` plots (see e.g., Figure 3.6, 3.7), as well as the transformation of the spectra through the `transform` `IRAF` task, while `POLSLT` only provides confirmation of the `RMS` for the interactive line identification during `wavelength calibration`.

The ‘check-specific’ methods were tested using synthetic spectra, which contained features with known and varying offsets introduced. The features refer to emission lines

Table 4.1: A comparison of the contents of a `POLSLT` pre-reduced `FITS` file to the `STOPs split` *O*- and *E*-beam `FITS` files. Table created using the ‘Astropy’ `fitsinfo` CLI tool.

Filename	No.	Name	Type	Cards	Dimensions	Format
<code>POLSLT</code>	0	‘Primary’	PrimaryHDU	161	-	-
	1	‘SCI’	ImageHDU	19	(3199, 1028)	float32
	2	‘VAR’	ImageHDU	8	(3199, 1028)	float32
	3	‘BPM’	ImageHDU	8	(3199, 1028)	uint8
<code>STOPs split ‘O’</code>	0	‘Primary’	PrimaryHDU	162	(3199, 474)	float32
<code>STOPs split ‘E’</code>	0	‘Primary’	PrimaryHDU	162	(3199, 474)	float32

in the `correlate` related tests and absorption skylines in the `skylines` related tests. The testing of the ‘check-specific’ methods are discussed in § 4.1.3 and § 4.1.4, respectively.

4.1.1 Testing the split Method

The `STOPs split` method accepts any `POLSLT` pre-reduced (‘mxgbp’- prefixed) `FITS` files as input and outputs `IRAF` compatible ([arc|beam][o|e]- prefixed) `FITS` file structures. As no ‘split’ `FITS` files are created during pure `POLSLT` reductions, the `STOPs split` method was tested by comparing the pre-reduced `POLSLT` files to the `split` method’s output files, ensuring the correct structure and data integrity of the files to be handed off to `IRAF`.

Table 4.1 shows the contents of a `FITS` file before and after splitting. The split `FITS` files contain a single ‘Primary’ extension which holds the respective polarization beams’ two-dimensional spectrum as well as a slightly modified copy of the ‘Primary’ header from the ‘pre-split’ file. The differences in the header and data are detailed below.

For the split `FITS` files, the header is left mostly untouched, and is only updated to represent the new data type and shape: the ‘BITPIX’ value is updated, from 8 to -32, and the ‘NAXIS’ value is updated, from 0 to 2; the ‘NAXIS1’ and ‘NAXIS2’ keywords are added, and their values are set to the new split ‘SCI’ data shape; and the ‘EXTEND’ keyword is removed.¹ This accounts for the discrepancy in the ‘Cards’ between the `POLSLT` and `STOPs` file header entries in Table 4.1.

After splitting it was confirmed that the split data was identical to the `POLSLT` ‘pre-split’ file by taking the difference between them, which showed a constant difference of zero. Each split `FITS` file, however, only includes half of the ‘pre-split’ data, for the relevant *O*- or *E*- polarization beam, with the data also being cropped at the top- and bottom-most rows of the `POLSLT` data, with the cropping defaulting to 40 pixels (see § 3.3.1). This accounts for the discrepancy in the ‘Dimensions’ between the `POLSLT` and `STOPs` files in Table 4.1.

This output file structure was chosen for `IRAF` compatibility, and was tested over multiple grating and articulation angles, as well as with various data sets to ensure that the `split` method was robust and reliable.

¹The ‘EXTEND’ keyword indicates that the `FITS` file contains multiple extensions while the ‘NAXIS1’ and ‘NAXIS2’ keywords indicate the shape and size of the data stored in the relevant extension.

Table 4.2: A comparison of the `POLSLALT` wavelength calibrated `FITS` file to the (`IRAF` wavelength calibrated) `STOPS join` `FITS` file. Table created using the `Astropy fitsinfo` CLI tool.

Filename	Ext. No.	Name	Type	Cards	Dimensions	Format
<code>POLSLALT</code>	0	'Primary'	Primary <code>HDU</code>	161	-	-
	1	'SCI'	Image <code>HDU</code>	21	(3199, 514, 2)	float32
	2	'VAR'	Image <code>HDU</code>	10	(3199, 514, 2)	float32
	3	'BPM'	Image <code>HDU</code>	10	(3199, 514, 2)	uint8
	4	'WAV'	Image <code>HDU</code>	21	(3199, 514, 2)	float32
<code>STOPS join</code>	0	'Primary'	Primary <code>HDU</code>	161	-	-
	1	'SCI'	Image <code>HDU</code>	21	(3199, 474, 2)	float32
	2	'VAR'	Image <code>HDU</code>	10	(3199, 474, 2)	float32
	3	'BPM'	Image <code>HDU</code>	10	(3199, 474, 2)	uint8
	4	'WAV'	Image <code>HDU</code>	21	(3199, 474, 2)	float32

4.1.2 Testing the join Method

The `join` method requires both an `IRAF` database with wavelength solutions² for both polarimetric beams, and the `POLSLALT` pre-reduced files as input, and outputs `POLSLALT spectra extraction` compatible ('wmxgbp'- prefixed) `FITS` files. Ensuring that the output format was correct was paramount as the `POLSLALT spectra extraction` method is unable to process the files otherwise, thus halting the reduction process. Thankfully, the `join` method output could be directly compared to the `POLSLALT wavelength calibration` method output files, ensuring that any changes introduced by the `STOPS` pipeline are well characterized.

Table 4.2 shows the `FITS` file information for both the `POLSLALT` and `STOPS` wavelength calibrated files. Other than the 'Dimensions' of each 'Image`HDU`' extension, the `FITS` files have identical structures.³

Although the 'Cards' count is the same, minor differences across the headers are present. The 'HISTORY' keyword, which would have contained the `POLSLALT` 'CRCLEAN' parameters, and which default to 'upper= 4.0, lower= 1.5, sigmaveto= 2.0', is instead modified to contain the implemented `CRR` parameters.⁴

Other minor differences may arise, such as the date-times stored in the 'SAL-TLM' and 'SMOSAIC' keywords, as they contain the date-times relating to the completion of the `POLSLALT` pre-reductions. This accounts for the differences in the 'Cards' between the `POLSLALT` and `STOPS` file header entries in Table 4.2.

Figure 4.1 shows the differences in the data between the `POLSLALT` and `STOPS` wavelength calibrated files. It can be seen that the 'VAR' extensions (Figure 4.1b) are identical. The difference in the 'SCI' extensions (Figure 4.1a) is due to the `CRR` applied by `STOPS`

²A custom wavelength solution may also be used.

³The 'Dimensions' differ due to the aforementioned cropping of the top- and bottom-most rows of the pre-reduced `FITS` files data.

⁴The `POLSLALT` pipeline performs `CRR` using a 10σ spike to cull cosmic rays. See the `source code` of `POLSLALT` for more information.



Figure 4.1: The difference of the `FITS` file extensions between the `POLSALT` and `STOPS` (`wmxgbp`- prefixed) wavelength calibrated files. Figures created using both the `POLSALT` and `STOPS` versions of the `POLSALT spectral extraction` input.

which rejects cosmic rays from the ‘SCI’ extension instead of masking the ‘BPM’ extension (Figure 4.1c) which is the method implemented by `POLSLALT`. The valid wavelength calibrated region is used as a mask and applied to the ‘BPM’ and ‘WAV’ extensions (Figure 4.1d). Slight differences arise near the centre of the frames, specifically Figure 4.1c and 4.1d, since the correction for the wollaston tilt, as implemented by `POLSLALT`, is reimplemented in Python 3 by `STOPS` and as such may be affected by rounding differences. The differences are fortunately minor and are at the edges of the two polarimetric spectral regions. The ‘WAV’ extensions contain the differing wavelength solutions and as such naturally differ. This accounts for the differences in the data between the `POLSLALT` and `STOPS` files.

Finally, the `STOPS` `join` method was tested to ensure compatibility and correctness of the output data in comparison to `POLSLALT`. This involved testing the `join` method with various data sets, with differing observation configurations, to ensure that the output files were accurate and consistent.

4.1.3 Cross Correlation Checks

The `correlate` method returns plots validating the wavelength solutions and so only has to accept the files output from the `POLSLALT spectra extraction` method (‘ecwmxgbp’-prefixed files).

The `STOPS` `correlate` method was tested by cross correlating synthetic *O*- and *E*-beam spectra with known offsets, with the aim of reacquiring said offsets, as shown in Figure 4.2. The spectra were generated with a feature in each `CCD` region, randomly offset in both the wavelength and intensity axes, Figure 4.2a. The features were purposefully chosen to be of low `SNRs` and `FWHM` to test the robustness of the `correlate` method. Non-synthetic spectra will include more features, with higher `SNRs` and `FWHM`, and as such will be more robust to the `correlate` method.

Through cross correlation, Figure 4.2b, the introduced offsets, or ‘max lag’, were reacquired. For spectral regions with few features or features with a low `SNR` (such as the left most `CCD` region of Figure 4.2b), correlation may fail to determine the correct offset. When a returned ‘max lag’ peak is not significant when compared to the noise in the correlation plots, the `SNR` of the features may be too low for an accurate calculation of the offset.

4.1.4 Sky Line Checks

The `skylines` method returns plots validating the wavelength solutions and so has to accept as input the files output from the `STOPS` `join` method.

In order to validate the `STOPS` `skylines` method, a synthetic two-dimension spectrum was created that contained sky lines. This is shown in Figure 4.3a, and consists of an average continuum (10 ‘counts’) with added noise (normal-sampled, $\sigma = 4.5$), skyline emission features (provided by `SALT`, see § 3.3.3), and the characteristic `RSS` chip gaps. Figure 4.3b shows the result, which successfully retrieves the skyline emission features for the synthetic spectrum. Note that the closest peaks ($\Delta\lambda$) are nearly never 0, since

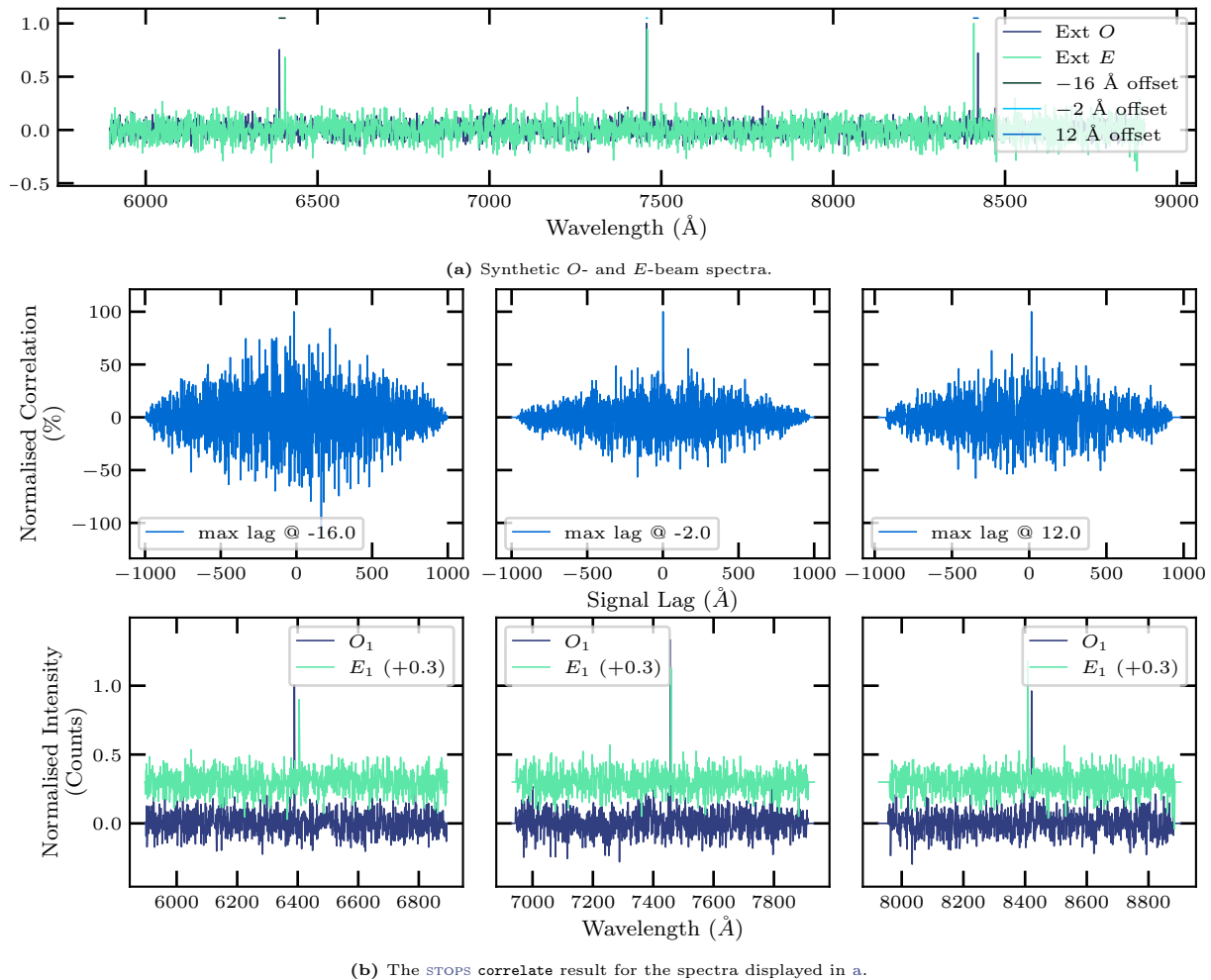
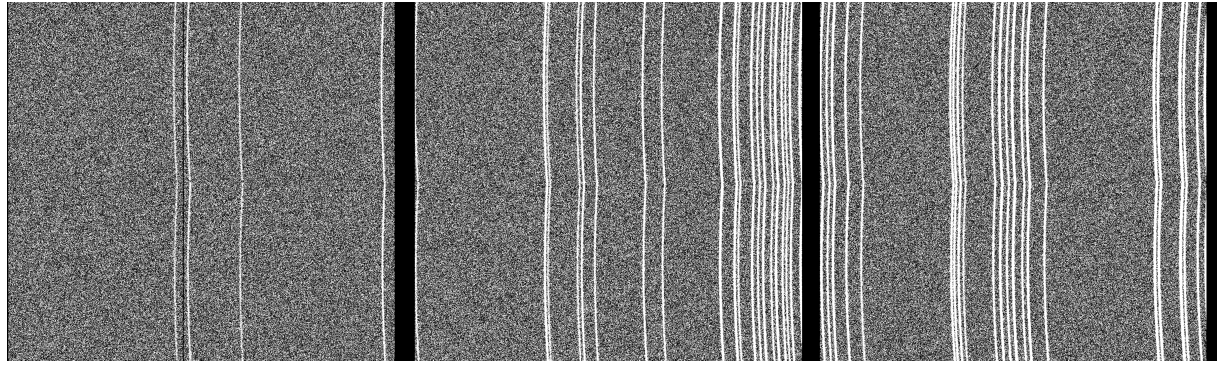
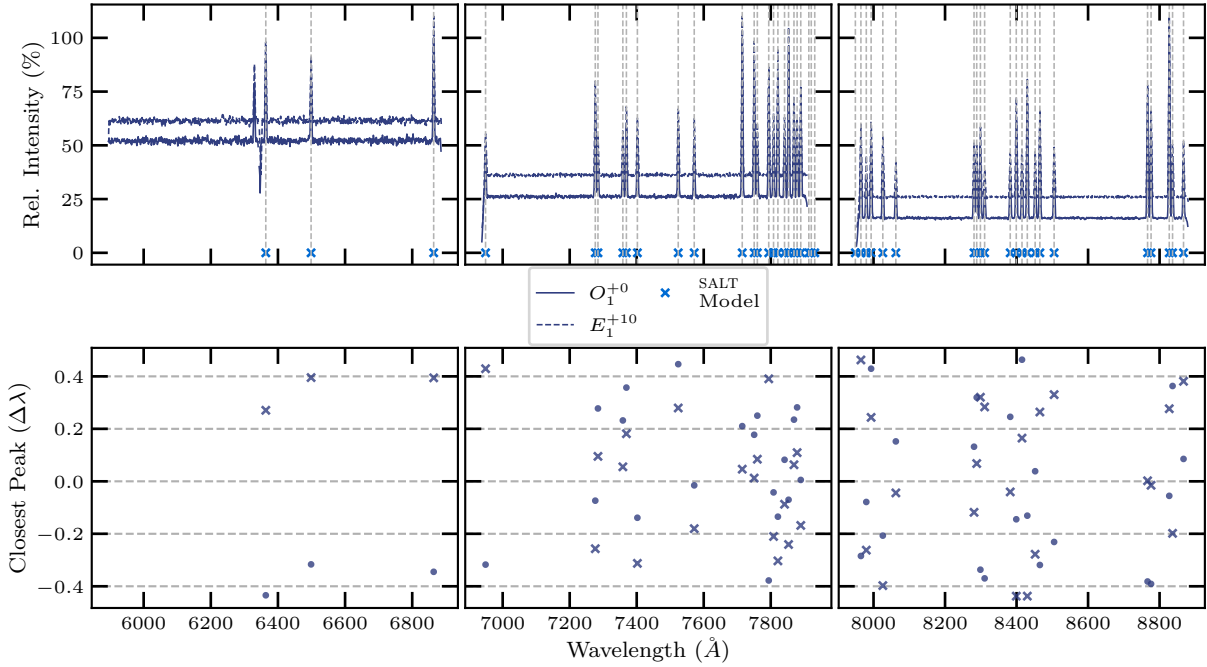


Figure 4.2: Reacquisition of offsets introduced to the O - and E -beam spectral features (a) by cross-correlation (b, bottom row).



(a) A generated two-dimensional spectrum consisting of noise, skyline emission features, and the characteristic RSS chip gaps.



(b) The `STOPs skylines` output for the synthetic spectrum displayed in a.

Figure 4.3: The `STOPs skylines` method output (b) for a synthetic two-dimensional spectrum (a). Figures generated using Python (a) and the `STOPs skylines` method (b).

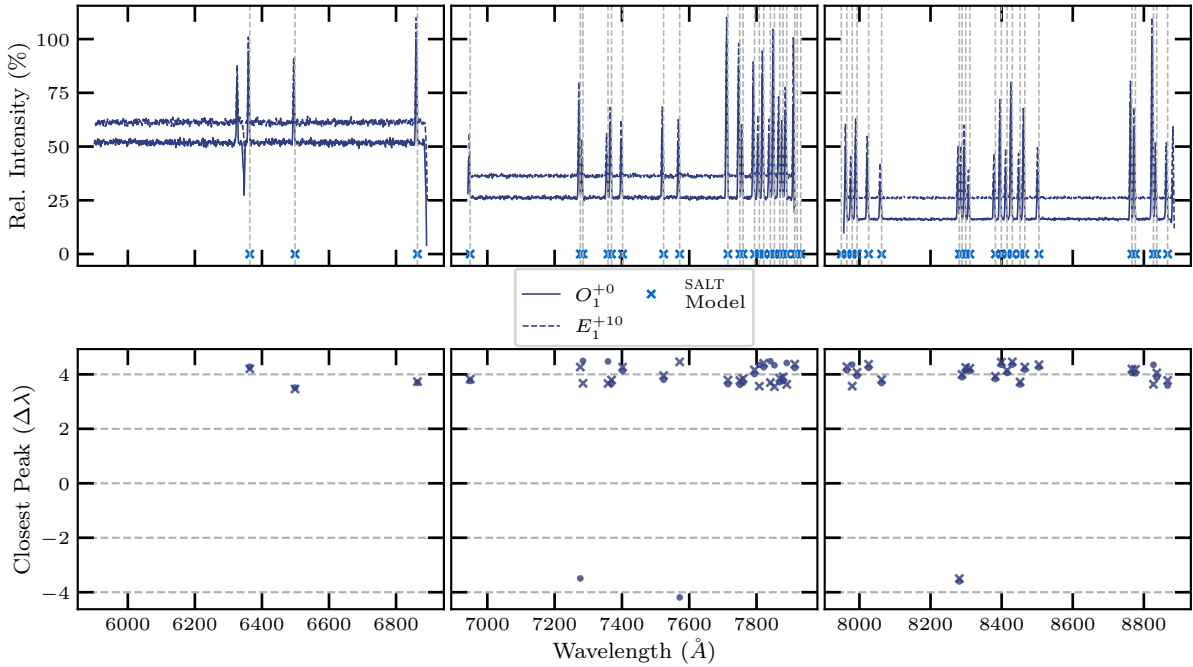


Figure 4.4: The `STOPSSkylines` output for a two-dimensional spectrum, as described in Figure 4.3b, with a constant offset of 4 \AA applied to all skyline emission features. Figure created using the `STOPSSkylines` method.

the skylines are only as accurate as the spectral pixel resolution ($\approx 1\text{ \AA}$ in our synthetic spectrum) while those as provided by `SALT` are not similarly limited. Additionally, the noise in the spectrum may shift a skylines' peak position, further contributing to, albeit small, discrepancies.

Figure 4.4 shows the result of the `STOPSSkylines` method when a constant offset of 4 \AA is applied to all skyline emission features in Figure 4.3a. In general, the offset is recovered, with the minor variation in the closest peaks once again noticed. The closest peaks near $\Delta\lambda \approx -4\text{ \AA}$ are the most notable outliers, and are due to misidentifications of skyline features with neighbors closer than 8 \AA .

4.2 Application of `STOPSS`

The `STOPSS` pipeline has been utilized for the reduction of a number of sources: this includes calibration tests using spectropolarimetric standards; and for scientific observations of transient sources, specifically [Gamma-ray Bursts \(GRBs\)](#) and blazars. The following sections summarize works in which observations were analysed using, in part, the `STOPSS` pipeline with [IRAF](#) wavelength calibrations, or from which the `STOPSS` pipeline was developed. The list of sources observed are summarized in [Table 4.3](#). In addition to the results discussed here, the `STOPSS` pipeline has also been extensively used for the analysis of the blazars presented in [Barnard et al. \(2022, 2024\)](#).

Table 4.3: Sources discussed from proceedings and publications within this section. Table adapted from observations presented in Buckley et al. (2021); Cooper and van Soelen (2023); Cooper et al. (2022); Schutte et al. (2022).

Source	Observation Date	Grating	Grating Angle (°)	Articulation Angle (°)	Exposure Time (sec)
4C +01.02	2016-07-09	PG0300	5.375	10.66	2400.82
	2017-07-25	PG0300	5.375	10.66	2400.83
Hiltner 600	2017-02-24	PG0900	12.500	24.91	135.60
			19.625	39.16	135.60
3C 279	2017-03-28	PG0900	12.498	24.91	480.81
			19.625	39.16	480.80
	2017-04-01	PG0900	12.500	24.92	480.78
			19.625	39.17	480.85
			12.500	24.92	720.83
	2017-05-17	PG0900	19.625	39.17	901.05
GRB 191221B	2019-12-21	PG0300	5.375	10.71	2400.84
EGGR 21	2020-01-10	PG0300	5.375	10.71	120.20
Hiltner 652	2022-06-10	PG0900	12.878	25.71	48.50

4.2.1 Spectropolarimetry and Photometry of the Early Afterglow of the Gamma-ray Burst GRB 191221B (Buckley et al., 2021)

Buckley et al. (2021) discusses the spectropolarimetric and photometric results of the early afterglow of GRB 191221B, a γ -ray burst initially detected by the Neil Gehrels *Swift* Observatory (*Swift*) Burst Alert Telescope (BAT) (Barthelmy et al., 2005) on 2019 December 21 (Laha et al., 2019). The afterglow was observed using the SALT/RSS in spectropolarimetric mode ≈ 3 h after the initial burst, with observations carried out during the re-brightening phase. Follow-up spectropolarimetric observations were also taken ≈ 10 h after the burst using the Very Large Telescope (VLT) Focal Reducer and Low Dispersion Spectrograph (FORS).

The SALT/RSS spectropolarimetric observations were reduced using a modified version of the POLSALT pipeline, allowing for relative flux calibrations of the spectra using the white dwarf, EGGR 21. GRB 191221B was observed at an average polarization level of $\Pi = 1.5 \pm 0.5\%$, and a polarization angle of $60 \pm 10^\circ$ across the $3900 - 8000 \text{ \AA}$. The VLT/FORS2 observations showed a similar polarization level ($\Pi = 1.2\%$) and polarization angle (60°) across the $3200 - 9200 \text{ \AA}$ wavelength region. These low polarization percentages are expected for afterglows this late, when the emission is understood to be dominated by the forward shock which exhibits no systematic orientation of the magnetic field configuration.

Figure 4.5 shows the normalized spectra of the SALT RSS and VLT FORS2 observations, offset by ± 0.05 , respectively. The spectra show a good agreement across the measured position of the proposed absorption features, with the FORS2 spectrum being able to resolve three close pairs of lines, namely, Fe II 5096/5114 \AA , Mg II 5481/5494 \AA , and Mg II 6002/6018 \AA , which were unresolved in the RSS spectrum.

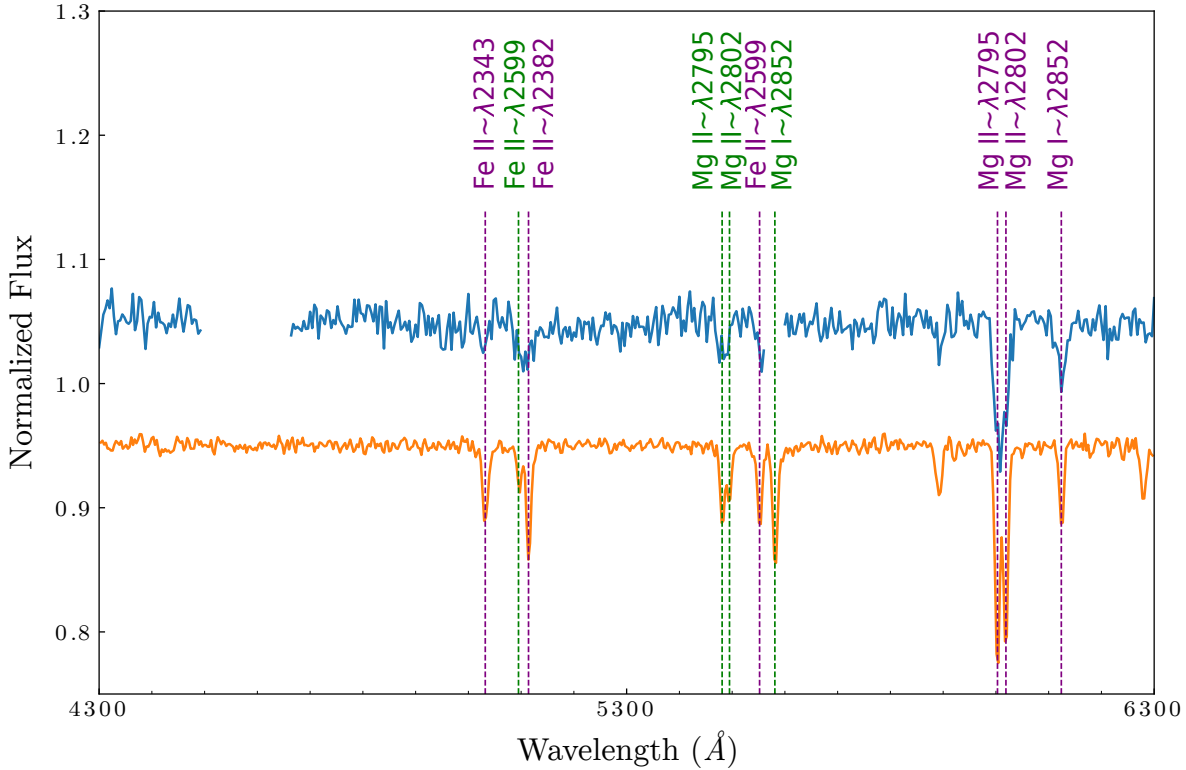


Figure 4.5: Comparison of the normalized (and offset by ± 0.05) spectra of GRB 191221B as obtained with the [SALT/RSS](#) (blue, ≈ 3 h post initial burst) and the [VLT/FORS2](#) (orange, ≈ 10 h post initial burst). Note the chip gap and region of sky subtraction from the [RSS](#) spectrum. Figure adapted from ([Buckley et al., 2021](#)).

Table 4.4 shows the measured absorption line properties, specifically for the [FORS2](#) spectrum due to its higher [SNR](#) and better line resolution than the [RSS](#) spectrum. Two distinct redshifts were acquired from the absorption line measurements, namely $z = 0.960 \pm 0.0017$ and $z = 1.142 \pm 0.0078$. Initial analysis of the spectrum by the [Swift/Ultraviolet Optical Telescope \(UVOT\)](#) team ([Kuin and Swift/UVOT Team, 2019](#)) placed the redshift at $z = 1.19$, which was later further refined by [Vielfaure et al. \(2019\)](#) who reported a redshift for the host galaxy of $z = 1.148$, as well as a fainter intervening system at $z = 0.961$, firmly agreeing with the measured redshifts found with [RSS](#) and [FORS2](#).

4.2.2 Development of Tools for the [SALT/RSS](#) Spectropolarimetry Reductions: Application to the Blazar 3C 279 (Proceedings of Science, HEASA 2021)

As discussed in [Cooper et al. \(2022, see also Appendix C\)](#), it was shown that alternative wavelength solutions, such as those created using [IRAF](#), are capable of being applied to [SALT](#) spectropolarimetric data. The ‘additional tools’ mentioned therein, which were the precursor to the [STOPs](#) pipeline, were used during the reduction of the blazar 3C 279.

The blazar 3C 279 was observed in linear spectropolarimetry mode, on 2017 May 17, using the PG0900 grating with two different grating angles (12.5° and 19.5°). The grating and articulation angles used for the observations (see Table 4.3) matched those of observations of the spectrophotometric standard star, Hiltner 600, observed on 2017 February 24, allowing the intensity to be relatively flux calibrated.

Table 4.4: Properties of the identified absorption lines within the spectra. The measured redshifts of the identified features correspond neatly to two distinct redshifts. Table adapted from [Buckley et al. \(2021\)](#).

Line ID	Rest Wavelength (Å)	Observed Wavelength (Å)	FWHM (Å)	EW (Å)	z
Fe II	2343	5032.35 ± 1.44	5.44 ± 1.43	0.83 ± 0.26	1.148
Fe II	2599	5096.67 ± 2.19	4.70 ± 2.26	0.45 ± 0.23	0.961
Fe II	2382	5114.49 ± 0.90	4.67 ± 0.96	1.10 ± 0.23	1.147
Mg II	2795	5481.56 ± 1.57	4.10 ± 1.67	0.67 ± 0.21	0.961
Mg II	2802	5494.59 ± 2.19	3.93 ± 2.29	0.45 ± 0.19	0.961
Fe II	2599	5552.48 ± 1.25	4.01 ± 1.25	0.62 ± 0.19	1.136
Mg I	2852	5581.78 ± 0.91	4.44 ± 0.91	1.05 ± 0.22	0.957
Mg II	2795	6002.98 ± 0.37	4.56 ± 0.40	2.08 ± 0.25	1.148
Mg II	2802	6018.71 ± 0.14	4.38 ± 0.43	1.83 ± 0.24	1.148
Mg I	2852	6124.64 ± 1.28	4.10 ± 1.30	0.69 ± 0.22	1.128

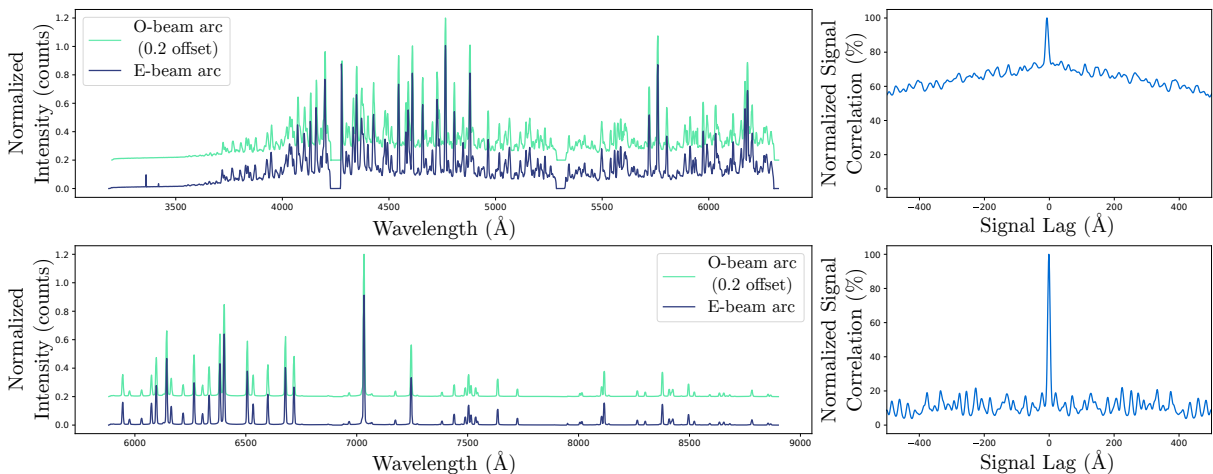


Figure 4.6: The spectra and cross correlation of the *O*- and *E*-beams of the ThAr (top) and Ne (bottom) arc lamps. Figure adapted from ([Cooper et al., 2022](#)).

Figure 4.6 shows the spectra and cross correlation of the *O*- and *E*-beams of the ThAr and Ne arc lamps, also with grating angles of 12.5° and 19.5° , respectively. The cross correlation of the arc lamps perpendicular polarization beams show clear peaks at 0 lag, indicating that the wavelength solutions are consistent across the two polarization beams.

Figure 4.7 shows the relative flux calibrated intensity, percentage of linear polarization, and polarization angle of the blazar 3C 279, across the visible spectrum. The spectra display a good overlap between the two grating angles, especially when considering the variable nature of blazars as well as the fact that the spectra are only relatively flux calibrated. Both the percentage of linear polarization and the polarization angle agree well across the grating angle overlap.

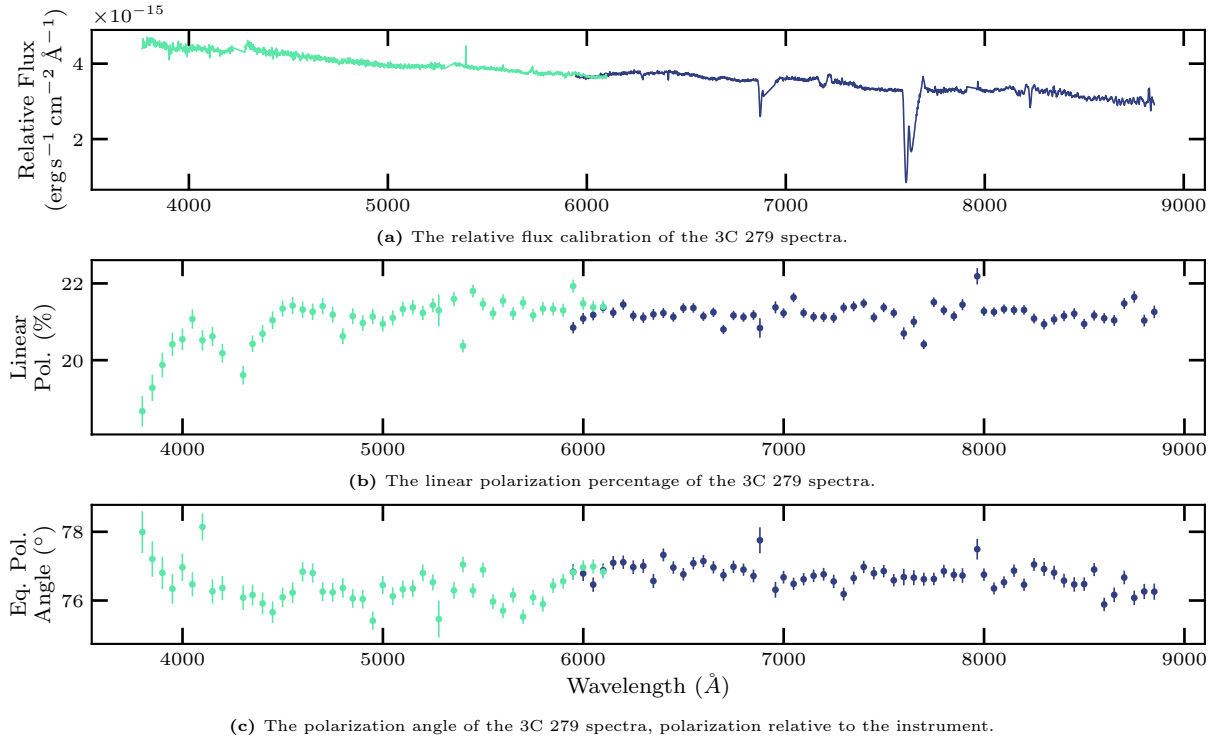


Figure 4.7: The relative flux calibrated spectra (a), linear polarization percentage (b), and polarization angle (c) of the blazar 3C 279 observed on 2017 May 17. Figure adapted from [Cooper et al. \(2022\)](#).

4.2.3 Spectropolarimetric observations of 3C 279

As was, in part, presented in [Cooper and van Soelen \(2023, see also Appendix C\)](#), the Flat Spectrum Radio Quasar (FSRQ) 3C 279 was observed with the SALT/RSS in linear spectropolarimetric mode in 2017 during periods of enhanced and flaring γ -ray activity.

Figure 4.8 shows the γ -ray photon flux from 3C 279 for energies between 0.1 – 100 GeV, observed using the *Fermi* Large Area Telescope (*Fermi*-LAT),⁵ with the dates of the optical observations noted by the vertical lines. The γ -ray flux was between 4 – 8 times brighter when compared to the mean quiescent state (horizontal line). Observations were taken with the PG0900 grating and a slit width of 1.5'', with two grating angles (12.5° and 19.625°), covering a wavelength range of $\lambda \approx 3300 - 8800 \text{ \AA}$. The spectrophotometric standard star, Hiltner 600, was also observed as part of these observations. See Table 4.3 for the details of each observation.

As a test of the STOPS pipeline, it was found that there was no noticeable effect on the polarization properties of spectropolarimetric data, when compared to the POLSALT pipeline. The measure of the goodness of fit for the wavelength solutions could also be measured, both through correlation and measuring the position of skyline features for both the *O*- and *E*-beams.

⁵Data from the *Fermi* Light Curve Repository (*Fermi* LCR) ([Abdollahi et al., 2023](#))

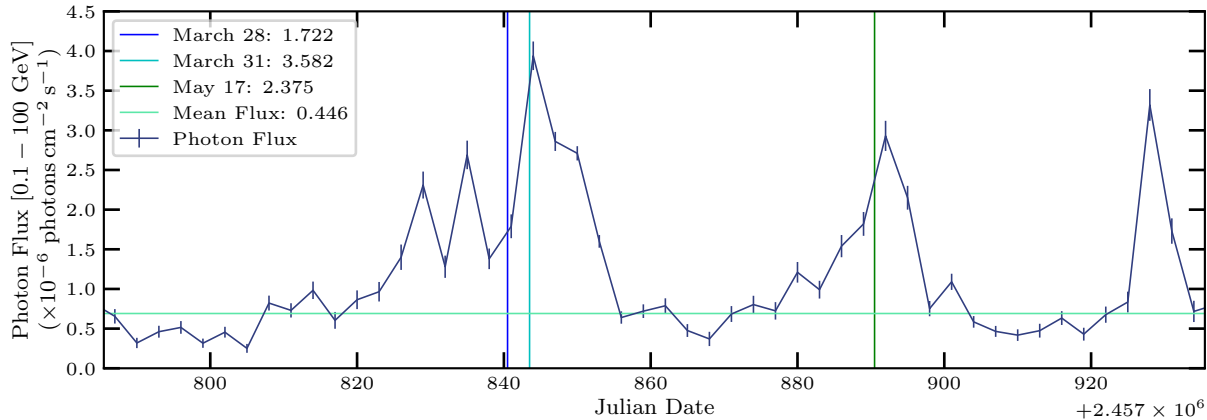


Figure 4.8: The *Fermi-LAT* photon flux [0.1 – 100 GeV] for 3C 279 as measured around the dates of the SALT/RSS spectropolarimetric observations (indicated by the vertical lines). Also included are the ‘mean’ γ -ray fluxes ($\times 10^{-6}$) for the observation dates, calculated using linear interpolation of the *Fermi-LAT* data points. The horizontal turquoise line shows the mean quiescent flux for this source. Figure created using data sourced from the *Fermi* Light Curve Repository (*Fermi* LCR).⁶

Figure 4.9 shows the spectropolarimetry results for the PG0900 observations of 3C 279, presenting, from top to bottom, the normalized, relative flux calibrated, spectra for both grating angles (12.5° and 19.625° , observed in that order), the percentage of linear polarization, and the polarization angle. It is important to note that, while the flux calibration did not produce an identical shape near the overlap regions of the spectrum (compare top two panels), the reductions are able to achieve very good agreements between the degree and angle of polarization (bottom two panels). The difference between the polarization percentage and polarization angle for the two grating angles is $\sim 0.25\%$ and $\sim 1.25^\circ$, respectively. The most notable disagreement of the polarization properties is seen, during the 2017 March 31 observation, but may be explained due to the flaring state of the blazar, the asynchronous times for the two observations, and a lower SNR near the edges of the RSS. The discrepancy in the shape of the flux calibrated spectra is attributed to poor fitting of the standard star near the end of the spectra, due to gaps between the standard flux points as obtained from the European Southern Observatory (ESO) catalog.⁷

The observations show a variation in the linear polarization across the observations, with the level and angle of polarization varying by $\sim 12\%$ and $\sim 24^\circ$, respectively. Surprisingly, the highest level of polarization is not found during the brightest γ -ray peak (2017 March 31), but rather during the dimmest γ -ray flux state (2017 March 28). Past observations of 3C 279 place the polarization during quiescence at $\Pi \approx 10\%$ (see e.g., Marshall et al., 2024), falling within the range observed during the peak in the γ -ray flare ($\Pi = 9.2 \pm 1.1\%$). 3C 279 is also known to show large, rapid minute-scale, variations in the polarization angle (Ackermann et al., 2016), possibly linked to repeating γ -ray activity (Blinov et al., 2021). An unordered magnetic field would lead to depolarization effects, and aligns with the polarization results in Figure 4.9. The disparity between the flaring γ -ray and apparent quiescent optical regimes may be due to for example, a turbulent magnetic field located in the optical emission region. An unordered magnetic field would lead to depolarization effects, and aligns with the observed spectropolarimetric results.

⁶[https://fermi.gsfc.nasa.gov/ssc/data/access/lat/LightCurveRepository/source.html?
source_name=4FGL_J1256.1-0547](https://fermi.gsfc.nasa.gov/ssc/data/access/lat/LightCurveRepository/source.html?source_name=4FGL_J1256.1-0547)

⁷Hiltner 600 is available from the ESO catalog at <https://www.eso.org/sci/observing/tools/standards/spectra/hilt600.html>.

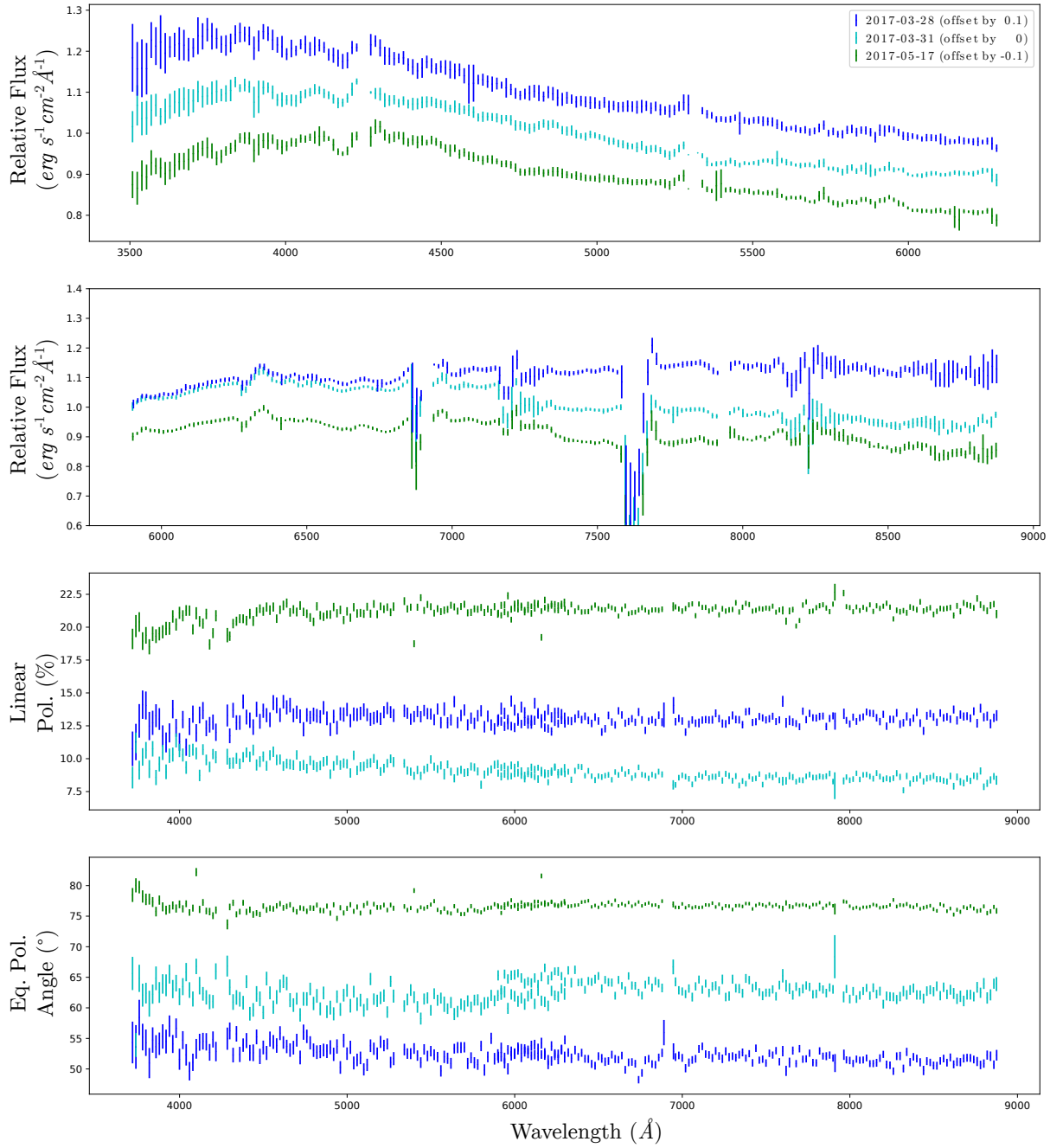


Figure 4.9: Spectropolarimetric results for 3C 279 during two distinct periods of flaring. The normalized relative flux is presented for both grating angles, 12.5° (top) and 19.625° (second from top). Figure sourced from (Cooper and van Soelen, 2023).

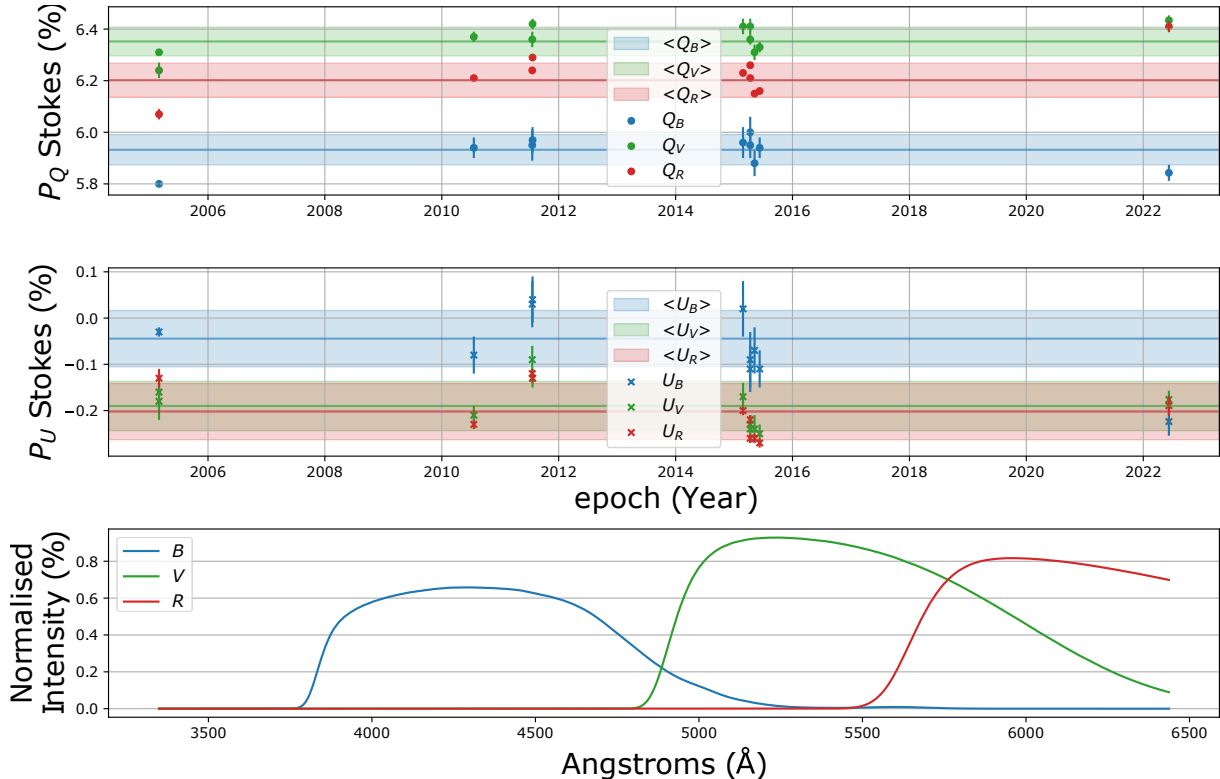


Figure 4.10: The reduced Q and U Stokes parameters for Hiltner 652, pre–2006 for published FORS1 data, 2010 – 2016 for published FORS2 data, and post–2022 for Stokes parameters observed with SALT and convolved with the Johnson-Cousins photometric system filter pass-bands. The horizontal lines and shaded regions refer to the FORS mean and 1σ regions, respectively. Finally, the bottom plot shows the Johnson-Cousins photometric system filter pass-band's used by POLSALT to calculate the Stokes parameters in the different filters. Figure sourced from (Cooper and van Soelen, 2023).

4.2.4 Comparison of Hiltner 652 to previous VLT/FORS observations

The spectropolarimetric observation of Hiltner 652 provided an opportunity to draw comparisons to previous observations of this source (presented in part in Cooper and van Soelen, 2023). Figure 4.10 shows the comparison between the reduced Q and U Stokes parameters for Hiltner 652 as observed with the VLT/FORS1 and VLT/FORS2 (as reported by Cikota et al., 2017; Fossati et al., 2007), and the SALT/RSS observations.

Photometric polarization results for Hiltner 652 were obtained from the spectropolarimetric results by running the POLSALT `specpolfilter.py` script.⁸ This script convolves the SALTICAM filter throughput with the relative flux (or intensity) spectrum to produce the weighted polarization and polarization error for each filter. Figure 4.10 shows that the Stokes parameters of Hiltner 652 are consistent across the different instruments, mostly falling within a standard deviation of historical results. Minor discrepancies are present, but can be due to multiple compounding effects, such as differing instrumental setups, and varying atmospheric conditions.

⁸See the POLSALT ‘Linear Polarization Reduction. Beta version’ wiki for documentation on the `specpolfilter.py` script.

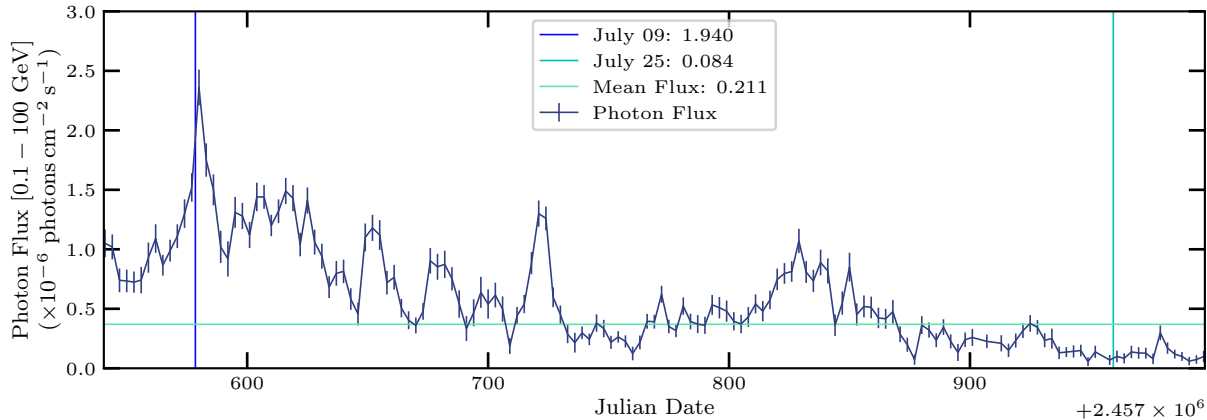


Figure 4.11: The *Fermi-LAT* photon flux [0.1 – 100 GeV] for 4C +01.02 as measured around the dates of the SALT/RSS spectropolarimetric observations (indicated by the vertical lines). Also included are the ‘mean’ γ -ray fluxes ($\times 10^{-6}$) for the observation dates, calculated using linear interpolation of the *Fermi-LAT* data points. The horizontal turquoise line shows the mean quiescent flux for this source. Figure created using data sourced from the *Fermi LCR*.⁹

4.2.5 Modeling the Spectral Energy Distributions and Spectropolarimetry of Blazars - Application to 4C +01.02 in 2016 – 2017 (Schutte et al., 2022)

Schutte et al. (2022) presented the results from spectropolarimetric observations and modeling of the SED for the blazar 4C +01.02 during a flaring and a quiescent state. The optical spectropolarimetric observations of the blazar were completed using the SALT/RSS in spectropolarimetric mode, with observations taken on 2016 July 09 and 2017 July 25, also noted in Table 4.3.

Figure 4.11 shows the photon flux of 4C +01.02 for 0.1 – 100 GeV energies as provided by the *Fermi LCR*. The figure shows that during the optical observations of 4C +01.02, the source was at γ -ray fluxes of $F \approx 1.9 \times 10^{-6}$ and $F \approx 0.1 \times 10^{-6}$ ph. cm $^{-2}$ s $^{-1}$, as compared to a quiescent ‘median’ flux of $\langle F \rangle = 0.21 \times 10^{-6}$ ph. cm $^{-2}$ s $^{-1}$.

The normalized, continuum-subtracted, intensity spectra as well as the polarization percentage for the 2016 and 2017 epochs are presented in Figure 4.12. The spectral features were identified using the known redshift of 4C 01.02 of $z = 2.1$. The quiescent state spectrum exhibits more prominent features than during the flaring state, with the CIV line being the most prominent feature present in both spectra. The increase in the spectral line intensity during the quiescent γ -ray state is due to the non-thermal continuum emission being fainter, as compared to the flaring state.

The linear polarization percentages averaged $\Pi = 10.04 \pm 1.03\%$ and $1.72 \pm 0.93\%$ during flaring and quiescence, respectively.

⁹https://fermi.gsfc.nasa.gov/ssc/data/access/lat/LightCurveRepository/source.html?source_name=4FGL_J0108.6+0134

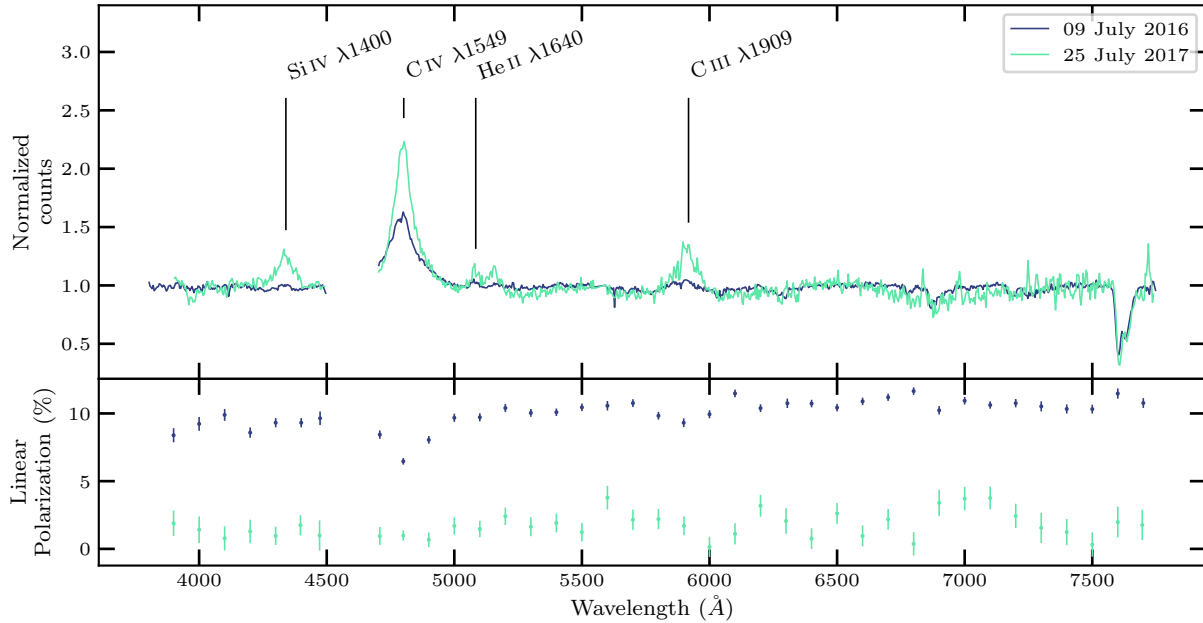


Figure 4.12: Spectropolarimetric results for 4C +01.02 during periods of flaring and quiescence. The spectra presented have been continuum subtracted and normalized. Figure adapted from (Schutte et al., 2022).

The **STOPS** pipeline has already proven its worth, aiding in the reduction of numerous spectropolarimetric observations beyond the select few presented above (see e.g., Barnard et al., 2024). Wavelength calibrations are, by far, the most time consuming part of spectropolarimetric data reductions. The **STOPS** software enables faster and thorough wavelength calibrations through external tools, such as **IRAF**, as well as providing methods to ensure the accuracy of the produced wavelength solutions. This decreases the time necessary for reductions while still ensuring their accuracy, allowing the analysis of the results to take precedence.

Chapter 5

Conclusions

This chapter contains an overview of the `STOPS` software, with a focus on its development and testing (§ 5.1), the findings from the application of `STOPS` to `SALT/RSS` spectro-polarimetric data (§ 5.2), and a discussion on the future of the `STOPS` software (§ 5.3).

5.1 A Broad Overview of `STOPS`

Means to provide a more streamlined wavelength calibration process for `SALT/RSS` spectropolarimetric data were desired, specifically when working with `SALT` arc lamps with poor uniform spectral coverage, e.g., the `Ar` arc lamp used in conjunction with the PG0300 grating. This led to the development of the `STOPS` software, and, more specifically, the `STOPS` `split` and `join` methods (see § 3.3.1, and 3.3.2), which allow alternate wavelength calibrations to replace the `POLSALT` wavelength calibration.

With the introduction of alternate wavelength solutions, the `STOPS` software was further developed to allow the user to quickly identify any faults in the wavelength solutions. This was achieved through the development of the `STOPS` `skylines` and `correlate` methods (see § 3.3.3, and 3.3.4), which allow for the identification of offsets in skyline features and the comparison of the wavelength solutions across *O*- and *E*-beams, respectively.

To ensure the accuracy and reproducibility of the `STOPS` software, testing was conducted, for each method, on both synthetic and real-world data (see § 4.1). A comparison of the `split` method's inputs and outputs showed that the data were unaffected during conversion from a dual beam to a single beam format, allowing accurate wavelength solutions to be found. The largest discrepancies introduced by the `split` method, other than the splitting of the *O*- and *E*-beams to separate files, are the cropping of the non-exposed regions of the `CCD`, and the removal of extensions, both of which are not used during `IRAF` wavelength calibrations.

Similarly, when comparing the output of the `STOPS` `join` and `POLSALT` wavelength calibration methods the alternate wavelength solutions are unaffected, although they differ slightly due to the different wavelength calibration method used, when converted back to the `POLSALT` format, thus providing `POLSALT` with accurate alternate wavelength

solutions for both polarimetric beams. The largest discrepancies introduced by the `join` method are the non-wavelength related processes as handled by `STOPS` to substitute the `POLSLT wavelength calibration`, specifically the handling of Wollaston corrections near the beam intersection (see § 2.2.2) and the `CRR` being applied to the ‘`SCI`’ extension instead of the ‘`BPM`’ extension. Both of these discrepancies, however, do not affect `POLSLT`, the rest of the reduction process, or the final results.

It is possible, and recommended, to ensure the accuracy of the wavelength solutions within whichever alternate wavelength calibration software the user decides to use, e.g., `IRAF`, or Python. The `STOPS skylines` and `correlate` methods were, therefore, developed to determine the accuracy of the wavelength solutions. To eliminate variability inherent in real-world data, synthetic data were generated and used to test these methods. By introducing known offsets to synthetic data, the recovery of these offsets through the `STOPS` check-specific methods ensured that the methods were functioning as intended.

The `skylines` method is able to recover offsets in generated skyline features within a symmetrical $\approx 4 \text{ \AA}$ region, limited by the nearest-neighbors of the relevant identifiable skyline, with an accuracy of $\approx 1 \text{ \AA}$ due to the limitations of the spectral resolution. The `correlate` method is able to recover offsets introduced to wavelength calibrated spectra, for each `CCD`, and for comparisons of the *O*- and *E*-beams within a single file, or for the same polarimetric beam across multiple files, with an accuracy of $\approx 1 \text{ \AA}$, limited once again by the spectral resolution.

5.2 Scientific results using `STOPS`

A number of publications have been produced during the development of `STOPS`. Most notably are the results for the papers discussed in § 4.2, which present the findings for a selection of sources, i.e., Buckley et al. (2021); Cooper and van Soelen (2023); Cooper et al. (2022); Schutte et al. (2022). Additionally, the `STOPS` software has been used extensively in Barnard (2022); Barnard et al. (2022, 2024).

Cooper et al. (2022), and later Cooper and van Soelen (2023), present results for the blazar 3C 279, reduced using alternate `IRAF` wavelength calibrations. It was shown that the `STOPS` software has no noticeable effect on the spectral and polarization properties, and that the `IRAF` wavelength solutions were accurate and reliable. The blazar was observed during periods of enhanced activity as well as during a period of flaring γ -ray activity on 31 March 2017. The normalized relative flux spectra of 3C 279 showed a consistent spectral shape across the various epochs, only deviating slightly during the epoch of flaring, as noted by the increase at shorter wavelengths in the $\sim 6000 - 9000 \text{ \AA}$ wavelength range. The linear polarization remained consistent across the wavelength range at each epoch but varied across epochs, with a minimum linear polarization occurring during the period of flaring. The angle of polarization was also consistent across the wavelength range while varying across epochs.

The linear polarization results seem counter-intuitive for the epoch of flaring. Periods of γ -ray flaring are generally associated with increased non-thermal, polarized synchrotron emission arising in the jet component, and thus a state of (relatively) low polarization is often related to periods of quiescence. Past measurements of the polarization of 3C 279

place the polarization during quiescence at $\Pi \approx 10\%$, falling within the observed $\Pi = 9.2 \pm 1.1\%$. 3C 279 is also known to show large, rapid minute-scale, variations in the polarization angle. The disparity between the flaring γ -ray and apparent quiescent optical regimes may be due to for example, a turbulent magnetic field located in the optical emission region. An unordered magnetic field would lead to depolarization effects, and aligns with the polarization results in Figure 4.9.

Cooper and van Soelen (2023) further reported on results for the standard star, Hiltner 652, reduced with alternative `IRAF` wavelength calibrations applied. The reduced Q and U Stokes parameters of Hiltner 652 showed no systematic deviation from previously published results, indicating that the wavelength calibration process did not introduce any errors into the polarization calculations.

Schutte et al. (2022) presented results for the blazar 4C +01.02, reduced using the `STOPS` software. The spectropolarimetric results were used, alongside multi-wavelength observations, to model the `SED` of the blazar across periods of quiescent and flaring activity. Using the known redshift for 4C +01.02 of $z = 2.1$, emission features in the normalized, continuum subtracted, spectra were identified. These features are more prominent during the quiescent state due to the fainter non-thermal continuum emission as compared to the flaring state. Optical spectropolarimetry of 4C 01.02 showed a consistent polarization percentage across the observed wavelength range, averaging $\Pi = 10.04 \pm 1.03\%$ and $1.72 \pm 0.93\%$, for the flaring and quiescent state, respectively.

It has been shown that the `STOPS` software allows for the integration of alternate wavelength calibrations with `POLSALT`, and that the software is accurate and reliable, meeting the objectives laid out at the offset of its development.

5.3 Future Development

It is possible to complete the data reductions of `SALT/RSS` spectropolarimetric data using only the `POLSALT` pipeline. This does not negate the fact that better tools and software better allow us to focus on the results of observations rather than the data reduction process. Due to the limitations inherent in software designed for use strictly as a pipeline, there is a lack of flexibility in data reduction processes, an over-reliance on the software to provide accurate results, and a lack of urgency when keeping ‘completed’ software up-to-date.

In this regard, the development of the `STOPS` software is a step in the right direction. Although `STOPS` was developed as a workaround to allow for the integration of alternate wavelength calibrations with `POLSALT`, it utilizes a well-supported programming language, Python 3, as well as actively developed `PyPI` packages, and is compatible with all devices capable of running Python. That said, the software is not without its limitations.

Future work would involve the continued development and maintenance of the `STOPS` software, further integration of the software with `POLSALT`, and possibly the development of a user-friendly interface or modification of the `POLSALT GUI` to include the `STOPS` functionality. Wavelength calibrations produced using Python are already supported, but further integration of non-standard wavelength solutions would also be beneficial, as the

current wavelength solutions are limited to Chebyshev and Legendre polynomials. Automation of the wavelength calibration process may also be considered, but development of this functionality depends heavily on the development of the [POLSLT](#) pipeline.

Bibliography

S. Abdollahi, M. Ajello, L. Baldini, J. Ballet, D. Bastieri, J. Becerra Gonzalez, R. Bellazzini, A. Berretta, E. Bissaldi, R. Bonino, A. Brill, P. Bruel, E. Burns, S. Buson, R. A. Cameron, R. Caputo, P. A. Caraveo, N. Cibrario, S. Ciprini, P. Cristarella Orestano, M. Crnogorcevic, S. Cutini, F. D'Ammando, S. De Gaetano, S. W. Digel, N. Di Lalla, L. Di Venere, A. Domínguez, V. Fallah Ramazani, S. J. Fegan, E. C. Ferrara, A. Fiori, H. Fleischhack, A. Franckowiak, Y. Fukazawa, P. Fusco, V. Gammaldi, F. Gargano, S. Garrappa, C. Gasbarra, D. Gasparrini, N. Giglietto, F. Giordano, M. Giroletti, D. Green, I. A. Grenier, S. Guiriec, M. Gustafsson, E. Hays, D. Horan, X. Hou, G. Jóhannesson, M. Kerr, D. Kocevski, M. Kuss, L. Latronico, J. Li, I. Liodakis, F. Longo, F. Loparco, L. Lorusso, B. Lott, M. N. Lovellette, P. Lubrano, S. Maldera, A. Manfreda, G. Martí-Devesa, M. N. Mazziotta, I. Mereu, M. Meyer, P. F. Michelson, T. Mizuno, M. E. Monzani, A. Morselli, I. V. Moskalenko, M. Negro, N. Omodei, E. Orlando, J. F. Ormes, D. Paneque, G. Panzarini, J. S. Perkins, M. Persic, M. Pesce-Rollins, R. Pillera, T. A. Porter, G. Principe, J. L. Racusin, S. Rainò, R. Rando, B. Rani, M. Razzano, S. Razzaque, A. Reimer, O. Reimer, M. Sánchez-Conde, P. M. Saz Parkinson, Jeff Scargle, L. Scotton, D. Serini, C. Sgrò, E. J. Siskind, G. Spandre, P. Spinelli, D. J. Suson, H. Tajima, D. J. Thompson, D. F. Torres, J. Valverde, T. Ventters, Z. Wadiasingh, S. Wagner, and K. Wood. The fermi-lat lightcurve repository*. *The Astrophysical Journal Supplement Series*, 265(2):31, March 2023. ISSN 1538-4365. doi: 10.3847/1538-4365/acbb6a. URL <http://dx.doi.org/10.3847/1538-4365/acbb6a>.

M. Ackermann, R. Anantua, K. Asano, L. Baldini, G. Barbiellini, D. Bastieri, J. Becerra Gonzalez, R. Bellazzini, E. Bissaldi, R. D. Blandford, E. D. Bloom, R. Bonino, E. Bottacini, P. Bruel, R. Buehler, G. A. Calandro, R. A. Cameron, M. Caragiulo, P. A. Caraveo, E. Cavazzuti, C. Cecchi, C. C. Cheung, J. Chiang, G. Chiaro, S. Ciprini, J. Cohen-Tanugi, F. Costanza, S. Cutini, F. D'Ammando, F. de Palma, R. Desiante, S. W. Digel, N. Di Lalla, M. Di Mauro, L. Di Venere, P. S. Drell, C. Favuzzi, S. J. Fegan, E. C. Ferrara, Y. Fukazawa, S. Funk, P. Fusco, F. Gargano, D. Gasparrini, N. Giglietto, F. Giordano, M. Giroletti, I. A. Grenier, L. Guillemot, S. Guiriec, M. Hayashida, E. Hays, D. Horan, G. Jóhannesson, S. Kensei, D. Kocevski, M. Kuss, G. La Mura, S. Larsson, L. Latronico, J. Li, F. Longo, F. Loparco, B. Lott, M. N. Lovellette, P. Lubrano, G. M. Madejski, J. D. Magill, S. Maldera, A. Manfreda, M. Mayer, M. N. Mazziotta, P. F. Michelson, N. Mirabal, T. Mizuno, M. E. Monzani, A. Morselli, I. V. Moskalenko, K. Nalewajko, M. Negro, E. Nuss, T. Ohsugi, E. Orlando, D. Paneque, J. S. Perkins, M. Pesce-Rollins, F. Piron, G. Pivato, T. A. Porter, G. Principe, R. Rando, M. Razzano, S. Razzaque, A. Reimer, J. D. Scargle, C. Sgrò, M. Sikora, D. Simone, E. J. Siskind, F. Spada, P. Spinelli,

- L. Stawarz, J. B. Thayer, D. J. Thompson, D. F. Torres, E. Troja, Y. Uchiyama, Y. Yuan, and S. Zimmer. Minute-timescale >100 MeV γ -ray variability during the giant outburst of quasar 3C 279 observed by *Fermi-LAT* in 2015 June. *The Astrophysical Journal Letters*, 824(2):L20, June 2016. doi: 10.3847/2041-8205/824/2/L20. URL <https://dx.doi.org/10.3847/2041-8205/824/2/L20>.
- Anaconda. Anaconda software distribution, 2020. URL <https://docs.anaconda.com/>.
- R. R. J. Antonucci and J. S. Miller. Spectropolarimetry and the nature of NGC 1068. *ApJ*, 297:621–632, October 1985. doi: 10.1086/163559.
- George B. Arfken and Hans J. Weber. Mathematical methods for physicists, 1999.
- Astropy Collaboration, T. P. Robitaille, E. J. Tollerud, P. Greenfield, M. Droettboom, E. Bray, T. Aldcroft, M. Davis, A. Ginsburg, A. M. Price-Whelan, W. E. Kerzendorf, A. Conley, N. Crighton, K. Barbary, D. Muna, H. Ferguson, F. Grollier, M. M. Parikh, P. H. Nair, H. M. Unther, C. Deil, J. Woillez, S. Conseil, R. Kramer, J. E. H. Turner, L. Singer, R. Fox, B. A. Weaver, V. Zabalza, Z. I. Edwards, K. Azalee Bostroem, D. J. Burke, A. R. Casey, S. M. Crawford, N. Dencheva, J. Ely, T. Jenness, K. Labrie, P. L. Lim, F. Pierfederici, A. Pontzen, A. Ptak, B. Refsdal, M. Servillat, and O. Streicher. Astropy: A community Python package for astronomy. *A&A*, 558:A33, October 2013. doi: 10.1051/0004-6361/201322068.
- Astropy Collaboration, A. M. Price-Whelan, B. M. Sipőcz, H. M. Günther, P. L. Lim, S. M. Crawford, S. Conseil, D. L. Shupe, M. W. Craig, N. Dencheva, A. Ginsburg, J. T. VanderPlas, L. D. Bradley, D. Pérez-Suárez, M. de Val-Borro, T. L. Aldcroft, K. L. Cruz, T. P. Robitaille, E. J. Tollerud, C. Ardelean, T. Babej, Y. P. Bach, M. Bachetti, A. V. Bakanov, S. P. Bamford, G. Barentsen, P. Barmby, A. Baumbach, K. L. Berry, F. Biscani, M. Boquien, K. A. Bostroem, L. G. Bouma, G. B. Brammer, E. M. Bray, H. Breytenbach, H. Buddelmeijer, D. J. Burke, G. Calderone, J. L. Cano Rodríguez, M. Cara, J. V. M. Cardoso, S. Cheedella, Y. Copin, L. Corrales, D. Crichton, D. D’Avella, C. Deil, É. Depagne, J. P. Dietrich, A. Donath, M. Droettboom, N. Earl, T. Erben, S. Fabbro, L. A. Ferreira, T. Finethy, R. T. Fox, L. H. Garrison, S. L. J. Gibbons, D. A. Goldstein, R. Gommers, J. P. Greco, P. Greenfield, A. M. Groener, F. Grollier, A. Hagen, P. Hirst, D. Homeier, A. J. Horton, G. Hosseinzadeh, L. Hu, J. S. Hunkeler, Ž. Ivezić, A. Jain, T. Jenness, G. Kanarek, S. Kendrew, N. S. Kern, W. E. Kerzendorf, A. Khvalko, J. King, D. Kirkby, A. M. Kulkarni, A. Kumar, A. Lee, D. Lenz, S. P. Littlefair, Z. Ma, D. M. Macleod, M. Mastropietro, C. McCully, S. Montagnac, B. M. Morris, M. Mueller, S. J. Mumford, D. Muna, N. A. Murphy, S. Nelson, G. H. Nguyen, J. P. Ninan, M. Nöthe, S. Ogaz, S. Oh, J. K. Parejko, N. Parley, S. Pasqual, R. Patil, A. A. Patil, A. L. Plunkett, J. X. Prochaska, T. Rastogi, V. Reddy Janga, J. Sabater, P. Sakurikar, M. Seifert, L. E. Sherbert, H. Sherwood-Taylor, A. Y. Shih, J. Sick, M. T. Silbiger, S. Singanamalla, L. P. Singer, P. H. Sladen, K. A. Sooley, S. Sornarajah, O. Streicher, P. Teuben, S. W. Thomas, G. R. Tremblay, J. E. H. Turner, V. Terrón, M. H. van Kerkwijk, A. de la Vega, L. L. Watkins, B. A. Weaver, J. B. Whitmore, J. Woillez, V. Zabalza, and Astropy Contributors. The Astropy Project: Building an Open-science Project and Status of the v2.0 Core Package. *AJ*, 156(3):123, September 2018. doi: 10.3847/1538-3881/aabc4f.

Astropy Collaboration, A. M. Price-Whelan, P. L. Lim, N. Earl, N. Starkman, L. Bradley, D. L. Shupe, A. A. Patil, L. Corrales, C. E. Brasseur, M. Nöthe, A. Donath, E. Tollerud, B. M. Morris, A. Ginsburg, E. Vaher, B. A. Weaver, J. Tocknell, W. Jamieson, M. H. van Kerckwijk, T. P. Robitaille, B. Merry, M. Bachetti, H. M. Günther, T. L. Aldcroft, J. A. Alvarado-Montes, A. M. Archibald, A. Bódi, S. Bapat, J. Barentsen, G. and Bazán, M. Biswas, M. Boquien, D. J. Burke, D. Cara, M. Cara, K. E. Conroy, S. Conseil, M. W. Craig, R. M. Cross, K. L. Cruz, F. D'Eugenio, N. Dencheva, H. A. R. Devillepoix, J. P. Dietrich, A. D. Eigenbrot, T. Erben, L. Ferreira, D. Foreman-Mackey, R. Fox, N. Freij, S. Garg, R. Geda, L. Glattly, Y. Gondhalekar, K. D. Gordon, D. Grant, P. Greenfield, A. M. Groener, S. Guest, S. Gurovich, R. Handberg, A. Hart, Z. Hatfield-Dodds, D. Homeier, G. Hosseinzadeh, T. Jenness, C. K. Jones, P. Joseph, J. B. Kalmbach, E. Karamehmetoglu, M. Kałuszyński, M. S. P. Kelley, N. Kern, W. E. Kerzendorf, E. W. Koch, S. Kulumani, A. Lee, C. Ly, Z. Ma, C. MacBride, J. M. Maljaars, D. Muna, N. A. Murphy, H. Norman, R. O'Steen, K. A. Oman, C. Pacifici, S. Pasqual, J. Pascual-Granado, R. R. Patil, G. I. Perren, T. E. Pickering, T. Rastogi, B. R. Roulston, D. F. Ryan, E. S. Rykoff, J. Sabater, P. Sakurikar, J. Salgado, A. Sanghi, N. Saunders, V. Savchenko, L. Schwardt, M. Seifert-Eckert, A. Y. Shih, A. S. Jain, G. Shukla, J. Sick, C. Simpson, S. Singanamalla, L. P. Singer, J. Singhal, M. Sinha, B. M. Sipőcz, L. R. Spitler, D. Stansby, O. Streicher, J. Šumák, J. D. Swinbank, D. S. Taranu, N. Tewary, G. R. Tremblay, M. de Val-Borro, S. J. Van Kooten, Z. Vasović, S. Verma, J. V. de Miranda Cardoso, P. K. G. Williams, T. J. Wilson, B. Winkel, W. M. Wood-Vasey, R. Xue, P. Yoachim, C. Zhang, A. Zonca, and Astropy Project Contributors. The Astropy Project: Sustaining and Growing a Community-oriented Open-source Project and the Latest Major Release (v5.0) of the Core Package. *ApJ*, 935(2):167, August 2022. doi: 10.3847/1538-4357/ac7c74.

S. Bagnulo, M. Landolfi, J. D. Landstreet, E. Landi Degl'Innocenti, L. Fossati, and M. Sterzik. Stellar spectropolarimetry with retarder waveplate and beam splitter devices. *Publications of the Astronomical Society of the Pacific*, 121(883):993, August 2009. doi: 10.1086/605654. URL <https://dx.doi.org/10.1086/605654>.

J. Barnard. Spectropolarimetric behaviour of a selection of high-energy blazars. Master's thesis, University of the Free State, November 2022. URL <http://hdl.handle.net/11660/12281>.

J. Barnard, B. van Soelen, J. Cooper, R. Britto, J. P. Marais, I. van der Westhuizen, D. Buckley, H. Schutte, M. Böttcher, B. Vaidya, S. Acharya, and A. Martin-Carrillo. Optical Spectropolarimetry Observations of the BL Lac-type object PKS 0537-441 after a period of quiescence. In *High Energy Astrophysics in Southern Africa 2021*, page 9, May 2022. doi: 10.22323/1.401.0009.

Joleen Barnard, B. van Soelen, S. Acharya, M. Böttcher, R. J. Britto, J. Cooper, D. A. H. Buckley, A. Martin-Carrillo, B. Vaidya, I. P. van der Westhuizen, and M. Zacharias. The optical spectropolarimetric behaviour of a selection of high-energy blazars. *MNRAS*, 532(2):1991–2005, August 2024. doi: 10.1093/mnras/stae1576.

S. I. Barnes, P. L. Cottrell, M. D. Albrow, N. Frost, G. Graham, G. Kershaw, R. Ritchie, D. Jones, R. Sharples, D. Bramall, J. Schmoll, P. Luke, P. Clark, L. Tyas, D. A. H.

- Buckley, and J. Brink. The optical design of the Southern African Large Telescope high resolution spectrograph: **SALT HRS**. In Ian S. McLean and Mark M. Casali, editors, *Ground-based and Airborne Instrumentation for Astronomy II*, volume 7014 of *Society of Photo-Optical Instrumentation Engineers (SPIE) Conference Series*, page 70140K, July 2008. doi: 10.1117/12.788219.
- Scott D Barthelmy, Louis M Barbier, Jay R Cummings, Ed E Fenimore, Neil Gehrels, Derek Hullinger, Hans A Krimm, Craig B Markwardt, David M Palmer, Ann Parsons, et al. The burst alert telescope (**BAT**) on the *Swift* midex mission. *Space Science Reviews*, 120:143–164, 2005.
- Erasmus Bartholinus. Experimenta crystalli islandici dis-diaclastici, quibus mira et insolita refractio detegitur (copenhagen, 1670). *Edinburgh Philosophical Journal*, 1:271, 1670.
- D. Scott Birney, Guillermo Gonzalez, and David Oesper. *Observational Astronomy – 2nd Edition*. Cambridge University Press, 2006. doi: 10.2277/0521853702.
- D Blinov, S. G. Jorstad, V. M. Larionov, N. R. MacDonald, T. Grishina, E. Kopatskaya, E. Larionova, L. Larionova, D. Morozova, A. Nikiforova, S. Savchenko, Y. Troitskaya, and I. Troitsky. Repeated pattern of gamma-ray flares in the light curve of the blazar 3C 279. *Monthly Notices of the Royal Astronomical Society*, 505(3):4616–4625, May 2021. ISSN 0035-8711. doi: 10.1093/mnras/stab1484. URL <https://doi.org/10.1093/mnras/stab1484>.
- M. Böttcher, A. Reimer, K. Sweeney, and A. Prakash. Leptonic and hadronic modeling of fermi-detected blazars. *The Astrophysical Journal*, 768(1):54, April 2013. doi: 10.1088/0004-637X/768/1/54. URL <https://dx.doi.org/10.1088/0004-637X/768/1/54>.
- D. G. Bramall, R. Sharples, L. Tyas, J. Schmoll, P. Clark, P. Luke, N. Looker, N. A. Dipper, S. Ryan, D. A. H. Buckley, J. Brink, and S. I. Barnes. The **SALT HRS** spectrograph: final design, instrument capabilities, and operational modes. In Ian S. McLean, Suzanne K. Ramsay, and Hideki Takami, editors, *Ground-based and Airborne Instrumentation for Astronomy III*, volume 7735 of *Society of Photo-Optical Instrumentation Engineers (SPIE) Conference Series*, page 77354F, July 2010. doi: 10.1117/12.856382.
- D. G. Bramall, J. Schmoll, L. M. G. Tyas, P. Clark, E. Younger, R. M. Sharples, N. A. Dipper, S. G. Ryan, D. A. H. Buckley, and J. Brink. The **SALT HRS** spectrograph: instrument integration and laboratory test results. In Ian S. McLean, Suzanne K. Ramsay, and Hideki Takami, editors, *Ground-based and Airborne Instrumentation for Astronomy IV*, volume 8446 of *Society of Photo-Optical Instrumentation Engineers (SPIE) Conference Series*, page 84460A, September 2012. doi: 10.1117/12.925935.
- Janus D. Brink, Moses K. Mogotsi, Melanie Saayman, Nicolaas M. Van der Merwe, Jonathan Love, and Alrin Christians. Preparing the **SALT** for near-infrared observations. In Heather K. Marshall, Jason Spyromilio, and Tomonori Usuda, editors, *Ground-based and Airborne Telescopes IX*, volume 12182 of *Society of Photo-Optical*

- Instrumentation Engineers (SPIE) Conference Series*, page 121822E, August 2022. doi: 10.1117/12.2627328.
- D. A. H. Buckley, J. Brink, N. S. Loaring, A. Swat, and H. L. Worters. The Southern African Large Telescope (**SALT**) calibration system. In Ian S. McLean and Mark M. Casali, editors, *Ground-based and Airborne Instrumentation for Astronomy II*, volume 7014, page 70146H. International Society for Optics and Photonics, SPIE, 2008. doi: 10.1117/12.790385. URL <https://doi.org/10.1117/12.790385>.
- D. A. H. Buckley, S. Bagnulo, R. J. Britto, J. Mao, D. A. Kann, J. Cooper, V. Lipunov, D. M. Hewitt, S. Razzaque, N. P. M. Kuin, I. M. Monageng, S. Covino, P. Jakobsen, A. J. van der Horst, K. Wiersema, M. Böttcher, S. Campana, V. D'Elia, E. S. Gorbovskoy, I. Gorbunov, D. N. Groenewald, D. H. Hartmann, V. G. Kornilov, C. G. Mundell, R. Podesta, J. K. Thomas, N. Tyurina, D. Vlasenko, B. van Soelen, and D. Xu. Spectropolarimetry and photometry of the early afterglow of the gamma-ray burst **GRB 191221B**. *MNRAS*, 506(3):4621–4631, September 2021. doi: 10.1093/mnras/stab1791.
- David A. H. Buckley, Gerhard P. Swart, and Jacobus G. Meiring. Completion and commissioning of the Southern African Large Telescope. In Larry M. Stepp, editor, *Society of Photo-Optical Instrumentation Engineers (SPIE) Conference Series*, volume 6267 of *Society of Photo-Optical Instrumentation Engineers (SPIE) Conference Series*, page 62670Z, June 2006. doi: 10.1117/12.673750.
- Christian Buil. *CCD astronomy : construction and use of an astronomical CCD camera; translated and adapted from the French by Emmanuel and Barbara Davoust*. Willmann-Bell, Richmond, Va, 1st english ed. edition, 1991. ISBN 0943396298.
- Eric B. Burgh, Kenneth H. Nordsieck, Henry A. Kobulnick, Ted B. Williams, Darragh O'Donoghue, Michael P. Smith, and Jeffrey W. Percival. Prime Focus Imaging Spectrograph for the Southern African Large Telescope: optical design. In Masanori Iye and Alan F. M. Moorwood, editors, *Instrument Design and Performance for Optical/Infrared Ground-based Telescopes*, volume 4841 of *Society of Photo-Optical Instrumentation Engineers (SPIE) Conference Series*, pages 1463–1471, March 2003. doi: 10.1117/12.460312.
- Subrahmanyan Chandrasekhar. Radiative transfer, 1950.
- Aleksandar Cikota, Ferdinando Patat, Stefan Cikota, and Tamar Faran. Linear spectropolarimetry of polarimetric standard stars with **VLT/FORS2**. *MNRAS*, 464(4):4146–4159, February 2017. doi: 10.1093/mnras/stw2545.
- Marshall H. Cohen. Genesis of the 1000-foot Arecibo dish. *Journal of Astronomical History and Heritage*, 12(2):141–152, July 2009.
- E. Collett. *Field Guide to Polarization*. Field Guides. SPIE Press, 2005. ISBN 9780819458681. URL <https://books.google.co.za/books?id=5lJwcCsLbLsC>.

- J. Cooper and B. van Soelen. *SALT* Spectropolarimetric Pipeline Comparisons. In *High Energy Astrophysics in Southern Africa 2022*, page 56, December 2023.
- J. Cooper, B. van Soelen, and R. Britto. Development of tools for *SALT/RSS* spectropolarimetry reductions: application to the blazar 3C 279. In *High Energy Astrophysics in Southern Africa 2021*, page 56, May 2022. doi: 10.22323/1.401.0056.
- M. Craig, S. Crawford, M. Seifert, T. Robitaille, B. Sipőcz, J. Walawender, Z. Vinícius, J. P. Ninan, M. Droettboom, J. Youn, E. Tollerud, E. Bray, N. Walker, Janga V. R., C. Stotts, H. M. Günther, E. Rol, Yoonsoo P. Bach, L. Bradley, C. Deil, A. Price-Whelan, K. Barbary, A. Horton, W. Schoenell, N. Heidt, F. Gasdia, S. Nelson, and O. Streicher. *astropy/ccdproc*: v1.3.0.post1, December 2017. URL <https://doi.org/10.5281/zenodo.1069648>.
- Steven M. Crawford, Martin Still, Pim Schellart, Luis Balona, David A. H. Buckley, Garith Dugmore, Amanda A. S. Gulbis, Alexei Kniazev, Marissa Kotze, Nicola Loaring, Kenneth H. Nordsieck, Timothy E. Pickering, Stephen Potter, Encarni Romero Colmenero, Petri Vaisanen, Theodore Williams, and Ewald Zietsman. PySALT: the *SALT* science pipeline. In David R. Silva, Alison B. Peck, and B. Thomas Soifer, editors, *Observatory Operations: Strategies, Processes, and Systems III*, volume 7737 of *Society of Photo-Optical Instrumentation Engineers (SPIE) Conference Series*, page 773725, July 2010. doi: 10.1117/12.857000.
- G. Dahlquist and Å. Björck. *Numerical Methods*. Dover Books on Mathematics. Dover Publications, 2003. ISBN 9780486428079. URL <https://books.google.co.ls/books?id=armfeHpJIwAC>.
- E. Landi Degl’Innocenti, S. Bagnulo, and L. Fossati. Polarimetric standardization, 2006.
- Egidio Landi Degl’Innocenti. The physics of polarization. *Proceedings of the International Astronomical Union*, 10(S305):1–1, 2014.
- Egidio Landi Degl’Innocenti and M. Landolfi. *Polarization in Spectral Lines*, volume 307. Springer Dordrecht, 2004. doi: 10.1007/978-1-4020-2415-3.
- Königlich Bayerische Akademie der Wissenschaften. *Denkschriften der Königlichen Akademie der Wissenschaften zu München für das Jahre 1820 und 1821*, volume 8. Die Akademie, 1824. URL <https://books.google.co.za/books?id=k-EAAAAAYAAJ>.
- J. F. Donati, M. Semel, B. D. Carter, D. E. Rees, and A. Collier Cameron. Spectropolarimetric observations of active stars. *MNRAS*, 291(4):658–682, November 1997. doi: 10.1093/mnras/291.4.658.
- I. V. Florinsky and A. N. Pankratov. Digital terrain modeling with the chebyshev polynomials. *Machine Learning and Data Analysis*, 1(12):1647 – 1659, 2015. doi: 10.48550/ARXIV.1507.03960. URL <https://arxiv.org/abs/1507.03960>.
- L. Fossati, S. Bagnulo, E. Mason, and E. Landi Degl’Innocenti. Standard Stars for Linear

- Polarization Observed with **FORS1**. In C. Sterken, editor, *The Future of Photometric, Spectrophotometric and Polarimetric Standardization*, volume 364 of *Astronomical Society of the Pacific Conference Series*, page 503, April 2007.
- Augustin Fresnel. *Oeuvres completes d'Augustin Fresnel: 3*. Imprimerie impériale, 1870.
- L. M. Freyhammer, M. I. Andersen, T. Arentoft, C. Sterken, and P. Nørregaard. On Cross-talk Correction of Images from Multiple-port **CCDs**. *Experimental Astronomy*, 12(3):147–162, January 2001. doi: 10.1023/A:1021820418263.
- G. Ghisellini, F. Tavecchio, L. Foschini, G. Ghirlanda, L. Maraschi, and A. Celotti. General physical properties of bright fermi blazars: Properties of bright fermi blazars. *Monthly Notices of the Royal Astronomical Society*, 402(1):497–518, November 2009. ISSN 0035-8711. doi: 10.1111/j.1365-2966.2009.15898.x. URL <http://dx.doi.org/10.1111/j.1365-2966.2009.15898.x>.
- David J Griffiths. Introduction to electrodynamics, 2005.
- George E. Hale. The Zeeman Effect in the Sun. *PASP*, 20(123):287, December 1908. doi: 10.1086/121847.
- George E. Hale. *16. On the Probable Existence of a Magnetic Field in Sun-Spots*, pages 96–105. Harvard University Press, Cambridge, MA and London, England, 1979. ISBN 9780674366688. doi: doi:10.4159/harvard.9780674366688.c19. URL <https://doi.org/10.4159/harvard.9780674366688.c19>.
- P. D. Hale and G. W. Day. Stability of birefringent linear retarders (wave plates). *Appl. Opt.*, 27(24):5146–5153, December 1988. doi: 10.1364/AO.27.005146. URL <https://opg.optica.org/ao/abstract.cfm?URI=ao-27-24-5146>.
- C. R. Harris, K. J. Millman, S. J. van der Walt, R. Gommers, P. Virtanen, D. Cournapeau, E. Wieser, J. Taylor, S. Berg, N. J. Smith, R. Kern, M. Picus, S. Hoyer, M. H. van Kerkwijk, M. Brett, A. Haldane, J. F. del Río, M. Wiebe, P. Peterson, P. Gérard-Marchant, K. Sheppard, T. Reddy, W. Weckesser, H. Abbasi, C. Gohlke, and T. E. Oliphant. Array programming with NumPy. *Nature*, 585(7825):357–362, September 2020. doi: 10.1038/s41586-020-2649-2. URL <https://doi.org/10.1038/s41586-020-2649-2>.
- E. Hecht. *Optics*. Pearson Education, Incorporated, 2017. ISBN 9780133977226. URL <https://books.google.co.za/books?id=ZarLoQEACAAJ>.
- Steve B. Howell. *Handbook of CCD Astronomy*, volume 5. Cambridge University Press, 2006.
- J. D. Hunter. Matplotlib: A 2d graphics environment. *Computing in Science & Engineering*, 9(3):90–95, 2007. doi: 10.1109/MCSE.2007.55.
- Christian Huygens. Treatise on light, 1690. translated by Thompson, s. p., 1690. URL <https://www.gutenberg.org/files/14725/14725-h/14725-h.htm>.

Mourad E. H. Ismail. *Classical and Quantum Orthogonal Polynomials in One Variable*. Encyclopedia of Mathematics and its Applications. Cambridge University Press, 2005. doi: 10.1017/CBO9781107325982.

James Janesick, James T. Andrews, and Tom Elliott. Fundamental performance differences between CMOS and CCD imagers: Part 1. In David A. Dorn and Andrew D. Holland, editors, *Society of Photo-Optical Instrumentation Engineers (SPIE) Conference Series*, volume 6276 of *Society of Photo-Optical Instrumentation Engineers (SPIE) Conference Series*, page 62760M, June 2006. doi: 10.1117/12.678867.

F.A. Jenkins and H.E. White. *Fundamentals of Optics*. International student edition. McGraw-Hill, 1976. ISBN 9780070323308. URL <https://books.google.co.za/books?id=dCdRAAAAMAAJ>.

Christoph U. Keller. Instrumentation for astrophysical spectropolarimetry. *Astrophysical Spectropolarimetry*, 1:303–354, 2002.

G. Kirchhoff and R. Bunsen. Chemische Analyse durch Spectralbeobachtungen. *Annalen der Physik*, 189(7):337–381, January 1861. doi: 10.1002/andp.18611890702.

Henry A. Kobulnicky, Kenneth H. Nordsieck, Eric B. Burgh, Michael P. Smith, Jeffrey W. Percival, Ted B. Williams, and Darragh O'Donoghue. Prime focus imaging spectrograph for the Southern African large telescope: operational modes. In Masanori Iye and Alan F. M. Moorwood, editors, *Instrument Design and Performance for Optical/Infrared Ground-based Telescopes*, volume 4841 of *Society of Photo-Optical Instrumentation Engineers (SPIE) Conference Series*, pages 1634–1644, March 2003. doi: 10.1117/12.460315.

N. P. M. Kuin and *Swift*/UVOT Team. GRB 191221B: *Swift*/UVOT redshift. *GRB Coordinates Network*, 26538:1, December 2019.

S Laha, KK Simpson, et al. GRB 191221b: *Swift* detection of a burst and a very bright optical candidate. *GRB Coordinates Network*, 26534:1, 2019.

Gerard Leng. Compression of aircraft aerodynamic database using multivariable chebyshev polynomials. *Advances in Engineering Software*, 28(2):133–141, 1997. ISSN 0965-9978. doi: [https://doi.org/10.1016/S0965-9978\(96\)00043-9](https://doi.org/10.1016/S0965-9978(96)00043-9). URL <https://www.sciencedirect.com/science/article/pii/S0965997896000439>.

Dave Litwiller. CCD vs. CMOS. *Photonics spectra*, 35(1):154–158, 2001.

Dongyue Liu and Bryan M. Hennelly. Improved wavelength calibration by modeling the spectrometer. *Applied Spectroscopy*, 76(11):1283–1299, 2022. doi: 10.1177/00037028221111796. URL <https://doi.org/10.1177/00037028221111796>. PMID: 35726593.

Etienne L. Malus. Sur une propriété de la lumière réfléchie. *Mém. Phys. Chim. Soc. d'Arcueil*, 2:143–158, 1809.

Herman L. Marshall, Ioannis Liodakis, Alan P. Marscher, Niccolò Di Lalla, Svetlana G. Jorstad, Dawoon E. Kim, Riccardo Middei, Michela Negro, Nicola Omodei, Abel L. Peirson, Matteo Perri, Simonetta Puccetti, Marco Laurenti, Iván Agudo, Giacomo Bonnoli, Andrei V. Berdyugin, Elisabetta Cavazzuti, Nicole Rodriguez Cavero, Immacolata Donnarumma, Laura Di Gesu, Jenni Jormanainen, Henric Krawczynski, Elina Lindfors, Greg Madjeski, Frédéric Marin, Francesco Massaro, Luigi Pacciani, Juri Poutanen, Fabrizio Tavecchio, Pouya M. Kouch, Francisco José Aceituno, Maria I. Bernardos, Víctor Casanova, Maya García-Comas, Beatriz Agís-González, César Husillos, Alessandro Marchini, Alfredo Sota, Dmitry Blinov, Ioakeim G. Bourbah, Sebastian Kielhmann, Evangelos Kontopodis, Nikos Mandarakas, Stylianos Romanopoulos, Raphael Skalidis, Anna Vervelaki, George A. Borman, Evgenia N. Kopatskaya, Elena G. Larionova, Daria A. Morozova, Sergey S. Savchenko, Andrey A. Vasilyev, Alexey V. Zhovtan, Carolina Casadio, Juan Escudero, Joana Kramer, Ioannis Myserlis, Efthalia Trainou, Ryo Imazawa, Mahito Sasada, Yasushi Fukazawa, Koji S. Kawabata, Makoto Uemura, Tsunefumi Mizuno, Tatsuya Nakaoka, Hiroshi Akitaya, Joseph R. Masiero, Dimitri Mawet, Georgia V. Panopoulou, Samaporn Tinyanont, Masato Kagitani, Vadim Kravtsov, Takeshi Sakanoi, Matthew Dattolo, Mark Gurwell, Garrett Keating, Ram-prasad Rao, Whee Yeon Cheong, Hyeon-Woo Jeong, Sincheol Kang, Sang-Hyun Kim, Sang-Sung Lee, Emmanouil Angelakis, Alexander Kraus, Antonio Hales, Seiji Kameno, Ruediger Kneissl, Hugo Messias, Hiroshi Nagai, Lucio A. Antonelli, Matteo Bachetti, Luca Baldini, Wayne H. Baumgartner, Ronaldo Bellazzini, Stefano Bianchi, Stephen D. Bongiorno, Raffaella Bonino, Alessandro Brez, Niccolò Bucciantini, Fiamma Capitanio, Simone Castellano, Chen-Ting Chen, Stefano Ciprini, Enrico Costa, Alessandra De Rosa, Ettore Del Monte, Alessandro Di Marco, Victor Doroshenko, Michal Dovčiak, Steven R. Ehlert, Teruaki Enoto, Yuri Evangelista, Sergio Fabiani, Riccardo Ferrazzoli, Javier A. Garcia, Shuichi Gunji, Kiyoshi Hayashida, Jeremy Heyl, Wataru Iwakiri, Philip Kaaret, Vladimir Karas, Fabian Kislat, Takao Kitaguchi, Jeffrey J. Kolodziejczak, Fabio La Monaca, Luca Latronico, Simone Maldera, Alberto Manfreda, Andrea Marinucci, Giorgio Matt, Ikuyuki Mitsuishi, Fabio Muleri, C. Y. Ng, Stephen L. O'Dell, Chiara Oppedisano, Alessandro Papitto, George G. Pavlov, Melissa Pesce-Rollins, Pierre-Olivier Petrucci, Maura Pilia, Andrea Possenti, Brian D. Ramsey, John Rankin, Ajay Ratheesh, Oliver J. Roberts, Roger W. Romani, Carmelo Sgrò, Patrick Slane, Paolo Soffitta, Gloria Spandre, Douglas A. Swartz, Toru Tamagawa, Roberto Taverna, Yuzuru Tawara, Allyn F. Tennant, Nicholas E. Thomas, Francesco Tombesi, Alessio Trois, Sergey S. Tsygankov, Roberto Turolla, Jacco Vink, Martin C. Weisskopf, Kinwah Wu, Fei Xie, and Silvia Zane. Observations of Low and Intermediate Spectral Peak Blazars with the Imaging X-Ray Polarimetry Explorer. *ApJ*, 972(1):74, September 2024. doi: 10.3847/1538-4357/ad5671.

Curtis McCully, Steve Crawford, Gabor Kovacs, Erik Tollerud, Edward Betts, Larry Bradley, Matt Craig, James Turner, Ole Streicher, Brigitte Sipőcz, Thomas Robitaille, and Christoph Deil. *astropy/astroscrappy*: v1.0.5 zenodo release, November 2018. URL <https://doi.org/10.5281/zenodo.1482019>.

- I. Newton and W. Innys. *Opticks:: Or, A Treatise of the Reflections, Refractions, Inflections and Colours of Light*. Opticks:: Or, A Treatise of the Reflections, Refractions, Inflections and Colours of Light. William Innys at the West-End of St. Paul's., 1730. URL <https://books.google.co.za/books?id=GnAFAAAAQAAJ>.

- Kenneth H. Nordsieck, Kurt P. Jaehnig, Eric B. Burgh, Henry A. Kobulnicky, Jeffrey W. Percival, and Michael P. Smith. Instrumentation for high-resolution spectropolarimetry in the visible and far-ultraviolet. In Silvano Fineschi, editor, *Polarimetry in Astronomy*, volume 4843 of *Society of Photo-Optical Instrumentation Engineers (SPIE) Conference Series*, pages 170–179, February 2003. doi: 10.1117/12.459288.
- D. O'Donoghue, D. A. H. Buckley, L. A. Balona, D. Bester, L. Botha, J. Brink, D. B. Carter, P. A. Charles, A. Christians, F. Ebrahim, R. Emmerich, W. Esterhuyse, G. P. Evans, C. Fourie, P. Fourie, H. Gajjar, M. Gordon, C. Gumede, M. de Kock, A. Koeslag, W. P. Koorts, H. Kriel, F. Marang, J. G. Meiring, J. W. Menzies, P. Menzies, D. Metcalfe, B. Meyer, L. Nel, J. O'Connor, F. Osman, C. Du Plessis, H. Rall, A. Riddick, E. Romero-Colmenero, S. B. Potter, C. Sass, H. Schalekamp, N. Sessions, S. Siyengo, V. Sopela, H. Steyn, J. Stoffels, J. Scholtz, G. Swart, A. Swat, J. Swiegers, T. Tiheli, P. Vaisanen, W. Whittaker, and F. van Wyk. First science with the Southern African Large Telescope: peering at the accreting polar caps of the eclipsing polar SDSS J015543.40+002807.2. *MNRAS*, 372(1):151–162, October 2006. doi: 10.1111/j.1365-2966.2006.10834.x.
- Darragh O'Donoghue. Correction of spherical aberration in the Southern African Large Telescope (SALT). In Philippe Dierickx, editor, *Optical Design, Materials, Fabrication, and Maintenance*, volume 4003 of *Society of Photo-Optical Instrumentation Engineers (SPIE) Conference Series*, pages 363–372, July 2000. doi: 10.1117/12.391526.
- Darragh O'Donoghue. Atmospheric dispersion corrector for the Southern African Large Telescope (SALT). In Richard G. Bingham and David D. Walker, editors, *Large Lenses and Prisms*, volume 4411 of *Society of Photo-Optical Instrumentation Engineers (SPIE) Conference Series*, pages 79–84, February 2002. doi: 10.1117/12.454874.
- Ferdinando Patat and Martino Romaniello. Error Analysis for Dual-Beam Optical Linear Polarimetry. *PASP*, 118(839):146–161, January 2006. doi: 10.1086/497581.
- Alba Peinado, Angel Lizana, Josep Vidal, Claudio Iemmi, and Juan Campos. Optimization and performance criteria of a stokes polarimeter based on two variable retarders. *Opt. Express*, 18(10):9815–9830, May 2010. doi: 10.1364/OE.18.009815. URL <https://opg.optica.org/oe/abstract.cfm?URI=oe-18-10-9815>.
- W. H. Press, S. A. Teukolsky, W. T. Vetterling, and B. P. Flannery. *Numerical Recipes 3rd Edition: The Art of Scientific Computing*. Cambridge University Press, 2007. ISBN 9780521880688. URL <https://books.google.co.za/books?id=1aA0dzK3FegC>.
- J. R. Priebe. Operational form of the mueller matrices. *J. Opt. Soc. Am.*, 59(2):176–180, February 1969. doi: 10.1364/JOSA.59.000176. URL <https://opg.optica.org/abstract.cfm?URI=josa-59-2-176>.
- Lawrence W. Ramsey, M. T. Adams, Thomas G. Barnes, John A. Booth, Mark E. Cornell, James R. Fowler, Niall I. Gaffney, John W. Glaspey, John M. Good, Gary J. Hill, Philip W. Kelton, Victor L. Krabbendam, L. Long, Phillip J. MacQueen, Frank B. Ray, Randall L. Ricklefs, J. Sage, Thomas A. Sebring, W. J. Spiesman, and M. Steiner.

- Early performance and present status of the Hobby-Eberly Telescope. In Larry M. Stepp, editor, *Advanced Technology Optical/IR Telescopes VI*, volume 3352 of *Society of Photo-Optical Instrumentation Engineers (SPIE) Conference Series*, pages 34–42, August 1998. doi: 10.1117/12.319287.
- SALT Ast. Ops. Proposal information for SALT call for proposals: 2024 semester 2. Technical Report 2430AB0001, SALT, June 2024. URL https://pysalt.salt.ac.za/proposal_calls/current/ProposalCall.html.
- Hester M. Schutte, Abraham Falcone, Andry Fitjavana Rajoelimanana, Markus Böttcher, David Buckley, Haocheng Zhang, Johannes P. Marais, Justin Cooper, Amanpreet Kaur, Brian Van Soelen, and Richard J. Britto. Modeling the Spectral Energy Distributions and Multi-Wavelength Polarization of Blazars. In *43rd COSPAR Scientific Assembly. Held 28 January – 4 February*, volume 43, page 1682, January 2021.
- Hester M. Schutte, Richard J. Britto, Markus Böttcher, Brian van Soelen, Johannes P. Marais, Amanpreet Kaur, Abraham D. Falcone, David A. H. Buckley, Andry F. Rajoelimanana, and Justin Cooper. Modeling the Spectral Energy Distributions and Spec-tropolarimetry of Blazars - Application to 4C+01.02 in 2016-2017. *ApJ*, 925(2):139, February 2022. doi: 10.3847/1538-4357/ac3cb5.
- Maria C. Simon. Wollaston prism with large split angle. *Appl. Opt.*, 25(3):369–376, February 1986. doi: 10.1364/AO.25.000369. URL <https://opg.optica.org/ao/abstract.cfm?URI=ao-25-3-369>.
- G. G. Stokes. On the Composition and Resolution of Streams of Polarized Light from different Sources. *Transactions of the Cambridge Philosophical Society*, 9:399, January 1852.
- Doug Tody. The **IRAF** Data Reduction and Analysis System. In David L. Crawford, editor, *Instrumentation in astronomy VI*, volume 627 of *Society of Photo-Optical Instrumentation Engineers (SPIE) Conference Series*, page 733, January 1986. doi: 10.1117/12.968154.
- Doug Tody. **IRAF** in the Nineties. In R. J. Hanisch, R. J. V. Brissenden, and J. Barnes, editors, *Astronomical Data Analysis Software and Systems II*, volume 52 of *Astronomical Society of the Pacific Conference Series*, page 173, January 1993.
- Stephen F. Tonkin. *Practical Amateur Spectroscopy*. The Patrick Moore Practical Astronomy Series. Springer London, 2013. ISBN 9781447101277. URL <https://books.google.fr/books?id=b2fgBwAAQBAJ>.
- C. Megan Urry and Paolo Padovani. Unified schemes for radio-loud active galactic nuclei. *Publications of the Astronomical Society of the Pacific*, 107:803, September 1995. ISSN 1538-3873. doi: 10.1086/133630. URL <http://dx.doi.org/10.1086/133630>.
- Pieter G. van Dokkum. Cosmic-Ray Rejection by Laplacian Edge Detection. *PASP*, 113(789):1420–1427, November 2001. doi: 10.1086/323894.

J. B. Vielfaure, M. Arabsalmani, K. E. Heintz, N. R. Tanvir, A. de Ugarte Postigo, D. B. Malesani, J. P. U. Fynbo, K. Wiersema, S. D. Vergani, D. Xu, G. Pugliese, S. Schulze, D. Burgarella, and Stargate Collaboration. [GRB](#) 191221B: [VLT](#)/X-shooter redshift. [GRB Coordinates Network](#), 26553:1, December 2019.

Pauli Virtanen, Ralf Gommers, Travis E. Oliphant, Matt Haberland, Tyler Reddy, David Cournapeau, Evgeni Burovski, Pearu Peterson, Warren Weckesser, Jonathan Bright, Stéfan J. van der Walt, Matthew Brett, Joshua Wilson, K. Jarrod Millman, Nikolay Mayorov, Andrew R. J. Nelson, Eric Jones, Robert Kern, Eric Larson, C J Carey, İlhan Polat, Yu Feng, Eric W. Moore, Jake VanderPlas, Denis Laxalde, Josef Perktold, Robert Cimrman, Ian Henriksen, E. A. Quintero, Charles R. Harris, Anne M. Archibald, Antônio H. Ribeiro, Fabian Pedregosa, Paul van Mulbregt, and SciPy 1.0 Contributors. SciPy 1.0: Fundamental Algorithms for Scientific Computing in Python. *Nature Methods*, 17:261–272, 2020. doi: 10.1038/s41592-019-0686-2.

L. Wang and J. C. Wheeler. Spectropolarimetry of supernovae. *ARA&A*, 46:433–474, September 2008. doi: 10.1146/annurev.astro.46.060407.145139.

Marsha J. Wolf, Matthew A. Bershady, Michael P. Smith, Kurt P. Jaehnig, Jeffrey W. Percival, Joshua E. Oppor, Mark P. Mulligan, and Ron J. Koch. Laboratory performance and commissioning status of the [SALT NIR](#) integral field spectrograph. In Christopher J. Evans, Julia J. Bryant, and Kentaro Motohara, editors, *Ground-based and Airborne Instrumentation for Astronomy IX*, volume 12184 of *Society of Photo-Optical Instrumentation Engineers (SPIE) Conference Series*, page 1218407, August 2022. doi: 10.1117/12.2630242.

William H. Wollaston. XII. A Method of Examining Refractive and Dispersive Powers, by Prismatic Reflection. *Philosophical Transactions of the Royal Society of London Series I*, 92:365–380, January 1802. doi: 10.1098/rstl.1802.0013.

Appendix A

The Modified Reduction Process

This section of the Appendix aims to provide a minimum working example of the commands necessary to reduce `POLSLT` data using `STOPS` and `IRAF`. It contains the commands necessary to activate all software and run through the reduction process but makes no attempt at discussion.

Both `POLSLT` and `IRAF` are launched from the default `CLI` but use independent interfaces during the reduction process. To distinguish which window is in focus, the ‘\$’ token is used for default `CLI` commands while the ‘c1>’ and ‘>>>’ tokens are used for `IRAF`’s ‘xgterm’ single- and multi-line commands, respectively. `CLI` commands may also require a specific Python environment. The environment being used is denoted using the ‘(salt)\$’ or ‘(base)\$’ tokens for the ‘salt’ or default ‘base’ environments.¹

General instructions for the reduction process (i.e., not `CLI` line-fed commands) may either be discussed outside a ‘Listing’ environment or included as part of a ‘Listing’ environment preceded with a comment ‘#’ token. Finally, `POLSLT` implements a `GUI` and thus takes no line-fed commands. As such, instructions referring to the `POLSLT` `GUI` also follow those of the general instructions.

As a final note, some parameters are distinguished using ‘<angle brackets>’. They signify necessary parameters that may vary from reduction to reduction. Notable uses of this notation include the date of observation, $\langle OBSDATE \rangle$ (formatted ‘YYYYMMDD’), the split science `FITS` files, $\langle O\text{-beam FILES} \rangle$ or $\langle E\text{-beam FILES} \rangle$, the split arc `FITS` files, $\langle O\text{-beam ARC} \rangle$ or $\langle E\text{-beam ARC} \rangle$, and a wildcard symbol, $\langle * \rangle$.

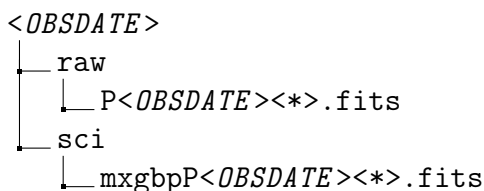


Figure A.1: The typical minimal file structure of data provided by `SALT`.

¹It is assumed a Python environment manager, such as ‘conda’, is installed.

Ensure the data is formatted in a file structure similar to that in Figure A.1. Data located in the ‘sci’ folder is often provided by **SALT** but is not strictly necessary to begin the reduction process. If ‘mxgbp’ prefixed data is available, the reductions may be begun starting at Listing A.2. The **POLSALT GUI** is launched from the default **CLI** running the commands in Listing A.1.

Listing A.1: Launching the **POLSALT GUI**

```
$ cd ~/polsalt-beta
$ conda activate salt
(salt)$ python -W ignore reducepoldataGUI.py &
```

Refer to Figure 3.1 for a depiction of the **POLSALT GUI**. To complete the **POLSALT** pre-calibrations, and with the **GUI** in focus:

- Ensure that the ‘**POLSALT** code directory’ is correct, i.e., ‘~/polsalt-beta’.
- Set the ‘Top level data directory’ to <OBSDATE>.
- Ensure ‘Raw data directory’ is correct.
- Ensure ‘Science data directory’ is correct.
- Select ‘Raw image reduction’ from the ‘Data reduction step’ drop down menu.
- Check the tick boxes of all raw images to be processed (include the arc) in the display box covering the lower half of the **GUI**.
- Proceed with the reductions by clicking the ‘OK’ button.

The pre-calibrated ‘mxgbp’ **FITS** files are now available in the ‘sci’ folder. The files may be split using **STOPS** by running the commands in Listing A.2.

Listing A.2: Splitting data using **STOPS**

```
$ cd <OBSDATE>/sci
$ conda activate
(base)$ python -m STOPS . split
```

The split *O*- and *E*-beam **FITS** files are now available. The **IRAF** wavelength calibrations are now run. The **IRAF** xgterm **CLI** is launched using Listing A.3.

Listing A.3: Launching **IRAF** in xgterm

```
$ cd ~/iraf
$ xgterm -sb &
cl> conda activate salt
cl> cl
cl> cd <OBSDATE>/sci
cl> noao
cl> twodspec
cl> longslit
cl> unlearn longslit
cl> longslit.dispaxis=1
```

The **IRAF** `identify` task requires an average feature width, ‘fwidth’, as a parameter. The width of a feature may be found in **IRAF** using the `implot` task² along with cursor commands, but may also be found using **FITS** viewing software, such as `ds9`.³ The `identify` task may be run using the commands in Listing A.4.

Listing A.4: Running the **IRAF** `identify` task

```
cl> mkscript 01_identify.cl
cl> # Add identify to 01_identify.cl twice, for both beams
cl> # Edit the parameters of 01_identify.cl in a text editor
cl> # Paste an identify script into the CLI, resulting in:
cl>
cl> identify ("<O-beam ARC>",
>>> "", "", section="middle line", database="database",
>>> coordlist="linelists$idheneare.dat", units="", nsum="10", match=-3.,
>>> maxfeatures=50, zwidth=100., ftype="emission", fwidth=8.,
>>> cradius=5., threshold=0., minsep=2., function="spline3", order=2,
>>> sample="*", niterate=0, low_reject=3., high_reject=3., grow=0.,
>>> autowrite=no, graphics="stdgraph", cursor="", aidpars="")
```

The `identify` task will launch an interactive window. Cursor commands refer to keys that provide unique functionality to the interactive **IRAF** tasks. The cursor commands for `identify` allow the arc lines to be identified using ‘m’ (and typing the relevant wavelength), while ‘d’ and ‘i’ will delete a single and all identified arc lines, respectively. The ‘f’ cursor command will perform a preliminary fit which can be quit using the ‘q’ cursor command. The ‘l’ cursor command will attempt to identify any unidentified arc lines. Once complete, a figure of the identified lines may be saved using ‘:labels coord’ and ‘:.snap eps’, and the task safely quit with the ‘q’ cursor command.⁴ The `identify` procedure is repeated, replacing $<O\text{-beam } ARC>$ with $<E\text{-beam } ARC>$.

The `reidentify` task may be run using the commands in Listing A.5.

Listing A.5: Running the **IRAF** `reidentify` task

```
cl> mkscript 02_reidentify.cl
cl> # Add reidentify to 02_reidentify.cl twice, for both beams
cl> # Edit the parameters of 02_reidentify.cl in a text editor
cl> # Paste a reidentify script into the CLI, resulting in:
cl>
cl> reidentify ("<O-beam ARC>",
>>> "<O-beam ARC>", "yes", "", "", interactive="no", section="middle
>>> line", newaps=yes, override=no, refit=yes, trace=yes, step="10",
>>> nsum="10", shift=".0.", search=0., nlost=0, cradius=5.,
>>> threshold=0., addfeatures=no, coordlist="linelists$idheneare.dat",
>>> match=-3., maxfeatures=50, minsep=2., database="database",
>>> logfiles="logfile", plotfile="", verbose=yes, graphics="stdgraph",
>>> cursor="", aidpars="")
```

²See https://astro.uni-bonn.de/~sysstw/lfa_html/iraf/plot.implot.html for documentation on the `implot` task.

³See <https://sites.google.com/cfa.harvard.edu/saoimageds9> for documentation on the `ds9` software.

⁴See https://astro.uni-bonn.de/~sysstw/lfa_html/iraf/noao.onedspec.identify.html for documentation on the `identify` task.

The `reidentify` task will run autonomously so long as the `interactive` parameter is set to “no”.⁵ Repeat the `reidentify` procedure, replacing $\langle O\text{-beam } ARC \rangle$ with $\langle E\text{-beam } ARC \rangle$ at both the ‘reference’ and ‘image’ parameter locations.

The `fitcoords` task may be run using the commands in Listing A.6.

Listing A.6: Running the `IRAF fitcoords` task

```
cl> mkscript 03_fitcoords.cl
cl> # Add fitcoords to 03_fitcoords.cl twice, for both beams
cl> # Edit the parameters of 03_fitcoords.cl in a text editor
cl> # Paste a fitcoords script into the CLI, resulting in:
cl>
cl> fitcoords ("<O-beam ARC> (exclude the file extension)" ,
>>> fitname="", interactive=yes, combine=no, database="database",
>>> deletions="deletions.db", function="chebyshev", xorder=6, yorder=6,
>>> logfiles="STDOUT,logfile", plotfile="plotfile",
>>> graphics="stdgraph", cursor="")
```

The `fitcoords` task will launch an interactive window. The x- and y-axis being plotted may be changed using the ‘x’ or ‘y’ cursor commands followed by the desired data axis (‘x’ for the x-axis, ‘y’ for the y-axis, or ‘r’ for the residuals).⁶ Repeat the `fitcoords` procedure, replacing $\langle O\text{-beam } ARC \rangle$ with $\langle E\text{-beam } ARC \rangle$.

The `transform` task may be run using the commands in Listing A.7.

Listing A.7: Running the `IRAF transform` task

```
cl> mkscript 04_transform.cl
cl> # Add transform to 04_transform.cl twice, for both beams
cl> # Edit the parameters of 04_transform.cl in a text editor
cl> # Paste a transform script into the CLI, resulting in:
cl>
cl> transform ("@<O-beam FILES>" ,
>>> "t//@<O-beam FILES>", "<O-beam ARC> (exclude the file extension)" ,
>>> minput="", moutput="", database="database", interptype="linear",
>>> x1="INDEF", x2="INDEF", dx="INDEF", nx="INDEF", xlog="no",
>>> y1="INDEF", y2="INDEF", dy="INDEF", ny="INDEF", ylog="no",
>>> flux="yes", blank="INDEF", logfiles="STDOUT,logfile")
```

The `transform` task will run autonomously.⁷ Repeat the `transform` procedure, replacing the $\langle O\text{-beam } FILES \rangle$ and $\langle O\text{-beam } ARC \rangle$ with $\langle E\text{-beam } FILES \rangle$ and $\langle E\text{-beam } ARC \rangle$ at both parameter locations. Inspect the transformed images, most notably the arc images, using any `FITS` viewer as a cursory check that the wavelength calibrations were completed without error.

The ‘gain’ and ‘read noise’ are now needed as the cosmic-ray rejection of the `STOPS` `join` method accepts them as parameters. These parameters may be found using the ‘`GAINSET`’ and ‘`ROSPEED`’ keywords in the `FITS` headers. The cosmic ray rejection

⁵See https://astro.uni-bonn.de/~sysstw/lfa_html/iraf/noao.onedspec.reidentify.html for documentation on the `reidentify` task.

⁶See https://astro.uni-bonn.de/~sysstw/lfa_html/iraf/noao.twodspec.longslit.fitcoords.html for documentation on the `fitcoords` task.

⁷See https://astro.uni-bonn.de/~sysstw/lfa_html/iraf/noao.twodspec.longslit.transform.html for documentation on the `transform` task.

defaults to *GAINSET*=‘FAINT’, and *ROSPEED*=‘SLOW’. If the gain and read noise values differ from the defaults, the parameters should be updated when running `join`.⁸

The `STOPS` `join` method may be run using the commands in Listing A.8.

Listing A.8: Joining the data using `STOPS`

```
$ cd <OBSDATE>/sci
$ conda activate
(base)$ python -m STOPS . join
```

The `STOPS` `skylines` method may be run on any ‘joined’ or transformed **FITS** files, *<FILE(S)>*, using the commands in Listing A.9.

Listing A.9: Running the `STOPS` `skylines` method

```
$ cd <OBSDATE>/sci
$ conda activate
(base)$ python -m STOPS . skylines <FILE(S)>
```

The ‘`sci/`’ directory may now be optionally organized by running the commands in Listing A.10, moving all the files relevant to the wavelength calibrations into either the ‘`database`’ or ‘`split_files`’ directories.

Listing A.10: Directory cleanup for `POLSALT`

```
$ cd <OBSDATE>/sci
$ mkdir split_files
$ mv *beam0* *beamE* *arc0* *arcE* split_files/
$ mv *.eps *.cl *.db database/
```

The `POLSALT spectra extraction` is now run. If the `POLSALT` GUI was closed it should now be reopened using Listing A.1. With the GUI in focus:

- Ensure all directories are still correct.
- Select ‘Spectra extraction’ from the ‘Data reduction step’ drop down menu.
- Check the tick boxes of all wavelength calibrated images to be processed (exclude the arc) in the display box covering the lower half of the GUI.
- Proceed with the reductions by clicking ‘OK’.

The `POLSALT spectra extraction` is interactive and will launch a separate GUI for the background subtraction and spectral extraction (see Figure 3.2). The background and spectral regions to be extracted may be adjusted, noting that adjustments affect both *O*- and *E*-beams. Once both background regions contain no trace and the spectral region fully contains only the science trace, the reduction may be completed by clicking ‘OK’.

⁸The read noise and gain may be determined from [SALT Ast. Ops. \(2024\)](#), specifically [Table 6.1](#) and [Table 6.2](#).

The `STOPs correlate` method may now be run on any ‘joined’ `FITS` files by running the commands in Listing A.11.

Listing A.11: Running the `STOPs correlate` method

```
$ cd <OBSDATE>/sci
$ conda activate
(base)$ python -m STOPs . correlate <FILE(S)>
```

The `POLSALT raw Stokes calculation`, `final Stokes calculation`, and `results visualisation` may now be completed. For the last time, if the `POLSALT GUI` was closed it should now be reopened using Listing A.1. With the `GUI` in focus:

- Ensure all directories are still correct.
- Select ‘Raw Stokes calculation’ from the ‘Data reduction step’ drop down menu.
- Check the tick boxes of all the extracted spectra images to be processed in the display box covering the lower half of the `GUI`.
- Proceed with the `raw Stokes calculation` by clicking ‘OK’.
- Select ‘Final Stokes calculation’ from the ‘Data reduction step’ drop down menu.
- Check the tick boxes of all the “raw Stokes” images to be processed in the display box covering the lower half of the `GUI`.
- Proceed with the `Final Stokes calculation` by clicking ‘OK’.
- Select ‘Results visualisation - interactive’ from the ‘Data reduction step’ drop down menu.
- Check the tick boxes of the “final Stokes” image to be visualized in the display box covering the lower half of the `GUI`.
- Proceed with the `visualisation` by clicking ‘OK’.

The `POLSALT visualisation` is interactive and will launch a separate `GUI` (See Figure 3.3). The `GUI` may be used to change the binning and parameters of the plot before saving the plot to a PDF file.

This concludes the minimum working example of the `POLSALT` reduction process when substituting the `POLSALT wavelength calibrations` with those done in `IRAF`. Aside from the final results, the file structure after reductions should resemble something akin to that provided in Figure A.2.

```

<OBSDATE>
├── raw
│   └── P<OBSDATE><*>.fits
└── sci
    ├── database
    │   ├── 01_identify.cl
    │   ├── 02_reidentify.cl
    │   ├── 03_fitcoords.cl
    │   ├── 04_transform.cl
    │   ├── deletions.db
    │   ├── fcarrE00<##>
    │   ├── fcarr000<##>
    │   ├── idarcE00<##>
    │   ├── idarc000<##>
    │   └── <*>.eps
    ├── split_files
    │   ├── arcE00<##>.fits
    │   ├── arc000<##>.fits
    │   ├── beamE<*>.fits
    │   ├── beam0<*>.fits
    │   ├── tarcE00<##>.fits
    │   ├── tarc000<##>.fits
    │   ├── tbeamE<*>.fits
    │   ├── tbeam0<*>.fits
    │   ├── <OBSDATE>_geom.txt
    │   ├── <OBSDATE>_filtered.txt
    │   ├── cwmxgbpP<OBSDATE><*>.fits
    │   ├── ecwmxgbpP<OBSDATE><*>.fits
    │   ├── mxgbpP<OBSDATE><*>.fits
    │   ├── wmxgbpP<OBSDATE><*>.fits
    │   └── <*>.log
    ├── <OBJ>_c0_h<*>_01.fits
    ├── <OBJ>_c0_1_stokes.fits
    ├── <OBJ>_c0_1_stokes_<BIN>_Ipt.txt
    └── <OBJ>_c0_1_stokes_<BIN>_Ipt.pdf

```

Figure A.2: The typical file structure after completing the reduction process.

Appendix B

STOPS Source Code

This section of Appendix includes all the major `STOPS` source code files related to the reduction process. Files such as those related to python initialization, testing directories, and other non-essential modules have been excluded for brevity and clarity.

Listing B.1: The source code for `__main__.py`

```
1 #!/usr/bin/env python3
2 # -*- coding: utf-8 -*-
3
4 """
5 The Command Line Interface (CLI) for STOPS, handling argument parsing,
6 class instantiation, processing, and logging.
7
8 Usage
9 -----
10 `python -m STOPS`
11
12 Suffix the above command with `-h` for help on usage.
13
14 Description
15 -----
16 This module is the entry point for the STOPS package. It provides
17 the CLI argument parser for the supplementary tools provided by STOPS.
18 The parser is built using the `argparse` module and is designed to be
19 user-friendly.
20
21 See Also
22 -----
23 IRAF:
24     For more information on the IRAF package, see the IRAF website:
25     https://iraf-community.github.io/
26
27 POLSALT:
28     For more information on the POLSALT pipeline, see the POLSALT website:
29     https://github.com/saltastro/polsalt
30
31 PYSALT:
32     For more information on the PYSALT package, see the PYSALT website:
33     https://astronomers.salt.ac.za/software/pysalt-documentation/
34
35 PYRAF:
36     For more information on the PYRAF package, see the PYRAF website:
37     https://pyraf.readthedocs.io/en/latest/
38
39 """
40
41 # MARK: Imports
```

```

42 import sys
43 import argparse
44 import logging
45 from pathlib import Path
46
47 from STOPS import __version__
48 from STOPS import Split, Join, CrossCorrelate, Skylines
49 from STOPS.utils import ParserUtils as Parser
50 from STOPS.utils.Constants import SPLIT_ROW, PREFIX, PARSE, SAVE_CORR, SAVE_SKY
51
52
53 # MARK: Constants
54 PROG = "STOPS"
55 DESCRIPTION = """
56 Supplementary TTools for Polsalt Spectropolarimetry (STOPS) is a
57 collection of supplementary tools created for SALT's POLSALT pipeline,
58 allowing for wavelength calibrations with IRAF. The tools provide
59 support for splitting and joining polsalt formatted data as well as
60 cross correlating complementary polarimetric beams.
61
62 Pre-release Reference:
63 DOI: 10.22323/1.401.0056
64 """
65
66
67 # MARK: Universal Parser
68 parser = argparse.ArgumentParser(
69     prog=PROG,
70     description=DESCRIPTION,
71     formatter_class=argparse.RawDescriptionHelpFormatter,
72 )
73 parser.add_argument(
74     "-V",
75     "--version",
76     action="version",
77     version=f"%(prog)s as of {__version__}",
78 )
79 parser.add_argument(
80     "-v",
81     "--verbose",
82     action="count",
83     default=PARSE['VERBOSE'],
84     help=(
85         "Counter flag which enables and increases verbosity. "
86         "Use -v or -vv for greater verbosity levels."
87     ),
88 )
89 parser.add_argument(
90     "-l",
91     "--log",
92     action="store",
93     type=Parser.parse_logfile,
94     help=(
95         "Filename of the logging file. "
96         "File is created if it does not exist. Defaults to None."
97     ),
98 )
99 parser.add_argument(
100    "data_dir",
101    action="store",
102    nargs="?",
103    default=PARSE['DATA_DIR'],
104    type=Parser.parse_path,
105    help=(
106        "Path of the directory which contains the working data. "
107        f"Defaults to the cwd -> '{PARSE['DATA_DIR']}' (i.e., '.')."
108    ),
109 )
110
111
112 # MARK: Split\Join Parent
113 split_join_args = argparse.ArgumentParser(add_help=False)
114 split_join_args.add_argument(

```

```

115     "-n",
116     "--no_arc",
117     action="store_true",
118     help="Flag to exclude arc files from processing.",
119 )
120 split_join_args.add_argument(
121     "-s",
122     "--split_row",
123     default=SPLIT_ROW,
124     type=int,
125     help=(
126         "Row along which the O and E beams are split. "
127         f"Defaults to polsalt's default -> {SPLIT_ROW}."
128     ),
129 )
130 split_join_args.add_argument(
131     "-p",
132     "--save_prefix",
133     nargs=2,
134     default=PREFIX,
135     help=(
136         "Prefix appended to the filenames, "
137         "with which the O and E beams are saved. "
138         f"Defaults to {PREFIX}."
139     ),
140 )
141
142
143 # MARK: Corr.\Sky. Parent
144 corr_sky_args = argparse.ArgumentParser(add_help=False)
145 corr_sky_args.add_argument(
146     "filenames",
147     action="store",
148     nargs="+",
149     type=Parser.parse_file,
150     help=(
151         "File name(s) of FITS file(s) to be processed."
152         "A minimum of one filename is required."
153     ),
154 )
155 corr_sky_args.add_argument(
156     "-b",
157     "--beams",
158     choices=[ "O", "E", "OE" ],
159     type=str.upper,
160     default=PARSE['BEAMS'],
161     help=(
162         "Beams to process. "
163         f"Defaults to {PARSE['BEAMS']}, but "
164         "may be given 'O', 'E', or 'OE' to "
165         "determine which beams are processed."
166     ),
167 )
168 corr_sky_args.add_argument(
169     "-ccd",
170     "--split_ccd",
171     action="store_false",
172     help=(
173         "Flag to NOT split CCD's. "
174         "Recommended to leave off unless the chip gaps "
175         "have been removed from the data."
176     ),
177 )
178 corr_sky_args.add_argument(
179     "-c",
180     "--continuum_order",
181     type=int,
182     default=PARSE['CONT_ORD'],
183     dest="cont_ord",
184     help=(
185         "Order of continuum to remove from spectra. "
186         "Higher orders recommended to remove most variation, "
187         "leaving only significant features."

```

```

188     ),
189 )
190 corr_sky_args.add_argument(
191     "-p",
192     "--plot",
193     action="store_true",
194     help="Flag for additional plot outputs.",
195 )
196
197
198 # MARK: Create subparser modes
199 subparsers = parser.add_subparsers(
200     dest="mode",
201     help="Operational mode of supplementary tools",
202 )
203
204
205 # MARK: Split Subparser
206 split_parser = subparsers.add_parser(
207     "split",
208     aliases=["s"],
209     help="Split mode",
210     parents=[split_join_args],
211 )
212 # 'children' split args here
213 # Change `split` defaults here
214 split_parser.set_defaults(
215     mode="split",
216     func=Split,
217 )
218
219
220 # MARK: Join Subparser
221 join_parser = subparsers.add_parser(
222     "join",
223     aliases=["j"],
224     help="Join mode",
225     parents=[split_join_args],
226 )
227 # 'children' join args here
228 join_parser.add_argument(
229     "-c",
230     "--coefficients",
231     dest="solutions_list",
232     nargs='*',
233     type=Parser.parse_file,
234     help=(
235         "Custom coefficients to use instead of the `IRAF` fitcoords "
236         "database. Use as either '-c <o_solution> <e_solution>' or "
237         "a regex descriptor '-c <*solution*extension>'."
238     ),
239 )
240 # Change `join` defaults here
241 join_parser.set_defaults(
242     mode="join",
243     func=Join,
244 )
245
246
247 # MARK: Correlate Subparser
248 corr_parser = subparsers.add_parser(
249     "correlate",
250     aliases=["x"],
251     help="Cross correlation mode",
252     parents=[corr_sky_args],
253 )
254 # 'children' correlate args here
255 corr_parser.add_argument(
256     "-o",
257     "--offset",
258     type=int,
259     default=PARSE['OFFSET'],
260     help=(

```

```

261     "Introduces an offset when correcting for "
262     "known offset in spectra or for testing purposes. "
263     f"Defaults to {PARSE['OFFSET']}. "
264     "(For testing, not used during regular operation.)"
265 ),
266 )
267 corr_parser.add_argument(
268     "-s",
269     "--save_prefix",
270     action="store",
271     nargs="?",
272     type=lambda path: Path(path).expanduser().resolve(),
273     const=SAVE_CORR,
274     help=(
275         "Prefix used when saving plot. "
276         "Excluding flag does not save output plot, "
277         f"flag usage of option uses default prefix {SAVE_CORR}, "
278         "and a provided prefix overwrites default prefix."
279     ),
280 )
281 # Change `correlate` defaults here
282 corr_parser.set_defaults(
283     mode="correlate",
284     func=CrossCorrelate,
285 )
286
287
288 # MARK: Skyline Subparser
289 sky_parser = subparsers.add_parser(
290     "skylines",
291     aliases=["sky"],
292     help="Sky line check mode",
293     parents=[corr_sky_args],
294 )
295 # 'children' skyline args here
296 sky_parser.add_argument(
297     "-t",
298     "--transform",
299     action="store_false",
300     help=(
301         "Flag to force transform images. "
302         "Recommended to use only when input image(s) "
303         "are prefixed 't' but are not yet transformed."
304     ),
305 )
306 sky_parser.add_argument(
307     "-s",
308     "--save_prefix",
309     action="store",
310     nargs="?",
311     type=lambda path: Path(path).expanduser().resolve(),
312     const=SAVE_SKY,
313     help=(
314         "Prefix used when saving plot. "
315         "Excluding flag does not save output plot, "
316         f"flag usage of option uses default prefix {SAVE_SKY}, "
317         "and a provided prefix overwrites default prefix."
318     ),
319 )
320 # Change `skylines` defaults here
321 sky_parser.set_defaults(
322     mode="skyline",
323     func=Skylines,
324 )
325
326
327 # MARK: Keyword Clean Up
328 args = parser.parse_args()
329
330 if len(sys.argv) == 1:
331     parser.print_help(sys.stderr)
332     sys.exit(2)
333

```

```
334 args.verbose = Parser.parse_loglevel(args.verbose)
335
336 if 'log' in args and args.log not in ['', None]:
337     args.log = args.data_dir / args.log
338
339 if "filenames" in args:
340     args.filenames = Parser.flatten(args.filenames)
341
342 if "solutions_list" in args and isinstance(args.solutions_list, list):
343     args.solutions_list = Parser.flatten(args.solutions_list)
344
345 # MARK: Begin logging
346 logging.basicConfig(
347     filename=args.log,
348     format="%(asctime)s - %(module)s - %(levelname)s - %(message)s",
349     datefmt="%Y-%m-%d %H:%M:%S",
350     level=args.verbose,
351 )
352
353 # MARK: Call Relevant Class(Args)
354 logging.debug(f"Argparse namespace: {args}")
355 logging.info(f"Mode:{args.mode}")
356 args.func(**vars(args)).process()
357
358
359 # Confirm all processes completed and exit without error
360 logging.info("All done! Come again!\n")
```

Listing B.2: The source code for split.py

```

1 #!/usr/bin/env python3
2 # -*- coding: utf-8 -*-
3
4 """Module for splitting ``polsalt`` FITS files."""
5
6 # MARK: Imports
7 import os
8 import sys
9 import logging
10 from copy import deepcopy
11 from pathlib import Path
12
13 import numpy as np
14 from astropy.io import fits as pyfits
15
16 from STOPS.utils.SharedUtils import find_files, find_arc
17 from STOPS.utils.Constants import SAVE_PREFIX, CROP_DEFAULT, SPLIT_ROW
18
19
20 # MARK: Split Class
21 class Split:
22     """
23         The `Split` class allows for the splitting of `polsalt` FITS files
24         based on the polarization beam. The FITS files must have basic
25         `polsalt` pre-reductions already applied (`mxbp...` FITS files).
26
27     Parameters
28     -----
29         data_dir : str / Path
30             The path to the data to be split
31         fits_list : list[str], optional
32             A list of pre-reduced `polsalt` FITS files to be split
33             within `data_dir`.
34             (The default is None, `Split` will search for `mxbp*.fits` files)
35         split_row : int, optional
36             The row along which to split the data of each extension in
37             the FITS file.
38             (The default is SPLIT_ROW (See Notes), the SALT RSS CCD's middle row)
39         no_arc : bool, optional
40             Decides whether the arc frames should be recombined.
41             (The default is False, `polsalt` has no use for the arc after
42             wavelength calibrations)
43         save_prefix : dict[str, list[str]], optional
44             The prefix with which to save the O & E beams.
45             Setting `save_prefix` = ``None`` does not save the split O & E beams.
46             (The default is SAVE_PREFIX (See Notes))
47
48     Attributes
49     -----
50         arc : str
51             Name of arc FITS file within `data_dir`.
52             `arc` = ```` if `no_arc` or not detected in `data_dir`.
53         o_files, e_files : list[str]
54             A list of the `O`- and `E`-beam FITS file names.
55             The first entry is the arc file if `arc` defined.
56         data_dir
57         fits_list
58         split_row
59         save_prefix
60
61     Methods
62     -----
63         split_file(file: os.PathLike)
64             -> tuple[astropy.io.fits.HDUList]
65             Handles creation and saving the separated FITS files
66         split_ext(hdulist: astropy.io.fits.HDUList, ext: str = 'SCI')
67             -> astropy.io.fits.HDUList
68             Splits the data in the `ext` extension along the `split_row`
69         crop_file(hdulist: astropy.io.fits.HDUList, crop: int = CROP_DEFAULT)
70             -> tuple[numumpy.ndarray]
71             Crops the data along the edge of the frame, that is,

```

```

72     `O`-beam cropped as [crop:], and
73     `E`-beam cropped as [:‐crop].
74     update_beam_lists(o_name: str, e_name: str)
75         -> None
76         Updates `o_files` and `e_files`.
77     save_beam_lists(file_suffix: str = 'frames')
78         -> None
79         Creates (Overwrites if exists) and writes the `o_files` and `e_files`
80         to files named `o_{file_suffix}` and `e_{file_suffix}`, respectively.
81     process()
82         -> None
83         Calls `split_file` and `save_beam_lists` on each file in `fits_list`
84         for automation.
85
86     Other Parameters
87     -----
88     **kwargs : dict
89         keyword arguments. Allows for passing unpacked dictionary to
90         the class constructor.
91
92     Notes
93     -----
94     Constants Imported (See utils.Constants):
95         SAVE_PREFIX
96         CROP_DEFAULT
97         SPLIT_ROW
98
99
100    # MARK: Split init
101    def __init__(
102        self,
103            data_dir: Path,
104            fits_list: list[str] = None,
105            split_row: int = SPLIT_ROW,
106            no_arc: bool = False,
107            save_prefix: Path | None = None,
108            **kwargs,
109        ) -> None:
110            self.data_dir = data_dir
111            self.fits_list = find_files(
112                data_dir=data_dir,
113                filenames=fits_list,
114                prefix="mxgbp",
115                ext="fits"
116            )
117            self.split_row = split_row
118            self.save_prefix = SAVE_PREFIX
119            if isinstance(save_prefix, dict):
120                self.save_prefix = save_prefix
121
122            self.arc = "" if no_arc else find_arc(self.fits_list)
123            self.o_files = []
124            self.e_files = []
125
126            logging.debug(f"__init__\n{repr(self)}")
127
128        return
129
130    def __repr__(self) -> str:
131        template = (
132            "Split(\n"
133            f"\tdata_dir={self.data_dir},\n"
134            f"\tfits_list=[\n\t\t{str.join(
135                map(str, self.fits_list)
136            )}\n\t],\n"
137            f"\tsplit_row={self.split_row},\n"
138            f"\tno_arc={self.arc == ''},\n"
139            f"\tsave_prefix={self.save_prefix}\n"
140            ")"
141
142        )
143
144        return template

```

```

145 # MARK: Split Files
146 def split_file(
147     self,
148     file: os.PathLike
149 ) -> tuple[pyfits.HDUList, pyfits.HDUList]:
150     """
151         Split the single FITS file into separated `O`- and `E`- FITS files.
152
153     Parameters
154     -----
155     file : os.PathLike
156         The name of the FITS file to be split.
157
158     Returns
159     -----
160     tuple[astropy.io.fits.HDUList, astropy.io.fits.HDUList]
161         Tuple containing the split O and E beam HDULists.
162     """
163
164     # Create empty HDUList
165     o_beam = pyfits.HDUList()
166     e_beam = pyfits.HDUList()
167
168     # Open file and split O & E beams
169     with pyfits.open(file) as hdul:
170         o_beam.append(hdul["PRIMARY"].copy())
171         e_beam.append(hdul["PRIMARY"].copy())
172
173         # Split specific extension
174         raw_split = self.split_ext(hdul, "SCI")
175
176         # o_beam[0].data = raw_split['SCI'].data[1]
177         # e_beam[0].data = raw_split['SCI'].data[0]
178         o_beam[0].data, e_beam[0].data = self.crop_file(raw_split)
179
180         # Handle prefix and names
181         pref = "arc" if file == self.arc else "beam"
182         o_name = self.save_prefix[pref][0] + file.name[-9:]
183         e_name = self.save_prefix[pref][1] + file.name[-9:]
184
185         # Add split data to O & E beam lists
186         self.update_beam_lists(o_name, e_name, pref == "arc")
187
188         # Handle don't save case
189         if self.save_prefix is None:
190             return o_beam, e_beam
191
192         # Handle save case
193         o_beam.writeto(o_name, overwrite=True)
194         e_beam.writeto(e_name, overwrite=True)
195
196     return o_beam, e_beam
197
198 # MARK: Split extensions
199 def split_ext(
200     self,
201     hdulist: pyfits.HDUList,
202     ext: str = "SCI"
203 ) -> pyfits.HDUList:
204     """
205         Split the data of the specified extension of `hdulist` into
206         its `O`- and `E`- beams.
207
208     Parameters
209     -----
210     hdulist : astropy.io.fits.HDUList
211         The FITS HDUList to be split.
212     ext : str, optional
213         The name of the extension to be split.
214         (Defaults to 'SCI')
215
216     Returns
217     -----
218     astropy.io.fits.HDUList

```

```

218         The HDUList with the split applied.
219         """
220         hdu = deepcopy(hdulist)
221         rows, cols = hdu[ext].data.shape
222
223         # if odd number of rows, strip off the last one
224         rows = int(rows / 2) * 2
225
226         # how far split is from center of detector
227         offset = int(self.split_row - rows / 2)
228
229         # split arc into o/e images
230         ind_rc = np.indices((rows, cols))[0]
231         padbins = (ind_rc < offset) | (ind_rc > rows + offset)
232
233         # Roll split_row to be centre row
234         image_rc = np.roll(hdu[ext].data[:rows, :], -offset, axis=0)
235         image_rc[padbins] = 0.0
236
237         # Split columns equally
238         hdu[ext].data = image_rc.reshape((2, int(rows / 2), cols))
239
240     return hdu
241
242     # MARK: Crop files
243     @staticmethod
244     def crop_file(
245         hdulist: pyfits.HDUList,
246         crop: int = CROP_DEFAULT
247     ) -> tuple[np.ndarray, np.ndarray]:
248         """
249             Crop the data with respect to the `O`/`E` beam.
250
251             Parameters
252             -----
253             hdulist : astropy.io.fits.HDUList
254                 The HDUList containing the data to be cropped.
255             crop : int, optional
256                 The number of rows to be cropped from the bottom and top
257                 of the `O` and `E` beam, respectively.
258                 (Defaults to 40)
259
260             Returns
261             -----
262             tuple[numumpy.ndarray, np.ndarray]
263                 Tuple containing the cropped O and E beam data arrays.
264             """
265             o_data = hdulist["SCI"].data[1, 0:-crop]
266             e_data = hdulist["SCI"].data[0, crop:]
267
268         return o_data, e_data
269
270     # MARK: Update beam lists
271     def update_beam_lists(
272         self,
273         o_name,
274         e_name,
275         arc: bool = True
276     ) -> None:
277         """
278             Update the `o_files` and `e_files` attributes.
279
280             Parameters
281             -----
282             o_name : str
283                 The filename of the O beam.
284             e_name : str
285                 The filename of the E beam.
286             arc : bool, optional
287                 Indicates whether the first entry should be the arc frame.
288                 (Defaults to True)
289
290             Returns

```

```

291     -----
292     None
293
294     """
295     if arc:
296         self.o_files.insert(0, o_name)
297         self.e_files.insert(0, e_name)
298     else:
299         self.o_files.append(o_name)
300         self.e_files.append(e_name)
301
302     return
303
304 # MARK: Save beam lists
305 def save_beam_lists(self, file_suffix: str = 'frames') -> None:
306     with open(f"o_{file_suffix}", "w+") as f_o, \
307          open(f"e_{file_suffix}", "w+") as f_e:
308         for i, j in zip(self.o_files, self.e_files):
309             f_o.write(i + "\n")
310             f_e.write(j + "\n")
311
312     return
313
314 # MARK: Process all Listed Images
315 def process(self) -> None:
316     """
317     Process all FITS images stored in the `fits_list` attribute
318
319     Returns
320     -----
321     None
322     """
323     for target in self.fits_list:
324         logging.debug(f"Processing {target}")
325         self.split_file(target)
326
327     self.save_beam_lists()
328
329     return
330
331
332 # MARK: Main function
333 def main(argv) -> None:
334     """Main function."""
335
336     return
337
338
339 if __name__ == "__main__":
340     main(sys.argv[1:])

```

Listing B.3: The source code for `join.py`

```

1 #!/usr/bin/env python3
2 # -*- coding: utf-8 -*-
3
4 """
5 Module for joining the split FITS files with an external wavelength solution.
6 """
7
8 # MARK: Imports
9 import os
10 import sys
11 import logging
12 import re
13 from pathlib import Path
14
15 import numpy as np
16 from numpy.polynomial.chebyshev import chebgrid2d as chebgrid2d
17 from numpy.polynomial.legendre import leggrid2d as leggrid2d
18 from astropy.io import fits as pyfits
19
20 # from lacosmic import lacosmic # Deprecated: ccdproc is ~6x faster
21 from ccdproc import cosmicray_lacosmic as lacosmic
22
23 from STOPS.utils.specpolpy3 import read_wollaston, split_sci
24 from STOPS.utils.SharedUtils import find_files, find_arc
25 from STOPS.utils.Constants import DATADIR, SAVE_PREFIX, SPLIT_ROW, CR_PARAMS
26
27
28 # MARK: Join Class
29 class Join:
30     """
31         The `Join` class allows for the joining of previously split files
32         and the appending of an external wavelength solution in the
33         `polsalt` FITS file format.
34
35     Parameters
36     -----
37     data_dir : str / Path
38         The path to the data to be joined
39     database : str, optional
40         The name of the `IRAF` database folder.
41         (The default is "database")
42     fits_list : list[str], optional
43         A list of pre-reduced `polsalt` FITS files to be joined
44         within `data_dir`.
45         (The default is ``None``, `Join` will search for `m*gbp*.fits` files)
46     solutions_list: list[str], optional
47         A list of solution filenames from which the wavelength solution
48         is created.
49         (The default is ``None``, `Join` will search for `fc*` files within
50         the `database` directory)
51     split_row : int, optional
52         The row along which the data of each extension in the FITS file
53         was split.
54         Necessary when Joining cropped files.
55         (The default is 517, the SALT RSS CCD's middle row)
56     save_prefix : dict[str, list[str]], optional
57         The prefix with which the previously split `O`- & `E`-beams were saved.
58         Used for detecting if cropping was applied during
59         the splitting procedure.
60         (The default is SAVE_PREFIX (See Notes))
61     verbose : int, optional
62         The level of verbosity to use for the Cosmic ray rejection
63         (The default is 30, i.e., logging.INFO)
64
65     Attributes
66     -----
67     fc_files : list[str]
68         Valid solutions found from `solutions_list`.
69     custom : bool
70         Internal flag for whether `solutions_list` uses the `IRAF`
71         or a custom format.

```

```

72     See Notes for custom solution formatting.
73     (Default (inherited from `solutions_list`) is False)
74     arc : str
75         Deprecated. Name of arc FITS file within `data_dir`.
76     data_dir
77     database
78     fits_list
79     split_row
80     save_prefix
81
82     Methods
83     -----
84     get_solutions(wavlist: list / None, prefix: str = "fc") ->
85         (fc_files, custom): tuple[list[str], bool]
86         Parse `solutions_list` and return valid solution files and if they are
87         non-`IRAF` solutions.
88     parse_solution(fc_file: str, x_shape: int, y_shape: int) ->
89         tuple[dict[str, int], np.ndarray]
90         Loads the wavelength solution file and parses keywords necessary for
91         creating the wavelength extension.
92     join_file(file: os.PathLike) -> None
93         Joins the files,
94         attaches the wavelength solutions,
95         performs cosmic ray cleaning,
96         masks the extension,
97         and checks cropping performed in `Split`.
98         Writes the FITS file in a `polsalt` valid format.
99     check_crop(hdu: pyfits.HDUList, o_file: str, e_file: str) -> int
100        Opens the split `O`- and `E`-beam FITS files and returns the amount of
101        cropping that was performed.
102     process() -> None
103        Calls `join_file` on each file in `fits_list` for automation.
104
105     Other Parameters
106     -----
107     no_arc : bool, optional
108         Deprecated. Decides whether the arc frames should be processed.
109         (The default is False, `polsalt` has no use for the arc after
110         wavelength calibrations)
111     **kwargs : dict
112         keyword arguments. Allows for passing unpacked dictionary to the
113         class constructor.
114
115     Notes
116     -----
117     Constants Imported (See utils.Constants):
118         DATADIR, SAVE_PREFIX, SPLIT_ROW, CR_PARAMS
119
120     Custom wavelength solutions must be formatted containing:
121         `x`, `y`, *coefficients...
122     where a solution are of order (`x` by `y`) and
123     must contain  $x \times y$  coefficients, all separated by newlines.
124     The name of the custom wavelength solution file must contain
125     either "cheb" or "leg" for Chebyshev or Legendre wavelength solutions,
126     respectively.
127
128     Cosmic ray rejection is performed using lacosmic [1]-
129     implemented in ccdproc via astroscrappy [2]_.
130
131     References
132     -----
133     .. [1] van Dokkum 2001, PASP, 113, 789, 1420
134         (article : https://adsabs.harvard.edu/abs/2001PASP..113.1420V)
135     .. [2] https://zenodo.org/records/1482019
136
137     """
138
139     # MARK: Join init
140     def __init__(self,
141                  data_dir: Path,
142                  database: str = "database",
143                  fits_list: list[str] = None,
144

```

```

145     solutions_list: list[Path] = None,
146     split_row: int = SPLIT_ROW,
147     no_arc: bool = True,
148     save_prefix: Path | None = None,
149     verbose: int = 30,
150     **kwargs,
151 ) -> None:
152     self.data_dir = data_dir
153     self.database = Path(data_dir) / database
154     self.fits_list = find_files(
155         data_dir=self.data_dir,
156         filenames=fits_list,
157         prefix="mxgbp",
158         ext="fits",
159     )
160     self.fc_files, self.custom = self.get_solutions(solutions_list)
161     self.split_row = split_row
162     self.save_prefix = SAVE_PREFIX
163     if isinstance(save_prefix, dict):
164         self.save_prefix = save_prefix
165
166     self.no_arc = no_arc
167     self.arc = find_arc(self.fits_list)
168
169     self.verbose = verbose < 30
170
171     logging.debug(f"__init__\n{repr(self)}")
172
173     return
174
175 # MARK: Join repr
176 def __repr__(self) -> str:
177     template = (
178         "Join(\n"
179         f"\tdata_dir={self.data_dir},\n"
180         f"\tdatabase={self.database},\n"
181         f"\tfits_list=[\n\t\t{self.fits_list}\n\t].join(\n"
182             map(str, self.fits_list)
183         )}\n\t],\n"
184         f"\tsolutions_list={self.fc_files},\n"
185         f"\tsplit_row={self.split_row},\n"
186         f"\tno_arc={self.no_arc},\n"
187         f"\tsave_prefix={self.save_prefix},\n"
188         f"\tverbose={self.verbose}\n"
189     )\n"
190     )
191
192     return template
193
194 # MARK: Find 2D WAV Functions
195 def get_solutions(
196     self,
197     wavlist: list[str] | None,
198     prefix: str = "fc",
199     reverse: bool = False,
200 ) -> tuple[list[str], bool]:
201     """
202         Get the list of wavelength solution files.
203
204     Parameters
205     -----
206     wavlist : list[str] / None
207         A list of custom wavelength solutions files.
208         If ``None``, `Join` will search for wavelength solutions
209         in the `database` directory.
210     prefix : str, optional
211         The prefix of the wavelength solution files.
212         (Defaults to "fc")
213     reverse : bool, optional
214         Whether to reverse the wavelength solution files.
215         Necessary when `wavlist` ordered ['O', 'E']
216         (Defaults to False)
217

```

```

218     Returns
219     -----
220     tuple[list[str], bool]
221         A tuple containing the list of wavelength solutions files and
222         a boolean indicating whether custom solutions were provided.
223
224     """
225     # No custom solutions
226     if not wavlist:
227         # Handle finding solutions
228         ws = []
229         for fl in os.listdir(self.database):
230             if os.path.isfile(
231                 self.database / fl
232             ) and (prefix == fl[0:len(prefix)]):
233                 ws.append(fl)
234
235     if len(ws) != 2:
236         # Handle incorrect number of solutions found
237         msg = (
238             f"Incorrect amount of wavelength solutions "
239             f"({len(ws)} fc... files) found in the solution "
240             f"dir.: {self.database}"
241         )
242         logging.error(msg)
243         raise FileNotFoundError(msg)
244
245     sols = {
246         i: j for i, j in zip(['O', 'E'], sorted(ws, reverse=reverse))
247     }
248     logging.debug(f"get_solutions - Found {sols} in {self.database}")
249
250     return sorted(ws, reverse=reverse), False
251
252     # Custom solution
253     if len(wavlist) >= 2:
254         if len(wavlist) > 2:
255             logging.warning(
256                 f" Too many solutions, only {wavlist[:2]} are considered"
257             )
258             wavlist = wavlist[:2]
259
260         for fl in wavlist:
261             if not os.path.isfile(os.path.join(self.data_dir, fl)):
262                 msg = (
263                     f"{fl} not found in the "
264                     f"data directory {self.data_dir}"
265                 )
266                 logging.error(msg)
267                 raise FileNotFoundError(msg)
268
269         sols = {
270             i: j for i, j in zip(
271                 ['O', 'E'],
272                 sorted(wavlist, reverse=reverse)
273             )
274         }
275         logging.debug(f"get_solutions - Found {sols} in {self.database}")
276
277     return sorted(wavlist, reverse=reverse), True
278
279     # MARK: Parse 2D WAV Function
280     def parse_solution(
281         self,
282         fc_file: str,
283         x_shape: int,
284         y_shape: int
285     ) -> tuple[dict[str, int], np.ndarray]:
286         """
287             Parse the 2D wavelength solution function from `fc_file`.
288
289         Parameters
290         -----

```

```

291     fc_file : str
292         The filename of the wavelength solutions file.
293     x_shape : int
294         The x-order of the 2D solution.
295     y_shape : int
296         The y-order of the 2D solution.
297
298     Returns
299     -----
300     tuple[dict[str, int], np.ndarray]
301         A tuple containing a dictionary of
302         the parameters of the solution function
303         and the function coefficients.
304
305     """
306     fit_params = {}
307
308     if self.custom:
309         # Load coefficients
310         coeff = np.loadtxt(fc_file)
311
312         fit_params["xorder"] = int(coeff[0].astype(int))
313         fit_params["yorder"] = int(coeff[1].astype(int))
314         coeff = coeff[2:]
315
316         f_type = 3
317         if "cheb" in str(fc_file):
318             f_type = 1
319         elif "leg" in str(fc_file):
320             f_type = 2
321         fit_params["function"] = f_type
322
323         fit_params["xmin"], fit_params["xmax"] = 1, x_shape
324         fit_params["ymin"], fit_params["ymax"] = 1, y_shape
325
326     else:
327         # Parse IRAF fc database files
328         file_contents = []
329         with open(self.database / fc_file) as fcfile:
330             for i in fcfile:
331                 file_contents.append(re.sub(r"\n\t\s*", "", i))
332
333         if file_contents[9] != "1.": # xterms - Cross-term type
334             msg = (
335                 "Cross-term not recognised (always 1 for "
336                 "FITCOORDS), redo FITCOORDS or change manually."
337             )
338             raise Exception(msg)
339
340         fit_params["function"] = int(file_contents[6][-1])
341
342         fit_params["xorder"] = round(float(file_contents[7][-1]), None)
343         fit_params["yorder"] = round(float(file_contents[8][-1]), None)
344
345         fit_params["xmin"] = int(file_contents[10][-1])
346         fit_params["xmax"] = x_shape
347         # int(file_contents[11][-1])# stretch fit over x
348         fit_params["ymin"] = int(file_contents[12][-1])
349         fit_params["ymax"] = y_shape
350         # int(file_contents[13][-1])# stretch fit over y
351
352         coeff = np.array(file_contents[14:], dtype=float)
353
354         coeff = np.reshape(
355             coeff,
356             (fit_params["xorder"], fit_params["yorder"]))
357     )
358
359     return fit_params, coeff
360
361     # MARK: Join Files
362     def join_file(self, file: os.PathLike) -> None:
363         """

```

```

364     Join the `O`- and `E`-beams, attach the wavelength solutions,
365     perform cosmic ray cleaning, mask the extensions,
366     and checks cropping performed by `Split`.
367     Write the FITS file in a `polsalt` valid format.
368
369     Parameters
370     -----
371     file : os.PathLike
372         The path of the FITS file to be joined.
373
374     See Also
375     -----
376     IRAF - `fitcoords` task
377         https://iraf.net/irafdocs/formats/fitcoords.php,
378     numpy 2D grid functions
379         https://numpy.org/doc/stable/reference/generated/numpy
380         Chebyshev: + '.polynomial.chebyshev.chebgrid2d.html'">''.polynomial.chebyshev.chebgrid2d.html'
381         Legendre: + '.polynomial.legendre.leggrid2d.html'">''.polynomial.legendre.leggrid2d.html'
382
383     """
384     # Create empty wavelength appended hdu list
385     whdu = pyfits.HDULIST()
386
387     # Handle prefix and names
388     pref = "arc" if file == self.arc else "beam"
389     o_file = self.save_prefix[pref][0] + file.name[-9:]
390     e_file = self.save_prefix[pref][1] + file.name[-9:]
391
392     # Open file
393     with pyfits.open(file) as hdu:
394         # Check if file has been cropped
395         cropsize = self.check_crop(hdu, o_file, e_file)
396
397         y_shape = int(hdu["SCI"].data.shape[0] / 2) - cropsize
398         x_shape = hdu["SCI"].data.shape[1]
399
400         # No differences in "PRIMARY" extension header
401         primary_ext = hdu["PRIMARY"]
402         primary_ext.header["HISTORY"] = f"CRCLEAN: {CR_PARAMS}"
403         whdu.append(primary_ext)
404
405         for ext in ["SCI", "VAR", "BPM"]:
406             whdu.append(pyfits.ImageHDU(name=ext))
407             whdu[ext].header = hdu[ext].header.copy()
408             whdu[ext].header["CTYPE3"] = "O,E"
409
410             # Create empty extensions with correct order and format
411             if ext == "BPM":
412                 whdu[ext].data = np.zeros(
413                     (2, y_shape, x_shape),
414                     dtype="uint8"
415                 )
416                 whdu[ext].header["BITPIX"] = "-uint8"
417             else:
418                 whdu[ext].data = np.zeros(
419                     (2, y_shape, x_shape),
420                     dtype=">f4"
421                 )
422                 whdu[ext].header["BITPIX"] = "-32"
423
424             # Fill in empty extensions
425             if cropsize:
426                 temp_split = split_sci(
427                     hdu,
428                     self.split_row,
429                     ext=ext
430                 )[ext].data
431                 whdu[ext].data[0] = temp_split[0, cropsize:]
432                 whdu[ext].data[1] = temp_split[1, 0:-cropsize]
433
434             else:
435                 whdu[ext].data = split_sci(
436                     hdu,

```

```

437             self.split_row,
438             ext=ext
439         )[ext].data
440     # End of hdu calls, close hdu
441
442     # MARK: Join (Wav. Ext.)
443     whdu.append(pyfits.ImageHDU(name="WAV"))
444     wav_header = whdu["SCI"].header.copy()
445     wav_header["EXTNAME"] = "WAV"
446     wav_header["CTYPE3"] = "O,E"
447     whdu["WAV"].header = wav_header
448
449     whdu["WAV"].data = np.zeros(
450         whdu["SCI"].data.shape,
451         dtype=">f4"
452     )
453
454     for num, fname in enumerate(self.fc_files):
455         params, coeffs = self.parse_solution(
456             fname,
457             x_shape,
458             y_shape
459         )
460
461         if params["function"] == 1: # Function type (1 = chebyshev)
462             # Set wavelength extension values to function
463             whdu["WAV"].data[num] = chebgrid2d(
464                 x=np.linspace(-1, 1, params["ymax"]),
465                 y=np.linspace(-1, 1, params["xmax"]),
466                 c=coeffs,
467             )
468
469         elif params["function"] == 2: # Function type (2 = legendre)
470             # Set wavelength extension values to function
471             whdu["WAV"].data[num] = leggrid2d(
472                 x=np.linspace(-1, 1, params["ymax"]),
473                 y=np.linspace(-1, 1, params["xmax"]),
474                 c=coeffs,
475             )
476
477         else:
478             msg = (
479                 "Function type not recognised, please wavelength "
480                 "calibrate using either Chebyshev or Legendre."
481             )
482             raise Exception(msg)
483
484     # MARK: Cosmic Ray Cleaning
485     # See utils.Constants for `CR_PARAMS` discussion
486     whdu["SCI"].data[num] = lacosmic(
487         whdu["SCI"].data[num],
488         # contrast=CR_PARAMS['CR_CONTRAST'],
489         # threshold=CR_PARAMS['CR_THRESHOLD'],
490         # neighbor_threshold=CR_PARAMS['CR_NEIGH_THRESH'],
491         # effective_gain=CR_PARAMS['GAIN'],
492         # background=CR_PARAMS['BACKGROUND'],
493         # readnoise=CR_PARAMS['READ_NOISE'],
494         # gain=CR_PARAMS['GAIN'],
495         # gain_apply=CR_PARAMS['GAIN_APPLY'],
496         # objlim=CR_PARAMS['OBJ_LIM'],
497         verbose=self.verbose,
498     )[0]
499
500     # MARK: WAV masking
501     # Left & Right Crop
502     whdu["WAV"].data[whdu["WAV"].data[:] < 3_000] = 0.0
503     whdu["WAV"].data[whdu["WAV"].data[:] >= 10_000] = 0.0
504
505     # Top & Bottom Crop (shift\tilt)
506     rpix_oc, cols, rbin, lam_c = read_wollaston(
507         whdu,
508         DATADIR + "wollaston.txt"
509     )

```

```

510
511     drow_oc = (rpix_oc - rpix_oc[:, int(cols / 2)][:, None]) / rbin
512
513     # Cropping as suggested
514     for c, col in enumerate(drow_oc[0]):
515         if np.isnan(col):
516             continue
517
518         if int(col) < 0:
519             whdu["WAV"].data[0, int(col):, c] = 0.0
520         elif int(col) > cropsize:
521             whdu["WAV"].data[0, 0: int(col) - cropsize, c] = 0.0
522
523     for c, col in enumerate(drow_oc[1]):
524         if np.isnan(col):
525             continue
526
527         if int(col) > 0:
528             whdu["WAV"].data[1, 0: int(col), c] = 0.0
529         elif (int(col) < 0) & (abs(int(col)) > cropsize):
530             whdu["WAV"].data[1, int(col) + cropsize:, c] = 0.0
531
532     # MARK: BPM masking
533     whdu["BPM"].data[0] = np.where(
534         whdu["WAV"].data[0] == 0,
535         1,
536         whdu["BPM"].data[0]
537     )
538     whdu["BPM"].data[1] = np.where(
539         whdu["WAV"].data[1] == 0,
540         1,
541         whdu["BPM"].data[1]
542     )
543
544     whdu.writeto(f"w{os.path.basename(file)}", overwrite=True)
545
546     return
547
548     # MARK: Check Crop
549     @staticmethod
550     def check_crop(
551         hdu: pyfits.HDUList,
552         o_file: str,
553         e_file: str
554     ) -> int:
555         """
556             Check if cropping is necessary when joining `O`- and `E`-beams.
557
558         Parameters
559         -----
560         hdu : astropy.io.fits.HDUList
561             The HDUList to check for cropping.
562         o_file : str
563             The name of the previously split `O`-beam FITS file.
564         e_file : str
565             The name of the previously split `E`-beam FITS file.
566
567         Returns
568         -----
569         int
570             The number of rows which were cropped by `Split`.
571
572         """
573         cropsize = 0
574
575         with pyfits.open(o_file) as o, \
576             pyfits.open(e_file) as e:
577             o_y = o[0].data.shape[0]
578             e_y = e[0].data.shape[0]
579
580             if hdu["SCI"].data.shape[0] != (o_y + e_y):
581                 # Get crop size, assuming crop same on both sides
582                 cropsize = int((hdu["SCI"].data.shape[0] - o_y - e_y) / 2)

```

```
583     return cropsize
584
585
586 # MARK: Process all Listed Images
587 def process(self) -> None:
588     """Process all FITS images stored in the `fits_list` attribute"""
589     for target in self.fits_list:
590         logging.debug(f"Processing {target}")
591         self.join_file(target)
592
593     return
594
595
596 def main(argv) -> None:
597     """Main function."""
598
599     return
600
601
602 if __name__ == "__main__":
603     main(sys.argv[1:])
```

Listing B.4: The source code for `cross_correlate.py`

```

1 #!/usr/bin/env python3
2 # -*- coding: utf-8 -*-
3
4 """Module for cross correlating polarization beams."""
5
6 # MARK: Imports
7 import sys
8 import logging
9 import itertools as iters
10 from pathlib import Path
11 from importlib.resources import files
12 from typing import Callable
13
14 import numpy as np
15 from numpy.polynomial import chebyshev
16 import matplotlib.pyplot as plt
17 import matplotlib.axes
18 from astropy.io import fits as pyfits
19 from scipy import signal
20
21 from STOPS.utils.SharedUtils import find_files, continuum
22 from STOPS.utils.Constants import SAVE_CORR, OFFSET
23 import STOPS.utils
24
25 # MARK: Logging init.
26 mpl_logger = logging.getLogger('matplotlib')
27 mpl_logger.setLevel(logging.INFO)
28
29
30 # MARK: Correlate class
31 class CrossCorrelate:
32     """
33         Cross correlate allows for comparing the extensions of multiple
34         FITS files, or comparing the $O$- and $E$-beams of a single FITS file.
35
36         Parameters
37         -----
38         data_dir : str / Path
39             The path to the data to be cross correlated
40         filenames : list[str]
41             The ecwma*gbp*.fits files to be cross correlated.
42             If only one filename is defined, correlation is done against the two
43             polarization beams.
44         split_ccd : bool, optional
45             Decides whether the CCD regions should each be individually
46             cross correlated.
47             (The default is True, which splits the spectrum up into its separate
48             CCD regions)
49         cont_ord : int, optional
50             The degree of a chebyshev to fit to the continuum.
51             (The default is 11)
52         plot : bool, optional
53             Decides whether the continuum fitting should be plotted
54             (The default is False, so no continua plots are displayed)
55         save_prefix : str, optional
56             The name or directory to save the figure produced to.
57             "." saves a default name to the current working. A default name is
58             also used when save_prefix is a directory.
59             (The default is None, i.e., The figure is not saved, only displayed)
60
61         Attributes
62         -----
63         data_dir
64         fits_list
65         beams : str
66             The mode of correlation.
67             'OE' for same file, and 'O' or 'E' for different files but same
68             extension.
69         ccds : int
70             The number of CCD's in the data.
71             Used to split the CCD's if split_ccd is True.

```

```

72     cont_ord : int
73         The degree of the chebyshev to fit to the continuum.
74     can_plot : bool
75         Decides whether the continuum fitting should be plotted
76     offset : int, DEPRECATED
77         The amount the spectrum is shifted, mainly to test the effect of the
78         cross correlation.
79         (The default is 0, i.e., no offset introduced)
80     save_prefix
81     wav_unit : str
82         The units of the wavelength axis.
83         (The default is Angstroms)
84     wav_cdelt : int
85         The wavelength increment.
86         (The default is 1)
87     alt : Callable
88         An alternate method of cross correlating the data.
89         (The default is None)
90
91     Methods
92     -----
93     load_file(filename: Path) -> tuple[np.ndarray, np.ndarray, np.ndarray]
94         Loads the data from a FITS file.
95     get_bounds(bpm: np.ndarray) -> np.ndarray
96         Finds the bounds for the CCD regions.
97     remove_cont(spec: list, wav: list, bpm: list, plot_cont: bool) -> None
98         Removes the continuum from the data.
99     correlate(filename1: Path, filename2: Path / None = None) -> None
100        Cross correlates the data.
101    ftcs(filename1: Path, filename2: Path / None = None) -> None
102        Cross correlates the data using the Fourier Transform.
103    plot(spec, wav, bpm, corrdbs, lagsdb) -> None
104        Plots the data.
105    process() -> None
106        Processes the data.
107
108    Other Parameters
109    -----
110    offset : int, optional
111        The amount the spectrum is shifted, mainly to test the effect of the
112        cross correlation.
113        (The default is 0, i.e., no offset introduced)
114    **kwargs : dict
115        keyword arguments.
116        Allows for passing unpacked dictionary to the class constructor.
117    ftcs : bool, optional
118        Boolean whether to use Fourier Transform for cross correlation.
119
120    See Also
121    -----
122    scipy:
123        https://docs.scipy.org/doc/scipy/reference/generated/scipy.signal.correlate.html
124        correlation:
125            scipy.signal.correlate.html
126    matplotlib custom style:
127        https://matplotlib.org/stable/users/explain/customizing.html
128
129    Notes
130    -----
131    Constants Imported (See utils.Constants):
132        SAVE_CORR:
133            The default save name for the correlation plot.
134        OFFSET:
135            The vertical offset of spectra in the output plot.
136        """
137
138    # MARK: Correlate init
139    def __init__(
140        self,
141        data_dir: Path,
142        filenames: list[str],
143        beams: str = "OE",
144        split_ccd: bool = True,

```

```

145     cont_ord: int = 11,
146     plot: bool = False,
147     offset: int = 0,
148     save_prefix: Path | None = None,
149     **kwargs,
150 ) -> None:
151     self.data_dir = data_dir
152     self.fits_list = find_files(
153         data_dir=self.data_dir,
154         filenames=filenames,
155         prefix="ecwmxgbp",
156         ext="fits",
157     )
158     self._beams = None
159     self.beams = beams
160
161     self.ccds = 1
162     if split_ccd:
163         # with pyfits.open(self.fits_list[0]) as hdu:
164         #     BPM == 2 near center of CCD (extract version != *_sc)
165         #     self.ccds = sum(hdu["BPM"].data.sum(axis=1)[0] == 2)
166         self.ccds = 3
167
168     self.cont_ord = cont_ord
169     self.can_plot = plot
170
171     self.offset = offset
172     if offset != 0:
173         # logging.warning("'offset' is only for testing.")
174         # Add an offset to the spectra to test cross correlation
175         # self.spec1 = np.insert(
176         #     self.spec1, [0] * offset, self.spec1[:, :offset], axis=-1
177         # )[ :, : self.spec1.shape[-1]]
178
179         err_msg = "Offset deprecated after testing finalized."
180         logging.error(err_msg)
181         raise DeprecationWarning(err_msg)
182
183     self.save_prefix = save_prefix
184     # Handle directory save name
185     if self.save_prefix and self.save_prefix.is_dir():
186         self.save_prefix /= SAVE_CORR
187         logging.warning((
188             f"Correlation save name resolves to a directory. "
189             f"Saving under {self.save_prefix}"
190         ))
191
192     self.wav_unit = "$\\AA$"
193     self.wav_cdelet = 1
194
195     self.alt = self.ftcs if kwargs.get("ftcs") else None
196
197     logging.debug(f"__init__ - \n{repr(self)}")
198
199     return
200
201 # MARK: Correlate repr
202 def __repr__(self) -> str:
203     template = (
204         "CrossCorrelate(\n"
205         f"\tdata_dir={self.data_dir},\n"
206         f"\tfits_list=[\n\t\tt{\\n\\t\\t}.join(\n"
207             map(str, self.fits_list)
208         )]\\n\\t],\\n"
209         f"\tbeams={self._beams},\\n"
210         f"\tsplit_ccd={self.ccds},\\n"
211         f"\tcont_ord={self.cont_ord},\\n"
212         f"\tplot={self.can_plot},\\n"
213         f"\toffset={self.offset},\\n"
214         f"\tsave_prefix={self.save_prefix},\\n"
215         f"\twav_unit={self.wav_unit},\\n"
216         f"\twav_cdelet={self.wav_cdelet},\\n"
217         f"\talt={self.alt},\\n"

```

```

218         ") \n"
219     )
220
221     return template
222
223     # MARK: Beams property
224     @property
225     def beams(self) -> str:
226         return self._beams
227
228     @beams.setter
229     def beams(self, mode: str) -> None:
230         if mode not in ['O', 'E', 'OE']:
231             err_msg = f"Correlation mode '{mode}' not recognized."
232             logging.error(err_msg)
233             raise ValueError(err_msg)
234
235         self._beams = mode
236
237     return
238
239     # MARK: Load file
240     def load_file(
241         self,
242         filename: Path
243     ) -> tuple[np.ndarray, np.ndarray, np.ndarray]:
244         """
245             Load the data from a FITS file.
246
247             Parameters
248             -----
249             filename : Path
250                 The name of the FITS file to load.
251
252             Returns
253             -----
254             tuple[np.ndarray, np.ndarray, np.ndarray]
255                 The spectrum, wavelength, and bad pixel mask.
256
257         """
258
259         # Open HDU
260         with pyfits.open(filename) as hdul:
261             spec = hdul["SCI"].data.sum(axis=1)
262             wav = (
263                 np.arange(spec.shape[-1])
264                 * hdul["SCI"].header["CDELT1"]
265                 + hdul["SCI"].header["CRVAL1"]
266             )
267             wav = np.array((wav, wav))
268             bpm = hdul["BPM"].data.sum(axis=1)
269
270             self.wav_cdelt = float(hdul["SCI"].header["CDELT1"])
271
272             if hdul["SCI"].header["CTYPE1"] != 'Angstroms':
273                 self.wav_unit = hdul["SCI"].header["CTYPE1"]
274
275         return spec, wav, bpm
276
277     # MARK: Get bounds
278     def get_bounds(self, bpm: np.ndarray, gap_length: int = 30) -> np.ndarray:
279         """
280             Find the bounds for a file based on the CCD count.
281
282             Parameters
283             -----
284             bpm : np.ndarray
285                 The bad pixel mask.
286             gap_length : int, optional
287                 The minimum length of a gap to be considered a CCD region.
288                 (Defaults to 30)
289
290             Returns

```

```

291     -----
292     np.ndarray
293         The bounds for the CCD regions.
294
295     """
296     if not 0 <= gap_length <= 60:
297         msg = f"An invalid gap length of {gap_length} was encountered."
298         logging.error(msg)
299         raise ValueError(msg)
300
301     # Check if get_bounds is needed
302     if self.ccds == 1:
303         return np.array(
304             [[(0, bpm[0].shape[-1]), (0, bpm[1].shape[-1])]]
305         ).astype(int)
306
307     # bounds.shape -> (0/E, CCD's, low./up. bound)
308     bounds = np.zeros((2, self.ccds, 2))
309
310     # Check if `BPM` contains any `2`'s
311     if np.any(bpm == 2):
312         for ext, ccd in iter.product(range(2), range(self.ccds)):
313             mid = np.where(bpm[ext] == 2)[0][ccd]
314             ccds = self.ccds * 2
315             bounds[ext, ccd] = (
316                 max(mid - bpm.shape[-1] // ccds, 0),
317                 min(mid + bpm.shape[-1] // ccds, bpm.shape[-1])
318             )
319
320         return bounds.astype(int)
321
322     for ext in range(len(self._beams)):
323
324         # Find min and max vals
325         min_val, max_val = 0, bpm[ext].shape[-1]
326
327         while True:
328             if bpm[ext][min_val] == 0:
329                 break
330             min_val += 1
331
332         while True:
333             if bpm[ext][max_val - 1] == 0:
334                 break
335             max_val -= 1
336
337         # Find ranges of non zero values
338         regions: list[np.ndarray] = np.split(
339             np.where(bpm[ext], min_val: max_val == 1)[0],
340             np.where(
341                 np.diff(np.where(bpm[ext], min_val: max_val == 1)[0]) != 1
342             )[0] + 1
343         )
344
345         # If less than 2 regions, raise error
346         if len(regions) < 2:
347             msg = "Less than 2 regions found in BPM. Returning bounds."
348             logging.error(msg)
349             raise ValueError(msg)
350
351         # Find `regions` longer than `gap_length`
352         regions = [
353             region for region in regions
354             if len(region) >= gap_length
355         ]
356
357         # Ensure 2 regions are found
358         if len(regions) < 2:
359             logging.debug(
360                 "get_bounds - Less than 2 regions found in BPM." +
361                 f"Calling get_bounds with gap_length = {gap_length - 10}"
362             )
363             return self.get_bounds(bpm, gap_length - 10)

```

```

364
365     elif len(regions) > 2:
366         logging.debug(
367             "get_bounds - More than 2 regions found in BPM. " +
368             f"Calling get_bounds with gap_length = {gap_length + 5}"
369         )
370         return self.get_bounds(bpm, gap_length - 10)
371
372     # Ensure region order correct
373     if regions[0][0] > regions[1][0]:
374         regions = regions[::-1]
375
376     # Assign bounds from regions
377     bounds[ext] = np.array([
378         (min_val, regions[0][0]),
379         (regions[0][-1], regions[1][0]),
380         (regions[1][-1], max_val),
381     ])
382
383     # Get lower and upper bound for each ccd, save to bounds
384     # Lower -> min is zero, Upper -> max is bpm length
385
386     # for ext in range(2):
387     #     cedge = ccdcenter(bpm[ext])
388     #     bounds[ext] = np.array(cedge)
389
390     logging.debug(f"get_bounds - found bounds at \n{bounds.astype(int)}")
391
392     return bounds.astype(int)
393
394     # MARK: Remove Continua
395     def remove_cont(
396         self,
397         spec: np.ndarray,
398         wav: np.ndarray,
399         bpm: np.ndarray,
400         plot_cont: bool
401     ) -> np.ndarray:
402         """
403             Remove the continuum from the data.
404
405             Parameters
406             -----
407             spec : np.ndarray
408                 The spectrum to remove the continuum from.
409             wav : np.ndarray
410                 The wavelength of the spectrum.
411             bpm : np.ndarray
412                 The bad pixel mask.
413             plot_cont : bool
414                 Decides whether the continuum fitting should be plotted
415
416             Returns
417             -----
418             spec : np.ndarray
419
420             """
421             # Mask out the bad pixels for fitting continua
422             okwav = np.where(bpm != 1)
423
424             # Define continua
425             ctm = continuum(
426                 wav[okwav],
427                 spec[okwav],
428                 deg=self.cont_ord,
429                 plot=plot_cont,
430             )
431
432             # Normalise spectra
433             spec /= chebyshev.chebval(wav, ctm)
434             spec -= 1
435
436             return spec

```

```

437
438     # MARK: Correlate
439     def correlate(
440         self,
441         filename1: Path,
442         filename2: Path | None = None,
443         alt: Callable = None
444     ) -> tuple[np.ndarray, np.ndarray, np.ndarray, list[list], list[list]]:
445         """
446             Cross correlates the data.
447
448         Parameters
449         -----
450             filename1 : Path
451                 The name of the first FITS file to cross correlate.
452             filename2 : Path, optional
453                 The name of the second FITS file to cross correlate.
454                 (Defaults to None)
455             alt : Callable, optional
456                 An alternate method of cross correlating the data.
457                 (Defaults to None)
458
459         Returns
460         -----
461             spec, wav, bpm, lagsdb, corrdb:
462                 tuple[np.ndarray, np.ndarray, np.ndarray, list[list], list[list]]
463
464         """
465         # mode: 0E -> '01' & 'E1', 0 -> '01' & '02', E -> 'E1' & 'E2'
466         # Load data
467         spec, wav, bpm = self.load_file(filename1)
468         if filename2 and self._beams != '0E':
469             def unpack(exts, *args):
470                 return [arr[exts] for arr in args]
471
472             if self._beams == '0':
473                 spec[-1], wav[-1], bpm[-1] = unpack(
474                     0, *self.load_file(filename2)
475                 )
476
477             else:
478                 spec[0], wav[0], bpm[0] = spec[-1], wav[-1], bpm[-1]
479                 spec[-1], wav[-1], bpm[-1] = unpack(
480                     -1, *self.load_file(filename2)
481                 )
482
483         bounds = self.get_bounds(bpm)
484
485         logging.debug(
486             f"correlate - data shape:\n{spec.shape}\n{wav.shape}\n{bpm.shape}"
487         )
488
489         corrdb = [[] for _ in range(self.ccds)]
490         lagsdb = [[] for _ in range(self.ccds)]
491         for ccd in range(self.ccds):
492             sig = []
493             for ext in range(2):
494                 lb, ub = bounds[ext, ccd]
495
496                 if self.cont_ord > 0:
497                     spec[ext, lb:ub] = self.remove_cont(
498                         spec[ext, lb:ub],
499                         wav[ext, lb:ub],
500                         bpm[ext, lb:ub],
501                         self.can_plot
502                     )
503
504                 # Invert BPM (and account for 2); zero bad pixels
505                 sig.append((
506                     spec[ext, lb:ub]
507                     * abs(bpm[ext, lb:ub].astype(np.int8) * -1 + 1)
508                 ))

```

```

510     # Finally(!!!) cross correlate signals and scale max -> 1
511     corrdb[ccd] = signal.correlate(*sig) if not alt else alt(*sig)
512     corrdb[ccd] /= np.max(corrdb[ccd])
513     # noinspection PyTypeChecker
514     lagsdb[ccd] = signal.correlation_lags(
515         sig[0].shape[-1],
516         sig[1].shape[-1]
517     ) * self.wav_cdel
518
519     return spec, wav, bpm, corrdb, lagsdb
520
521 # MARK: ftcs alternate
522 def ftcs(
523     self,
524     signal1: np.ndarray,
525     signal2: np.ndarray
526 ) -> np.ndarray:
527     """
528     Cross correlates the data using the Fourier Transform.
529
530     Parameters
531     -----
532     signal1 : np.ndarray
533         The first signal to cross correlate.
534     signal2 : np.ndarray
535         The second signal to cross correlate.
536
537     Returns
538     -----
539     np.ndarray
540         The correlation data using the Fourier Transform.
541
542     """
543     logging.debug(
544         f"ftcs - data shape:\n{tspec.wav/bpm: {signal1.shape}}"
545     )
546
547     # Invert BPM (and account for 2); zero bad pixels
548     ft_spec1 = np.fft.fft(signal1)
549     ft_spec2 = np.fft.fft(signal2)
550
551     if self.can_plot:
552         plt.plot(ft_spec1)
553         plt.plot(ft_spec2)
554         plt.show()
555
556     # Cross correlate signals
557     # ft_spectrum1 * np.conj(ft_spectrum2)
558     corr_entry = signal.correlate(ft_spec1, ft_spec2)
559
560     return np.fft.ifft(corr_entry)
561
562 # MARK: Plot
563 def plot(self, spec, wav, bpm, corrdb, lagsdb) -> None:
564     """
565     Plot the data.
566
567     Parameters
568     -----
569     spec : np.ndarray
570         The spectrum.
571     wav : np.ndarray
572         The wavelength.
573     bpm : np.ndarray
574         The bad pixel mask.
575     corrdb : np.ndarray
576         The cross correlation data.
577     lagsdb : np.ndarray
578         The `lags` data.
579
580     Returns
581     -----
582     None

```

```

583
584     """
585     plt.style.use([
586         files(STOPS.utils).joinpath('STOPS.mplstyle'),
587         files(STOPS.utils).joinpath('STOPS_correlate.mplstyle'),
588     ])
589     bounds = self.get_bounds(bpm)
590
591     fig, axs = plt.subplots(2, self.ccds, sharey="row")
592
593     if self.ccds == 1:
594         # Convert axs to a 2D array
595         # noinspection PyTypeChecker
596         axs: np.ndarray[matplotlib.axes.Axes] = np.swapaxes(
597             np.atleast_2d(axs), 0, 1
598         )
599
600     # for ext, ccd in iters.product(range(2), range(self.ccds)):
601
602     for ccd in range(self.ccds):
603         axs[0, ccd].plot(
604             lagsdb[ccd],
605             corrdb[ccd] * 100,
606             color='C4',
607             label=f"max lag @ {lagsdb[ccd][corrdb[ccd].argmax()]} - (bounds[1, ccd, "
608                   "0] - bounds[0, ccd, 0])}",
609         )
610
611     for ext in range(2):
612         lb, ub = bounds[ext, ccd]
613         logging.debug(f"fl-{ext}: {wav[ext, lb]}:{wav[ext, ub - 1]}")
614
615         axs[1, ccd].plot(
616             wav[ext, lb:ub],
617             spec[ext, lb:ub]
618             * abs(bpm[ext, lb:ub].astype(np.int8) * -1 + 1)
619             + OFFSET * ext,
620             label=(
621                 f"${self._beams if self._beams != 'OE' else self._beams[ext]}"
622                 f"_{ext + 1 if self._beams != 'OE' else 1}$$"
623                 f"{' (' + str(OFFSET * ext) + ')'} if ext > 0 else ''}"
624             ),
625         )
626
627     axs[0, 0].set_ylabel("Normalised Correlation\n($\\%$)")
628     for ax in axs[1:, 0]:
629         ax.set_ylabel("Normalised Intensity\n(Counts)")
630     xcol = int(self.ccds != 1)
631     axs[0, xcol].set_xlabel(f"Signal Lag ({self.wav_unit})")
632     axs[-1, xcol].set_xlabel(f"Wavelength ({self.wav_unit})")
633     for ax in axs.flatten():
634         leg = ax.legend()
635         leg.set_draggable(True)
636
637     plt.show()
638
639     # Handle do not save
640     if not self.save_prefix:
641         return
642
643     # Handle save
644     fig.savefig(fname=self.save_prefix)
645
646     return
647
648     # MARK: Process all listed images
649     def process(self) -> None:
650         """
651         Process the data.
652
653         Returns
654         -----
655         None

```

```

655
656     """
657     if self._beams != 'OE' and len(self.fits_list) == 1:
658         # change mode to OE with warning
659         logging.warning((
660             f"`{self._beams}` correlation not possible for "
661             "a single file. correlation `mode` changed to 'OE'."
662         ))
663         self._beams = 'OE'
664
665     # OE `mode` (same file, diff. ext.)
666     if self._beams == 'OE':
667         for fl in self.fits_list:
668             logging.info(f"'OE' correlation of {fl}.")
669             spec, wav, bpm, corr, lags = self.correlate(fl, alt=self.alt)
670             self.plot(spec, wav, bpm, corr, lags)
671
672     return
673
674     # O/E `mode` (diff. files, same ext.)
675     for fl1, fl2 in itertools.combinations(self.fits_list, 2):
676         logging.info(f"{self._beams} correlation of {fl1} vs {fl2}.")
677         spec, wav, bpm, corr, lags = self.correlate(fl1, fl2, alt=self.alt)
678         self.plot(spec, wav, bpm, corr, lags)
679
680     return
681
682
683 # MARK: Main function
684 def main(argv) -> None:
685     return
686
687
688 if __name__ == "__main__":
689     main(sys.argv[1:])

```

Listing B.5: The source code for `skylines.py`

```

1 #!/usr/bin/env python3
2 # -*- coding: utf-8 -*-
3
4 """
5 Module for analyzing the sky lines of a wavelength calibrated image.
6 """
7
8 # MARK: Imports
9 import sys
10 import logging
11 from pathlib import Path
12 from importlib.resources import files
13
14 import numpy as np
15 import matplotlib.pyplot as plt
16 import matplotlib.axes
17 from astropy.io import fits as pyfits
18 from scipy import signal
19
20 from STOPS.utils.SharedUtils import find_files, get_arc_lamp
21 from STOPS.utils.Constants import SAVE_SKY, FIND_PEAK_PARAMS
22 import STOPS.data
23 import STOPS.utils
24 import STOPS.data.RSS_arc
25
26
27 # print(
28 #     [logging.getLogger(name) for name in logging.root.manager.loggerDict]
29 # )
30 mpl_logger = logging.getLogger('matplotlib')
31 mpl_logger.setLevel(logging.INFO)
32 pil_logger = logging.getLogger('PIL')
33 pil_logger.setLevel(logging.INFO)
34
35
36 # MARK: Skylines Class
37 class Skylines:
38     """
39         Class representing the Skylines object.
40
41     Parameters
42     -----
43     data_dir : Path
44         The directory containing the data files.
45     filenames : list[str]
46         The list of filenames to be processed.
47     beam : str, optional
48         The beam mode, by default "OE".
49     plot : bool, optional
50         Flag indicating whether to plot the continuum, by default False.
51     save_prefix : Path / None, optional
52         The prefix for saving the data, by default None.
53     **kwargs
54         Additional keyword arguments.
55
56     Attributes
57     -----
58     data_dir : Path
59         The directory containing the data files.
60     fits_list : list[str]
61         The list of fits file paths.
62     beams : str
63         The beam mode.
64     can_plot : bool
65         Flag indicating whether to plot the continuum.
66     save_prefix : Path / None
67         The prefix for saving the data.
68     wav_unit : str
69         The unit of wavelength.
70
71     Methods

```

```

72     -----
73     checkLoad(self, path1: str) -> np.ndarray:
74         Checks and loads the data from the given path.
75     transform(self, wav_sol: np.ndarray, spec: np.ndarray) -> np.ndarray:
76         Transforms the input wavelength and spectral data based on
77         the given wavelength solution.
78     rmvCont(self) -> np.ndarray:
79         Removes the continuum from the spectrum.
80     process(self) -> None:
81         Placeholder method for processing the data.
82
83     See Also
84     -----
85     matplotlib custom style:
86         https://matplotlib.org/stable/users/explain/customizing.html
87
88     Notes
89     -----
90     Constants imported (see utils.Constants):
91         SAVE_SKY:
92             The default save name for the skylines plot.
93         FIND_PEAK_PARAMS:
94             The default parameters for finding peaks in the spectrum.
95     """
96
97     # MARK: Skylines init
98     def __init__(
99         self,
100        data_dir: Path,
101        filenames: list[str],
102        beams: str = "OE",
103        split_ccd: bool = False,
104        cont_ord: int = 11,
105        plot: bool = False,
106        transform: bool = True,
107        save_prefix: Path | None = None,
108        **kwargs,
109    ) -> None:
110         self.data_dir = data_dir
111         self.fits_list, self.arc_list = find_files(
112             data_dir=self.data_dir,
113             filenames=filenames,
114             prefix="wmxgbp", # t[o/e]beam
115             ext="fits",
116             sep_arc=True,
117         )
118         if self.arc_list:
119             self.arc_lamp = get_arc_lamp(self.arc_list[0])
120
121         self._beams = None
122         self.beams = beams
123         self.ccds = 1
124         if split_ccd:
125             # See cross_correlate for initial implementation
126             self.ccds = 3
127
128         self.cont_ord = cont_ord
129         self.can_plot = plot
130         self.must_transform = transform
131
132         self.save_prefix = save_prefix
133         # Handle directory save name
134         if self.save_prefix and self.save_prefix.is_dir():
135             self.save_prefix /= SAVE_SKY
136             logging.warning((
137                 f"Skylines save name resolves to a directory. "
138                 f"Saving under {self.save_prefix}"
139             ))
140
141         self.max_difference = 5
142
143         self.wav_unit = "$\\AA$"
144

```

```

145     logging.debug(f"__init__\n{repr(self)}")
146
147     return
148
149 # MARK: Skylines repr
150 def __repr__(self) -> str:
151     template = (
152         "Skylines(\n"
153         f"\tdata_dir={self.data_dir},\n"
154         f"\tfits_list=[\n\t\t{"'\n\t\t'.join(
155             map(str, self.fits_list)
156         )}\n\t],\n"
157         f"\tbeams={self.beams},\n"
158         f"\tplot={self.can_plot},\n"
159         f"\tsave_prefix={self.save_prefix},\n"
160         f"\twav_unit={self.wav_unit}\n"
161         ") \n"
162     )
163
164     return template
165
166 # MARK: Beams property
167 @property
168 def beams(self) -> str:
169     return self._beams
170
171 @beams.setter
172 def beams(self, mode: str) -> None:
173     if mode not in ['O', 'E', 'OE']:
174         err_msg = f"Correlation mode '{mode}' not recognized."
175         logging.error(err_msg)
176         raise ValueError(err_msg)
177
178     self._beams = mode
179
180     return
181
182 # MARK: Find Peaks
183 def find_peaks(
184     self,
185     spec: np.ndarray,
186     axis: int | None = None,
187     min_height: float = 0.5,
188     **kwargs,
189 ) -> tuple[list[np.ndarray], list[dict]]:
190     """
191         Finds the peaks in the given spectral data.
192
193     Parameters
194     -----
195     spec : np.ndarray
196         The spectral data.
197     axis: int / None, optional
198         The axis along which the peaks are found.
199     min_height : float, optional
200         The minimum height of the peaks, by default 0.5.
201
202     Returns
203     -----
204     peaks, properties : tuple[list[np.ndarray], list[dict]]
205         The peaks and their properties.
206     """
207     peaks = []
208     props = []
209     row_means = []
210
211     for ext in range(len(self.beams)):
212         row_mean = spec[ext] if axis is None else np.mean(
213             spec[ext], axis=axis
214         )
215
216         peak, prop = signal.find_peaks(
217             row_mean,

```

```

218         prominence=min_height * np.max(row_mean),
219         width=0,
220         **kwargs,
221     )
222     peaks.append(peak)
223     props.append(prop)
224     row_means.append(row_mean)
225
226     if self.can_plot:
227         fig, axis = plt.subplots(2, 1)
228         for ext in range(len(self.beams)):
229             axis[ext].plot(
230                 row_means[ext],
231                 label=f"'E' if ext else 'O'")
232
233             axis[ext].plot(
234                 peaks[ext],
235                 row_means[ext][peaks[ext]],
236                 "x",
237                 label=f"'E' if ext else 'O'" peaks"
238             )
239             axis[ext].legend()
240         plt.show()
241
242     logging.debug(f"find_peaks - peaks: {[len(i) for i in peaks]}")
243     # logging.debug(
244     #     f"find_peaks - props: {[key for key in props[0].keys()]}"
245     # )
246
247     return peaks, props
248
249 # MARK: Min. of Diff. Matrix
250 @staticmethod
251 def min_diff_matrix(
252     a: np.ndarray,
253     b: np.ndarray,
254     max_diff: int = 100
255 ) -> tuple[np.ndarray, np.ndarray, np.ndarray]:
256     """
257         Find the minimum difference between the elements of two arrays.
258
259     Parameters
260     -----
261     a : np.ndarray
262         The first 1d array.
263     b : np.ndarray
264         The second 1d array.
265     max_diff : int, optional
266         The maximum difference allowed, by default 100.
267
268     Returns
269     -----
270     a : np.ndarray (len(a))
271         The elements of the first array.
272     min_vals : np.ndarray (len(a))
273         The minimum difference between the elements of the two arrays.
274     min_idxs : np.ndarray (len(a))
275         The indices of the minimum difference between
276         the elements of the two arrays.
277     """
278
279     # Compute the difference matrix using transpose
280     diff = a - b[:, np.newaxis]
281
282     # Find the minimum value in each row (A) of `diff`
283     min_idxs = np.abs(diff).argmin(axis=0)
284
285     min_vals = np.array([diff[j, i] for i, j in enumerate(min_idxs)])
286     # TODO: Recalculate min_val after selecting best min_val and
287     # TODO: removing the corresponding row/column
288
289     logging.debug(
290         f"min_diff_matrix - min_vals={np.round(min_vals, 2).astype(int)}"
291     )

```

```

291     logging.debug(f"min_diff_matrix - min_idxs={min_idxs}")
292
293     max_mask = (min_vals <= max_diff) & (min_vals >= -1 * max_diff)
294
295     return a[max_mask], min_vals[max_mask], min_idxs[max_mask]
296
297 # MARK: Load File Data
298 def load_file_data(
299     self,
300     filename: Path
301 ) -> tuple[np.ndarray, np.ndarray, np.ndarray]:
302     """
303         Loads the data from the given file.
304
305     Parameters
306     -----
307     filename : Path
308         The path to the file to be loaded.
309
310     Returns
311     -----
312     spec, wav, bpm : tuple[np.ndarray, np.ndarray, np.ndarray]
313         The wavelength, spectral, and bad pixel mask data.
314     """
315
316     # Load data from self.beams extension
317     with pyfits.open(filename) as hdul:
318         exts = [0, 1]
319         if len(self.beams) != 2:
320             exts = 0 + int(self.beams == 'E')
321
322         spec2d = np.atleast_3d(hdul["SCI"].data[exts])
323         wav2d = np.atleast_3d(hdul["WAV"].data[exts])
324         bpm2d = np.atleast_3d(hdul["BPM"].data[exts].astype(bool))
325
326         logging.info(
327             f"load_file_data - {filename.name} - shape: {spec2d.shape}"
328         )
329
330     return spec2d, wav2d, bpm2d
331
332 # MARK: Load Sky or Arc Lines
333 @staticmethod
334 def load_lines(
335     filename: str | Path | None = None,
336     dtype: list[tuple] = [('wav', float), ('flux', float)],
337     skip_header: int = 3,
338     skip_footer: int = 1
339 ) -> np.ndarray:
340     """
341         Loads the sky or arc lines from the given file.
342
343     Parameters
344     -----
345     filename : str / Path / None, optional
346         The path to the file to be loaded.
347         Defaults to loading the skylines from `data/sky.salt`.
348     dtype : list[tuple], optional
349         The data type of the sky lines.
350         (Default is [('wav', float), ('flux', float)])
351     skip_header : int, optional
352         The amount of lines to skip of the `filenames` header.
353         (Default is 3)
354     skip_footer : int, optional
355         The amount of lines to skip of the `filename`'s footer.
356         (Default is 1)
357
358     Returns
359     -----
360     sky_lines : np.ndarray['wav', 'flux']
361         The sky lines from the file.
362     """
363     lines: np.ndarray = None

```

```

364     usecols = None
365     if filename:
366         filename = files(STOPS.data.RSS_arc).joinpath(filename)
367         usecols = (0, 1)
368     else:
369         filename = files(STOPS.data).joinpath('sky.salt')
370
371     lines = np.genfromtxt(
372         filename,
373         dtype=dtype,
374         skip_header=skip_header,
375         skip_footer=skip_footer,
376         usecols=usecols
377     )
378
379     logging.debug(
380         f"load_lines - {filename.name} - shape: {lines.shape}"
381     )
382
383     return lines
384
385 # MARK: Mask Traces
386 def mask_traces(
387     self,
388     spec: np.ndarray,
389     bpm: np.ndarray,
390     max_traces: int = 1,
391     tr_pad: int = 5,
392     bg_margin: int = 10,
393     lr_margins: list[int] = [10, 10],
394     h_min: float = 0.5,
395     h_rel: float = 1 - 0.05,
396 ) -> np.ndarray:
397     """
398         Masks the traces in the bad pixel mask.
399
400     Parameters
401     -----
402     spec : np.ndarray
403         The spectral data.
404     bpm : np.ndarray
405         The bad pixel mask.
406     max_traces : int, optional
407         The maximum number of traces to be masked.
408         (Default is 1)
409     tr_pad : int, optional
410         The amount to pad traces by.
411         (Default is 5)
412     bg_margin : int, optional
413         The margin size for the background.
414         (Default is 10)
415     lr_margins : list[int, int], optional
416         The left and right background margins at the spectrum edge.
417         (Default is [10, 10])
418     h_min: float, optional
419         The minimum height of a detected peak.
420         (Default is 0.5)
421     h_rel: float, optional
422         The relative height for the properties of a detected peak.
423         (Default is 1)
424
425     Returns
426     -----
427     bpm : np.ndarray
428         The updated bad pixel mask.
429     """
430
431     # Base mask
432     bpm[:, :bg_margin] = True
433     bpm[:, -bg_margin:] = True
434     bpm[:, :, :lr_margins[0]] = True
435     bpm[:, :, -lr_margins[1]:] = True
436
437     # Get the traces

```

```

437     traces, tr_props = self.find_peaks(
438         spec,
439         axis=1,
440         min_height=h_min,
441         rel_height=h_rel
442     )
443
444     for ext in range(len(self.beams)):
445         # Mask the traces
446         for i in range(len(traces[ext][:max_traces])):
447             lb = max(
448                 0,
449                 int(tr_props[ext]['left_ips'][i]) - tr_pad
450             )
451             ub = min(
452                 spec.shape[-1],
453                 int(tr_props[ext]['right_ips'][i]) + tr_pad
454             )
455             bpm[ext, lb: ub] = True
456             # TODO: Relocate targets after initial masking
457
458         logging.info(
459             f"mask_traces - {min(max_traces, len(traces))} " +
460             f"of {len(traces)} traces masked."
461         )
462
463     return bpm
464
465     # MARK: Transform Spectra
466     def transform(
467         self,
468         spec: np.ndarray,
469         wav_sol: np.ndarray,
470         row_max: int | None = None,
471         res_plot: bool = False,
472     ) -> tuple[np.ndarray, np.ndarray]:
473         """
474             Transforms the input wavelength and spectral data
475             based on the given wavelength solution.
476
477         Parameters
478         -----
479         spec : np.ndarray
480             The spectral data.
481         wav_sol : np.ndarray
482             The wavelength solution.
483         row_max : int, optional
484             The row along which the spectral data is to be transformed.
485             (Default is None)
486         res_plot : bool, optional
487             Flag indicating whether to plot the results.
488             (Default is False)
489
490         Returns
491         -----
492         spec, wav : np.ndarray
493             The transformed wavelength and spectral data.
494
495         """
496         # Create arrays to return
497         cs = np.zeros_like(spec)
498         cw = np.zeros_like(wav_sol.mean(axis=1))
499
500         for ext in range(len(self.beams)):
501
502             if row_max:
503                 avg_max = row_max
504             else:
505                 # Get middle row (to interpolate the rest of the rows to)
506                 avg_max = np.mean(spec[ext], axis=1).argmax()
507
508             # Correct extensions based on wavelength
509             # Get wavelength values at row with most trace

```

```

510         cw[ext] = wav_sol[ext, avg_max]
511
512     # Spec ext
513     for row in range(cs.shape[1]):
514         cs[ext, row] = np.interp(
515             cw[ext],
516             wav_sol[ext, row],
517             spec[ext, row]
518         )
519     # f_2d = interpolate.interp2d(
520     #     wav_sol[ext, row],
521     #     np.arange(rows),
522     #     spec[ext],
523     # )
524     # cs[ext] = f_2d(cw[ext], np.arange(rows))
525
526     # Plot results
527     if res_plot:
528         fig, axs = plt.subplots(2, 1, figsize=[20, 4])
529         for ext in range(len(self.beams)):
530             axs[ext].imshow(
531                 cs[ext],
532                 vmax=cs[ext].mean() + 2 * cs[ext].std(),
533                 vmin=cs[ext].mean() - 2 * cs[ext].std()
534             )
535
536             logging.debug(
537                 f"E' if ext else 'O'} Average continuum = " +
538                 f"{np.median(np.median(cs[ext], axis=0)):4.3f}"
539             )
540
541             axx = axs[ext].twinx()
542             axx.hlines(
543                 np.median(np.median(cs[ext], axis=0)),
544                 0,
545                 cs[ext].shape[-1],
546                 colors='black'
547             )
548             axx.plot(
549                 cs[ext].mean(axis=0),
550                 "k",
551                 label=f"mean {'E' if ext else 'O'}"
552             )
553             axx.plot(
554                 np.median(cs[ext], axis=0),
555                 "r",
556                 label=f"median {'E' if ext else 'O'}"
557             )
558             axx.legend()
559         plt.show()
560
561     logging.info(f"transform - {cs.shape} transformed.")
562
563     return cs, cw
564
565     # MARK: Plot
566     def plot(
567         self,
568         spectra,
569         wavelengths,
570         peaks,
571         properties,
572         arc: bool = False,
573     ) -> None:
574         plt.style.use([
575             files(STOPS.utils).joinpath('STOPS.mplstyle'),
576             files(STOPS.utils).joinpath('STOPS_skylines.mplstyle'),
577         ])
578         plt.rcParams['figure.subplot.hspace'] *= len(self.beams)
579
580     def norm(vals):
581         return (vals - np.min(vals)) / (np.max(vals) - np.min(vals))
582

```

```

583     # Load known lines
584     if arc:
585         lines = self.load_lines(filename=self.arc_lamp)
586     else:
587         lines = self.load_lines()
588
589     # noinspection PyTypeChecker
590     lines = lines[
591         (lines['wav'] > wavelengths[1][0][0].min()) &
592         (lines['wav'] < wavelengths[1][0][0].max())
593     ]
594
595     # Create plot for results
596     fig, axs = plt.subplots(2, self.ccds, sharex='col', sharey='row')
597
598     # Convert axs to a 2D array if ccd count is 1
599     if self.ccds == 1:
600         # noinspection PyTypeChecker
601         axs: np.ndarray[matplotlib.axes.Axes] = np.swapaxes(
602             np.atleast_2d(axs),
603             0,
604             1
605         )
606
607     for fl in range(len(self.arc_list if arc else self.fits_list)):
608
609         # set color cycle
610         # private deprecated
611         # color = next(axs[0, 0]._get_lines.prop_cycler)['color']
612         color = axs[0, 0]._get_lines.get_next_color()
613
614         for ext in range(len(self.beams)):
615
616             ccdrange = spectra[1][fl][ext].shape[-1] // self.ccds
617             for ccd in range(self.ccds):
618                 # MARK: plot spectrum
619                 # (transformed)
620                 axs[0, ccd].plot(
621                     wavelengths[1][fl][ext][
622                         ccdrange * ccd:ccdrange * (ccd + 1)
623                     ],
624                     norm(spectra[1][fl][ext][
625                         ccdrange * ccd:ccdrange * (ccd + 1)
626                     ]) * 100 + 10 * ext + 30 * fl,
627                     color=color,
628                     linestyle='dashed' if ext else 'solid',
629                     label=f"${{{self.beams[ext]}}}_{{{fl + 1}}}^{+{10 * ext + 30 * fl}}$" if ccd == 0 else None,
630                 )
631
632                 # MARK: plot dev
633                 # noinspection PyTypeChecker
634                 sky_wavs, dev, peak_idx = self.min_diff_matrix(
635                     lines['wav'],
636                     wavelengths[1][fl][ext][peaks[1][fl][ext]],
637                     max_diff=self.max_difference,
638                 )
639
640                 # # MARK: width/width_init
641                 # width = properties[1][fl][ext]['widths'][peak_idx]
642                 # width_i = np.zeros_like(width)
643
644                 # sky_i, i_dev, i_idx = self.min_diff_matrix(
645                 #     lines['wav'],
646                 #     wavelengths[0][fl][ext][peaks[0][fl][ext]],
647                 #     max_diff=self.max_difference,
648                 # )
649
650                 # width_i = np.array([
651                 #     properties[0][fl][ext]['widths'][
652                 #         np.where(wav == sky_i)[0][0]
653                 #     ]
654                 #     if wav in sky_i else 1000

```

```

655     #         for wav in sky_wavs
656     #     ])
657     # width_ratio = (width / width_i) - 1
658     # width_ratio[width_ratio < 0] = 0
659
660     # ylolims = width_ratio > self.max_difference
661     # width_ratio[
662     #     width_ratio > self.max_difference
663     # ] = self.max_difference // 2
664
665     ok = np.where(
666         (sky_wavs >= wavelengths[1][fl][ext].data[
667             ccdrange * ccd
668         ]) &
669         (sky_wavs <= wavelengths[1][fl][ext].data[
670             ccdrange * (ccd + 1)
671         ])
672     )
673     axs[1, ccd].plot(
674         sky_wavs[ok],
675         dev[ok],
676         # yerr=(width_ratio[ok] * 0, width_ratio[ok]),
677         # lolims=ylolims[ok],
678         "."
679         if ext else "x",
680         # fmt="."
681         if ext else "x",
682         alpha=0.8,
683         color=color,
684         # markeredgecolor='white',
685         # markeredgewidth=0.5,
686         # label=f"${self.beams[ext]}_{{{fl + 1}}}$",
687     )
688
689     logging.debug(
690         f"plot - RMS: {np.sqrt(np.mean(dev[ok] ** 2)):.2f}"
691     )
692
693     for ccd in range(self.ccds):
694         ccdrange = spectra[1][0][0].shape[-1] // self.ccds
695
696         # spectrum
697         # noinspection PyTypeChecker
698         ok = np.where(
699             (lines['wav'] >= wavelengths[1][0][0].data[ccdrange * ccd]) &
700             (lines['wav'] <= wavelengths[1][0][0].data[ccdrange * (ccd+1)])
701         )
702         # noinspection PyTypeChecker
703         axs[0, ccd].plot(
704             lines['wav'][ok],
705             lines['flux'][ok] * 0,
706             'x',
707             color='C4',
708             label="\text{sc}\{salt\}\nModel" if ccd == 0 else None,
709         )
710         # noinspection PyTypeChecker
711         for x in lines['wav'][ok]:
712             axs[0, ccd].axvline(x, ls='dashed', c='0.7')
713
714         axs[0, 0].set_ylabel("Rel. Intensity ($\\%$)")
715         axs[1, 0].set_ylabel(
716             "Closest Peak ($\\Delta\\lambda$)")
717
718         # for ax in axs[:, 0]:
719         #     ax.legend(loc='upper left', ncols=(fl + 1) * (ext + 1) + 1)
720         leg = fig.legend(
721             loc='center',
722             ncol=min(8, len(spectra[0])) + 1,
723             columnspacing=0.5,
724             bbox_to_anchor=(
725                 np.mean((
726                     plt.rcParams['figure.subplot.left'],
727                     plt.rcParams['figure.subplot.right']
728                 )),
729                 np.mean((

```

```

728         plt.rcParams['figure.subplot.bottom'],
729         plt.rcParams['figure.subplot.top']
730     ),
731 )
732 leg.set_draggable(True)
733 for ax in axs[1, :]:
734     ax.grid(axis='y')
735
736 axs[-1, 0 if self.ccds == 1 else 1].set_xlabel(
737     f"Wavelength ({self.wav_unit})"
738 )
739
740 # plt.tight_layout()
741
742 plt.show()
743
744 # Save results
745 if self.save_prefix:
746     fig.savefig(fname=self.save_prefix)
747
748 return
749
750 # MARK: Process all listed images
751
752 def process(self, arc: bool = False) -> None:
753     files = self.fits_list
754     if arc:
755         files = self.arc_list
756
757     logging.info(f"Processing '{self.beams}' lines.")
758
759     spectra = [[], []]
760     wavs = [[], []]
761     peaks = [[], []]
762     peak_props = [[], []]
763
764     for fl in files:
765         # Load data
766         spec2d, wav2d, bpm2d = self.load_file_data(fl)
767
768         # Mask traces in BPM
769         bpm2d = self.mask_traces(
770             spec2d,
771             bpm2d,
772             max_traces=0,
773             bg_margin=15,
774             h_min=0.05
775         )
776         m_spec2d = np.ma.masked_array(spec2d, mask=bpm2d) # spec2d
777         m_wav2d = np.ma.masked_array(wav2d, mask=bpm2d) # wav2d
778
779         # Initial spectra
780         spec_i = np.mean(m_spec2d, axis=-2)
781         wav_i = np.mean(m_wav2d, axis=-2)
782
783         # Transform data
784         t_spec2d, t_wav = self.transform(
785             m_spec2d,
786             m_wav2d,
787             res_plot=self.can_plot
788         )
789
790         # Final spectra
791         spec_f = np.mean(t_spec2d, axis=-2)
792         wav_f = t_wav
793
794         # Find peaks
795         peaks_i, props_i = self.find_peaks(
796             spec_i,
797             **FIND_PEAK_PARAMS
798         )
799         peaks_f, props_f = self.find_peaks(
800

```

```
801         spec_f,
802         **FIND_PEAK_PARAMS
803     )
804
805     spectra[0].append([*spec_i])
806     spectra[1].append([*spec_f])
807     wavs[0].append([*wav_i])
808     wavs[1].append([*wav_f])
809     peaks[0].append([*peaks_i])
810     peaks[1].append([*peaks_f])
811     peak_props[0].append([*props_i])
812     peak_props[1].append([*props_f])
813
814     # Plot results
815     self.plot(spectra, wavs, peaks, peak_props, arc=arc)
816
817     if arc:
818         return
819     elif self.arc_list:
820         self.process(arc=True)
821
822     return
823
824
825 # MARK: Main function
826 def main(argv) -> None:
827     """main function."""
828
829     return
830
831
832 if __name__ == "__main__":
833     main(sys.argv[1:])
```

Appendix C

Proceedings

Development of [STOPS](#) and it's application to spectropolarimetric observations was presented at conferences, with the following proceedings included here.

- HEASA 2021 – [Cooper, van Soelen, and Britto \(2022\)](#)
- HEASA 2022 – [Cooper and van Soelen \(2023\)](#)

Development of tools for the SALT/RSS spectropolarimetry reductions: application to the blazar 3C 279

Justin Cooper,^{a,*} Brian van Soelen^a and Richard J. Britto^a

^a*University of the Free State,
205 Nelson Mandela Drive, Bloemfontein, South Africa*

E-mail: CooperJ@ufs.ac.za, VanSoelenB@ufs.ac.za

Blazars represent a subset of AGN with relativistic jets, where the direction of the jet lies very close to our line of sight. The highly Doppler boosted emission from the blazar's jet results in high apparent luminosities, and blazars display variability on periods from less than one day up to years. At optical wavelengths, the observed emission of the blazar is a superposition of the polarised non-thermal synchrotron emission, arising from the jet, and the unpolarised thermal emission, arising from the accretion disc, broad line region, torus and host galaxy. Polarimetry observations can serve as an important tool for diagnosing the emission from blazars. The RSS spectrograph, on SALT, can operate in spectropolarimetry mode and is currently being used to undertake spectropolarimetric observations of transient blazar sources. We present additional tools developed to work in conjunction with the current SALT spectropolarimetry reduction pipeline, POLSALT, that aims to streamline the reduction of the SALT polarisation data, including the testing of the wavelength calibration of the individual O and E beams. This was applied to observations of 3C 279 during 2017.

*** *High Energy Astrophysics in Southern Africa (HEASA2021)* ***

*** *13 - 17 September, 2021* ***

*** *Online* ***

*Speaker

1. Introduction

Active Galactic Nuclei (AGN) are the centres of galaxies powered by accretion onto a supermassive black hole. The accretion can power relativistic jets which produce non-thermal emission over multiple wavelengths [1]. Blazars are a subclass of AGN where the direction of the jet lies very close to our line of sight. The highly Doppler boosted emission from the jet results in high apparent luminosities.

At optical wavelengths the observed emission is a superposition of polarised non-thermal synchrotron emission, arising from the jet, and unpolarised thermal emission, arising from the disc, broad line region, torus, and host galaxy [2].

The Robert Stobie Spectrograph (RSS) on the Southern African Large Telescope (SALT) [3] [4] is capable of long-slit spectropolarimetry and has been used to observe blazars in flaring and quiescent states. Data reduction of these observations is processed using the SALT spectropolarimetry reduction package POLSALT.¹ POLSALT allows for the full reduction, from pre-reduction to the extraction of the target spectra, and the measuring of the polarisation. However, it does not allow for much flexibility with the wavelength calibrations, nor does it provide tools to confirm that the wavelength calibrations lead to similar wavelength calibrated spectra for the O and E beams.

In order to streamline the data reduction we are developing additional tools to work in conjunction with POLSALT. We present the overview of this pipeline and demonstrate its application to an observation of 3C 279 taken in 2017.

2. Pipeline Overview

The tools being developed are designed to work in conjunction with POLSALT and provide a method to perform the wavelength calibrations using conventional `IRAF` methods [5]. They also allow easy comparisons to be made between the wavelength solutions of the O and E beam, to determine their quality and reliability.

The workflow for reductions is depicted in figure 1. It summarises the steps followed to reduce spectropolarimetric data. Steps that are performed using POLSALT are indicated in blue; steps performed by the new tools are shown in orange, while the `IRAF` calibration is shown in green.

If the wavelength solutions are found with `IRAF`, the tools split the multi-extension FITS files into the correct format for `IRAF` and the `IRAF` wavelength calibration is performed. The files are then written back into multi-extension FITS files in the correct format for POLSALT to complete the extraction and measurement of polarisation.

The cross-correlation between the O and E beam spectra, named correlation in figure 1, and relative flux calibrations are optional, though correlation is suggested. Relative flux calibrations may be performed assuming a standard and published standard spectra can be acquired. We performed the relative flux calibrations using the `ASTROPY` [6, 7] and `SCIPY`² packages.

¹<https://github.com/saltastro/polsalt>

²<http://www.scipy.org/>

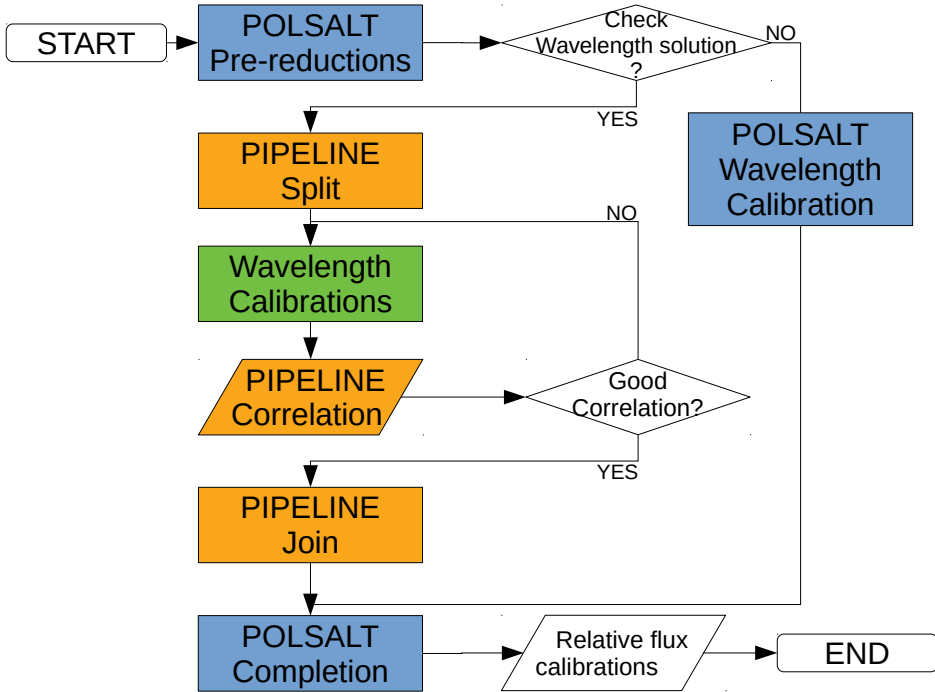


Figure 1: The flow diagram of the SALT RSS spectropolarimetry reductions steps.

POS (HEAS2021) 056

2.1 Pre-reduction

The first step in the pipeline uses **POLSLT** and this performs the pre-reductions, the over-scan subtraction, gain and cross talk corrections, and mosaicing. After the pre-reduction is performed, the next step is to either undertake the wavelength calibration with **POLSLT**, or to split the files into the correct format for **IRAF**.

2.2 FITS split

Once all pre-reductions are complete, the tool **SPLIT** converts the multi-extension FITS files into multiple, single extension O or E beam FITS files. This is done as some **IRAF** tasks do not handle multi-extension FITS files well. The O and E beam frames are cropped to remove any non-exposed rows to accommodate the standard **IRAF** tasks and the FITS files saved with updated header information.

2.3 Wavelength calibration

If the **POLSLT** pipeline is used, the wavelength calibration is performed using the wavelength calibration tools which form part of **PYSALT** [8].

If the files have been formatted for **IRAF**, standard wavelength calibration methods are followed, using the **NOAO** package and the **identify**, **re-identify**, and **fitcoords** tasks. This allows greater control of the resultant wavelength solution.

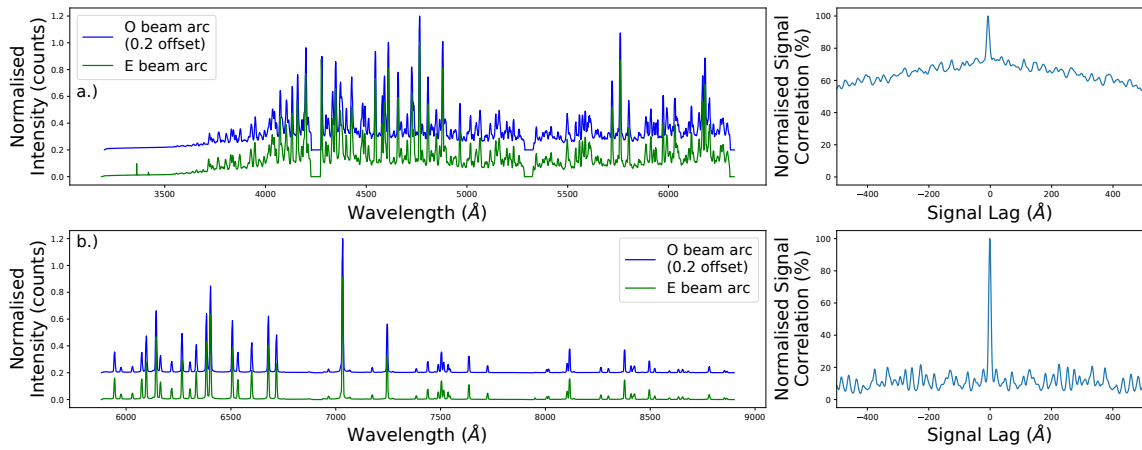


Figure 2: Comparison of the O and E beams for a.) ThAr and b.) Ne arc lamp spectra as well as the cross-correlation of their O and E beams.

2.4 Correlation

Our tool CORRELATE allows a comparison to be made between the O and E beam solutions, by performing a cross-correlation between the two arc or target observations, after the wavelength solution as been applied by `IRAF`. This is important as the polarisation is calculated from the difference between the O and E beam and, therefore, accurate wavelength solutions are required. The comparison between the O and E beams for a ThAr and Ne arc spectra and their cross-correlations, with a near zero lag, are shown in figure 2.a) and figure 2.b), respectively. Figure 2's Signal Lag plots show a clear peak at zero lag but also show an important distinction between noisy and quiet spectra in the non-peaking region.

2.5 FITS join

Once the `IRAF` wavelength calibrations are complete, the tool JOIN performs cosmic-ray cleaning using the LACOSMIC package [9], applies a wollaston correction which accounts for the physical shift of the spectra on the CCD, and then formats the single extension O and E beam FITS files into the multi-extension format required by `POLSALT`. This includes saving the wavelength solution found in `IRAF` as an additional extension. Currently only wavelength solutions fit with a Chebychev function are recognised but further development is planned to recognise Legendre functions.

2.6 Completion - extraction and polarisation measurement

After the wavelength solution is found, the final step is performed using `POLSALT`, which performs the curvature corrections, background subtraction, spectral extraction, and the raw and final stokes calculations. The binning and plotting also form part of the `POLSALT` completion.

3. Application to 3C 279

The blazar 3C 279 was observed in linear spectropolarimetry mode, on 2017 May 17, using the the PG0900 grating with two different grating angles (12.5° and 19.5°). The spectrophotometric

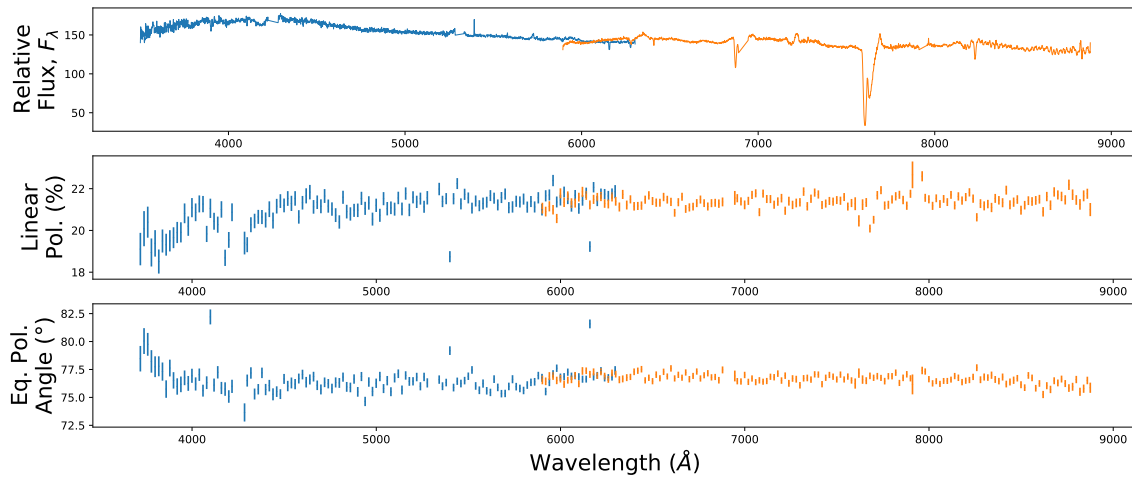


Figure 3: Reduced observations of 3C 279, taken with grating angle 12.5° (blue line) and 19.5° (orange line). Top: relative flux calibrated spectra. Middle: degree of linear polarisation. Bottom: Polarisation angle (relative to instrument).

standard star Hiltner 600 was observed on 2017 February 24, using the same configuration and was used for relative flux calibrations.

The target and standard were reduced following the steps discussed about. The flux correction was performed using `ASTROPY` and `SCIPY` python packages to correct the flux shape.

The results are shown in figure 3, indicating a good overlap between the observations taken at two different grating angles, with the polarisation measurements generally agree well where the observations overlap.

Figure 2 shows the comparison of the O and E beams for this observations. The cross-correlation is very close to zero lag, indicating the wavelength solution is similar for both the O and E beams.

4. Discussion and Conclusions

Creating an independent 2D wavelength solution for the O and E beams using `IRAF` allows for more flexibility in obtaining the wavelength solutions and provides a tool to directly compare the O and E beam solutions. This is useful for difficult cases, such as arc line identification for the PG0300 spectral grating, because there are fewer arc lines in some parts of the spectra and it is more complicated to create a consistent solution across the full wavelength range covered.

The cross-correlation plot cannot only be considered when deciding on whether to proceed onward with the reductions or to return to wavelength calibrations as depicted in figure 1. The comparison of the spectra is as important since the cross-correlation may show zero lag but lines in the spectra could still be mis-identified in both beams. The cross-correlation serves as a method to check the similarity of the wavelength solutions but not the accuracy of said solutions.

The tools developed create an alternative to the `POLSALT` wavelength calibration and add a method to check the consistency of the wavelength solutions, as can be seen with the application to 3C 279. These assist with the wavelength calibration, in particular for observations taken with

the PG0300 and PG0900 RSS gratings, that have been used for numerous observations of blazar sources.

Acknowledgments

The observational data presented was obtained with the Southern African Large Telescope (SALT) under the proposal 2016-2-LSP-001 (PI: D.A.H. Buckley). This work is based on the research supported in part by the National Research Foundation of South Africa (Grant Numbers: 116300).

References

- [1] C.M. Urry and P. Padovani, *Unified Schemes for Radio-Loud Active Galactic Nuclei*, *PASP* **107** (1995) 803 [[astro-ph/9506063](#)].
- [2] M. Böttcher, B. Van Soelen, R.J. Britto, D.A.H. Buckley, J.P. Marais and H. Schutte, *Salt spectropolarimetry and self-consistent sed and polarization modeling of blazars*, *Galaxies* **5** (2017) .
- [3] E.B. Burgh, K.H. Nordsieck, H.A. Kobulnicky, T.B. Williams, D. O'Donoghue, M.P. Smith et al., *Prime focus imaging spectrograph for the southern african large telescope: optical design*, in *Instrument Design and Performance for Optical/Infrared Ground-based Telescopes*, vol. 4841, pp. 1463–1471, International Society for Optics and Photonics, 2003.
- [4] H.A. Kobulnicky, K.H. Nordsieck, E.B. Burgh, M.P. Smith, J.W. Percival, T.B. Williams et al., *Prime Focus Imaging Spectrograph for the Southern African Large Telescope: operational modes*, in *Instrument Design and Performance for Optical/Infrared Ground-based Telescopes*, M. Iye and A.F.M. Moorwood, eds., vol. 4841, pp. 1634 – 1644, International Society for Optics and Photonics, SPIE, 2003, [DOI](#).
- [5] D. Tody, *The IRAF Data Reduction and Analysis System*, in *Instrumentation in astronomy VI*, D.L. Crawford, ed., vol. 627 of *Society of Photo-Optical Instrumentation Engineers (SPIE) Conference Series*, p. 733, Jan., 1986, [DOI](#).
- [6] Astropy Collaboration, T.P. Robitaille, E.J. Tollerud, P. Greenfield, M. Droettboom, E. Bray et al., *Astropy: A community Python package for astronomy*, *A&A* **558** (2013) A33 [[1307.6212](#)].
- [7] Astropy Collaboration, A.M. Price-Whelan, B.M. Sipőcz, H.M. Günther, P.L. Lim, S.M. Crawford et al., *The Astropy Project: Building an Open-science Project and Status of the v2.0 Core Package*, *AJ* **156** (2018) 123 [[1801.02634](#)].
- [8] S.M. Crawford, M. Still, P. Schellart, L. Balona, D.A.H. Buckley, G. Dugmore et al., *PySALT: the SALT science pipeline*, in *Observatory Operations: Strategies, Processes, and Systems III*, D.R. Silva, A.B. Peck and B.T. Soifer, eds., vol. 7737 of *Society of Photo-Optical Instrumentation Engineers (SPIE) Conference Series*, p. 773725, July, 2010, [DOI](#).

- [9] P.G. Van Dokkum, *Cosmic-ray rejection by laplacian edge detection*, *Publications of the Astronomical Society of the Pacific* **113** (2001) 1420.

POS (HEASA2021) 056

SALT Spectropolarimetric Pipeline Comparisons

J. Cooper^{a,*} and B. van Soelen^a

^a*University of the Free State, Physics Dept.,*

PO Box 339, Bloemfontein, 9300

E-mail: Justin.jb78@gmail.com, vanSoelenB@ufs.ac.za

Blazars are active galactic nuclei (AGN) with jets aligned very closely to our line of sight. The optical emission of blazars is often dominated by the polarised, non-thermal emission arising in the jets, with an underlying unpolarised, thermal emission component arising from the host galaxy, dusty torus, and accretion disk components.

Coupled with multi-wavelength observations, optical spectropolarimetry of blazars during both flaring and quiescent states can be used to disentangle the polarised and unpolarised components in their spectral energy distributions, providing better constraints for the non-thermal particle distribution. To this end, spectropolarimetry of blazars during different states of activity was taken with the Southern African Large Telescope (SALT) using the Robert Stobie Spectrograph (RSS). For RSS spectropolarimetry, reductions are performed using the POLSALT pipeline. In order to streamline the spectropolarimetric reductions, we have implemented supplementary interactive tools which provides additional wavelength calibration to improve the accuracy of the wavelength calibration for the O & E beam.

Here we present a brief overview of the tools and the results for Hiltner 652, a spectropolarimetric standard, as well as results for the blazars 3C 279. The reduced, P_Q and P_U , Stokes parameters of Hiltner 652 show no major deviation from previously published results which reassures us that there is no interference introduced into the Stokes parameter calculations when wavelength calibrations are handled by our supplementary tools. The $\sim 6000 - 9000 \text{ \AA}$ range of 3C 279 shows a notable dip in the normalized spectrum during a period of flaring when compared to epochs of enhanced activity. The degree of polarisation for 3C 279 of 13.2%, 9.5%, and 21.2% for the epochs 2017 March 28, 2017 March 31, and 2017 May 17, respectively, remains fairly constant across the observed wavelength ranges while still varying with the blazars' state of quiescence or flaring.

High Energy Astrophysics in Southern Africa 2022 - HEASA2022
28 September - 1 October 2022
Brandfort, South Africa

*Speaker

1. Introduction

Blazars are a radio-loud sub-set of Active Galactic Nuclei (AGN), where the jet is aligned very closely to our line of sight and whose observed emission varies over time scales from hours to decades [1]. The optical emission observed from blazars is often dominated by the polarised, non-thermal emission arising in the jets, but there is also underlying non-polarised, thermal emission arising from the host galaxy, dusty torus, and accretion disk components [2]. When a blazar varies between flaring and quiescent states, the relative strength of the thermal component to the non-thermal component changes.

The Spectral Energy Distribution (SED) of blazars shows two clear components: a lower energy component produced through leptonic synchrotron processes (covering the radio to the UV/soft X-ray regimes) and a higher energy component (covering the X-ray to the γ -ray regimes) which can be produced through either leptonic or hadronic processes [3]. Optical spectropolarimetry observations, coupled with multi-wavelength observations during both flaring and quiescent states, can be used to disentangle the polarised and non-polarised components in the blazar's SED, providing better constraints for the non-thermal particle distribution [4, 5].

To this end, spectropolarimetric observations of blazars during different states of activity were taken using SALT [6] and the RSS [7]. RSS spectropolarimetry data is reduced with the dedicated POLSALT pipeline [8]. In order to facilitate the blazar observations we have developed supplementary tools to provide a more interactive approach to the wavelength calibration, allowing for improved accuracy for the O & E beam wavelength solutions [9]. Furthermore, spectropolarimetric standards, which were also observed with SALT and the RSS, were reduced alongside the blazar observations to test that the developed tools correctly performed the wavelength calibration. Here we present an overview of the pipeline as well as the preliminary results of a spectropolarimetric standard, namely Hiltner 652, and for the blazar 3C 279.

2. Pipeline Overview

RSS spectropolarimetry data is currently reduced using the POLSALT pipeline [8]. This python package allows for a full reduction from pre-reduction to extracted spectrum, and measured polarisation. However, the wavelength calibration component of the package does not allow for flexibility, nor provide a tool to confirm that the wavelength calibrations of the O & E beams are in agreement. This flexibility is most notably missed when performing calibrations of observations taken using the PG0300 grating¹ due to the very sparse spectral features of the Argon arc lamp used by SALT as well as second order contamination which differs between the O & E beams.

The developed tools work in conjunction with the existing pipeline and provide a method to perform the wavelength calibrations using conventional IRAF [10] methods. Figure 1 shows the typical workflow for data reductions of spectropolarimetric SALT data. Items in blue refer to processing steps completed entirely using POLSALT while items in orange refer to processing steps completed using the developed tools. The single green item refers to the wavelength calibration

¹This grating has been decommissioned and replaced by the PG0700, and is not available for general use as of November 2022.

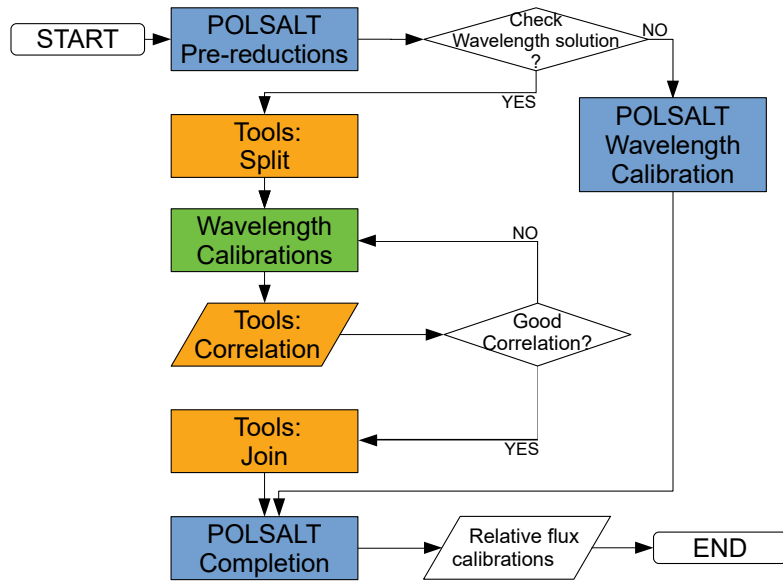


Figure 1: A general workflow for data reductions using a combination of **POLSALT** and our developed tools.

Source	Observation date	Grating angle (°)	Slit width (")	Exposure time (sec)	Wavelength range (Å)
Hiltner 652	2022 June 10	12.878	2	48.5	3350 - 6440
3C 279	2017 March 28	12.5	1.5	480.8	3300 - 6300
3C 279	2017 March 28	19.625	1.5	480.8	5800 - 8800
3C 279	2017 March 31	12.5	1.5	480.8	3300 - 6300
3C 279	2017 March 31	19.625	1.5	480.8	5800 - 8800
3C 279	2017 May 17	12.5	1.5	720.8	3300 - 6300
3C 279	2017 May 17	19.625	1.5	720.8	5800 - 8800

Table 1: All spectropolarimetric observations taken with SALT and the RSS and used as part of development and testing of the supplementary tools.

done in **IRAF**. Additional tools to cross-check that the wavelength calibration is consistent across both beams have also been implemented.²

3. Observations

The spectropolarimetric observations were taken using the RSS mounted on SALT, in **LINEAR** mode. The spectropolarimetric standard, Hiltner 652, was observed in 2022 and the blazar 3C 279, was observed in 2017, as summarized in Table 1. All observations presented here were observed using the PG0900 and were reduced following the reduction workflow as described in Figure 1.

²A further, in-depth, discussion of the developed tools can be found at [9].

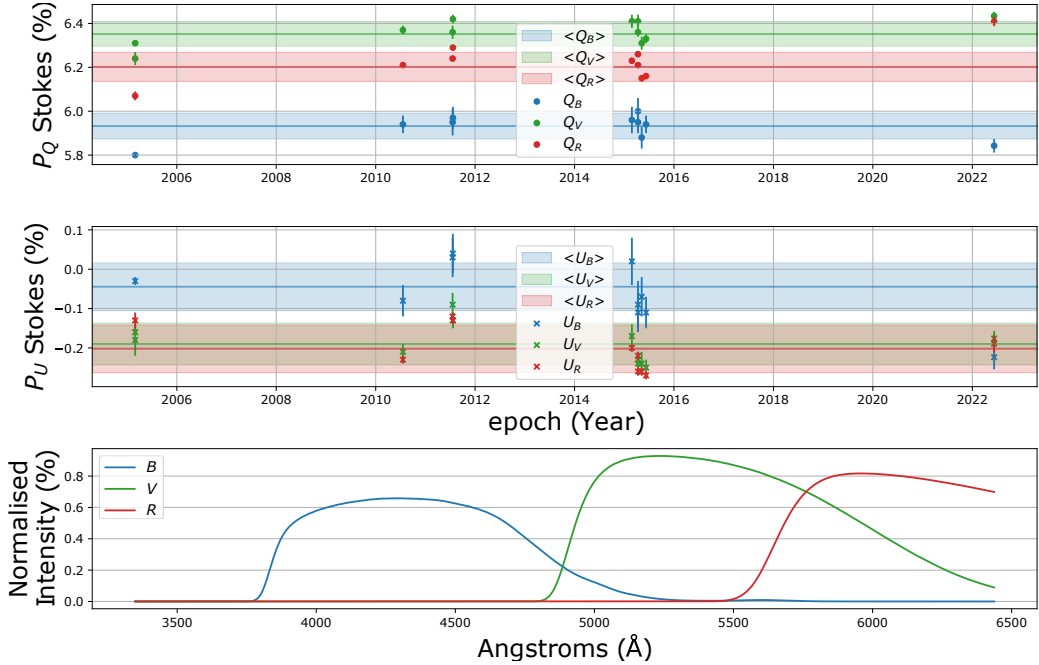


Figure 2: The reduced Q and U Stokes parameters for Hiltner 652 obtained with SALT in 2022 (post 2020) calculated by convolving the spectropolarimetry with the Johnson-Cousins filter pass-bands. This is compared to the published FORS1 [11] and FORS2 [12] observation results (top and middle panels). The average of the FORS reduced Stokes parameters as well as their standard deviation are plotted as the horizontal lines and shaded regions, respectively. Hiltner 652 was observed by SALT in 2022, by FORS1 from 1999 to 2006 (shown as average value at March 2005), and by FORS2 from 2010 to 2016. Finally, the Johnson-Cousins filter pass-band's used by POLSALT to calculate the stokes parameters in the different filters are shown in the bottom panel.

4. Results

The linear Stokes parameters, Q & U , normalized to the total intensity, referred to henceforth as the reduced Stokes parameters, P_Q & P_U , are relative quantities which are used to calculate the polarisation properties, and from which the fraction of linear polarisation may be easily calculated as $P_L = \sqrt{P_Q^2 + P_U^2}$ [13]. The reduced Stokes parameters of Hiltner 652, convolved against the Johnson-Cousins filter pass-bands, as performed by POLSALT, are shown in Figure 2 and are compared against published filtered reduced Stokes parameters obtained with FORS1 [11] and FORS2 [12]. The bottom panel of Figure 2 also shows the filter band-passes for the wavelength range covered by the SALT spectropolarimetry; note that the full R band is not covered by the observation setup.

The reduced Stokes parameters of Hiltner 652 fall within or near the 1σ level of the previously published reduced Stokes parameters over the course of multiple years. This shows that Hiltner 652 is not only a good standard for spectropolarimetric observations but also that using POLSALT with the supplementary wavelength calibrations correctly calculated the Stokes parameters.

The blazar 3C 279 was observed during periods of enhanced and flaring γ -ray activity for energies of 0.1 – 100 GeV and were sourced from the Fermi Light Curve Repository (Fermi LCR)

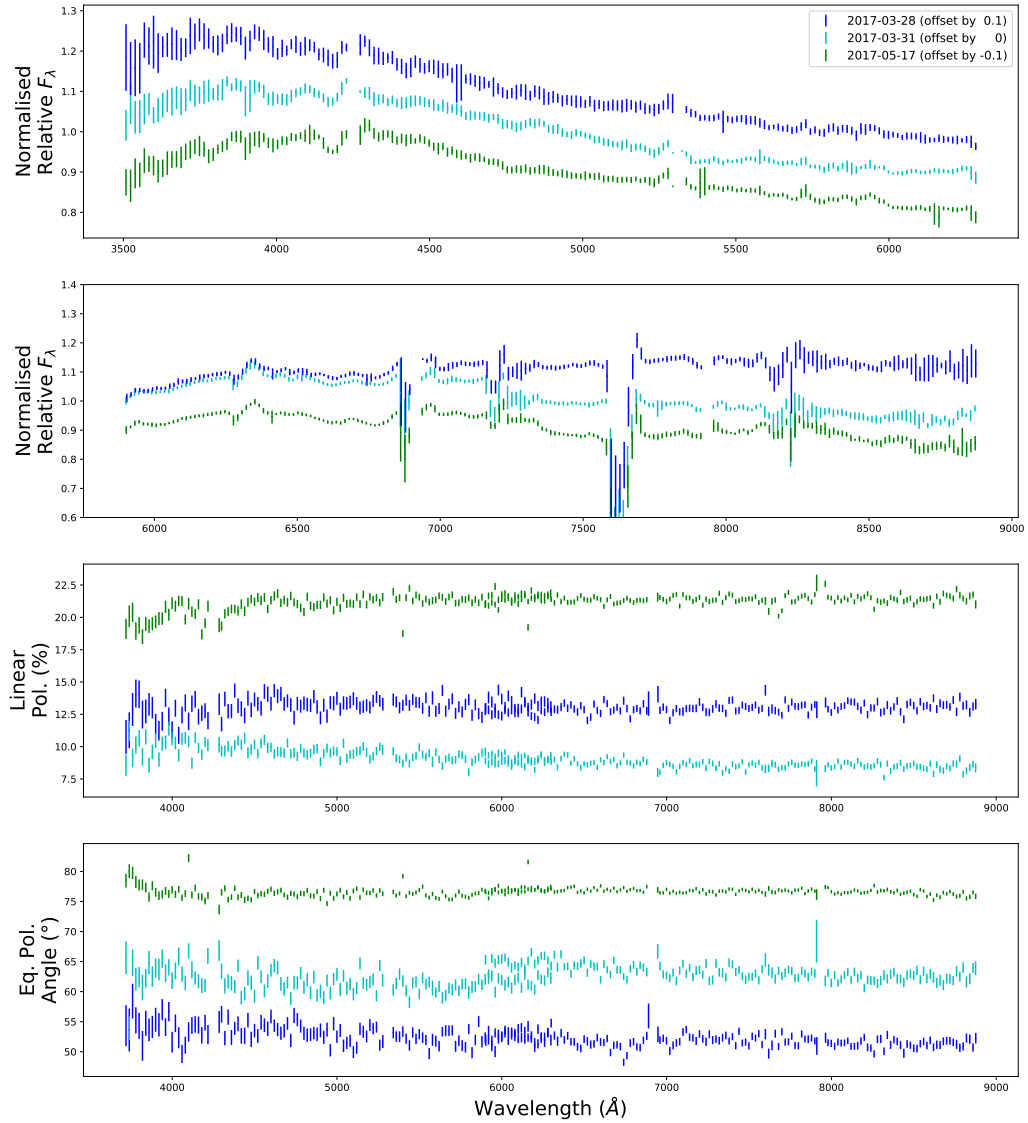


Figure 3: Optical spectropolarimetric observations of 3C 279 during two different periods of flaring. The relative flux calibrated spectra for the grating angles 12.5° (top), observed first at each epoch, and 19.625° (second from top), the degree of polarisation (third from top), and the polarisation angle (bottom).

[14]. 3C 279 was observed at fluxes of 1.58×10^{-6} , 2.87×10^{-6} , and 2.00×10^{-6} ph cm $^{-2}$ s $^{-1}$ as compared to a ‘quiescent’ median flux of 4.59×10^{-7} ph cm $^{-2}$ s $^{-1}$.

Figure 3 shows the relative flux calibrated spectra normalized to the spectrum’s mean (and offset as indicated), degree of polarisation, and polarisation angle for 3C 279. The relative flux was normalized to better compare how the shape of the spectrum changes during the differing γ -ray states. 3C 279 showed variable flux and polarisation during the three observations, with the polarisation changing by $\sim 12.23\%$ and the angle changing by $\sim 24.22^\circ$. The relative spectral shape remains similar over all three observations, however the second observation (2017-03-31) appears to show a slightly brighter spectrum in the blue. There is also a relatively good agreement

in the polarisation at the wavelength overlap for the different grating angles. The difference of the polarisation and degree of polarisation is on the order of 0.25 % and 1.25°, respectively.

5. Discussion and Conclusions

In this paper we have considered the observations of a spectropolarimetric standard, Hiltner 652, and a flaring blazar, 3C 279, to test our supplementary tools used for the reduction of spectropolarimetric data obtained with the RSS. The results serve to confirm that the supplementary tools' wavelength reductions, in combination with POLSALT, produces the correct polarisation behavior. Our results for Hiltner 652 agree well with the historical results obtained using the FOcal Reducer and low dispersion Spectrograph (FORS1 and FORS2) mounted at the Very Large Telescope (VLT).

For 3C 279, there is similarly good agreement between the polarisation for the observations taken at two grating angles where the wavelength ranges overlap. Some disagreement is found which may be due to the inherent nature of flaring blazars which cause the polarisation angle to drastically vary and the two observations at different grating angles are not taken simultaneously. Additionally, the disagreement may be due to a lower Signal-to-Noise Ratio (SNR) at the edges of the RSS, which would introduce a larger systematic error. The lower SNR could originate from either blaze effects, or from the extraction of the trace, which is currently limited to a rectangular aperture in the current POLSALT pipeline.

The results show that our supplementary wavelength calibrations for POLSALT increase the efficiency of the data reduction and produce acceptable results. This reduction procedure has been used for the reduction of a number of blazar observations undertaken as part of a long term monitoring campaign [15].

Acknowledgments

All observations taken in this study were obtained using the RSS mounted on SALT under the programme ID 2016-2-LSP-001 (PI DAH Buckley).

References

- [1] C.M. Urry and P. Padovani, *Unified Schemes for Radio-Loud Active Galactic Nuclei*, *Publications of the Astronomical Society of the Pacific* **107** (1995) 803 [[astro-ph/9506063](#)].
- [2] G. Ghisellini, F. Tavecchio, L. Foschini, G. Ghirlanda, L. Maraschi and A. Celotti, *General physical properties of bright Fermi blazars*, *Monthly Notices of the Royal Astronomical Society* **402** (2010) 497 [[0909.0932](#)].
- [3] M. Böttcher, A. Reimer, K. Sweeney and A. Prakash, *Leptonic and hadronic modeling of fermi-detected blazars*, *The Astrophysical Journal* **768** (2013) 54.

- [4] H.M. Schutte, M. Böttcher, J. Barnard, A. Dmytriiev, B. van Soelen, A. Falcone et al., *Modeling the Multi-wavelength Polarization and Spectral Energy Distributions of Blazars*, in *44th COSPAR Scientific Assembly. Held 16-24 July*, vol. 44, p. 1869, July, 2022.
- [5] H.M. Schutte, R.J. Britto, M. Böttcher, B. van Soelen, J.P. Marais, A. Kaur et al., *Modeling the spectral energy distributions and spectropolarimetry of blazars—application to 4C+01.02 in 2016-2017**, *The Astrophysical Journal* **925** (2022) 139.
- [6] E.B. Burgh, K.H. Nordsieck, H.A. Kobulnicky, T.B. Williams, D. O'Donoghue, M.P. Smith et al., *Prime Focus Imaging Spectrograph for the Southern African Large Telescope: optical design*, in *Instrument Design and Performance for Optical/Infrared Ground-based Telescopes*, M. Iye and A.F.M. Moorwood, eds., vol. 4841 of *Society of Photo-Optical Instrumentation Engineers (SPIE) Conference Series*, pp. 1463–1471, Mar., 2003, DOI.
- [7] H.A. Kobulnicky, K.H. Nordsieck, E.B. Burgh, M.P. Smith, J.W. Percival, T.B. Williams et al., *Prime focus imaging spectrograph for the Southern African large telescope: operational modes*, in *Instrument Design and Performance for Optical/Infrared Ground-based Telescopes*, M. Iye and A.F.M. Moorwood, eds., vol. 4841 of *Society of Photo-Optical Instrumentation Engineers (SPIE) Conference Series*, pp. 1634–1644, Mar., 2003, DOI.
- [8] S. Crawford and K. Nordsieck, “Polsalt.” <https://github.com/saltastro/polsalt>, 2020.
- [9] J. Cooper, B. van Soelen and R. Britto, *Development of tools for SALT/RSS spectropolarimetry reductions: application to the blazar 3C279*, in *High Energy Astrophysics in Southern Africa 2021*, p. 56, May, 2022, DOI.
- [10] D. Tody, *The IRAF Data Reduction and Analysis System*, in *Instrumentation in astronomy VI*, D.L. Crawford, ed., vol. 627 of *Society of Photo-Optical Instrumentation Engineers (SPIE) Conference Series*, p. 733, Jan., 1986, DOI.
- [11] L. Fossati, S. Bagnulo, E. Mason and E. Landi Degl'Innocenti, *Standard Stars for Linear Polarization Observed with FORS1*, in *The Future of Photometric, Spectrophotometric and Polarimetric Standardization*, C. Sterken, ed., vol. 364 of *Astronomical Society of the Pacific Conference Series*, p. 503, Apr., 2007.
- [12] A. Cikota, F. Patat, S. Cikota and T. Faran, *Linear spectropolarimetry of polarimetric standard stars with VLT/FORS2*, *Monthly Notices of the Royal Astronomical Society* **464** (2017) 4146 [1610.00722].
- [13] E. Landi Degl'Innocenti, S. Bagnulo and L. Fossati, *Polarimetric Standardization*, in *The Future of Photometric, Spectrophotometric and Polarimetric Standardization*, C. Sterken, ed., vol. 364 of *Astronomical Society of the Pacific Conference Series*, p. 495, Apr., 2007, DOI [astro-ph/0610262].

- [14] S. Abdollahi, M. Ajello, L. Baldini, J. Ballet, D. Bastieri, J.B. Gonzalez et al., *The fermi-lat light curve repository*, 2023. 10.48550/ARXIV.2301.01607.
- [15] J. Barnard, B. van Soelen, J. Cooper, R. Britto, J.P. Marais, I. van der Westhuizen et al., *Optical Spectropolarimetry Observations of the BL Lac-type object PKS 0537-441 after a period of quiescence*, in *High Energy Astrophysics in Southern Africa 2021*, p. 9, May, 2022, DOI.